

STUDIES IN COSMIC RAYS

THESIS PRESENTED

BY

MILIND MANOHAR BEMALKHEDKAR

FOR THE DEGREE OF  
DOCTOR OF PHILOSOPHY  
OF THE  
GUJARAT UNIVERSITY

MARCH 1974

PHYSICAL RESEARCH LABORATORY

AHMEDABAD 380009

INDIA

043



B5608

## S T A T E M E N T

The majority of variations in the cosmic ray intensity observed at the earth are known to be due to solar modulation of Galactic cosmic rays. The present thesis deals with a special class of diurnal anisotropy with maximum around 09 hour direction in the interplanetary space. The studies are made with the Gulmarg neutron monitor as well as with the worldwide network of neutron monitors. In addition a neutron multiplicity meter was attached to the Gulmarg neutron monitor to study the possibility of using the multiplicity spectrum as a representation of the primary spectrum during various cosmic ray intensity variations.

A ground based neutron monitor looks into a small region of the sky, determined by its 'Asymptotic cone of acceptance' and, as earth spins, it scans this region of the sky around the spin-axis in all directions during the course of a day. As a result, any spatial anisotropy in the cosmic ray intensity perpendicular to the spin-axis produces a diurnal variation in the monitor counting rate, the time of maximum being a function of the local time at the monitor. On the other hand, any isotropic change in intensity, like the Forbush decrease, causes a simultaneous change in the monitor counting rate at all longitudes and latitudes. To separate out these two different types of cosmic ray intensity variations, it is therefore necessary to use a

large number of cosmic ray monitors spaced at various longitudes and latitudes.

The neutron monitor at Gulmarg was set up in September 1967. The author was actively involved in this work. The monitor is of IGY type and has twenty Boron-tri-fluoride counters with a total counting rate of  $\approx 260,000$  counters hour<sup>-1</sup>. The station of the monitor has geographic latitude 34.07°N and longitude 74.42°E and is located 2743 meters above sea level. The specialized location of the monitor, with the geomagnetic cutoff rigidity of 11.91 GV of the station, makes it an important station in the worldwide network of the monitors. The neutron multiplicity meter designed and built by the author has been operated in association with the Gulmarg neutron monitor for the period October, 1967 - October, 1971.

The salient features of the results presented in the thesis are as follows:

The investigation of the diurnal variation in the cosmic ray intensity on individual days has revealed a new class of diurnal variation showing a maximum around 09 hour direction in the interplanetary space. It is shown to occur during the recovery phase of Forbush decreases as well as during quiet periods. The amplitude of this anomalous diurnal variation is, in general, larger when preceded by a Forbush decrease. The rigidity spectrum of the anomalous

diurnal variation has an exponent around zero, the same as that for the average diurnal variation exhibiting maximum around 18 hours in the interplanetary space.

It is shown that the Forbush decreases associated with the diurnal variation exhibiting morning maximum, are 27 day recurrent in nature and are preceded by east limb solar flares on most of the occasions. Recurrent Forbush decreases preceded by west limb flares exhibit only the average diurnal variation in their recovery phases. Further, the non-recurrent Forbush decreases also show predominantly the characteristics of the average diurnal variation during their recovery phase.

A qualitative model of the transient modulation by solar corotating corpuscular streams of enhanced solar wind velocity, emanating from the active regions on the solar disc, is proposed to explain the anomalous diurnal anisotropy in the recovery phase of 27 day recurrent Forbush decreases. The enhanced convection of the cosmic ray particles in the corotating stream, in a quasi-equilibrium state with the simultaneous inward diffusion from all sides, produces depression in cosmic ray intensity inside the stream. When the earth is engulfed by such a corotating stream from east of the earth-sun line, it experiences a smaller transient modulation depth on the west than on the east of the earth-sun line. At this specialized location inside the stream, there is therefore a larger inward diffusion from the west than



from the east of the earth-sun line, which is shown to result in the anomalous diurnal variation in the cosmic ray intensity with maximum around the garden hose direction. From this model, the cosmic ray diffusion coefficients, parallel and perpendicular to the interplanetary magnetic field inside the corotating stream, are derived and compared with the average values. It is found that, while the value of the field perpendicular diffusion coefficient inside the stream is of the same order as quoted by Jokipii and Coleman (1968), the field parallel diffusion coefficient is smaller by a factor of two. The recent measurements on Pioneer 10, however, indicate that the average value of the field parallel diffusion coefficient is much higher than the value quoted by Jokipii and Coleman (1968). The smaller value inside the corotating stream is understandable in terms of the enhanced magnetic field irregularities associated with high velocity solar wind in the stream producing larger turbulence.

Modifications in the configuration of a corotating stream due to the occurrence of east limb flares in the long lived active regions or in nearby regions on the solar disc, are discussed to explain the increased probability for the anomalous diurnal variation to occur. If the flare occurs in the active region producing the corotating stream, it may widen the angular extent of the stream increasing the transient modulating depth on the east than on west of the

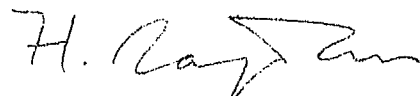
earth-sun line, when the stream engulfs the earth. Or, if the flare occurs in the nearby active regions on the solar disc, the plasma cloud from the flare may interact with the stream and again produce a larger modulating depth on east of the earth-sun line. On the other hand the plasma cloud from a west limb flare, preceding the Forbush decrease caused by the corotating stream, cannot interact with the stream unless the angular dimensions of the cloud are sufficiently large. But it does create a region of depressed cosmic ray intensity on the west of the stream, which results in less diffusion of cosmic ray particles from the west, producing the diurnal variation in the intensity with maximum around 18 hours in the interplanetary space.

In contrast to the anomalous diurnal variation during the recovery phase of recurrent Forbush decreases, the anomalous diurnal variation during the quiet periods is attributed to the enhanced flux of cosmic ray particles in the garden hose direction resulting from short circuiting of the heliolatitudinal density gradients by interplanetary magnetic field irregularities moving radially outward from the sun. The 27 day recurrence tendency of the quiet time anomalous diurnal variation also, has led us to postulate quasi-stable regions on the solar disc which produce a larger number of magnetic field irregularities.

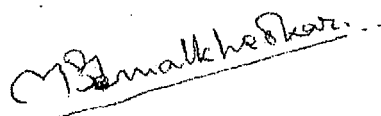
To investigate the possibility of determining the energy spectra of cosmic ray intensity variations from a single station, a continuous record of neutron multiplicity spectrum in the Gulmarg neutron monitor is obtained for the period October, 1967 - October, 1971. The average multiplicity spectrum in the Gulmarg neutron monitor shows a mean multiplicity  $\approx 1.4$  for 12 Boron-tri-fluoride counters and is an increasing function of the number of counters used. The mean multiplicity measured in various other neutron monitors, when normalized to the cutoff rigidity of Gulmarg (11.91 GV), shows a systematic increase with the altitude of the station. Measurement of the multiplicity spectrum during Forbush decreases has not shown any significant change in the spectrum beyond statistical errors, when compared to the spectrum during quiet periods.

The thesis is divided into five chapters. The first chapter describes the present knowledge of the propagation of cosmic rays in the interplanetary medium and its relation to time variations in the cosmic ray intensity. The second chapter discusses the experimental and the analytical methods of relating the time variations in the intensity observed by ground based neutron monitors to the cosmic ray intensity variations in the interplanetary space. This essentially involves discussion of the atmospheric and geomagnetic effects on cosmic ray intensity and brings out

the concept of the "Asymptotic cone of acceptance" in the interplanetary space for a cosmic ray monitor on the ground. The third chapter describes the Gulmarg neutron monitor and the associated electronic circuits. The fourth chapter presents a description of the associated neutron multiplicity meter and the results on multiplicity measurements in the Gulmarg neutron monitor including time variations observed in the multiplicity counting rates. Fifth chapter discusses the results on the anomalous diurnal anisotropy with maximum around 09 hour direction in the interplanetary space. The chapter further includes a discussion of the models of the transient modulating stream corotating with the sun which causes the anomalous diurnal anisotropy in the cosmic ray intensity, as well as of the short circuiting of the heliolatitudinal density gradients to produce the quiet time anomalous diurnal variation.



(H. RAZDAN)



(M. M. BEMALKHEDKAR)

## LIST OF PUBLICATIONS

M. M. BEMALKHEDKAR

Physical Research Laboratory

Ahmedabad, India.

1. Multiplicity Spectrum of a IGY Neutron Monitor at Gulmarg.  
- Bemalkhedkar M.M., N.W.Nerurkar and H. Razdan.  
Proc. 10th symposium on Cosmic Rays, Elementary Particle Physics and Astrophysics, Aligarh, India, 167, 1967.
2. On Forbush Decreases in Various Multiplicities in Gulmarg Neutron Monitor.  
- Bemalkhedkar M.M. and R.K. Kaul  
Proc. 11th symposium on Cosmic Rays, Astrophysics, Geophysics and Elementary Particle Physics, Delhi India, 2, 399, 1969.
3. Bunch Pulser.  
- Bemalkhedkar M.M.  
Journal of Institution of Telecommunication Engineers, 15, 676, 1969.
4. Anomalous Diurnal Variation of Cosmic Rays with Maximum along the Garden Hose Direction.  
- Razdan H. and M.M. Bemalkhedkar  
Proc. 12th International Conference on Cosmic Rays, Hobart, Australia, 2, 697, 1971.

5. Anomalous Recurrent Diurnal Anisotropy in Cosmic Ray Intensity with Maximum along the Garden Hose Direction.  
- Razdan H. and M.M. Bemalkhedkar Cosmic Electrodynamics, 3, 297, 1972.
6. Latitude Variation of 510 KeV Line Intensity and Absorption Length of Atmospheric Gamma Radiation.  
- Bemalkhedkar M.M. and H. Razdan. Proc. 13th International Cosmic Ray Conference, Denver, U.S.A., 2, 933, 1973.
7. Diurnal Anisotropy of Cosmic Rays Associated with Forbush Decreases and Solar Flares.  
- Bemalkhedkar M.M., G. Subramanian and H. Razdan. Proc. 13th International Cosmic Ray Conference, Denver, U.S.A., 2, 1293, 1973.
8. High Energy Cosmic Ray Intensity Increases of Non-Solar Origin and the Unusual Forbush Decrease of August 1972.  
- Agrawal S.P., A.G. Ananth, M.M. Bemalkhedkar, L.V.Kargathra, U.R. Rao and H. Razdan. Accepted for publication in J. Geophys. Res., 1974.

## A C K N O W L E D G E M E N T S

It is a great pleasure to acknowledge my deep indebtedness to Prof. H. Razdan for his inspiring guidance, active encouragement and moral support during the entire research work presented in this thesis. I also express my deep indebtedness to Prof. N.W. Nerurkar for his guidance in the early stages of the research work. The research facilities provided by late Prof. V.A. Sarabhai and Prof. D. Lal at Physical Research Laboratory, Ahmedabad and at High Altitude Research Laboratory, Gulmarg are gratefully acknowledged.

Thanks are due to Messrs M.U. Khan and S. Bakaya for fruitful discussions during the designing of neutron multiplicity meter and other electronic circuits of the Gulmarg neutron monitor, and to Messrs R.K. Kaul, K.S. Lali and Quasim Ali for the efficient running of the neutron monitor. The cooperation from wiring group for wiring electronic circuits as well as from Workshop, Carpentry, Drafting and Photography sections in Physical Research Laboratory and High Altitude Research Laboratory is acknowledged.

Thanks are also due to the Directors of various cosmic ray laboratories and World-data-centre for providing the cosmic ray data. Special mention must be made of Prof. C.P. Sonett and Dr.S.J. Bames for kindly providing the interplanetary magnetic field and solar wind data.

I had the privilege of having a number of discussions with Prof. R.P. Kane and Dr. G. Subramanian during the data analysis and the interpretation of the results. I express my sincere thanks to them for the same. The data analysis was carried out on IBM 360 Computer at Physical Research Laboratory and I am thankful to Mr. S.R. Thakore, Dr.Dinesh Patel and their group at the Computer centre for their generous co-operation.

The author expresses his thanks to Mr. K.S. Patel, Mr. J.G. Vora and Mrs. U.K. Modi for the computational help. Thanks are also due to Mr. M.V. Joseph for efficient typing of the thesis.

The entire research programme received financial support from Department of Atomic Energy, Government of India.

Finally, I wish to express my deep gratitude towards my parents for their moral support during the entire research work.

*M.M. Bemalkhedkar*

Date : 20-03-1974

(M.M. Bemalkhedkar)



# I N D E X

## CHAPTER I

	<u>Cosmic Rays and their Modulations</u>	Page No.
I.1	General survey	1
I.2	Characteristics of the Interplanetary medium	4
I.3	Propagation of cosmic rays in the interplanetary medium	10
I.4	Time variations in the cosmic ray intensity	22
	I.4 a) Eleven year variation	22
	I.4 b) Forbush decreases	28
	I.4 c) Diurnal variation	34
	I.4 d) Semidiurnal variation	45
	I.4 e) 27 day variation	48
	I.4 f) Solar flare increases	50
I.5	Origin of cosmic rays	55

## CHAPTER II

### Techniques of the study of cosmic ray time variations

II.1	Comparison of cosmic ray detectors	60
II.2	Atmospheric pressure correction in a neutron monitor	62
II.3	Geomagnetic field and asymptotic cones of acceptance	66
II.4	Variational coefficients	73
II.5	Rigidity dependence in cosmic ray intensity	78
II.6	Numerical techniques	79
	II.6 a) Harmonic analysis	79
	II.6 b) Correction of harmonic coefficients for secular changes in the data	81

II.6 c)	Method of superposed epoch or the Chree analysis	83
II.6 d)	'Principle of least squares' and regression analysis	88
II.6 e)	$\chi^2$ square test for goodness of fit	88

### CHAPTER III

#### GULMARG NEUTRON MONITOR

III.1	Description of the neutron monitor	90
III.2	3000 Volt Power supply for the neutron monitor	93
III.3	Low voltage supplies	98
III.4	Camera control and the clock circuit	98

### CHAPTER IV

#### Multiplicity measurements in Gulmarg Neutron Monitor

IV.1	Introduction	100
IV.2	Neutron multiplicity meter	101
IV.3	Bunch Pulser for continual checking of neutron multiplicity meter	105
IV.4	Corrections of the multiplicity counting rates for chance coincidence and life time of neutrons in the monitor	110
IV.5	Neutron multiplicity spectrum and the mean multiplicity	113
IV.6	Latitude and altitude variation of mean multiplicity	116
IV.7	Multiplicity spectrum during Forbush decreases	122

CHAPTER V

Anomalous diurnal variation in cosmic ray intensity

V.1	Introduction	132
V.2	Enhanced anomalous diurnal variation with morning maximum during the years 1965-1967	135
V.2 a)	General characteristics	135
V.2 b)	Rigidity spectrum of the enhanced anomalous diurnal variation	142
V.2 c)	The solar and geomagnetic phenomena preceding the Forbush decreases associated with the anomalous diurnal variation	146
V.3	Statistical analysis of anomalous diurnal variation in the recovery phase of Forbush decreases during the years 1960-1970	155
V.4	Recurrent Forbush decreases and solar flares	171
V.5	Corotating corpuscular streams and the anomalous diurnal variation in the cosmic ray intensity	175
V.6	Quiet time anomalous diurnal variation	186
V.7	Concluding remarks	198

\*\*\*\*\*

# CHAPTER I

## COSMIC RAYS AND THEIR MODULATIONS

### I.1. General survey of cosmic rays

The primary cosmic rays, impinging on the top of the earth's atmosphere, consist mainly of 86.25% protons, 12.44% alpha particles and remaining 1.31% heavy nuclei. In addition, they also contain electrons, though their abundance does not exceed 0.2% of the total cosmic rays (Hulsizer, 1949; Critchfield, 1950). The energies of cosmic rays are observed to extend upto  $\approx 10^{20-21}$  eV (Suga et al., 1971) and have an integral energy spectrum  $\sim E^{-1.5}$ . Cosmic rays being charged particles, their trajectories undergo bending in the geomagnetic field causing particles with rigidities greater than the minimum to arrive at a place on earth from a given direction. The geomagnetic field also causes the direction of the primary particles at the top of the atmosphere to be different from their asymptotic directions in the interplanetary space. Their propagation in the interplanetary medium is basically governed by the scattering and bending of their trajectories in the solar magnetic fields stretched out by the solar wind. Beyond the region of solar influence, the galactic cosmic rays are found to be isotropic within the experimental errors (Hayakawa, 1969). Further, their intensity has been constant during the last 10<sup>8</sup> years (Honda et al., 1960; Arnold et al., 1961; Geiss, 1963;

Hayakawa, 1969). The present theories consider the origin of the galactic cosmic rays to be in the supernovae explosions (Ginzburg, 1958) and/or in pulsars (Gold, 1969). During their travel in the galactic space, the cosmic rays undergo random collisions with moving magnetic field irregularities and become isotropic. These collisions impart energy to the cosmic ray particles through Fermi acceleration mechanism (Fermi, 1949) and lead to a power law energy spectrum of cosmic rays with a negative exponent.

Eventhough, the galactic intensity of cosmic rays is isotropic and constant in time, their interaction with the interplanetary magnetic field gives rise to spatial anisotropies and time variations in their intensity near the orbit of the earth. Cosmic rays diffuse into the solar modulating region against the convection by irregularities in the interplanetary magnetic field moving radially outward with the solar wind. The balance between the outward convection and the inward diffusion of cosmic rays results in the steady state cosmic ray density profile in the interplanetary medium having a radial, positive, integral density gradient between 3% to 9% per AU above 400 MeV per nucleon (O'Gallagher, 1972). The recent measurements on the deep-space probe Pioneer 10 (Lentz et al., 1973; Teegarden et al., 1973; Van Allen, 1973) have however indicated, that within about 1-4 AU, the radial cosmic ray

particle density gradient is significantly less than the above value. Any imbalance between the convection and diffusion causes a change in the cosmic ray density profile resulting in a change of cosmic ray flux. Further, the anisotropic diffusion of cosmic rays in the interplanetary magnetic field gives rise to spatial anisotropies in the cosmic ray intensity. These manifest themselves as periodic variations in the intensity recorded by an earthbound detector scanning various directions in the interplanetary space as the earth rotates. The amplitude and direction of such anisotropies are dependent upon the scale size and the spatial distribution of the irregularities in the magnetic field. Thus, time variations in the cosmic ray intensity provide a probe to study macroscopically, the interplanetary magnetic field structure, its irregularities and their spatial and temporal variations. In all these studies, the direct measurements of cosmic ray density gradient and the interplanetary magnetic field by satellite detectors play an important role. However, satellite measurements have a limitation that they refer to only localized regions of the interplanetary space near the satellite and that the measurements are not continuous over long periods. Also, since all the satellites are in the plane of ecliptic, we have no direct measurements from the higher heliolatitudes. The detailed discussions of the experimental results on modulation of cosmic rays and

the models derived therefrom, have been reviewed by Singer (1958), Webber (1962,1968), Dorman (1963,1969), Obayashi (1964), Biswas and Fichtel (1965), Forbush (1966), Quenby (1967), Parker (1969), McCracken and Rao (1970), Jokipii (1971), Lockwood (1971), Pomerantz and Duggal (1971) and Rao (1972).

## I.2. Characteristics of the interplanetary medium

The sun emits continuously a corpuscular radiation known as the solar wind, containing mainly protons and electrons in equal numbers, which moves radially outwards due to hydromagnetic expansion of the solar corona. The rate of expansion (outward flow) starts from very low velocities beneath the corona. The velocity increases steadily outward, surpassing the speed of sound at a radial distance of a few solar radii by De Laval nozzle action arising from the solar gravitational force (Parker, 1963, 1965; Dessler, 1967). The velocity reaches its average interplanetary value of  $300\text{--}400 \text{ km sec}^{-1}$  beyond a distance of about 30 solar radii. The average density of solar wind particles at the orbit of the earth is  $\approx 8 \text{ particles cm}^{-3}$  (Hundhausen, 1970). The solar wind velocity following a large solar flare can reach as high a value as  $2000 \text{ km sec}^{-1}$  for a short period together with an increase in the density (Gruenwaldt et al., 1972). The other characteristics of the solar wind and the interplanetary magnetic field

are listed in the table 1.1.

At a heliocentric distance  $\approx 3-7$  AU, the solar wind undergoes a shock transition from supersonic to subsonic flow because of the inward pressure of the galactic hydrogen (Axford et al., 1963, Burlaga, 1967; O'Gallagher, 1968; Pathak and Sarabhai, 1970; Simpson and Wang, 1970; Jokipii, 1971). Beyond the shock transition, the solar wind protons undergo charge exchange with galactic neutral hydrogen, thereby transferring the solar wind energy to the outflowing neutral atomic hydrogen.

The interplanetary magnetic field results from the extension of the lines of force of the general solar dipole field by the outflowing solar wind. In addition to this, the rotation of the sun twists the interplanetary magnetic field in the form of an Archimedean spiral (Parker, 1958). In polar coordinate system  $(r, \theta, \phi)$ , the interplanetary magnetic field is described by the equations

$$B_r(r, \theta, \phi) = B \left[ \theta, \phi + \frac{r}{V_s} \right] \cdot \frac{(R_\odot)^2}{r} \quad \dots (1.1)$$

$$B_\phi(r, \theta, \phi) = B \left[ \theta, \phi + \frac{r}{V_s} \right] \cdot \frac{(R_\odot \Omega)}{V_s} \cdot \frac{R_\odot}{r} \cdot \sin \theta \quad \dots (1.2)$$

where  $R_\odot$  is the solar radius,  $V_s$  is the solar wind velocity and  $\Omega$  is the angular velocity of the sun. Evidence for the spiral structure has been experimentally obtained by McCracken (1962) through the study of propagation of



solar cosmic rays and by Ness et al.(1964) through direct satellite measurements. The spiral angle  $\chi$  at a distance  $r$  from the sun, also known as "garden hose angle" is given by

$$\tan \chi = \frac{\Omega r}{V_s} \quad \dots (1.3)$$

Near the orbit of the earth, the garden hose angle is  $\approx 45^\circ$ , while strength of the magnetic field is  $\approx 5$  gamma.

The average interplanetary magnetic field contains many small scale irregularities due to turbulence in the solar wind velocity. The average irregularities are of the scale  $10^5$ - $10^8$  km and move radially outward with the solar wind (Smith et al.,1962; Ness et al.,1964).

The interplanetary magnetic field is divided into alternate sectors of opposite polarity (Wilcox and Ness, 1965) as shown in figure 1.1. The source of the sector structure is probably associated with the pattern of the weak photospheric sectors, two of each polarity, though at times six sectors have been noticed. The sector pattern corotates with the sun. The average sector contains a coherent internal structure. The magnitude of the magnetic field, solar wind velocity as well as plasma density rise to a peak near the leading edge of the sector and decline in the following portion as is shown in figure 1.2.

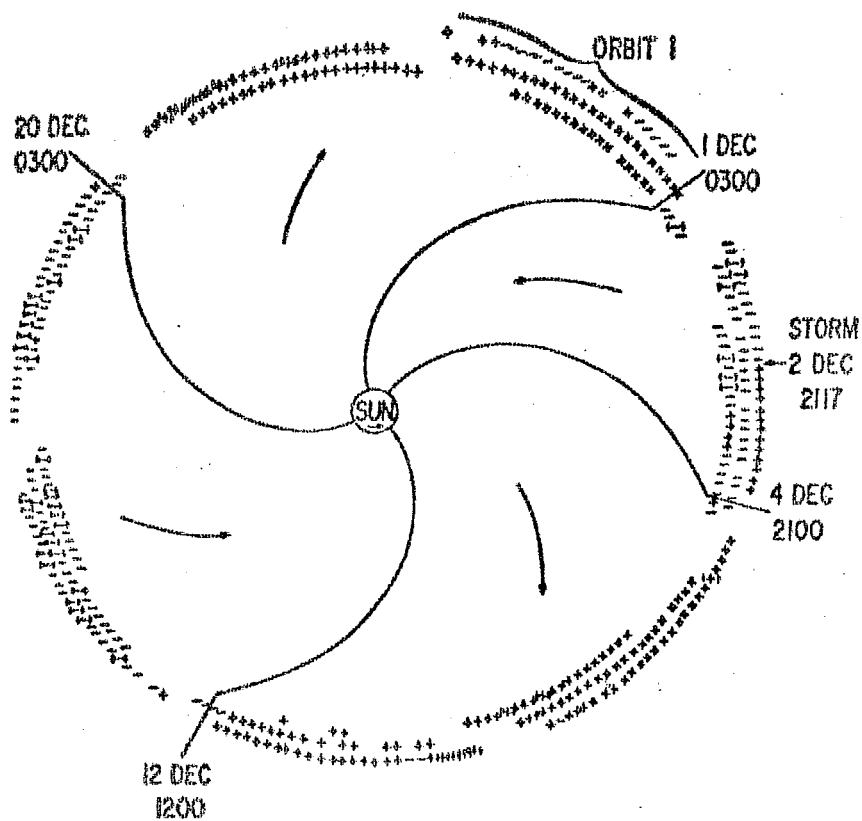
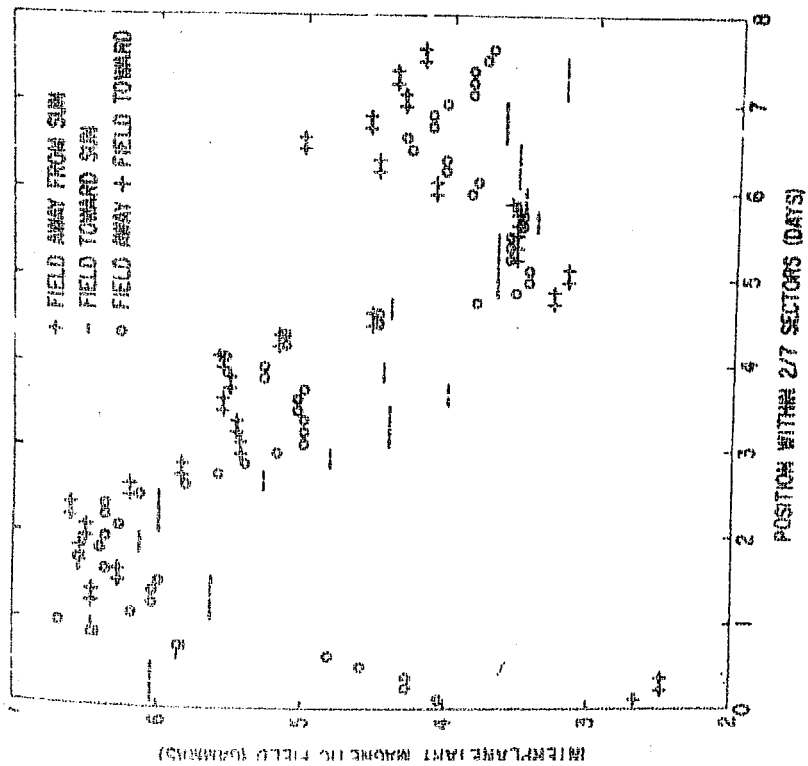
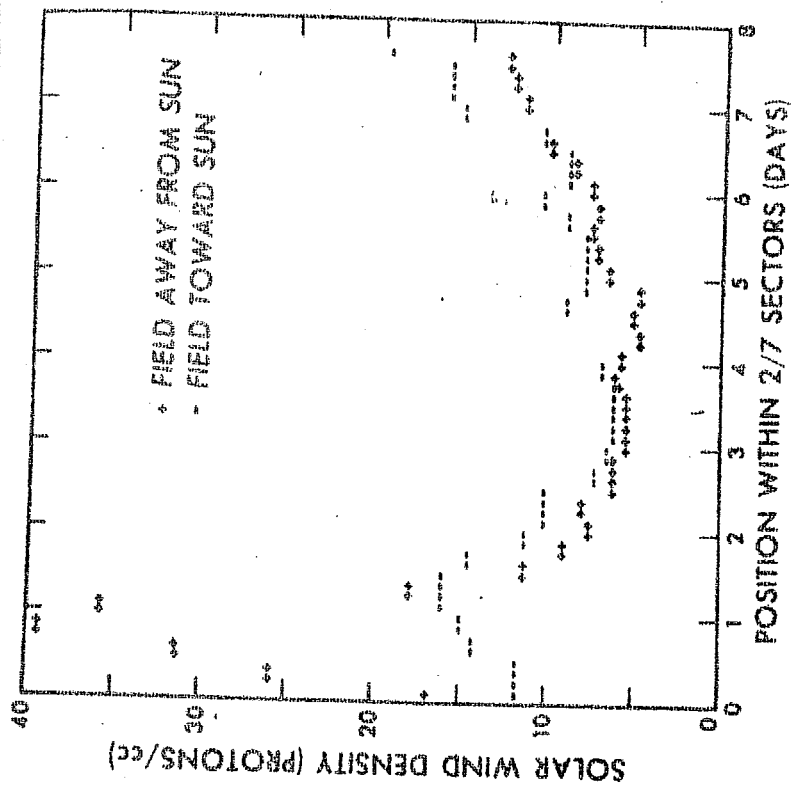


Figure 1.1 The sector structure of the interplanetary spiral magnetic field in the plane of ecliptic, measured by instruments aboard IMP-1 in 1963 (Wilcox and Ness, 1965). A plus sign indicates the field lines pointed away from the sun, and a minus sign towards the sun.



a



b

Figure 1.2a, b Variation of interplanetary magnetic field and the plasma density inside a sector of the interplanetary magnetic field (Wilcox and Ness, 1965).

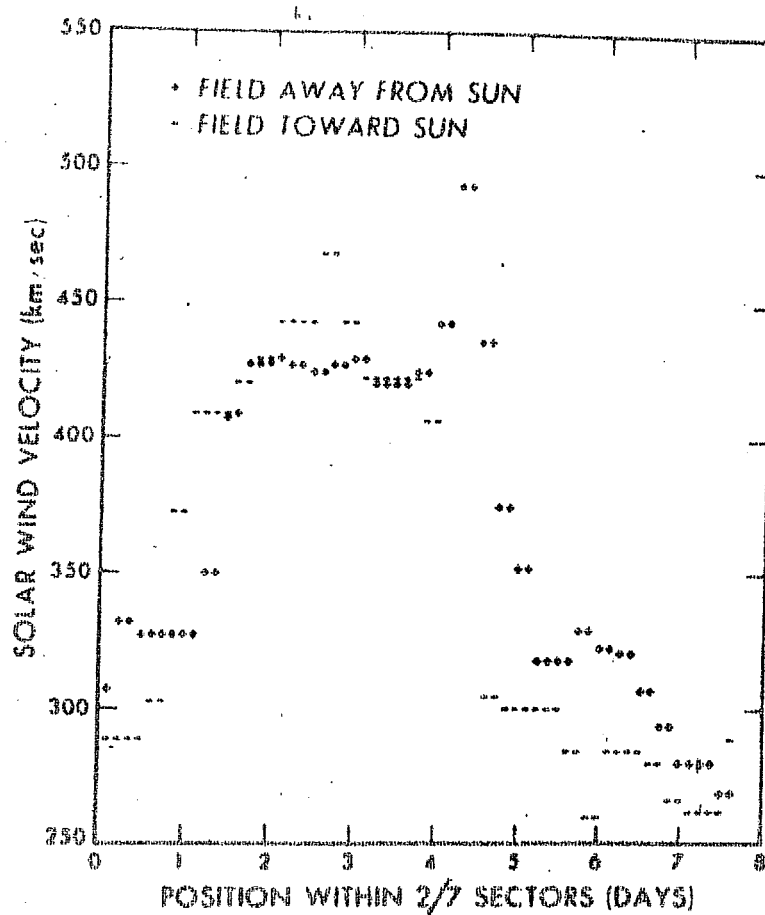


Figure 1.2c Variation of solar wind velocity inside a sector of the interplanetary magnetic field (Wilcox and Ness, 1965).

Table 1.1 Properties of the solar wind and the interplanetary magnetic field

Description	Average value at the base of the solar corona	Quiet day value at the orbit of the earth	Maximum value at the earth
Solar wind velocity	Very small	320 km sec <sup>-1</sup>	2000 km sec <sup>-1</sup>
Solar wind flow direction	Radial	1.6°E *	11.6°E to 8.4°W *
Proton or electron density	10 <sup>8</sup> cm <sup>-3</sup>	8 cm <sup>-3</sup>	54 cm <sup>-3</sup>
Helium to proton density ratio		0.045	0.15
Debye length	0.7 cm	2000 cm	
Proton temperature	2 x 10 <sup>6</sup> °K	4.8 x 10 <sup>4</sup> °K	8 x 10 <sup>5</sup> °K
Electron temperature		(1 - 1.5) x 10 <sup>5</sup> °K	8 x 10 <sup>5</sup> °K
Electrical conductivity	6 x 10 <sup>16</sup> sec <sup>-1</sup>	6 x 10 <sup>11</sup> sec <sup>-1</sup>	
Viscosity	0.7 gm cm <sup>-1</sup> sec <sup>-1</sup>	Very small	
Magnetic field	1 gauss	5 γ	80 γ
Direction of the field line	Radial	~ 45°W *	
Scale size of irregularities		≤ 0.01 AU	
Magnetic Reynolds number	6 x 10 <sup>10</sup>	6 x 10 <sup>7</sup>	

\* The direction east or west is with respect to the earth sun line.

### I.3. Propagation of cosmic rays in the interplanetary medium

Theoretical investigations of the kinetics of cosmic rays in the interplanetary magnetic fields and the resulting time variations in the cosmic ray intensity have been carried out by Ahluwalia and Dessler (1962), Stern (1964), Parker (1964,65), Axford (1965), Gleeson and Axford (1967), Gleeson (1969), Fisk and Axford (1970), Forman and Gleeson (1970) and Jokipii (1971). Basically, there have been two approaches to study this problem. Ahluwalia, Dessler, Stern, Parker and Jokipii considered the motion of individual particles in the interplanetary magnetic field using the guiding center concept. On the other hand, Axford, Gleeson, Fisk and Forman analysed the hydromagnetic equations of the cosmic ray gas in the interplanetary magnetic field. Both the methods lead to similar conclusions about the kinetics of cosmic rays and are described below.

In the guiding centre formalism, the drift velocity of the guiding centre perpendicular to the interplanetary magnetic field  $\underline{B}$  may be expressed as (Parker, 1964),

$$\underline{u}_{\perp} = \frac{c \underline{E} \times \underline{B}}{B^2} + \frac{1}{2} \frac{mv_{\perp}^2}{qB^4} c \frac{\underline{B}}{B} \times \frac{\partial}{\partial \underline{n}} (B^2/2) + \frac{mv_{\parallel}^2}{qB^4} c \frac{\underline{B}}{B} \times \left[ \underline{B} \cdot \frac{\partial}{\partial \underline{n}} \right] \underline{B} \dots (1.4)$$

where  $m$  is the mass of the particle,  $q$  the charge of the particle,  $v_{\parallel}$  and  $v_{\perp}$  the components of the velocity of the particle parallel and perpendicular to the magnetic field respectively,  $c$  the velocity of light and  $\underline{E}$  is

the electric field induced perpendicular to the solar equatorial plane due to the motion of the interplanetary magnetic field, in 15 hour direction relative to the earth. The electric field  $\tilde{E}$  is given by

$$\tilde{E} = - \frac{\tilde{V}_s \times \tilde{B}}{c} \quad \dots (1.5)$$

where  $\tilde{V}_s$  is the solar wind velocity (Ahluwalia and Dessler, 1962). The first of the three terms in the equation (1.4) represents the electric drift in 15 hour direction and is shown in figure 1.3. The second term corresponds to the drift due to gradient in the magnetic field. The third term represents the drift due to curvature of the field lines. Application of Compton-Getting effect (1935) to the flux due to streaming velocity  $u_r$  will give the anisotropy of cosmic rays. Parker has shown from equation (1.4) that in the case of smooth magnetic fields, the resultant streaming velocity is zero as also argued by Stern (1964). The streaming will, however, be non-zero if there are enough irregularities beyond the earth's orbit to wipe out the streaming in 15 hour direction resulting from the curvature and gradient drift of the particles. Parker has further postulated a field aligned inward diffusion of cosmic rays to make the average radial component of streaming zero, for the sun is neither a source nor a sink of cosmic rays. Parker (1965) and Jokipii (1971) consider the effect of interplanetary magnetic field irregularities on the motion of cosmic rays. By using Fokker-Planck equation

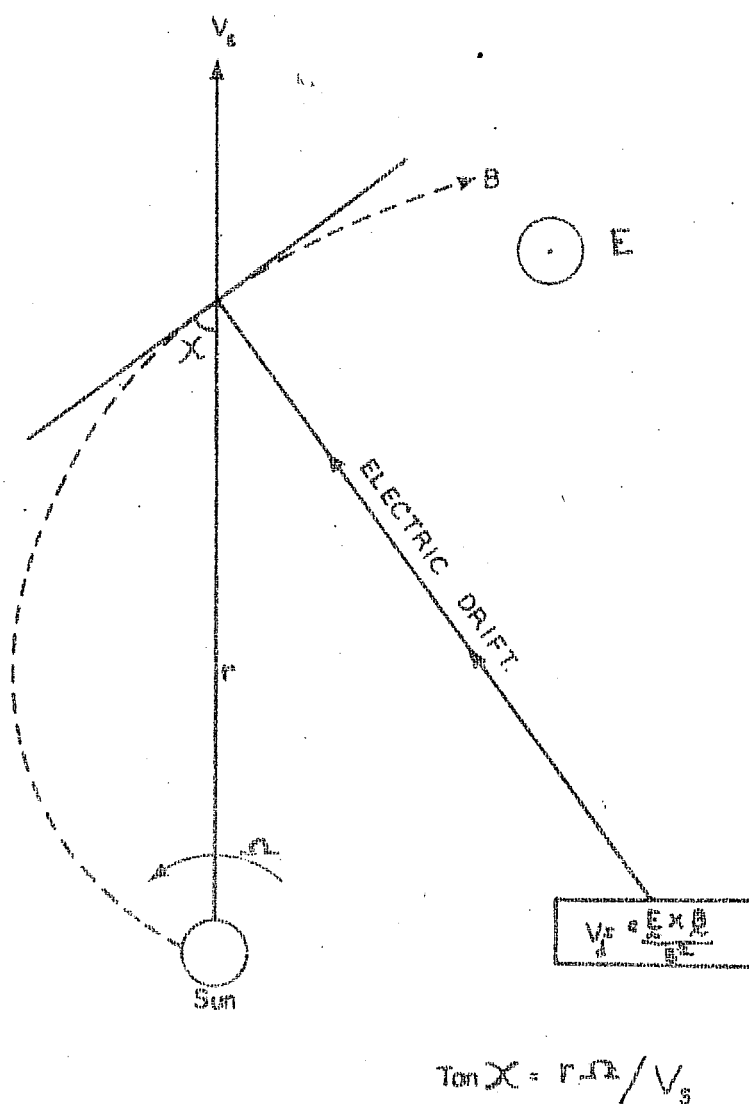


Figure 1.3 The electric drift ( $\underline{E} \times \underline{B}$ ) of cosmic ray particles in the interplanetary space. The electric field results from the motion of interplanetary magnetic field in 15 hour direction relative to the earth.



for the scattering of cosmic rays by these irregularities, they have calculated the field parallel and perpendicular diffusion coefficients in the interplanetary medium.

An alternative theory of cosmic ray propagation developed by Axford (1965) considers the Boltzman equation of cosmic ray gas in the interplanetary magnetic field. He postulates the presence of small scale irregularities superposed on the average interplanetary magnetic field  $B_0$  throughout the solar modulation region and has studied the motion of cosmic rays under scattering by these irregularities which move radially outward with the solar wind. If  $\underline{E}$  is the electric field associated with the motion of the average interplanetary magnetic field  $B_0$  relative to earth in the 15 hour direction (Ahluwalia and Dessler, 1962), the Boltzman equation for the cosmic ray gas may be written as

$$\frac{\partial f}{\partial t} + \left[ \underline{v} \cdot \frac{\partial}{\partial \underline{r}} \right] f + \frac{e}{m} \left[ \underline{E} + \frac{\underline{v} \times \underline{B}_0}{c} \right] \cdot \frac{\partial}{\partial \underline{v}} (f) = \left[ \frac{df}{dt} \right]_c \quad \dots (1.6)$$

where  $f(\underline{r}, \underline{v}, t)$  is the distribution function for the component of the cosmic radiation with particle charge  $e$  and mass  $m$ . The term on the right hand side represents the effect of collisions with the fluctuating part (irregularities) of the interplanetary magnetic field.

The zero-order and first-order moments of this equation yield the equation of continuity and the momentum equation respectively.

The continuity equation,

$$\frac{d\rho}{dt} + \frac{\partial}{\partial \underline{r}} \cdot (\rho \underline{u}) = 0 \quad \dots(1.7)$$

states that the time rate of change of cosmic ray mass density  $\rho$  is equal to divergence of the mass flux ( $\rho \underline{u}$ ) due to the average hydrodynamic or streaming velocity  $\underline{u}$  of the particles. Likewise, if  $U$  is the number density ( $\rho/m$ ) of particles, the momentum equation is given by

$$\begin{aligned} \frac{d(\rho \underline{u})}{dt} + \frac{\partial}{\partial \underline{r}} \cdot \underline{\underline{S}} + \left[ \underline{u} \cdot \frac{\partial}{\partial \underline{r}} \right] (\rho \underline{u}) + \rho \underline{u} \left[ \frac{\partial}{\partial \underline{r}} \cdot \underline{u} \right] - e U \left[ \underline{E} + \frac{\underline{v} \times \underline{B}_0}{c} \right] \\ = \int \left[ \frac{d\underline{f}}{dt} \right]_c \cdot m \underline{v} d^3v \quad \dots(1.8) \end{aligned}$$

where  $\underline{\underline{S}}$  is the stress tensor. If divergence of the streaming velocity  $\underline{u}$  is zero, because no accumulation of particles takes place in the interplanetary medium, the momentum conservation equation may be written after rearranging, in the form,

$$\frac{d\underline{u}}{dt} + (\underline{u} \cdot \frac{\partial}{\partial \underline{r}}) \underline{u} = - \frac{1}{Um} \left[ \frac{\partial}{\partial \underline{r}} \cdot \underline{\underline{S}} \right] + \frac{e}{m} \left[ \underline{E} + \frac{(\underline{v} \times \underline{B}_0)}{c} \right] + \frac{1}{U} \int \left[ \frac{d\underline{f}}{dt} \right]_c \underline{v} d^3v \dots(1.9)$$

The simple mean free path treatment for the cosmic ray particles undergoing collisions with irregularities in the interplanetary magnetic field  $\underline{B}_0$ , gives

$$\int \left[ \frac{d\underline{f}}{dt} \right]_c \underline{v} d^3v = \frac{U}{\tau} (\underline{v}_s - \underline{u}) \quad \dots(1.10)$$

where  $\tau$  is the mean collision interval and  $\underline{v}_s$  is the solar wind velocity.

If the off-diagonal terms of the stress tensor  $\underline{S}$  are zero and the diagonal terms are equal to  $\Pi = \frac{1}{3} U m \underline{v}^2$ , and the inertial terms negligible, we get

$$0 = - \frac{\underline{v}^2}{3 U} \left[ \frac{\partial U}{\partial \underline{r}} \right] + \frac{e}{m} \left[ \underline{E} + \frac{(\underline{u} \times \underline{B}_0)}{c} \right] + \frac{1}{\tau} (\underline{v}_s - \underline{u}) \dots (1.11)$$

where  $\underline{u}$  is substituted for  $\underline{v}$  in the  $\underline{v} \times \underline{B}_0$  term as an approximation. Elimination of  $\underline{u}$  between the equations (1.7) and (1.11) gives the diffusion equation

$$\underline{u} = \underline{K} \cdot \left[ \frac{3}{v \lambda} \underline{v}_s - \frac{1}{U} \cdot \frac{\partial U}{\partial \underline{r}} \right] \dots (1.12)$$

where  $\lambda$  is the mean free path of the particles and the diffusion tensor  $\underline{K}$  is of the form

$$\underline{K} = \begin{bmatrix} \frac{1}{3} v \lambda & 0 & 0 \\ 0 & \frac{\frac{1}{3} v \lambda}{1 + \omega^2 \tau^2} & - \frac{\frac{1}{3} v \lambda \omega \tau}{1 + \omega^2 \tau^2} \\ 0 & \frac{\frac{1}{3} v \lambda \omega \tau}{1 + \omega^2 \tau^2} & \frac{\frac{1}{3} v \lambda}{1 + \omega^2 \tau^2} \end{bmatrix} \dots (1.13)$$

Similar form of diffusion tensor has been also obtained by Parker (1965) by using Fokker-Planck equation to describe cosmic ray propagation in the interplanetary medium.

Writing

$$K_{||} = \frac{1}{3} v \lambda \dots (1.14)$$

and

$$K_{\perp} = \frac{K_{||}}{1 + \omega^2 \tau^2} \dots (1.15)$$

we have

$$\tilde{K} \approx \begin{bmatrix} K_{\parallel} & 0 & 0 \\ 0 & K_{\perp} & -K_{\perp} \omega \tau \\ 0 & K_{\perp} \omega \tau & K_{\perp} \end{bmatrix} \dots (1.16)$$

The components of the streaming velocity in the solar equatorial plane are then given as

$$u_{\parallel} = V_{s\parallel} - K_{\parallel} \left[ \frac{\partial}{\partial \tilde{r}} (\log_e U) \right]_{\parallel} \dots (1.17)$$

$$u_{\perp} = V_{s\perp} - K_{\perp} \left[ \frac{\partial}{\partial \tilde{r}} (\log_e U) \right]_{\perp} - \omega \tau K_{\perp} \cdot \left[ \frac{\frac{\partial}{\partial \tilde{r}} (\log_e U) \times \underline{B}}{B_0} \right] \dots (1.18)$$

Application of Compton-Getting effect (1935) to the cosmic ray flux due to streaming velocity  $\underline{u}$  (equations 1.17 and 1.18), gives the anisotropy of cosmic ray flux. In the limit when  $\tau$ , the time interval of collision between the particles and the field irregularities becomes infinity,  $K_{\parallel}$  becomes infinity, and the field parallel inward diffusion can exactly counter balance the convection component  $V_{s\parallel}$  giving uniform particle density along the field lines. Also, in this case,  $u_{\perp}$  is zero if  $V_{s\perp}$ , the electric drift in Ahluwalia and Dessler's model is balanced by a field perpendicular density gradient  $\left[ \frac{\partial U}{\partial \tilde{r}} \right]_{\perp} = 3 \frac{e U E}{mc^2}$  and is equivalent to the point raised by Stern (1964). Thus the Parker's model (1964) and Axford's model (1965) of cosmic ray propagation lead to similar results.

The basic equations of Axford (1965) have been modified by Gleeson (1969) and Forman and Gleeson (1970) by rigorous calculation of the collision term (Equation 1.6, term on r.h.s.) for individual energy intervals, which inherently includes the Compton-Getting effect, and the cosmic ray streaming vectors  $\tilde{S}(r, T)$  is then expressed as

$$\tilde{S}(r, T) = CUV_{\tilde{s}} - K_{\parallel} \left[ \frac{\partial U}{\partial r} \right]_{\parallel} - K_{\perp} \left[ \frac{\partial U}{\partial r} \right]_{\perp} - \frac{v^2}{3\omega} \frac{(\omega\tau)^2}{[1+(\omega\tau)^2]} \left[ \frac{\frac{\partial U}{\partial r} \times \tilde{B}}{\tilde{B}} \right] \dots (1.19)$$

or equivalently

$$\begin{aligned} \tilde{S}(r, T) = CUV_{\tilde{s}_{\parallel}} - K_{\parallel} \left[ \frac{\partial U}{\partial r} \right]_{\parallel} - K_{\perp} \left[ \frac{\partial U}{\partial r} \right]_{\perp} - \frac{v^2}{3\omega} \frac{(\omega\tau)^2}{[1+(\omega\tau)^2]} \left[ \frac{\frac{\partial U}{\partial r} \times \tilde{B}}{\tilde{B}} \right] \\ + \frac{CU}{B^2} \left[ \frac{\tilde{E} \times \tilde{B}}{\tilde{B}} \right] \dots (1.20) \end{aligned}$$

where  $T$  is the kinetic energy of the particles,  $C$  the Compton-Getting factor,  $U$  the particle density,  $\left[ \frac{\partial U}{\partial r} \right]_{\parallel}$

and  $\left[ \frac{\partial U}{\partial r} \right]_{\perp}$  the cosmic ray particle density gradients

parallel and perpendicular to the interplanetary magnetic field  $\tilde{B}$  respectively,  $K_{\parallel}$  and  $K_{\perp}$  the corresponding diffusion coefficients which are functions of the particle rigidity  $P$ ,  $\tau$  the average collision time interval of the particles with field irregularities,  $\omega$  the gyrofrequency of the particles,  $\tilde{E}$  the induced electric field due to the magnetized solar wind plasma flowing with velocity  $V_{\tilde{s}}$  relative to the observer (Ahluwalia and Dessler, 1962) and  $V_{\tilde{s}_{\parallel}}$  is the component of the solar wind velocity parallel

to the magnetic field.

The term  $\tilde{C}UV_s$  denotes streaming due to convection by the solar wind.  $K_{\parallel} \left[ \frac{\partial U}{\partial r} \right]_{\parallel}$  and  $K_{\perp} \left[ \frac{\partial U}{\partial r} \right]_{\perp}$  are the streamings due to the particle density gradients parallel and perpendicular to the interplanetary magnetic field in the solar equatorial plane. The fourth term denotes the streaming in the solar equatorial plane resulting from the particle density gradient across the heliolatitudes and is normally negligible (Subramanian, 1971). In the second expression for the streaming (1.20) the last term corresponds to the streaming perpendicular to the magnetic field due to the electric drift (Ahluwalia and Dessler, 1962) and is obtained in the explicit form by resolving the radial convection term along and perpendicular to the interplanetary magnetic field.

It is to be noted that while  $K_{\parallel}$  is the isotropic diffusion coefficient given by  $K_{\parallel} = \frac{1}{3} v^2 \tau$  where  $v$  is the particle velocity and  $\tau$  the mean collision time,  $K_{\perp}$  is composed of two parts (Jokipii and Parker, 1969) given as,

$$K_{\perp} = \frac{K_{\parallel}}{[1 + (\omega \tau)^2]} + K'(\tilde{B}, \tilde{r}, t) \quad \dots (1.21)$$

where  $t$  denotes time. The first term represents field perpendicular diffusion due to resonant scattering while the second term is the contribution due to the random walk of the field lines (figure 1.4).

The diffusion coefficients  $K_{\parallel}$  and  $K_{\perp}$  are derived from the interplanetary magnetic field measurements from satellites. The interplanetary magnetic field is a function of space and time, and present satellite measurements are not able to provide the complete information about it. The magnetic field data consists of a mean value over an ensemble taken over a certain time at the location of the satellite. Let the averages over an ensemble of identical systems be denoted by the symbol  $\langle \rangle$ . If  $B_i(\underline{r}, t)$  is the magnetic field vector at  $i^{\text{th}}$  point in the space, the correlation functions

$$R_{ij \dots k}(\underline{r}_1, t_1; \underline{r}_2, t_2; \dots \underline{r}_n, t_n) = B_i(\underline{r}_1, t_1) \cdot B_j(\underline{r}_2, t_2) \dots B_k(\underline{r}_n, t_n) \dots (1.22)$$

for all values of  $n$ , as a function of  $\underline{r}_1, t_1; \underline{r}_2, t_2; \dots \underline{r}_n, t_n$ ; describe the interplanetary magnetic field (Jokipii, 1971). In this notation,  $\langle B_i(\underline{r}, t) \rangle$  denotes the average magnetic field. Now define the fluctuating part of the magnetic field as

$$B_{1i}(\underline{r}, t) = B(\underline{r}, t) - \langle B \rangle \dots (1.23)$$

Then the two point correlation of  $B_{1i}$  is

$$\langle B_{1i}(\underline{r}_1, t_1) \cdot B_{1j}(\underline{r}_2, t_2) \rangle = R_{ij}(\underline{r}_1, t_1, \underline{r}_2, t_2) \dots (1.24)$$

Using the power spectrum of the interplanetary magnetic field irregularities derived from such correlation functions, the field parallel diffusion coefficient for particles of

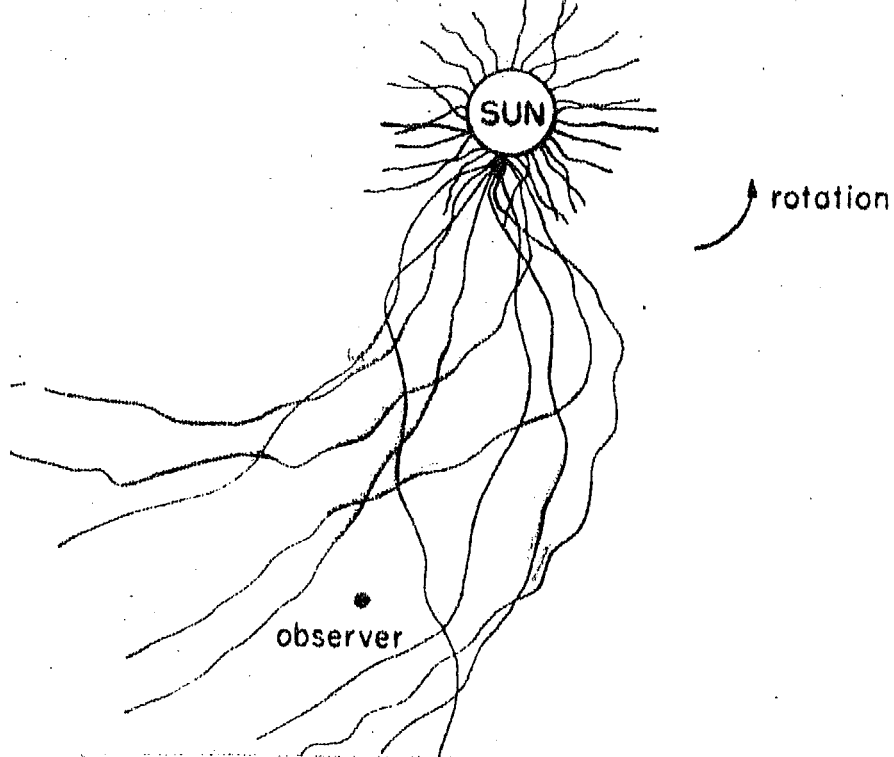
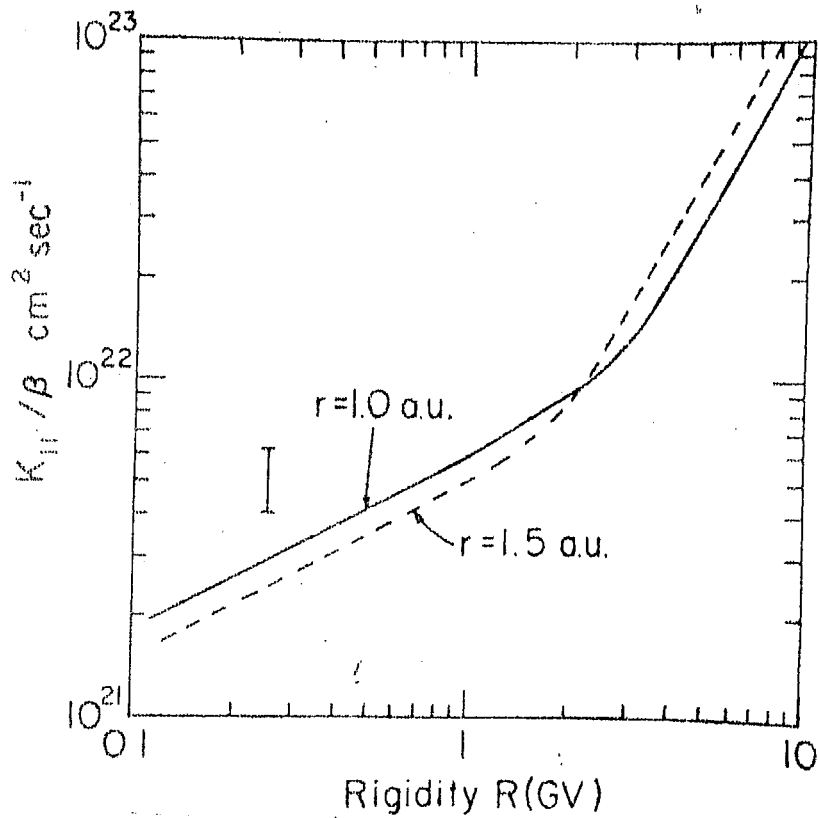


Figure 1.4 Schematic illustration of the random walk of magnetic field lines in the interplanetary space (Jokipii and Parker, 1969).





rigidity  $P < 1$  GV is obtained as

$$K_{\parallel} \simeq 5 \times 10^{21} P^{\frac{1}{2}} \beta \text{ cm}^2 \text{ sec}^{-1} \quad \dots(1.25)$$

where  $P$  is the particle rigidity and  $\beta = v/c$ . At higher rigidities, the expression becomes

$$K_{\parallel} \simeq 1.5 \times 10^{21} P \beta \text{ cm}^2 \text{ sec}^{-1} \quad \dots(1.26)$$

The dependence of  $K_{\parallel}$  on rigidity is shown in figure 1.5.

The field perpendicular diffusion coefficient  $K_{\perp}$  for rigidities below 1 GV, may be expressed in the form

$$K_{\perp} \simeq 2 \times 10^{21} \beta \text{ cm}^2 \text{ sec}^{-1} \quad \dots(1.27)$$

At higher rigidities  $K_{\perp}$  remains the same within a factor of 2. From the above equations (1.26) and (1.27) it turns out that  $K_{\perp}$  is not as small as was thought previously

[ $K_{\perp} / K_{\parallel} \simeq .01$ , Parker, 1964; Axford, 1965]. Typically the ratio  $K_{\perp} / K_{\parallel}$  is  $\simeq 0.15$  at 5 GV (Jokipii and Coleman, 1968).

The upper limit on the rigidity of the cosmic ray particles which undergo solar modulation through scattering by irregularities in the interplanetary magnetic field results from the sector structure of the interplanetary magnetic field shown in figure 1.1. In the average field of  $\simeq 5$  gamma at the orbit of the earth, particles of rigidity  $\simeq 100$  GV have gyroradii comparable to the sector width at the earth's orbit. So, beyond  $\simeq 100$  GV, the interplanetary magnetic field is not able to affect cosmic rays near the earth (Ahluwalia and Dessler, 1962).

#### I.4. Time variations in the cosmic ray intensity

Time variations in the cosmic ray intensity resulting from the cosmic ray particle interaction with the interplanetary magnetic field irregularities, fall into two categories: periodic and nonperiodic. Among the periodic variations are (1) the eleven year variation (2) the 27 day variation (3) the diurnal variation and (4) the semidiurnal variation. The Forbush decreases and the solar flare increases are the nonperiodic variations observed in the cosmic ray intensity. A summary of all these time variations in the cosmic ray intensity is given below:

##### I.4. a) Eleven year variation:

The cosmic ray intensity undergoes an eleven year variation in antiphase with the solar activity with a lag of a few months (Forbush, 1958). In a high latitude neutron monitor, the variation has an amplitude of 20%. Figure 1.6 shows the yearly normalized cosmic ray flux measured by ionization chambers from 1937 to 1957 and by neutron monitors at Deep River and Ottawa from 1958 to 1970 (Forbush, 1958; Rao, 1972). In the same figure is also shown the yearly mean Zurich sunspot number. The anticorrelation between the solar activity and the cosmic ray intensity is obvious. Use of sunspot number as a parameter of solar activity yields a lag of 6-9 months between the maximum in the cosmic ray intensity and the minimum in the solar activity.

This gives the radius of the modulating region to be about 100 AU. However, taking the intensity of the green coronal emission line at  $5303 \text{ \AA}^0$  as the index of the solar activity, the lag is found to be only one month yielding a value  $\approx 7$  AU for the radius of the modulating region (Pathak and Sarabhai, 1970; Simpson and Wang, 1970). The geomagnetic index  $K_p$  representing the solar activity also yields a value of  $\approx 7$  AU for the radius of the modulating region (Rao, 1972). Burlaga (1967) and Jokipii (1971) have arrived at a value of 3-5 AU regarding the dimensions of the modulation region from the study of decay curve of solar cosmic rays.

The interplanetary parameters determining the eleven year modulation of the cosmic ray intensity can be obtained from the equation (1.19) of the streaming of the cosmic ray gas. In the first case, assuming the scattering to be isotropic and the contribution due to  $\left[ \frac{\partial U}{\partial r} \times B \right]$  term negligible, the streaming equation can be written as

$$S(r, T) = CU V_s - K \left[ \frac{\partial U}{\partial r} \right] \quad \dots(1.28)$$

Further, the average radial streaming is zero, since the sun is neither a permanent source nor a sink of cosmic rays. Resolving the terms in the equation along the radial direction, we have,

$$CU V_s - K \left[ \frac{\partial U}{\partial r} \right] = 0 \quad \dots(1.29)$$

$$\text{i.e. } \frac{dU}{U} = \frac{C V_s}{K} dr \quad \dots(1.30)$$

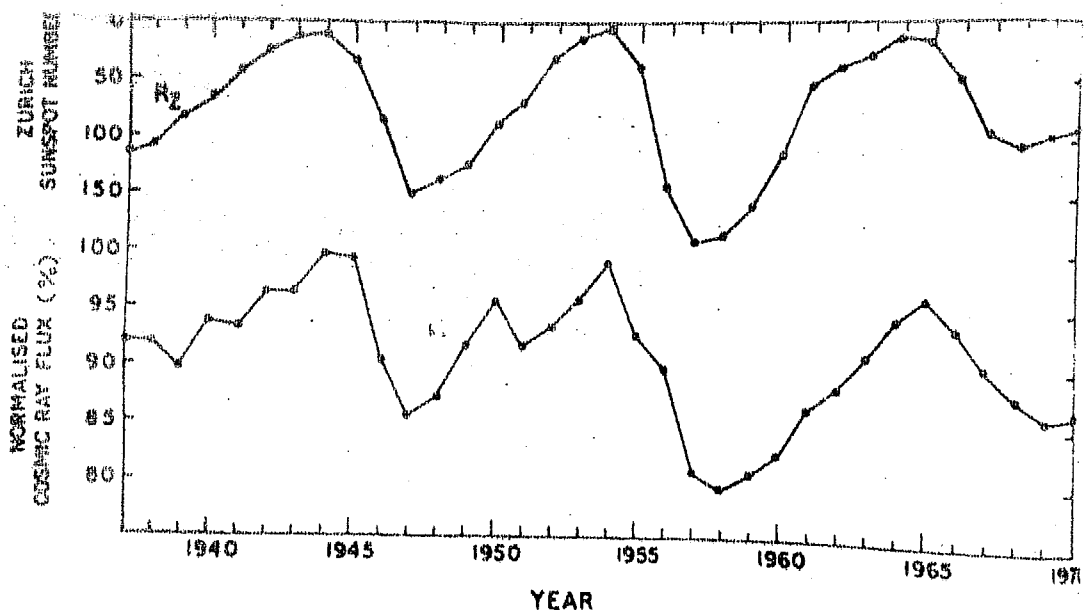


Figure 1.6 Eleven year variation in the cosmic ray intensity from 1937-1970. The figure also shows the eleven year variation in the Zurich sunspot number for the same period.

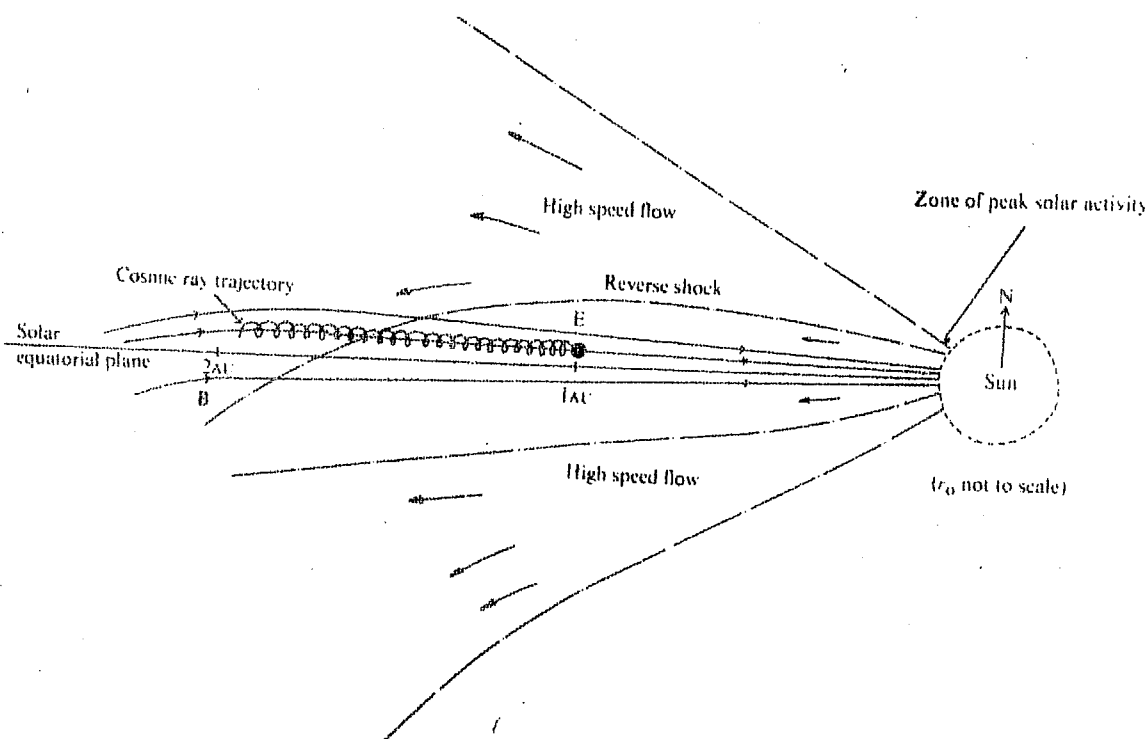


Figure 1.7 Schematic representation of possible plasma flow configuration in a solar meridian plane to explain the observed lack of long term anticorrelation between the solar wind velocity and the cosmic ray intensity (Hedgecock et al., 1972).

Integrating the equation from  $r = 0$  at the sun, to the boundary of the modulation region at  $r = R$ , the cosmic ray particle density at any point  $r$  inside the modulation region is given as

$$U = U_0 \cdot \exp \left[ - \frac{C V_s}{K} \cdot (R - r) \right] \quad \dots (1.31)$$

where  $U_0$  is the interstellar cosmic ray particle density beyond  $r = R$ .

In the case of anisotropic scattering, equation (1.31) gets modified by the inclusion of a heliolatitudinal dependence in the cosmic ray particle density. In the extreme case when field perpendicular diffusion is zero, the expression for the particle density is

$$U = U_0 \cdot \exp \left[ - \frac{C V_s}{K_{\parallel}} (R-r) \left\{ 1 + \frac{1}{3} \left[ \frac{\Omega \sin \theta}{V_s} \right]^2 (R^2 + rR + r^2) \right\} \right] \dots (1.32)$$

where  $\Omega$  is the angular velocity of the sun,  $K_{\parallel}$  the field parallel diffusion coefficient and  $\theta$  the co-heliolatitude.

Equations (1.31, 1.32) indicate that the cosmic ray particle density at a distance  $r$  from the sun, would increase with reduction in the solar wind velocity  $V_s$ , reduction in the modulation depth  $R$  or with an increase in the diffusion coefficient  $K$ . The observed eleven year modulation of cosmic ray intensity in antiphase with solar activity therefore indicates, that either solar wind velocity  $V_s$  or the diffusion coefficient  $K$  or the radius of the modulation boundary  $R$  should show a corresponding variation with a periodicity of eleven years. Pathak and

Sarabhai (1970) have indicated that R and K vary over a solar cycle as

$$R = \text{const.} + \frac{r}{K} \dots (1.33)$$

where  $r = 1$  AU. The diffusion coefficient K may vary significantly at certain times (Jokipii, 1971). However, a systematic variation in either K or R, required by eleven year modulation of cosmic rays, is not observed (Mathews et al., 1971a). The solar wind velocity measurements by satellite detectors (Mathews et al., 1971a; and Hedgecock et al., 1972), show that the velocity did not change significantly over the years 1962-1972. The above authors have attributed the lack of anticorrelation in the cosmic ray intensity with solar wind velocity to the off ecliptic modulation of cosmic rays. The mechanism proposed by them is indicated in figure 1.7, showing the possible plasma flow configuration in a solar meridian plane with a greater number of high speed streams from activity centres north and south of the solar equator, squeezing the low latitude flow. However, the northern activity has dominated over the southern one during the present solar cycle, which bends the whole plasma flow pattern towards south at low latitudes beyond the earth's orbit. The transition of the flow in the latitudes may either be gradual or a reverse hydromagnetic shock may be produced at times as indicated in the figure. Cosmic rays arriving near zero degrees heliolatitude, must spend much time in the northern high

speed flow region. This might result in the observed modulation of cosmic ray intensity even though the solar wind velocity has not varied much near the earth.

In the section I.3 (page 21) it was mentioned that the diffusion coefficients  $K_{\parallel}$  and  $K_{\perp}$  are functions of particle rigidity  $P$ . So, the fractional 11 year modulation  $\frac{\Delta U}{U}$  will be different at different rigidities. The average form of the variational spectrum of eleven year modulation of cosmic ray intensity above 2 GV is  $P^{-1}$  or  $\sim k/\beta P$  where  $\beta = v/c$  (O'Gallagher and Simpson, 1967; Hatton et al., 1968; Lockwood and Webber, 1968; Ormes and Webber, 1968). However, values of the spectral exponent ranging from -0.5 to -2.0 have been quoted at different phases of the 11 year cycle [Stozhkov and Charakhchyan, 1968; Stoker et al., 1971; Kane, 1972]. Recently, Carmichael and Stoker (1970), Stoker and Carmichael (1971) and Carmichael and Katzman (1971) have pin-pointed at least four occasions during the period (1966-1970) when there were sudden long lasting step-like alterations in the spectral form of the eleven year modulation. Kane (1972) has suggested that these step-like changes in the spectral exponent may be associated with sudden changes in the radius of the modulation region.

The eleven year modulation shows a broad peak at rigidities around 2 GV. While the modulation is same for all particles of a given rigidity above 2 GV, Webber (1969)

concludes that the peak modulation occurs at  $\approx 0.5$  GV for electrons, at  $\approx 1$  GV for protons and  $\approx 2$  GV for alpha particles and heavies. The charge dependence at low rigidities is consistent with the energy loss of the particles due to deceleration in diffusion against the solar wind (Gleeson and Axford, 1968 and Gleeson, 1971).

#### I.4 b) Forbush decreases:

Forbush decreases in the cosmic ray intensity are identified as world wide depressions in the intensity occurring in a period of a few hours to a day or two, followed by gradual recovery lasting from a few days to months. A typical Forbush decrease profile is shown in figure 1.8. The experimental observations and the derived theoretical models of Forbush decreases have been recently reviewed by Lockwood (1971).

Basically there have been two types of models for explaining Forbush decreases: 1) Magnetic tongue or bottle model, and 2) Blast-wave model.

The first theoretical model to explain a Forbush decrease on the basis of ordered magnetic field structure was the magnetic tongue model of Dorman (1957) and Gold (1959) shown in figure 1.9a. The magnetic field lines in the expanding cloud of high density plasma, emanating from a solar flare, are stretched in the form of an ordered loop structure. The cloud starts from an active region on the sun with zero cosmic ray intensity inside. As it expands



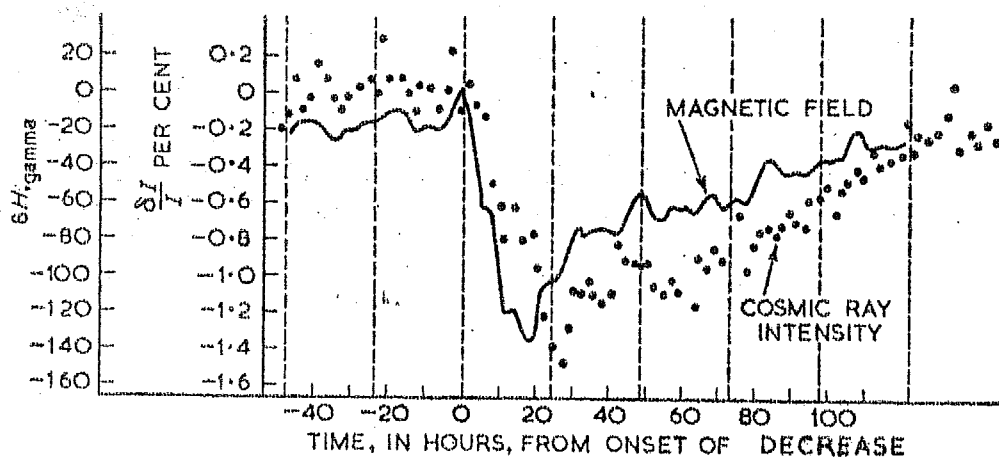


Figure 1.8 Average Forbush decrease profile showing the fast decrease and the slow recovery in the cosmic ray intensity (Derman, 1957). The figure also shows simultaneous variation in geomagnetic field.

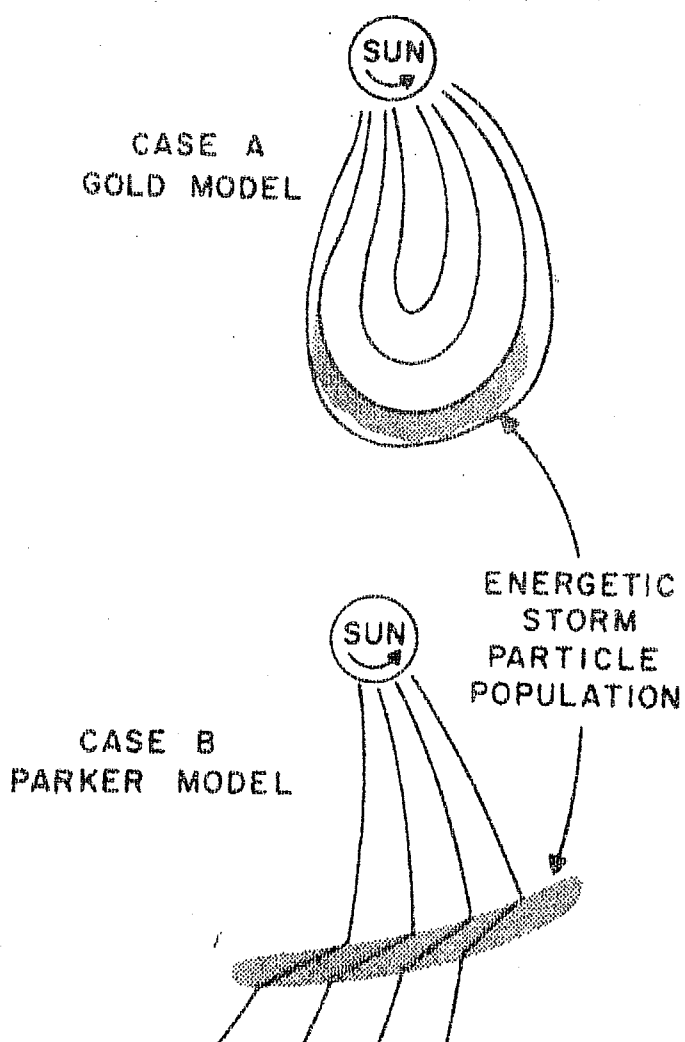


Figure 1.9a,b Schematic representation of the Gold's bottle model and Parker's blastwave model to explain a Forbush decrease.

due to enhanced solar wind behind it, cosmic ray particles start diffusing in, from all directions. As this magnetic bottle engulfs the earth, a cosmic ray detector starts sampling the cosmic ray flux inside the bottle and registers a sudden decrease in the intensity. The intensity inside the bottle is, however, continuously being replenished by diffusion of particles from outside and the intensity recovers to its value outside the bottle in the course of a few days or longer.

In the other model proposed by Parker (1961, 1963) shown in figure 1.9b, the dense magnetic fields in the blast-wave moving ahead of the fast plasma from a solar flare, sweep out the cosmic ray particles and cause a transient decrease in the cosmic ray intensity. The cosmic ray intensity recovers in the region behind the shock wave in the course of a few days due to diffusion from sides. The envisaged shock thickness is of the order of 0.05 - 0.1 AU. In the next more realistic model, Parker (1963) also includes the motion of <sup>magnetic field</sup> irregularities due to outward convection, in determining the cosmic ray density changes.

In another interesting model of Forbush decreases, Laster et al. (1962) have evaluated the energy loss of cosmic rays trapped in an expanding cloud of disordered magnetic fields, as they collide with the outward moving field irregularities. The energy loss process referred to as 'diffusive deceleration' is essentially an 'Inverse

Fermi acceleration' mechanism. The mechanism leads to a rigidity spectrum of the form  $P^{-1}$  for a Forbush decrease. The spectral value is close to the one observed experimentally, although experimental values indicate a large spread as is discussed later (page 34).

It may be noted that all the models of the Forbush decrease lead to a gradual recovery of the intensity within about a weeks time. At present there is no established model to explain some of the Forbush decreases with recovery periods of weeks or months in length. Roelof (1971) has studied the cosmic ray intensity during the nearly  $3\frac{1}{2}$  months recovery period of Forbush decrease of June 8, 1969 and reports that the nearly rigidity independent modulation during this period can be explained if the scattering mean free path of cosmic rays were rigidity independent in the range 1-15 GV during this period.

The detailed characteristics of the Forbush decreases and the associated geomagnetic phenomena have been investigated by various authors since the last two decades. Lockwood (1958) and Bachelet et al.(1960) have shown that the onset of a typical Forbush decrease is preceded by a worldwide geomagnetic storm by about 1-6 hours. Further, the difference in the onset times at different stations (different longitudes) have been studied by Fenton et al. (1959) Lockwood and Razdan (1963), Ables et al.(1967), Mercer and Wilson (1968) and Dorman (1969). They

conclude that the onset is earliest along a direction  $30^{\circ}\text{W}$  to  $50^{\circ}\text{W}$  of the earth-sun line. Fenton et al., (1959), Lockwood and Razdan (1963) and Mathews et al. (1968) have further reported instances when the onset of a Forbush decrease was observed along the garden hose direction even before the sudden commencement (SC) of geomagnetic storm. This is explained to be due to reconnection of the magnetic field lines inside the cloud with the region outside, which allows an early sampling of the particles at earth from the inner regions of the plasma cloud (McCracken, 1962; Lockwood and Razdan, 1963). This anisotropic depression along the garden hose direction vanishes when the earth is completely immersed in the plasma cloud. In addition to this, about one third of the Forbush decreases are accompanied by north-south anisotropies perpendicular to the solar equatorial plane (Duggal and Pomerantz, 1970). The north-south anisotropy indicates temporary differences in modulation process in north and south directions arising probably because of solar flares occurring at higher latitudes on the solar disc, causing enhanced plasma-flow at an angle to the solar equatorial plane.

Many of the Forbush decreases are preceded by short lived universal time increases upto a few percent, during the 12 hour period just before the onset. The amplitude of the preincrease is higher in a direction between the sunward and the garden hose direction. Dorman (1963)

has explained it as an extra flux due to reflection of cosmic ray particles from the approaching shockfront of the plasma cloud (albedo mechanism). However, Lockwood (1971) has put a word of caution in estimating the amount of pre-increase particularly in view of the enhanced diurnal variation during such periods due to the presence of large anisotropies.

The recovery phases of many of the Forbush decreases are characterized by short lived enhancements and/or long lived anisotropies both in the equatorial plane and/or in north-south direction. The sudden universal time enhancements of a few percent for a few hours during or just after the decrease phase, are attributed to a reduction in primary cutoff rigidity of a station following a geomagnetic storm (Dorman 1963, 1969; Yoshida et al., 1968). The enhancement is maximum for neutron monitors having cutoff-rigidity 4-5 GV, while as it is negligible at stations with cutoff-rigidity below the atmospheric cutoff (1.4 GV). There is, however, at least one instance of a Forbush decrease (August 4, 1972) when the sudden universal time enhancement in the cosmic ray intensity just after the decrease phase (post-increase) cannot be attributed to a reduction in cutoff rigidity. The detailed analysis of this sudden universal time enhancement along-with spatial anisotropies prior, during and after the Forbush decrease, have been reported by the author (Agrawal et al., 1973). The post increase is

explained to be due to 'pile up' of cosmic ray particles just behind the interplanetary shock causing the large and very fast decrease ( $\approx 6\%$  per hour) in the intensity. The pile up results from the diffusion of the particles from higher heliolatitudes into the cavity behind the shock and the simultaneous radially outward convection inside the cavity.

The rigidity dependence of Forbush decreases has been studied by many authors. But it is still in a controversial state. Webber (1962) finds the spectrum to be of the form  $P^{-m}$  with  $m$  between 0.5 to 1.0. McDonald and Webber (1960), Lockwood (1960), Nerurkar and Webber (1964), Rao (1965), Balsubrahmanyam and Venkatesan (1969) and Mathews et al. (1971) find that the rigidity dependence is the same as that of the eleven year variation with  $m \approx 1.0$ . On the other hand, McCracken (1960), Kane (1966), Lockwood and Webber (1969), Kane and Winckler (1969), Lockwood et al. (1970) and Lockwood (1971) report a smaller rigidity dependence. It is, of course, extremely important to resolve this point, since it will have significant implications on the Forbush decrease mechanism.

#### I.4 c) Diurnal variation:

The average diurnal variation in the cosmic ray intensity observed in the ground based neutron monitors has an amplitude  $\approx 0.4\%$  in the solar equatorial plane in the interplanetary space with maximum along the 18 hour direction as shown in figure 1.10. (Bercovitch, 1963 and Rao et al., 1963).

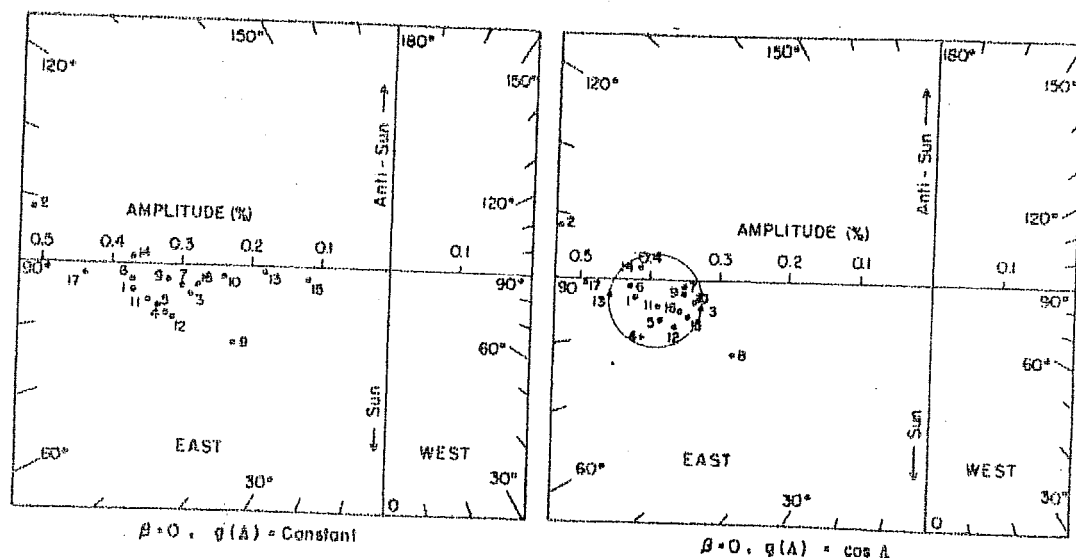


Figure 1.10 Vector diagram of diurnal anisotropy in the cosmic ray intensity in the interplanetary space during the year 1958 (Rao et al., 1963).

5608

The amplitude varies with the geographic latitude  $\lambda$  as  $\cos \lambda$  and is rigidity independent in the range 1-100 GV. The above estimate of diurnal amplitude in the interplanetary space from ground based monitors was made by the use of variational coefficients (discussed in section II.4) which include particles of rigidities upto 500 GV. However, from an improved calculation including the upper rigidity limit at  $\simeq 90$  GV, Subramanian (1971) has concluded that neutron monitors yield an average diurnal amplitude of  $\simeq 0.6\%$  in the interplanetary space, as is expected from the corotation concept described in this section later. Theoretical models of the average diurnal variation in the cosmic ray intensity have been put forward by Ahluwalia and Dessler (1962), Stern (1964), Parker (1964,1965), Axford (1965), Gleeson and Axford (1967), Gleeson (1969), Fisk and Axford (1970), and Forman and Gleeson (1970).

Ahluwalia and Dessler (1962) were the first to realize that as a result of the motion of interplanetary magnetic field lines in 15 hour direction, an observer on the earth experiences an  $\underline{E} \times \underline{B}$  drift of the particles in the 15 hour direction due to the electric field  $\underline{E}$  developed perpendicular to the solar equatorial plane. By the application of Compton-Getting effect (1935), this of course gives average direction of the diurnal anisotropy along 15 hour direction instead of the observed 13 hour direction. The above conclusion has been contradicted by Stern (1964)



on the grounds that in the conservative system with  $\partial B / \partial t = 0$ ,  $\underline{E} \times \underline{B}$  drift of the cosmic ray particles will be exactly cancelled by the resulting gradients of the particle density which produce streaming in the opposite direction (Liouville's theorem). This is followed by Parker's model (1964) of diurnal variation, who has taken into consideration, Stern's objection. He hypothesizes a smooth interplanetary spiral magnetic field between the sun and the earth, and an irregular field beyond. In this model, the density gradients, which would otherwise cancel the  $\underline{E} \times \underline{B}$  drift, would be wiped out by the irregularities beyond the earth's orbit. In addition to this, Parker has noted that the sun is neither a permanent source nor a sink of cosmic rays. So, he has postulated an inward diffusion of cosmic rays along the interplanetary magnetic field lines, which when combined with the  $\underline{E} \times \underline{B}$  drift along the 15 hour direction, results in the cosmic ray streaming along 18 hour direction on an average basis.

Essentially the same conclusion as above, has been arrived at by Axford (1965) by solving hydromagnetic equations of the cosmic rays gas in the interplanetary medium (Section I.3). Quenby (1965) has extended the work of Axford to the relativistic case whileas Gleeson (1969) and Forman and Gleeson (1970) have improved upon the basic equations of Axford for the study of diurnal variation. Gleeson has obtained a set of continuity and momentum

equations for cosmic rays in the interplanetary medium applying to small energy intervals, which incorporate improved expression for collision of cosmic ray particles with interplanetary magnetic field irregularities and inherently include terms due to the Compton-Getting effect. The expression of streaming of cosmic ray gas in the interplanetary medium due to Forman and Gleeson (1970) is already presented in section I.3 (equation 1.19). Excluding the small contribution to the streaming due to gradients perpendicular to the solar equatorial plane, the streaming may be expressed as

$$\underline{S}(\underline{r}, T) = CUV_s - K_{||} \left[ \frac{\partial U}{\partial \underline{r}} \right]_{||} - K_{\perp} \left[ \frac{\partial U}{\partial \underline{r}} \right]_{\perp} \quad \dots(1.34)$$

Resolving the streaming vector  $\underline{S}$  along and perpendicular to the radial direction, the corotation streaming along the azimuthal direction (18 hour) is given by

$$S_{\phi} = CUV_s \cdot \frac{(K_{||} - K_{\perp}) \sin \chi \cdot \cos \chi}{K_{||} \cdot \cos^2 \chi + K_{\perp} \cdot \sin^2 \chi} \quad \dots(1.35)$$

where  $\chi$  is the garden hose angle. Now the amplitude of anisotropy is given by (Gleeson, 1969; Forman and Gleeson, 1970) as,

$$\underline{r} = \frac{3 \underline{S}}{vU} \quad \dots(1.36)$$

where  $U$  is the particle density and  $v$  their velocity.

This gives

$$\underline{r} = 3 \frac{C V_s}{v} \cdot \frac{(K_{||} - K_{\perp}) \tan \chi}{[K_{||} + K_{\perp} \cdot \tan^2 \chi]} \quad \dots(1.37)$$

The expression gets simplified when  $K_{\parallel} \gg K_{\perp}$ . In this case

$$r = \frac{3 CV_s}{v} \tan \chi = \frac{3 CV_r}{v} \dots (1.38)$$

where  $V_r$  is the velocity of corotation.

At relativistic energies, the Compton-Getting term  $C$  is of the form  $C = \frac{1}{3} \left[ 2 - \frac{T}{U} \cdot \frac{\partial U}{\partial t} \right] \dots (1.39)$

where  $T$  is the kinetic energy of the particles. Further, if  $U(T) \sim T^{-\gamma}$  where  $\gamma$  is the exponent of the differential energy spectrum of cosmic rays, then

$$C = \frac{1}{3} (2 + \gamma) \dots (1.40)$$

So, the corotation anisotropy (equation 1.38) can be written as

$$r = \frac{3 CV_r}{v} = (2 + \gamma) \cdot \frac{V_r}{v}, \text{ when } K_{\parallel} \gg K_{\perp} \dots (1.41)$$

For a solar wind velocity of  $400 \text{ km sec}^{-1}$ , garden hose angle  $\chi = 45^\circ$  and the cosmic ray spectral exponent  $\gamma = 2.5$ , equation (1.41) yields the corotation anisotropy  $\simeq 0.6\%$ .

On individual days, corotation picture may not be necessarily true and one has to use the exact formula of streaming (1.19) to obtain the amplitude and phase of the anisotropy. However, the recent analyses of Hashim et al. (1971) and Rao et al. (1972) show that the diurnal variation on most of the days can be individually explained in terms of the radially outward convection and the inward diffusion of the cosmic ray particles along the interplanetary magnetic field lines.

## GALACTIC COSMIC RAYS

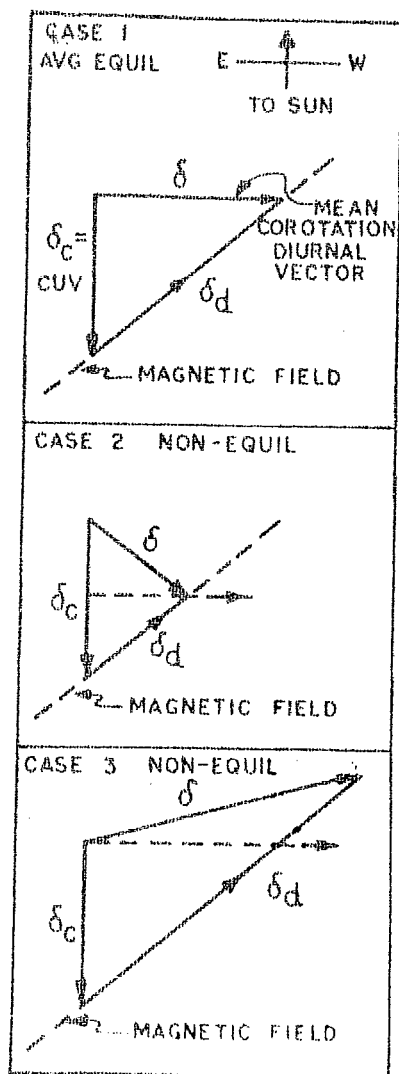


Figure 1.11 The convection-diffusion model to explain the diurnal anisotropy in the cosmic ray intensity on individual days (Rao et al., 1971a).

These authors have essentially extended the model of McCracken et al.(1971) for explaining anisotropies at various times during a solar flare increase and its decay in the energy range 10-50 MeV. The model is shown in figure 1.11. The total anisotropy is expressed as

$$\delta_{\sim} = \delta_{\sim c} + \delta_{\sim d} \quad \dots(1.42)$$

where  $\delta_c$  and  $\delta_d$  are convection and diffusion anisotropies respectively. It may be mentioned that Barnden (1973a,b) has developed a technique of studying the cosmic ray propagation in the interplanetary space by considering the region where the particle suffered its last collision before it came to the earth. The technique, known as "origin of scatter technique", though a very involved one, has been found by him to be useful in studying the diurnal and the semidiurnal variation in the cosmic ray intensity on individual days.

The behaviour of the diurnal anisotropy on individual days has been found to be complicated both in terms of amplitude as well as time of maximum. For example, during the years 1964-65, the diurnal variation has a component with maximum at 15 hours and a minimum at 09 hours in addition to the dominant average component with maximum at 18 hours (Patel et al.,1968). A few instances of large diurnal variation with maximum along the 21 hour direction, have been reported by Mathews et al.(1969) and Hashim and Thambyahpillai (1969). These have been attributed

essentially to a depression in the cosmic ray intensity along the garden hose direction rather than the streaming along the antigarden hose direction. An evidence of variability of the diurnal variation is reported by Duggal and Pomerantz (1962) showing a progressive rotation of the diurnal vector in the anticlockwise direction and completing a cycle of 24 hours over a period of about eight days. Another important class of diurnal variation is the one with maximum along the garden hose direction (Razdan and Bemalkhedkar, 1971, 1972) and is studied in detail in the present thesis.

The spectral index of the diurnal variation in the cosmic ray intensity on individual days shows large departures from its average value  $\simeq 0.0$  (Sarabhai and Subramanian, 1965). They have thus concluded that corotational theory is insufficient to account for the characteristics of the diurnal variation on individual days.

The amplitude and time of maximum of diurnal variation in the cosmic ray intensity is found to exhibit a long term variation too. The amplitude of the diurnal anisotropy is significantly lower during each of the sunspot minimum epoch as compared to that during periods of maximum solar activity (Duggal et al., 1967). Forbush (1967, 1969) and Duggal et al. (1970a, b) have indicated a 20-22 year periodicity in the diurnal anisotropy of cosmic rays from the ionization chamber measurements from 1937-67. Forbush

has shown that the amplitude of 20 year anisotropy in the diurnal variation oscillates around zero with direction of maximum changing from the antigarden hose to garden hose direction and vice versa. Thus the total diurnal anisotropy is composed of two parts (figure 1.12). One component is the corotation component directed along  $90^\circ$  east (18 hours) of the earth sun line, which is well correlated with the geomagnetic activity. It exhibits a solar cycle variation with minimum amplitude near sunspot minimum. In contrast to this, the other component varies sinusodially around zero with a periodicity of 20 years <sup>and</sup> has a mean amplitude in the interplanetary space greater by 40% than that of the corotation component. The direction of the second component lies along the Archimedian spiral. Rao (1972) has, however, concluded from neutron monitor data, that the diurnal anisotropy essentially remained constant over the last solar cycle and that the ion-chamber results mentioned above have to be taken with certain reservation due to uncertainties in the temperature correction for the meson component.

The diurnal variation in cosmic ray intensity has exhibited a strange behaviour in the year 1954. From, July to September 1954, the diurnal vector constantly pointed in 03 hour direction in the interplanetary space [Conforto and Simpson, 1957; Marsden and Begum, 1959; Venkatesan and Dattner, 1959; and Razdan, 1960] and has an amplitude  $\approx 0.39 \pm 0.03\%$  (Thomson, 1971). Pomerantz and Duggal (1971)

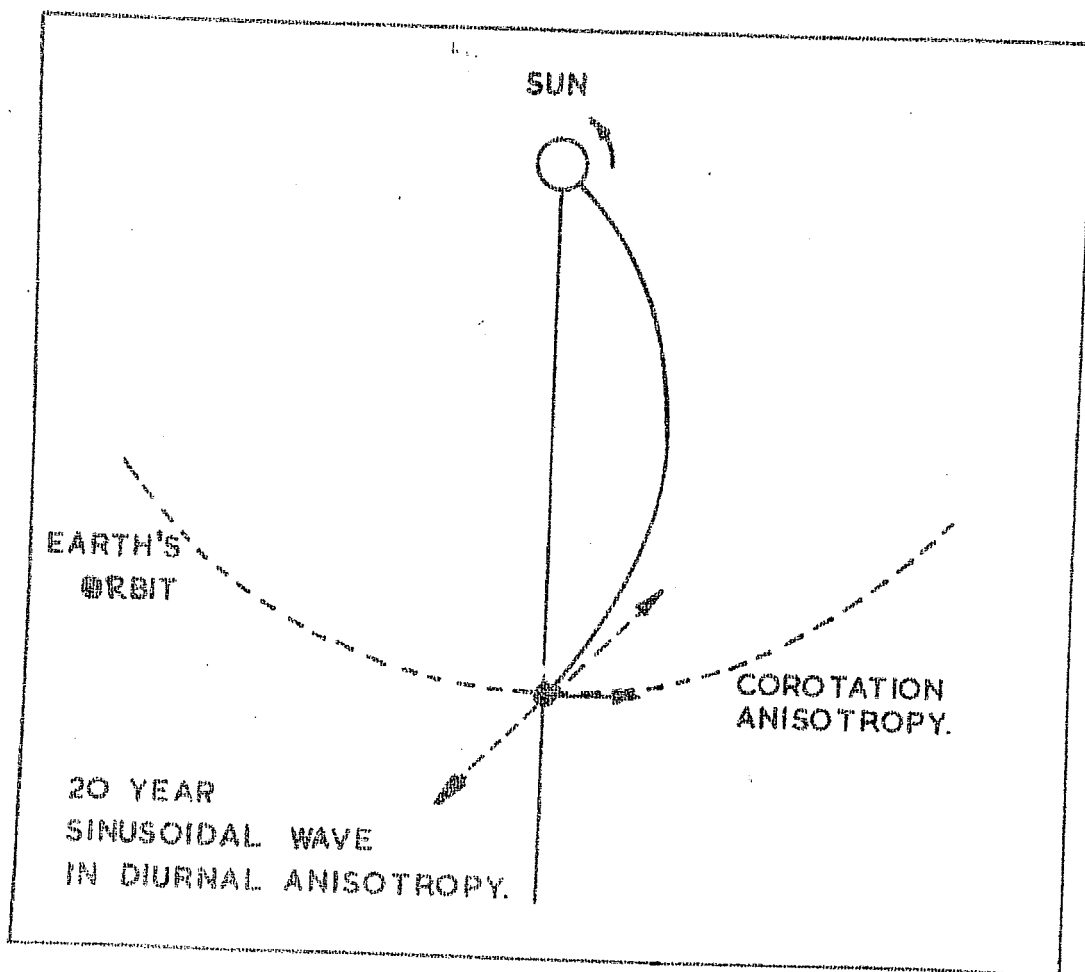


Figure 1.12 The diurnal anisotropy resolved into two components: 1) The corotation anisotropy pointing in the 13 hour direction in the interplanetary space and 2) The 20-22 year sinusoidal wave in the anisotropy pointing in the field aligned direction.



have suggested that during this period the 20 year component of diurnal variation (Forbush, 1967,1969) was at its peak and the anisotropy pointed in the garden hose direction. The resultant of 20 year component and the corotation component of diurnal variation in cosmic ray intensity produced the small diurnal anisotropy along the 03 hour direction. However, Thomson (1971) has attributed the 03 hour anisotropy in 1954 to large north-south gradients in particle density, and to a low value of the upper limiting rigidity  $\simeq 30$  GV of the modulation. Svalgaard (1968,1972), Friis - Christensen et al.(1971) and Wilcox (1972) have shown that during this period, the interplanetary magnetic field comprised of only one sector with field lines pointing away from the sun. So, a positive particle density gradient in the northern direction during this period has been postulated by Thomson (1972) to explain the prolonged period of the diurnal variation with maximum in the 03 hour direction.

#### I.4 d) Semidiurnal variation:

The existence of a semidiurnal wave in the cosmic ray intensity was pointed out by Nicolson and Sarabhai (1948), Elliot and Dolber (1950,51), Elliot (1952) and Forbush and Venkatesan (1960). A number of workers have studied its characteristics (see Pomerantz and Duggal, 1971). It emerges that around 10 GV, the amplitude of the semidiurnal anisotropy in the interplanetary medium is  $\simeq 0.1\%$  with phase  $\simeq 135^\circ$  west of the earth sun line. The amplitude of the

anisotropy has a rigidity dependence  $\sim P^{+1}$  upto about 100 GV. Beyond  $\approx 100$  GV, the anisotropy is zero. The semidiurnal anisotropy shows  $\cos^2 \lambda$  dependence where  $\lambda$  is the geographic latitude. The phase of the semidiurnal anisotropy has remained essentially constant over the last solar cycle. However, the amplitude has varied considerably as in the case of diurnal variation.

Sarabhai and Subramanian (1966) and Lietti and Quenby (1968) have proposed two alternative causes for semidiurnal variation in the cosmic ray intensity: 1) Symmetrical density gradient of cosmic rays across heliolatitudes and 2) the pitch angle distribution of cosmic rays. In the case of heliolatitudinal density gradients, the gyrocentres of the particles reaching earth lie at higher heliolatitudes having larger cosmic ray particle density and produce the semidiurnal anisotropy with maximum along 03 hour and 15 hour directions respectively. In the pitch angle distribution hypothesis, the cosmic ray intensity distribution around the magnetic field line has a maximum in a plane perpendicular to the field line. However, when projected in the equatorial plane, this also gives rise to a semidiurnal variation in the intensity. The observations of the semidiurnal variation and other cosmic ray intensity variations do not indicate whether either or both of the above mechanisms are operative.

Subramanian (1971) has looked for the heliolatitudinal density gradient in the cosmic ray particle density, as required by the earlier estimation of the diurnal anisotropy  $\simeq 0.4\%$  (Bercovitch, 1963; Rao et al., 1963) compared to the anisotropy  $\simeq 0.6\%$  predicted by the corotation theory. The revised value of the diurnal anisotropy (Subramanian, 1971), however, concurs with the one predicted by the corotation theory thereby precluding any such heliolatitudinal density gradients. A change of  $\simeq 15^\circ$  in the heliolatitude of the earth during an year, would further produce an annual variation  $\simeq 1\%$  in the mean intensity of earth-bound neutron monitors at high latitudes, at least in the interplanetary magnetic field sectors of same polarity (Gleeson, 1969). Such a variation in the intensity has not been reported so far. Nagashima et al. (1971) have pointed out that the semidiurnal anisotropy due to heliolatitudinal density gradients, if any, will have zero component perpendicular to the solar equatorial plane, while the pitch angle anisotropy will still be present in that plane. From the spherical harmonics of the anisotropy resulting from the inclination of the earth's rotation axis and the ecliptic north pole, they have concluded that, semidiurnal variation in the cosmic ray intensity can be explained by the pitch angle distribution of the cosmic rays.

Recently Barnden (1973b), using the 'Origin of Scatter' technique, has attributed semidiurnal variation to the asymmetrical daily variation of cosmic ray intensity having

deeper minimum (relative to equidistant intermediate levels) than its maximum. The asymmetrical daily variation occurs due to nonlinearity in  $U(r)$  the cosmic ray number density at a distance  $r$  from the sun and  $\mathcal{L}(r)$  the fraction of the particle flux arriving at the earth from a given direction, which was last-scattered in the volume element at  $r$  when  $U(r) = 1.0$ . The non-linearity of  $U(r)$  and  $\mathcal{L}(r)$  results from the radial dependence of the diffusion coefficient and the converging nature of the interplanetary magnetic field. The model also predicts a positive spectral exponent for the semidiurnal variation.

#### I. 4 c) 27 day variation:

27 day recurrent changes in the cosmic ray intensity manifest themselves as small isotropic decreases without any obvious correlation with solar flares but are closely correlated with recurrent (M-region) geomagnetic storms. It was shown by Simpson et al. (1953) and Simpson (1954) that these changes are not produced by the geomagnetic disturbances but are of solar origin and are associated with central meridian passage (CMP) of active coronal regions and unipolar magnetic (UM) regions on the solar disc. The 27 day recurrent decrease is a quasi-permanent phenomenon found to last even upto 18 solar rotations and shows close correlation with enhanced 5303 Å<sup>0</sup> emission from the solar active regions (Mori et al., 1964 and Pathak, 1969).

The rigidity dependence of the 27 day variation is seen to be similar to that of Forbush decreases although in general the percent decrease in the intensity is smaller (Fonger, 1953; Lockwood, 1960; Webber, 1962; and Bukata et al. 1968). In fact it is difficult to distinguish small recurrent Forbush decreases from 27 day variation. In this context it is important to note that Ballif and Jones (1969) Antonucci et al. (1971), Ballif et al. (1971), McDonald and Desai (1971) and Bemalkhedkar et al. (1973) conclude that almost all Forbush decreases are associated with 27 day recurrent solar, corotating, corpuscular streams emanating from active regions on the solar disc. Verschell et al. (1973) have classified Forbush decreases in two categories: 1) Forbush decreases associated with solar flares and 2) Forbush decreases associated with corotating 27 day recurrent solar streams emanating from either the solar active regions or from the coronal magnetic holes, discussed by Krieger et al. (1973). On the other hand, from Forbush decreases  $> 4\%$  in high latitude neutron monitors for the year 1966-72 and multiple spacecraft observations of interplanetary magnetic field, Barnden (1973c) finds that all the Forbush decreases  $> 4\%$  are associated with shock waves from solar flares. It is not clear at present whether the Forbush decreases can be attributed solely to the 27 day recurrent solar corotating streams or to transient plasma clouds and/or shock waves from solar flares. Probably both exist in

the sun-earth region simultaneously and interact in a complicated manner to cause the Forbush decrease.

#### I. 4 f) Solar flare increases:

A typical solar flare increase in ground based neutron monitor shows a simple time profile having a rapid rise to a maximum intensity within a few hours followed by a slow exponential decay phase lasting upto a few days. The increase in intensity in a high latitude neutron monitor may vary from a few percent to a few hundreds of percent. The increase in intensity of low energy particles measured by satellite detectors, can reach a value of a few thousands of percent. Figure 1.13 shows examples of such increases in the ground based neutron monitors and in the satellite detectors in the interplanetary space. The solar cosmic rays contain ions of charge  $1 \leq Z \leq 26$  as well as electrons. Rigidities of these, normally do not exceed a few GeV. The energy spectrum of the solar particles is normally very steep. The power law exponent  $\gamma$  of the energy spectrum lies in the range -12 to -40 for protons and -27 to -61 for  $\alpha$  particles and heavies (Biswas et al., 1962 a,b; 1963; Fichtel and Guss, 1961 and Biswas and Fichtel, 1964, 1965).

Injection of the flare particles in the solar system takes place within about  $\pm 1$  minute of the optical flash of the solar flare and is accompanied by X-ray and radio bursts.

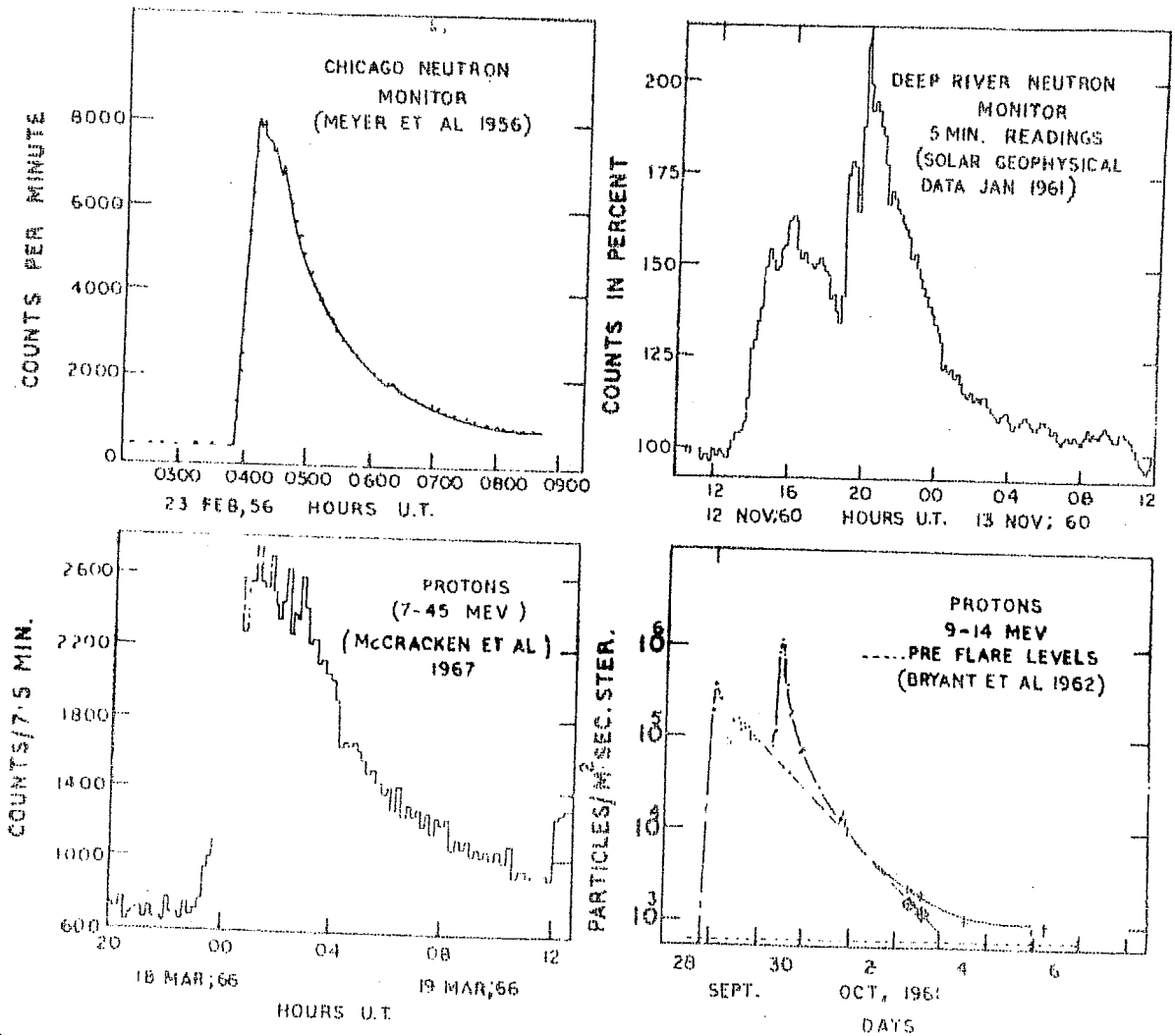


Figure 1.13 Typical profile of solar flare increases in the ground based neutron monitor as well as in the low energy proton detectors aboard space-crafts.

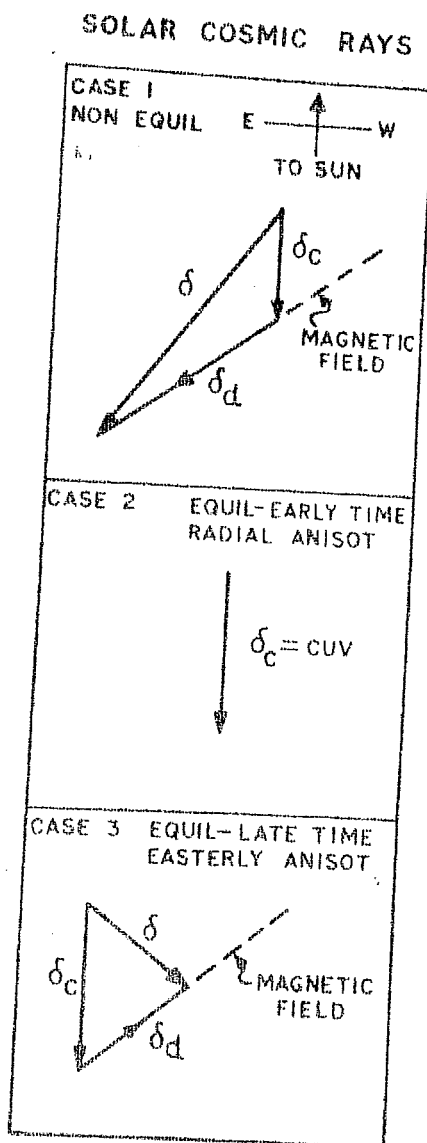


Figure 1.14 The convection diffusion model to explain the propagation of solar cosmic rays in the interplanetary medium (McCracken et al., 1971).



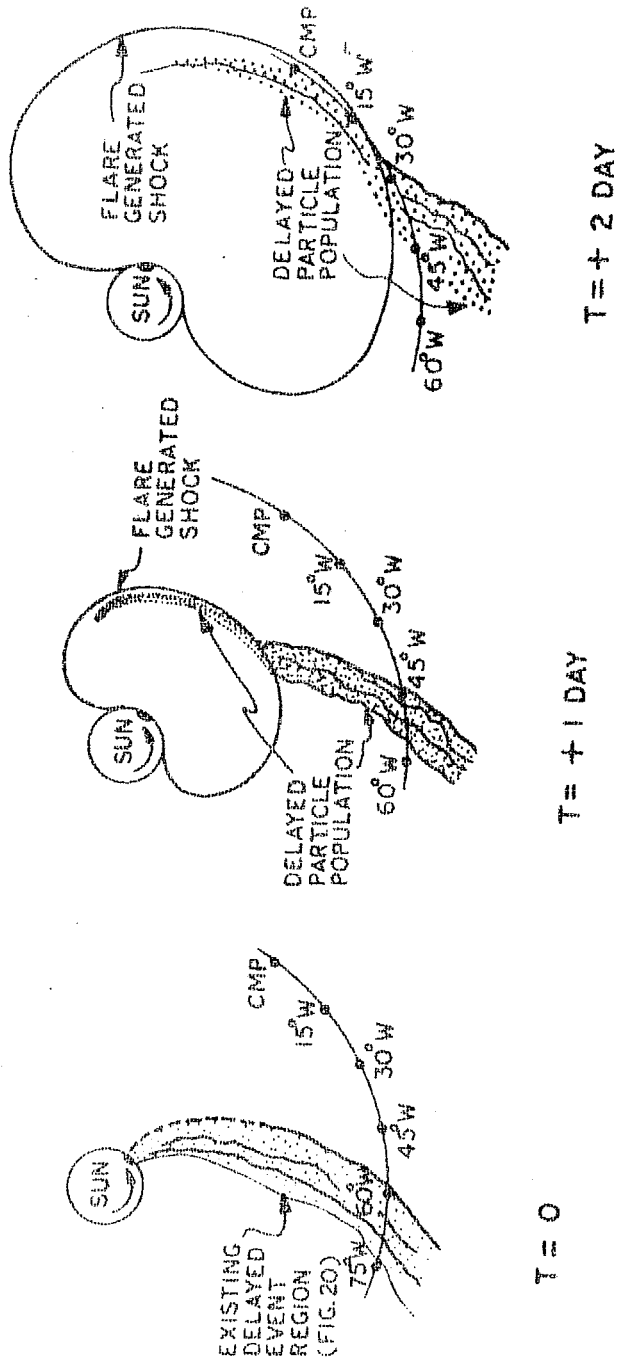


Figure 1.15 A model of propagation of low energy solar cosmic rays in the interplanetary space, which are apparently not related to any solar flare event (Kahler, 1969).

Observation of the solar cosmic rays at the earth shows a marked preference for the preceding west limb flares (McCracken et al., 1967; Lin and Anderson, 1967; Cline and McDonald, 1963 and Lin, 1970). The time of flight of these particles detected at the earth approximately agrees with the path length of the Archimedean spiral line from the sun to the earth; which has confirmed Parker's garden hose model of the interplanetary magnetic field (McCracken, 1962). Velocity dispersion is a very characteristic feature of these increases and the electron population usually arrives first. This is followed by protons and then all other heavy ions all at a time, since their  $A/Z$  being roughly the same, all the heavy ions exhibit similar behaviour during the transit. Biswas et al. (1963) and Durgaprasad et al. (1968) have reported instances when the proton to helium was dependent upon the time of observation during the flare event.

The anisotropies in the  $\simeq 10$  MeV solar particles detected in satellite detectors at various stages in a flare increase are depicted in figure 1.14 (McCracken et al., 1971; Rao et al., 1971). These authors have offered an explanation for the varying anisotropies during the different phases of the flare increase in terms of the radially outward convection of the particles by solar wind and field aligned diffusion of solar cosmic rays.

At early times during a flare increase ( $T < 1$  day), the outward field aligned diffusion dominates over the

convection giving anisotropy along the garden hose direction. At late times ( $1 \text{ day} \lesssim T \lesssim 4 \text{ days}$ ), the initial large density gradients are smeared over the whole region and the solar particles move under the outward convection producing radial anisotropy. At very late times, ( $T > 4 \text{ days}$ ), convection of the solar particles results in a positive radial density gradient. The combined action of reversed field aligned diffusion in the inward direction and the outward radial convection leads to anisotropy along 15 hour direction in the interplanetary space.

At low energies (few MeV) satellite observations many times show a second increase during the decay phase of a flare associated increase. The energy spectrum of these increases is considerably steeper than that of the first increase, and are common at energies  $\simeq 5 \text{ MeV}$ . Bryant et al. (1965), Fan et al. (1968) and Anderson (1969) have suggested that such increases are due to the low energy ions and electrons generated in the solar active regions. These particles adhere to the field lines for a time of the order of  $10^4$ - $10^5$  seconds. When the flare occurs, the high energy particles produced during the flare first arrive at the earth. The low energy particles already present near the sun around such regions, are then convected out and arrive at the earth in the course of a day or two. The various phases in the phenomenon are shown in figure 1.15 (Kahler, 1969).

Such low energy increases are some times seen without any preceding solar flare or any flare increase and are associated with 27 day recurrent solar corotating streams (Fan et al., 1968 and Lin et al., 1968).

### I. 5 Origin of cosmic rays:

Except for the solar flare type increases, the sun is not the source of the bulk of cosmic rays. The sun essentially modulates the intensity of cosmic rays in the Galaxy, which causes time variations in the intensity such as diurnal variation, Forbush decrease and eleven year variation. The cosmic ray intensity has essentially remained constant for the past  $10^8$  years (Honda et al., 1960; Arnold et al., 1961; Geiss, 1963; and Hayakawa, 1969). The various characteristics of cosmic rays indicate that their origin is in our own Galaxy. These are summarized below.

The energy density of cosmic rays in our Galaxy is  $\approx 10^{-12}$  erg cm<sup>-3</sup> (Ginzburg, 1958) and is comparable to that of the star light, the turbulent motion of the interstellar gas and the galactic magnetic field ( $10^{-5}$ - $10^{-6}$ ) gauss. On the basis of equipartition<sup>ti</sup> of energy, this indicates a galactic origin of cosmic rays. In comparison, the intergalactic magnetic field is estimated to be an order of magnitude lower (Ginzburg, 1958).

Anand et al. (1968), Clark et al. (1968, 1970, 1971) and Garmire (1970) have reported a finite flux  $\approx 10^{-4}$  photons cm<sup>-2</sup> sec<sup>-1</sup> strad<sup>-1</sup> of the diffused cosmic gamma rays of energy

>100 MeV in the direction of the galactic centre. The flux in the anticentre direction is  $\approx 3 \times 10^{-5}$  photons  $\text{cm}^{-2} \text{sec}^{-1} \text{strad}^{-1}$  (Clark et al.). Cowsik and Hutcheon (1971) have evaluated the contribution from different processes to the observed flux. The Inverse-Compton scattering of  $2.7^\circ$  universal black body radiation has negligible contribution. The gamma rays arising from  $\pi^0$  decay contribute to only 10% ( $\approx 1 \times 10^{-5}$  photons  $\text{cm}^{-2} \text{sec}^{-1} \text{strad}^{-1}$ ) of the flux as is also pointed out by Clark et al. (1970). The Inverse-Compton scattering of the star light from the centre of the Galaxy by galactic electrons provides the major part ( $\approx 8 \times 10^{-5}$  photons  $\text{cm}^{-2} \text{sec}^{-1} \text{strad}^{-1}$ ) of the flux. The authors conclude that the total flux from all the above processes is in good agreement with the observed one. Their calculations agree with the variation in the flux with galactic longitude obtained by Clark et al. If the rate of cosmic ray injection is correlated with the distribution of matter density in the Galaxy, the calculated fluxes would be higher by an order of magnitude. This further suggests a uniform distribution of cosmic rays and hence of their sources in the Galaxy.

To a first approximation, the chemical composition of cosmic rays is similar to that of the cosmic abundances. However, the ratio of light (Li, Be, B) to heavy nuclei in the cosmic rays is five orders of magnitude greater compared to that in the cosmic abundances (Waddington, 1962).

These extra light nuclei are assumed to be produced by spallation of medium and heavy nuclei in the cosmic radiation with the matter (hydrogen) encountered during their travel, and the ratio of abundances of (Li, Be, B) to medium and heavy nuclei can therefore be used to estimate the path length traversed by the cosmic rays. A similar parameter is the ratio of  $^3\text{He} / (^3\text{He} + ^4\text{He})$  on the assumption  $^3\text{He}$  is the fragmentation product of  $^4\text{He}$ . These methods yield the total path length traversed by cosmic rays  $\approx 3-6.5 \text{ gm cm}^{-3}$  (Hayakawa et al., 1953; Biswas et al., 1968; Biswas and Ramadurai, 1971). Considering the entire motion of the cosmic rays within our Galaxy having matter density of  $2 \times 10^{-26} \text{ gm cm}^{-3}$ , the path length turns out to be  $\approx 2 \times 10^{26} \text{ cm}$ . The observed cosmic ray positron flux produced through decay of  $\pi^+$  mesons arising in the cosmic ray interactions with galactic matter, again yields a similar value for the path length. The path length is four orders of magnitude higher than the radius of the Galaxy ( $5 \times 10^{22} \text{ cm}$ ). However, in the galactic magnetic field ( $\approx 10^{-6}$  gauss), a proton of as high an energy as  $10^{17} \text{ eV}$ , has a gyroradius of only  $3 \times 10^{20} \text{ cm}$  and such a particle can gyrate a number of times to yield the path length mentioned above, thus suggesting that the major fraction of matter traversed is in the interstellar space (Daniel and Stephens, 1969).

Supernovae explosions have been considered as one of the probable sources of injecting cosmic rays in the galactic space (Ginzburg, 1953). In a supernova explosion, one expects a much higher abundance of heavy nuclei compared to the cosmic abundance. This would be consistent with the (30-50) times higher abundance of nuclei with  $Z \gtrsim 20$  in cosmic rays than the cosmic average (Waddington, 1962). Ginzburg (1953) has estimated the optical energy output from a supernova explosion to be  $\approx 10^{43-50}$  erg. If the supernovae explosions occur at the rate of one per 30 years, the power output in the optical range would be  $W_{\text{SN.O}} \approx 10^{39-41}$  erg sec<sup>-1</sup>. If we assume the accelerated electrons as the source of the synchrotron radiation observed in the supernovae remnants, we have,  $W_{\text{SN.e}} \approx 10^{37-39}$  erg sec. Presumably, protons are also accelerated in the supernovae. Detailed calculations (Ginzburg, 1953) show that the transfer of energy to protons and nuclei is probably 10-1000 times greater than to electrons. The average power output in the form of cosmic rays from a supernova explosion would be  $W_{\text{SN.c.r.}} \approx 10^{33-40}$  erg sec. Such an energy output would certainly be sufficient to maintain the loss of energy by cosmic rays through interactions with the galactic matter (Ginzburg, 1953). Cosmic rays injected into the galactic space undergo random scattering with moving magnetic field irregularities and become isotropic. Further, Fermi (1949) has shown that cosmic rays can gain energy during such collisions and lead to a power law energy spectrum with a negative exponent.

Gold (1969) has proposed pulsars as another possible source of cosmic rays. Pulsars are rotating neutron stars surrounded by Strong magnetic fields and are formed in the central core of a star during the stage of supernova explosion. The neutron star loses energy in two ways: 1) the synchrotron radio emission by electrons, though pulsed gamma ray emission at  $10^3$  eV has been observed by Chatterjee et al. (1969) from the pulsar CPO 950, and 2) loss of relativistic gas crossing out of the magnetosphere of the neutron star. It is shown that the total energy loss in the form of relativistic gas is  $\simeq 10^{52}$  ergs. So, even one pulsar from a supernova per hundred years, would be able to provide the galaxy, a mean energy rate of  $3 \times 10^{42}$  ergs  $\text{sec}^{-1}$  in the form of cosmic rays, which would allow a high rate of leakage out of the Galaxy.

Recently, Ostriker (1970) and Cowsik (1971a,b) have developed a white dwarf model for injecting cosmic rays in the galactic space. The model is similar to the pulsar mechanism, using the high magnetic fields in the white dwarfs [Magagauss fields; Kemp et al., 1970; Angle and Landstreet, 1970; Landstreet and Angle, 1971] and the rapid rotation at the time of their formation through stellar collapse. Cowsik (1971a,b) have concluded that white dwarfs are favourable candidates for cosmic rays of energies  $\ll 10^{13}$  eV.



## CHAPTER II

## TECHNIQUES OF THE STUDY OF COSMIC RAY TIME VARIATIONS

## I.1. Comparison of cosmic ray detectors

Studies of the time variations in cosmic ray intensity are carried out by continuous monitoring of cosmic ray intensity using a variety of techniques in various energy ranges from a few MeV to  $\approx 10^{21}$  eV. Cosmic rays of energies  $< 10^9$  eV have been mainly studied by balloon borne and satellite detectors, whereas the extensive air shower technique is used for studying particles above  $10^{12}$  eV. In the intermediate energy range, the ground based ionization chambers, Geiger-Müller telescopes, plastic scintillation telescopes and neutron monitors have been extensively used over the past few decades for the continuous monitoring of the cosmic ray intensity. The lower energy limit for these detectors is set by the atmospheric absorption of the cosmic ray particles. In addition to simplicity and relative ease in the operation of the ground based detectors, they have a further advantage, that the geomagnetic field acts as a momentum spectrum-analyser of primary cosmic rays resulting in an increase in cutoff rigidity from poles to equator. The ground based detectors measure the intensity of the secondary particles produced by the interaction of primary cosmic rays in the earth's atmosphere. Ionization chambers, Geiger-Müller telescopes and plastic scintillation telescopes respond basically to the hard component ( $\mu$  - mesons) in

the atmosphere, whereas 92% of the counting rate in a neutron monitor is due to nucleonic component of the secondary cosmic rays (Huges and Marsden, 1966). The mean rigidity response of neutron monitors is therefore lower than that of the meson monitors. The mean rigidity response is defined as

$$\text{Mean rigidity response } \langle P^{-\gamma} \rangle^{\frac{1}{1-\gamma}} = \frac{\int_{P_c}^{\infty} S(P) \cdot dN/dP \cdot dP}{\int_{P_c}^{\infty} P^{-\gamma} \cdot S(P) \cdot dN/dP \cdot dP} \dots (2.1)$$

where  $P_c$  is the geomagnetic cutoff-rigidity of the station,  $\gamma$  the spectral exponent of the variation under study,  $S(P)$  the specific yield function (Lockwood and Webber, 1967) and  $dN/dP$  is the primary differential rigidity spectrum of cosmic rays. For  $\gamma = 1$ , as in the case of eleven year variation, the mean rigidity response for a neutron monitor at sea level varies from  $\simeq 10$  GV at the geomagnetic latitude  $\simeq 55^\circ$  to  $\simeq 41$  GV near the equator (Trivandrum, India).

In comparison the meson monitor at equator has a mean rigidity response  $\simeq 47$  GV. The mean rigidity response further increases to  $\simeq 80-100$  GV for an underground meson monitor depending upon the depth below ground. Thus all these detectors are supplementary to each other in the study of cosmic ray intensity variations in the different rigidity ranges.

Among all the ground based detectors, neutron monitors are found to be the most suitable for the study of solar modulation of the cosmic ray intensity. This is because of their lower rigidity response as well as due to easy

\* correction for the atmospheric effects. Study of the spatial anisotropies in the cosmic ray intensity by such ground based detectors needs analysis of data from the monitors distributed at various latitudes and longitudes forming a grid all over the earth. To meet this requirement, a large number of neutron monitors have been set up at various places during the IGY and later.

## II.2. Atmospheric pressure correction to total counting rates in a neutron monitor

The intensity of secondary cosmic radiation in the atmosphere undergoes changes due to the variations in the atmospheric pressure. An increase in the atmospheric pressure results in a greater absorption of secondary cosmic rays and hence a decrease in their intensity at ground and vice versa. The pressure corrected counting rate  $N_{\text{corr}}$  in a neutron monitor is therefore given, to a first approximation, by the formula (Elliot, 1952),

$$N_{\text{corr}} = N_{\text{obs}} (1 - \beta \cdot \Delta p) \quad \dots(2.2)$$

where  $N_{\text{obs}}$  is the observed counting rate,  $\Delta p$  is the change in pressure from standard mean atmospheric pressure at the station and  $\beta$  is the pressure coefficient having a negative value. Precisely, the relation is

$$N_{\text{corr}} = N_{\text{obs}} \cdot \exp \left[ - \beta (p_{\text{obs}} - \bar{p}) \right] \quad \dots(2.3)$$

where  $p_{\text{obs}}$  is the atmospheric pressure observed at the time

of  $N_{\text{obs}}$  and  $\bar{p}$  is the standard mean atmospheric pressure of the station.

Various methods [Mathews, 1959; McCracken and Johns, 1959; and Lindgren, 1962], suggested for determining the pressure coefficient from the above equation, suffer from the draw back that the primary cosmic ray intensity at the top of the atmosphere is constantly changing. The method of successive differencing used by Lapointe and Rose (1962), Bachelet et al. (1965) and Griffiths et al. (1966) is, however, considerably more reliable in this regard. The method is as follows:

If  $N_1$  is the counting rate on day 1 having daily mean pressure  $p_1$ , then the counting rate  $\bar{N}_1$  on that day for the mean standard pressure  $\bar{p}$  at the station can be found from the relation,

$$N_1 = \bar{N}_1 \cdot \exp [-\beta \cdot (p_1 - \bar{p})] \quad \dots(2.4)$$

Similarly on the subsequent day 2, we would have,

$$N_2 = \bar{N}_2 \cdot \exp [-\beta \cdot (p_2 - \bar{p})] \quad \dots(2.5)$$

and hence

$$\ln \left[ \frac{N_1}{N_2} \right] = \ln \left[ \frac{\bar{N}_1}{\bar{N}_2} \right] - \beta \cdot (p_1 - p_2) \quad \dots(2.6)$$

If the periods are chosen when the primary intensity does not change appreciably from one day to the next, then

$\bar{N}_1 \approx \bar{N}_2$  and  $\ln \left[ \frac{\bar{N}_1}{\bar{N}_2} \right]$  is approximately zero. With this

assumption,  $\beta$  can be determined by means of a regression

analysis of  $\ln \left[ \frac{N_1}{N_2} \right]$  on  $(p_1 - p_2)$ .

McCracken and Johns (1959), Bachelet et al.(1965) and Carmichael et al.(1968), Carmichael and Bercovitch (1969) have studied the latitude and altitude dependence of the pressure coefficient for neutron monitors. Figure 2.1 shows the latitude variation of the pressure coefficient at sea level obtained by Carmicheal and Bercovitch. The coefficient increases from about 0.94 percent per millimeter of Hg at about 16 GV cutoff rigidity to about 1.04 percent per millimeter of Hg at about 2 GV and then onward it remains constant upto the poles. Likewise, the pressure coefficient is found to increase upto an atmospheric depth of about  $600 \text{ gm cm}^{-2}$ , and thereafter it decreases upto the sea level. The increase in the pressure coefficient with increasing latitude and atmospheric depth is understood in terms of the reduction in the energy and hence absorption length of the particles contributing significantly to the counting rate in the monitor. The anomalous decrease in the pressure coefficient below  $600 \text{ gm cm}^{-2}$  has been explained by Carmichael and Bercovitch (1969) and Singh et al.(1970) as due to obliquely incident cosmic rays having an apparently smaller absorption length, which contribute more at higher altitudes than near sea level.



### II.3. Geomagnetic field and asymptotic cones of acceptance:

The geomagnetic field, to a first approximation, is that due to a magnetic dipole located near the centre of the earth. The equivalent dipole would be off-set by 436 km from the centre of the earth, displaced toward the Pacific ocean. Further, it is tilted with respect to the earth's rotation axis by approximately  $11^\circ$  (handbook of Geophys, USAF Geophysics Research Directorate, the Macmillan Company, 1960). The north geomagnetic pole is located in Greenland at  $81.0^\circ\text{N}$ ,  $84.7^\circ\text{W}$  in the geographic system of coordinates. The corresponding south geomagnetic pole is in antartica at  $75.0^\circ\text{S}$ ,  $120.4^\circ\text{E}$ . The geomagnetic latitude  $\lambda_m$  and longitude  $\psi_m(\text{east})$ , of a point having geographic latitude  $\theta$  and longitude  $\phi$ , are given by

$$\sin \lambda_m = \left[ \cos 78.3^\circ \cdot \cos \theta \cdot \cos (\phi - 291^\circ) \right] + \sin 78.3^\circ \cdot \sin \theta \quad \dots(2.7)$$

and

$$\cos \psi_m = \left[ \sin 78.3^\circ \cdot \cos \theta \cdot \cos (\phi - 291^\circ) - \cos 78.3^\circ \sin \theta \right] \cos \lambda_m \quad \dots(2.8)$$

The geomagnetic dipole has a magnetic moment of  $8.06 \times 10^{25}$  gauss  $\text{cm}^3$ .

The geomagnetic field produces two major effects on the cosmic ray particles. Firstly, it acts as a momentum spectrum analyser and, at each geomagnetic latitude, the particles arrive only above a threshold magnetic rigidity

from a particular zenithal and azimuthal direction. This effect has been extensively used for understanding the rigidity spectrum of various cosmic ray intensity variations. The second consequence of the geomagnetic field on cosmic rays is the change in the asymptotic direction of approach of the particles in the interplanetary space from the direction of incidence on the surface of the earth, so that the intensity observed at any station at a particular local time has to be related to a different direction in space. The correction becomes complicated since a ground based monitor records the secondaries in the atmosphere produced by primary cosmic ray particles of all the rigidities from the geomagnetic cutoff to infinity and the geomagnetic bending for each rigidity is different. Both these effects are discussed in detail below.

The cutoff-rigidities of cosmic ray particles in the centered dipole geomagnetic field have been worked out by Störmer (1936), Lemaitre and Vallarta (1936, a, b) and Alpher (1950). At a geomagnetic latitude  $\lambda_m$ , the cosmic ray particles arriving from a zenith angle  $\theta$  and azimuth  $\phi$  are subject to a cutoff-rigidity given by (Alpher, 1950):

$$P_c = \frac{300 \times M \cos^4 \lambda_m}{a^2 \left[ 1 + \sqrt{1 - \sin \theta \cdot \cos \phi \cdot \cos^3 \lambda_m} \right]^2} \quad \dots (2.9)$$

in units of GV where  $M$  is the earth's magnetic moment in Gauss and  $a$  is the earth's radius in Störmer unit (C)



defined as

$$1 \text{ Störmer Unit} = C = \left[ \frac{\text{Magnetic moment of the earth}}{\text{rigidity of particle}} \right]^{\frac{1}{2}}$$

$$= \left[ \frac{M}{pc/Ze} \right]^{\frac{1}{2}} \quad \dots(2.10)$$

In the above expression,  $p$  is the momentum,  $Ze$  is the charge of the particle and  $c$  is the velocity of light.

For vertically incident particles, the expression for cutoff-rigidity reduces to

$$P_c = 14.9 \cos^4 \lambda_m \quad \dots(2.11)$$

The reduction in cutoff-rigidity from equator to poles results in an increase in the integral cosmic ray intensity with increasing latitude as is verified from the latitude surveys conducted by Carmichael et al. (1965) and in earlier surveys quoted by Webber (1962). The surveys also show that the increase in the intensity continues only upto  $\simeq 55^\circ$  geomagnetic latitude and there onwards it remains constant. The constancy of the intensity above  $\simeq 55^\circ$  latitude, known as the "latitude knee" results from the atmospheric absorption of all the primary particles having rigidity less than  $\simeq 1.5 \text{ GV}$ . Therefore any reduction in the cutoff-rigidity beyond  $55^\circ$  geomagnetic latitude does not increase the integral cosmic ray intensity. The latitude surveys have shown a disagreement with the expected latitude distribution of the cosmic ray intensity at various longitudes for a centered dipole geomagnetic field. This has led to the study of the influence of higher moments of the earth's magnetic field on

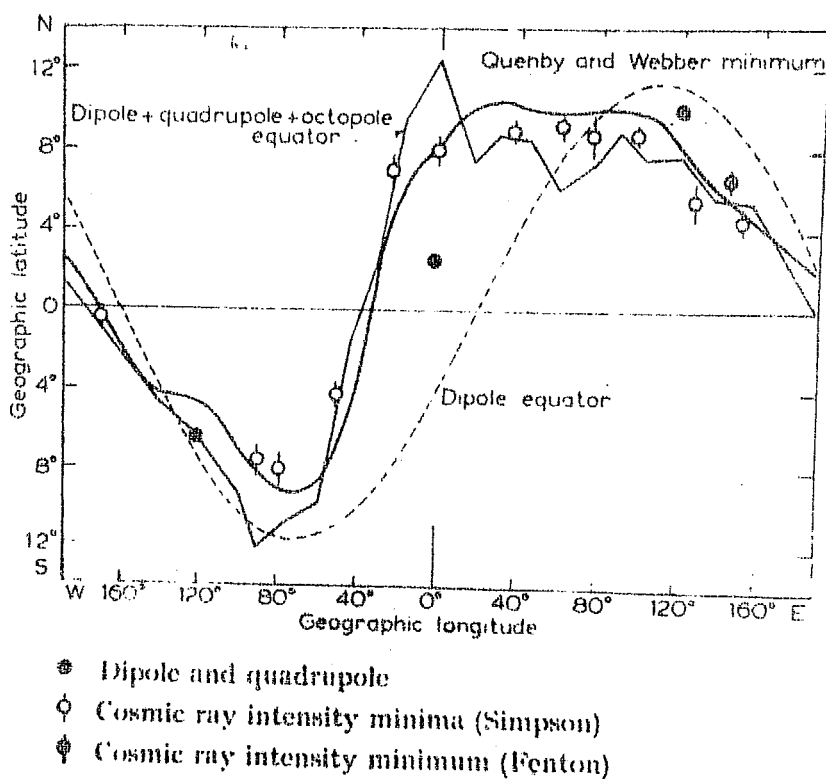


Figure 2.2 Comparison of observed and calculated cosmic ray equator.  
 Observed - Katz et al. (1958)  
 Calculated - Kellog and Schwartz (1959)  
 Quenby and Webber (1959)

cutoff-rigidities [Quenby and Webber, 1959 ; and Wenk, 1961], which has shown better agreement with the results from the latitude surveys and has revealed a longitudinal dependence in the cutoff-rigidities. The maximum cutoff-rigidity of  $\approx 17$  GV is observed in the Indian zone near the geomagnetic equator. Figure 2.2 shows the comparison of the observed cosmic ray equator (Katz et al., 1958) and the calculated ones by Kellogg and Schwartz (1959) using terms upto Octopoles of the earth's magnetic field as well as by Quenby and Webber (1959) using spherical harmonics of the earth's magnetic field up to sixth degree. The deformed geomagnetic field under the pressure of solar wind also leads to a change in the cutoff-rigidity at a particular station at different local times as shown by Ahluwalia and McCracken (1965), Razdan and Summers (1965) and Smart et al. (1969).

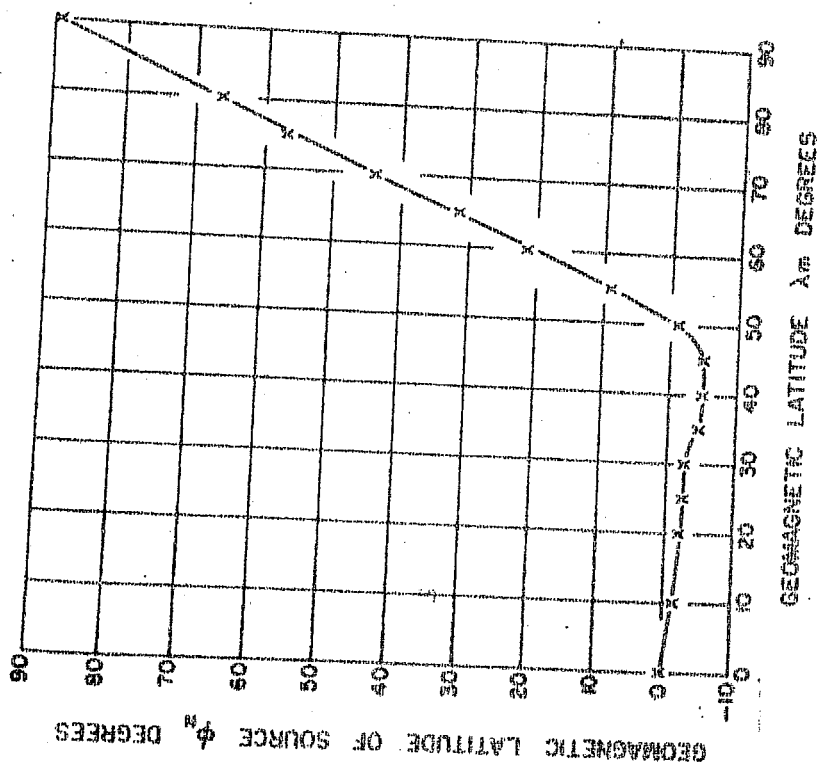
A cosmic ray detector on the ground responds in varying degrees to primary cosmic ray particles of different rigidities impinging on the top of the atmosphere from different directions. These primary cosmic ray particles of different rigidities above the geomagnetic cutoff come from different asymptotic directions outside the deflecting geomagnetic field. Therefore, in order to find out the mean asymptotic direction of approach of the cosmic ray particles contributing significantly to the counting rate in a ground based detector, a combined weightage is assigned to every accessible asymptotic direction in terms of the primary

rigidity spectrum and the zenithal dependence of the counting rate in the monitor. Asymptotic cone of acceptance of a ground based cosmic ray detector is then defined by the solid angle containing the asymptotic directions of approach of primary cosmic ray particles that contribute significantly to its counting rate [Lapointe and Rose, 1961; McCracken, 1962]. The mean asymptotic direction  $A_m$  is given by

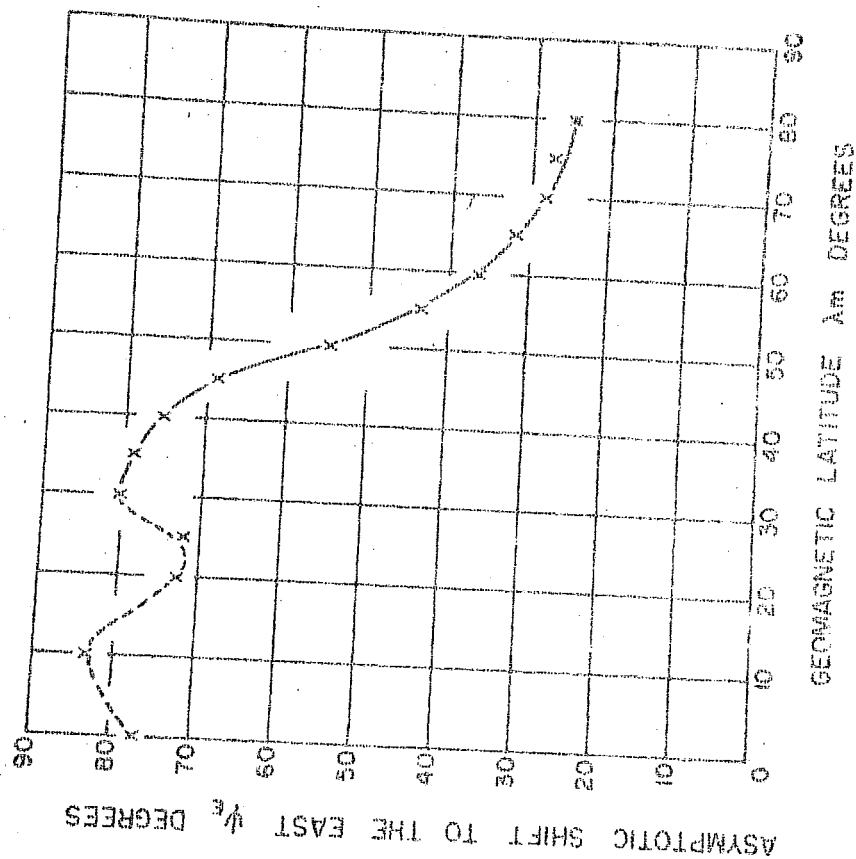
$$A_m = \frac{\int_{P_c}^{\infty} P^{-\gamma} \cdot S(P) \cdot A(P) \cdot dP}{\int_{P_c}^{\infty} P^{-\gamma} \cdot S(P) \cdot dP} \quad \dots(2.12)$$

where  $A(P)$  is the asymptotic direction of approach for a particle of rigidity  $P$ ,  $P^{-\gamma}$  is the primary differential rigidity spectrum,  $P_c$  the geomagnetic cutoff-rigidity at the station and  $S(P)$  the specific yield function (Treiman, 1952; and Lockwood and Webber, 1967).

The calculations of Lapointe and Rose (1961) and McCracken (1962) reveal that for monitors located at geographic latitudes less than  $\cong 55^\circ$ , the asymptotic cone of acceptance lies to the east of the station meridian and with  $\pm 10^\circ$  of the equatorial plane. The asymptotic cones of very high latitude monitors make an appreciable angle with the equatorial plane. Figure 2.3 a,b,c show the mean asymptotic latitude, longitudinal shift in the mean asymptotic direction from station-meridian and the width of the

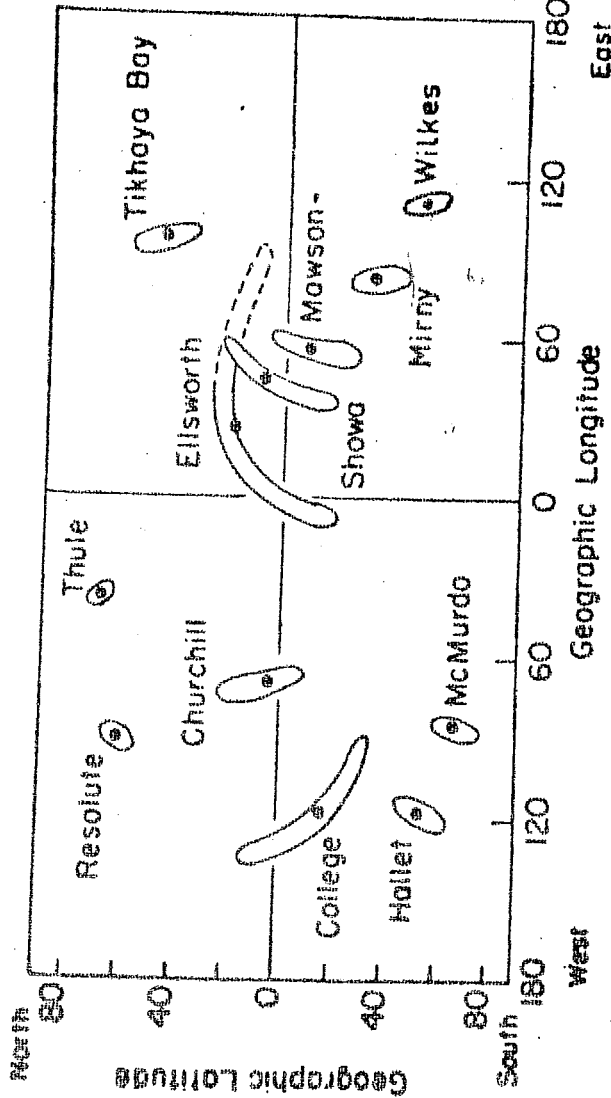
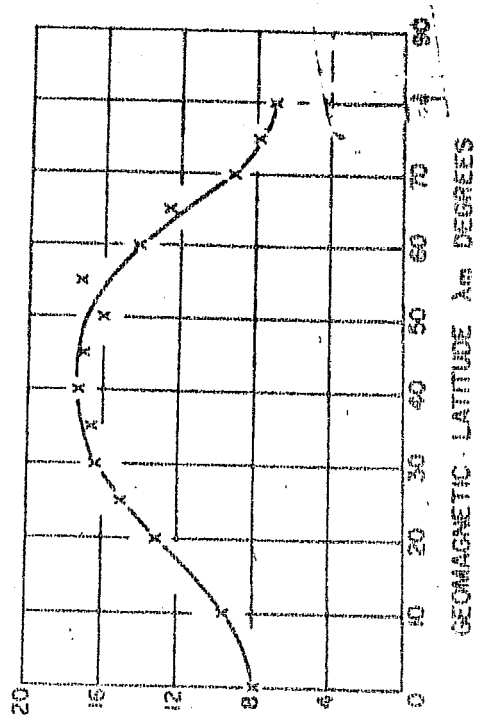
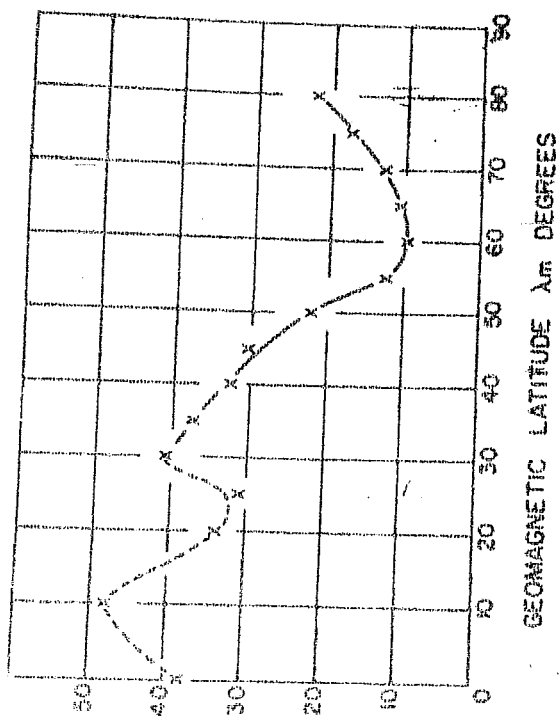


a



b

Figure 2.3a, b. The mean asymptotic latitude and longitudinal shift in the mean asymptotic direction from vertical for neutron monitors at various geomagnetic latitudes (Lapointe and Rose, 1961).



d

Figure 2.3c The width of the asymptotic cones of acceptance of neutron monitors (Lapointe and Rose, 1961).  
Figure 2.3d The actual asymptotic cones of acceptance for different neutron monitors (McCracken, 1962).

asymptotic cone of acceptance at various geographic latitudes as calculated by Lapointe and Rose (1961) for a simple dipole geomagnetic field. Figure 2.3 d, shows explicitly, the asymptotic cones of acceptance for different stations (McCracken, 1962), taking into account the spherical harmonics upto sixth degree in the geomagnetic field. It is seen that the the longitudinal width of the asymptotic cones decreases from  $\approx 50^\circ$  near the equator to  $\approx 20^\circ$  near the poles, while the eastward shift in the mean asymptotic direction decreases from  $\approx 55^\circ$  near the equator to  $\approx 30^\circ$  near the poles. The higher harmonics in the geomagnetic field make a considerable contribution in the asymptotic coordinates of stations at very high geographic latitudes. For different stations at such high latitudes, the longitudinal shifts in the asymptotic direction can differ by more than three hours. At lower latitudes, this difference due to deviations from dipole geomagnetic field is smaller. All these factors make middle latitude stations the most suitable for the study of cosmic ray anisotropies in the equatorial plane.

#### II.4. Variational coefficients

The effect of the characteristics of asymptotic cones of acceptance (described in the last section) on the spatial anisotropy in cosmic ray intensity, has been discussed by Rao et al. (1963). The fractional change in the counting rate of a ground based monitor due to particles arriving

in the solid angle  $\Omega_i$  at the top of the atmosphere is given by

$$\frac{dN(\Omega_i)}{N} = \int_{P_c}^{\infty} W(P) \cdot \frac{\Delta J_i(P)}{J_o(P)} \cdot \frac{Y(\Omega_i, P)}{Y(4\pi, P)} \cdot dP \quad \dots (2.13)$$

where  $J_i(P)$  is the differential cosmic ray rigidity spectrum within  $i^{\text{th}}$  solid angle  $\Omega_i$  and is expressed as  $J_i(P) = J_o(P) + \Delta J_i(P)$  where  $J_o(P)$  is the "average" differential spectrum while the change  $\Delta J_i(P)$  is different from one  $\Omega_i$  to the next.  $N$  is the average counting rate of the monitor over all directions,  $W(P)$  are the coupling coefficients discussed by Dorman (1957).  $Y(\Omega_i, P)$  are the weighting functions (derived from the zenithal and azimuthal response of the monitor) integrated over the zenith angle and azimuthal angle in the solid angle  $\Omega_i$ .  $Y(4\pi, P)$  is its average over all the solid angles in the space.

It is assumed that the variational spectrum of the anisotropy  $\frac{\Delta J_i(P)}{J_o(P)}$  of the primary cosmic rays is a power law of the form  $AP^\gamma$  where  $A$  is a function of the asymptotic direction and  $P$  the rigidity in GV. So, the observed anisotropy  $\frac{dN(\Omega_i)}{N}$  can be expressed as

$$\frac{dN(\Omega_i)}{N} = A \cdot v(\Omega_i, \gamma) \quad \dots (2.14)$$

where

$$v(\Omega_i, \gamma) = \int_{P_c}^{\infty} W(P) \cdot P^\gamma \cdot \frac{Y(\Omega_i, P)}{Y(4\pi, P)} \cdot dP \quad \dots (2.15)$$



$v(\Omega_i, \chi)$  is called the "variational coefficient" of the monitor for the solid angle  $\Omega_i$  and the soectral index  $\chi$ .

Let A, the amplitude of the anisotropy, be expressed in terms of the asymptotic latitude  $\lambda$  and the asymptotic longitude  $\psi$  as

$$A = f(\psi) \cdot \cos \lambda \quad \dots(2.16)$$

The expression for the anisotropy observed at the ground based detector due to particles coming in the solid angle  $\Omega_i$  can then be written as

$$\frac{dN(\Omega_i)}{N} = f(\psi) \cdot v(\Omega_i, \chi) \cdot \cos \lambda \quad \dots(2.17)$$

Summing over all the solid angles  $\Omega_i$ , we get

$$\frac{dN(\psi_j)}{N} = f(\psi_j) \left[ \sum_i v(\Omega_i, \chi) \right] \cdot \cos \lambda \quad \dots(2.18)$$

$$= f(\psi_j) \cdot V(\psi_j, \chi) \quad \dots(2.19)$$

where  $\frac{dN(\psi_j)}{N}$  is the anisotropy due to particles arriving from the  $j^{\text{th}}$  asymptotic longitude  $\psi_j$  and  $V(\psi_j, \chi)$  is the corresponding total variational coefficient.

Let the anisotropy be expanded as an arbitrary function of the angle  $\eta$  in the form of a Fourier series

$$f(\eta) = J_0(P) \sum_{m=1}^{\infty} \alpha_m \cdot \cos m(\eta - C_m) \quad \dots(2.20)$$

where  $\alpha_m$  and  $C_m$  are the arbitrary amplitude and phase constants.  $C_m$  is also the asymptotic direction of viewing from which the maximum of  $m^{\text{th}}$  harmonic is seen. The

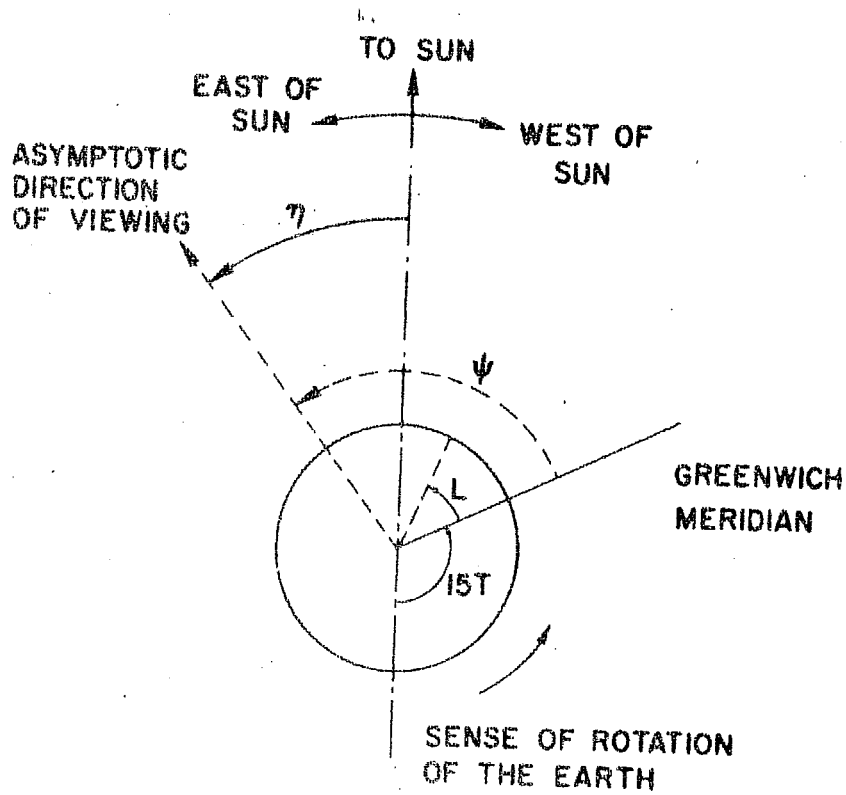


Figure 2.4 The angles employed to specify the asymptotic direction of viewing in equation 2.21.

asymptotic angle  $\eta$  is measured east of the earth-sun line (figure 2.4) and can be expressed as

$$\eta = \psi + 15 T - 180^\circ \quad \dots(2.21)$$

where  $\psi$  is the asymptotic longitude of the station and  $T$  is the local time measured in hours. Thus

$$f(\psi) = J_0(P) \left[ \sum_{m=1}^{\infty} \alpha_m \cos m(\psi + 15T - 180^\circ - C_m) \right] \dots(2.22)$$

Substituting this expression for  $f(\psi)$  in the equation defining the observed fractional change (anisotropy) in the counting rate due to change  $\Delta J(\psi_j)$  in the primary intensity from the asymptotic direction  $\psi_j$ , and then summing over all the asymptotic directions, we have

$$\frac{\Delta N(\text{Total})}{N} = \sum_j V(\psi_j, \delta) \sum_{m=1}^{\infty} \alpha_m \cos \left[ m(\psi + 15T - 180^\circ - C_m) \right] \quad \dots(2.23)$$

$$= \sum_{m=1}^{\infty} \alpha_m B_m \cos \left[ m(15T - C_m - 180^\circ) + \delta_m \right] \dots(2.24)$$

where

$$B_m^2 = \left[ \sum_j V(\psi_j, \delta) \cdot \sin(m\psi_j) \right]^2 + \left[ \sum_j V(\psi_j, \delta) \cdot \cos(m\psi_j) \right]^2 \dots(2.25)$$

and

$$\tan \delta_m = \frac{\sum_j V(\psi_j, \delta) \cdot \sin(m\psi_j)}{\sum_j V(\psi_j, \delta) \cdot \cos(m\psi_j)} \quad \dots(2.26)$$

$(\alpha_m B_m)$  and  $(-m C_m + \delta_m)$  are the amplitude and phase constants of the  $m^{\text{th}}$  harmonic of the cosmic ray intensity variation at the detector. The universal time of maximum

intensity of the  $m^{\text{th}}$  harmonic is given as

$$T_m = \frac{180 m + m C_m - \delta_m}{15 m} \text{ hours} \quad \dots(2.27)$$

The local time of maximum for a detector at a geographic longitude  $L^0$  is given by

$$t_m = \frac{180 m + m C_m - (\delta_m - mL)}{15 m} \text{ hours} \quad \dots(2.28)$$

The quantity  $\frac{\delta_m - mL}{15 m}$  is also known as the "geomagnetic bending" of the cosmic ray flux.

## II. 5. Rigidity dependence of cosmic ray anisotropies

The method of studying rigidity dependence of the cosmic ray anisotropy developed by Rao et al.(1963) is described below. The variational spectrum is expressed as

$$\frac{\delta J(P)}{J(P)} = F(\lambda) \cdot a \cdot P^{\gamma} \text{ for } P_l < P < P_u \quad \dots(2.29)$$

$$= 0 \text{ for } P < P_l \text{ and for } P > P_u \quad \dots(2.30)$$

where  $P_l$  and  $P_u$  are the lower and upper limits of rigidity beyond which isotropy prevails,  $a$  is the amplitude of the anisotropy in the free space,  $\gamma$  is the spectral index and  $F(\lambda)$  is the dependence of the anisotropy on the latitude  $\lambda$ .

The spectral exponent  $\gamma$  is determined by varying the parameters in the above equation until the variance among the theoretically normalized anisotropy values in the interplanetary space, obtained from various stations is minimized.

Using this method, Rao et al.(1963) and Mori (1968) have

shown that for the average diurnal variation, with  $0 < P_E < 9$  GV, the spectral index  $\gamma$  is  $\simeq 0$ . The upper cutoff-rigidity of diurnal variation in the cosmic ray intensity is strongly dependent upon the level of solar activity (Agrawal and Rao, 1969; Jacklyn et al., 1970).

## II.6. Numerical techniques

### II.6 a) Harmonic analysis:

To determine the diurnal and semi-diurnal variation in the cosmic ray intensity, the data is subjected to Fourier (harmonic) analysis. Following is a general description of a Fourier series and the scheme of calculating the various harmonic coefficients.

Any periodic function  $y = f(\theta)$  can be expressed in the form of a trigonometric Fourier series,

$$Y = f(\theta) = a_0 + \sum_{n=1}^{\infty} a_n \cos(n\theta) + \sum_{n=1}^{\infty} b_n \sin(n\theta) \dots (2.31)$$

The function has a period  $2\pi$ . The coefficients in the series are given by

$$a_0 = \frac{1}{2\pi} \int_{-\pi}^{+\pi} f(\theta) \cdot d\theta \dots (2.32)$$

$$a_n = \frac{1}{\pi} \int_{-\pi}^{+\pi} f(\theta) \cdot \cos(n\theta) \cdot d\theta \dots (2.33)$$

$$b_n = \frac{1}{\pi} \int_{-\pi}^{+\pi} f(\theta) \cdot \sin(n\theta) \cdot d\theta \dots (2.34)$$

The series may be written in the alternative form as,

$$Y = f(\theta) = \frac{1}{2} a_0 + \sum_{n=1}^{\infty} r_n \cdot \cos (n \theta - \phi_n) \quad \dots(2.35)$$

$$\text{where } r_n = \sqrt{a_n^2 + b_n^2} \quad \dots(2.36)$$

$$\cos \phi_n = a_n / r_n \quad \dots(2.37)$$

$$\sin \phi_n = b_n / r_n \quad \dots(2.38)$$

$$\text{i.e. } \phi_n = \tan^{-1} b_n / a_n \quad \dots(2.39)$$

The condition  $n \theta = \phi_n$  then gives the argument for the maximum contribution from the harmonic amplitude  $r_n$ .

A periodic function having a period different from  $2\pi$  can be reduced to the above form in the following manner. If  $t$  is the independent variable and the given function  $Y = f(t)$ , we write

$$t = k + m\theta \quad \dots(2.40)$$

If limits for  $t$  are  $g$  and  $h$ , and  $\theta$  is to have limits from  $0$  to  $2\pi$  we have

$$g = k + 0 \text{ and } h = k + 2\pi m \quad \dots(2.41)$$

This gives  $k = g$  and  $m = (h-g)/2\pi$ . The derived transformation is therefore,

$$t = g + \frac{(h-g)}{2\pi} \cdot \theta \quad \dots(2.42)$$

$$\text{or } \theta = 2\pi \cdot \frac{(t-g)}{(h-g)} \quad \dots(2.43)$$

In cosmic ray studies, the data is normally analysed for periods of 24 hours (one day) or its higher harmonics.

If  $t$  is the time in hours, we have for hourly data,  $g = 1$  and  $h = 24$ , while the direction of the anisotropy is to be measured from  $t = 0$  hours. The argument of the harmonic series is

$$\Theta = 2\pi \cdot \frac{(t-1)}{23} + 0.5 \quad \dots(2.44)$$

The numerical scheme to find the harmonic coefficients is described by Scarborough (1966).

In the case of hourly data, the period of  $360^\circ$  is divided into 24 intervals of  $15^\circ$  width each. The standard error  $\sigma_{r_n}$  in the amplitude  $r_n$  of the  $n^{\text{th}}$  harmonic is then

$\sigma/\sqrt{12}$  where  $\sigma$  is the standard error in the hourly counting rate. The standard error in the time of maximum of the  $n^{\text{th}}$  harmonic is  $\sigma_{\phi_n} = \sigma_{r_n}/r_n$

In the case of bi-hourly data (interval  $30^\circ$ ) having standard error  $\sigma$ , the standard error in the amplitude of the  $n^{\text{th}}$  harmonic is given by  $\sigma_{r_n} = \sigma/\sqrt{6}$ , while the standard error in the time of maximum is given by the same formula namely,  $\sigma_{\phi_n} = \sigma_{r_n}/r_n$ .

## II.6 b) Correction of harmonic coefficients for secular changes in the data:

The experimental data used for harmonic analysis may contain a systematic linear variation or periodic secular variation of large periods. Such variations, to some extent,

distort the results of harmonic analysis. These effects may be eliminated as follows:

1) Linear variation:

The extreme ordinates at the end of the period are interpolated in the intermediate ordinates and these differences are then subtracted from the data. This removes the linear trend in the data.

2. Secular variations:

The secular variations are determined by the method of moving averages and are filtered out by subtracting from the data.

Let  $x_1, x_2, x_3, \dots, x_n$  be a series of data spaced at equal intervals  $\tau$  and let the total period be  $T = n\tau$ . The successive sums in the sliding intervals are formed as

$$\sum_{i=1}^n x_i, \quad \sum_{i=2}^{n+1} x_i, \quad \sum_{i=3}^{n+2} x_i,$$

Mean values of these sums corresponding to the central terms  $\frac{n}{2}, (\frac{n}{2} + 1), \dots$  form a series,

$$\bar{x}_{n/2} = \frac{1}{n} \sum_{i=1}^n x_i, \quad \bar{x}_{(\frac{n}{2} + 1)} = \frac{1}{n} \sum_{i=2}^{n+1} x_i,$$

These represent the secular variations. If the period  $T$  is divided in even number of intervals, the value  $\bar{x}_{n/2}$  actually corresponds to  $x_{(n/2 + \frac{1}{2})}$ . The actual value of



$\bar{x}_{n/2}$  is then given by

$$\left[ \bar{x}_{n/2} + \bar{x}_{(n/2 - 1)} \right] / 2$$

Subtracting these values from the actual data at corresponding intervals of time leaves only, those variation of period T in the data, which may be calculated by harmonic analysis.

#### II.6 c) Method of superposed Epoch or the Chree analysis for small variations:

This method is especially useful in detecting small non-periodic as well as periodic variations. Values of the observed quantity corresponding to onset of these small phenomena observed at different times are entered in a vertical column numbered zero. The values succeeding this epoch are consecutively written in the columns 1,2,3 ...etc. The preceding values are entered in the columns -1,-2,-3 ... etc. The table contains n lines if n phenomena are superposed. The mean value of the observed quantity in each column is found and plotted against the column number. Presence of the phenomena is clearly then, brought out, with onset in the column zero. The stray variations in the other columns are averaged out resulting in their total or partial cancellation.

#### II.6 d) 'Principle of least square' and regression analysis:

The 'Principle of least squares', first formulated by Legendre can be expressed as follows:

"The most probable value of any observed quantity is such that the sum of the squares of the deviations of the observations from this value is least". For example, if  $x_1, x_2, \dots, x_n$  are the observed values of any given quantity then the most probable value  $X$  is such that

$$(x_1 - X)^2 + (x_2 - X)^2 + \dots + (x_n - X)^2$$

is least. If  $\bar{x}$  is the arithmetic mean of  $x_1, x_2, \dots, x_n$ , so that

$$\sum_{i=1}^n x_i = n \bar{x} \quad \dots(2.45)$$

$$\text{i.e.} \quad \sum_{i=1}^n (x_i - \bar{x}) = 0 \quad \dots(2.46)$$

We have,

$$\sum_{i=1}^n (x_i - X)^2 = \sum_{i=1}^n [(x_i - \bar{x}) + (\bar{x} - X)]^2 \quad \dots(2.47)$$

$$= \left[ \sum_{i=1}^n (x_i - \bar{x})^2 \right] + n (\bar{x} - X)^2 \quad \dots(2.48)$$

which is clearly least when  $X = \bar{x}$ . This gives that the most probable value of a measured quantity is the arithmetic mean of the observations.

One of the other useful applications of the 'Method of least squares' is in fitting of a curve to set of

experimental data points. Let  $y_1, y_2, \dots, y_n$  be the measured quantity  $y$  for the values  $x_1, x_2, \dots, x_n$  of another quantity  $x$  and let a linear relation between the two (the method can be extended to any degree curve) variables  $x$  and  $y$  to be computed. The linear relation can be expressed as

$$y = a_1 x + b_1 \quad \dots(2.49)$$

where  $a_1$  and  $b_1$  are constants. The experimental values of  $y_i$  for different values of  $x_i$  will, in general, not be the same as those calculated from the above equation. The difference (error) will be  $(a_1 x_i + b_1 - y_i)$ . To obtain the linear best fit to the data, the constants  $a_1$  and  $b_1$  are so chosen that the sum of squares of the 'errors' is least, that is,

$$\sum_{i=1}^n (a_1 x_i + b_1 - y_i)^2 \text{ is least.}$$

The partial differentiation with respect to  $a_1$  and  $b_1$  then gives

$$\sum_{i=1}^n x_i (a_1 x_i + b_1 - y_i) = 0 \quad \dots(2.50)$$

$$\sum_{i=1}^n (a_1 x_i + b_1 - y_i) = 0 \quad \dots(2.51)$$

Solution of these equations gives

$$a_1 = \frac{\sum_{i=1}^n x_i y_i - \sum_{i=1}^n x_i \cdot \sum_{i=1}^n y_i}{n \sum_{i=1}^n x_i^2 - \left[ \sum_{i=1}^n x_i \right]^2} \quad \dots(2.52)$$

and

$$b_1 = \frac{\sum_{i=1}^n y_i \cdot \sum_{i=1}^n x_i^2 - \sum_{i=1}^n x_i \cdot \sum_{i=1}^n x_i y_i}{n \sum_{i=1}^n x_i^2 - \left[ \sum_{i=1}^n x_i \right]^2} \quad \dots(2.53)$$

where  $a_1$  is the slope of the line with respect to x-axis and  $b_1$  is the intercept on the y-axis. The above treatment assumes that only  $y_i$  are subject to experimental errors. However, it may happen that  $x_i$  may also be experimentally obtained and are liable to error. In this case, a regression line of x on y is also to be found by similar method, which will give  $a_2$  and  $b_2$  as the coefficients in the relation

$$x = a_2 y + b_2 \quad \dots(2.54)$$

The quantity

$$r = \sqrt{a_1 \cdot a_2} \quad \dots(2.55)$$

is known as the regression coefficient between x and y and is a measure of the dependence between the two. The maximum value of the regression coefficient is unity and the relation between x and y is taken to be significant

if  $r > 0.5$ . The standard errors in the coefficients  $a_1$ ,  $b_1$  and  $r$  are

$$\sigma_{a_1} = \frac{\sqrt{\frac{\sum_{i=1}^n (a_1 x_i + b_1 - y_i)^2}{n-2}}}{\sqrt{n \sum_{i=1}^n x_i^2 - \left\{ \sum_{i=1}^n x_i \right\}^2}} \quad \dots (2.56)$$

$$\sigma_{b_1} = \frac{\sqrt{\frac{\sum_{i=1}^n (a_1 x_i + b_1 - y_i)^2}{n-2}}}{\sqrt{n \sum_{i=1}^n x_i^2 - \left\{ \sum_{i=1}^n x_i \right\}^2}} \cdot \frac{\sum_{i=1}^n x_i^2}{(n-2)} \quad \dots (2.57)$$

$$\sigma_r = \frac{1 - r^2}{\sqrt{n}} \quad \dots (2.58)$$

Some of the other complicated functional forms can be made suitable for linear regression analysis by slight modifications. For example, taking natural logarithm of both sides of the equation

$$y = a e^{bx} \quad \dots (2.59)$$

can be expressed as

$$\log_e y = \log_e a + bx \quad \dots (2.60)$$

Similarly, the equation

$$y = a x^b \quad \dots (2.61)$$

can be expressed in the form

$$\log_e y = \log_e a + b \log_e x \quad \dots (2.62)$$

## II.6 e) $\chi^2$ - test for goodness of fit:

A test for estimating the confidence level in similarity between a histogram derived from experimentally observed values and another hypothesized one, is described below. The method involves comparison of frequencies in every interval in the histogram with corresponding frequencies expected from the hypothesized frequency distribution. A quantity  $(f_{oj} - f_{ej})^2 / f_{ej}$  is calculated for every interval where  $f_{oj}$  is the observed frequency in the  $j^{\text{th}}$  interval and  $f_{ej}$  is the expected frequency in the same interval from the hypothesized distribution. The quantity  $\chi^2$  is then defined as

$$\chi^2 = \sum_{j=1}^n \frac{(f_{oj} - f_{ej})^2}{f_{ej}} \quad \dots(2.63)$$

where  $n$  is the total number of intervals. A value of  $\chi^2 = 0$ , corresponds to the exact (theoretical) agreement between the observed and the hypothesized distribution, whereas the increasing values of  $\chi^2$  indicate less and less agreement between the two. The probability  $\gamma_{\chi^2}$  that the value of  $\chi^2$  will lie between  $\chi^2$  and  $\chi^2 + d\chi^2$ , on the basis of normal distribution, is given by

$$\gamma_{\chi^2} = \exp \left[ -\frac{\chi^2}{2} \right] \cdot (\chi^2)^{\frac{n-2}{2}} / \frac{n}{2} \cdot \left[ \frac{n-2}{2} \right]! \quad \dots(2.64)$$

The probability that the  $\chi^2$  value will be equal to or

greater than a calculated value of  $\chi^2$  for  $(n-3)$  degrees of freedom (Smith and Duncan, 1944) is listed in  $\chi^2$  - tables mentioned in standard statistical tables. Normally, if the observed value of  $\chi^2$  is less than the  $\chi^2$  value corresponding to 5% rejection level mentioned in the table, the agreement between the observed and hypothesized frequency distributions is taken to be satisfactory.

It should be mentioned that the  $\chi^2$  -test does not indicate as to whether a single value in the histogram is responsible for the difference in the observed and hypothesized frequency distributions or it is due to an over all difference in the two distributions. Further, if the observed and the hypothesized distributions differ in a negative way on one side of the central point and in a positive way on the other side by small magnitudes, the  $\chi^2$ -test does not bring out this difference, since the signs of the deviations from the expected values do not affect the value of  $\chi^2$ .

C H A P T E R    I I IGULMARG NEUTRON MONITORIII.1. Description of the neutron monitor

The neutron monitor at Gulmarg (geog. long.  $74.42^{\circ}$ , lat.  $34.07^{\circ}$ , and altitude 2743 meters) is shown schematically in figure 3.1. The author was actively involved in setting up this monitor in September 1967. The monitor is of IGY type, and consists of twenty Boron-tri-fluoride ( $\text{BF}_3$ ) proportional counters of active length 86.3 cm and diameter 3.8 cm. The counters are filled with Boron-tri-fluoride gas at pressure 45 cm of Hg and are operated at a nominal voltage  $\approx 2500$  volts with a plateau of  $\approx 100$  volts on both sides. The counters are surrounded by 5.1 cm of paraffin acting as thermalizer and then by a layer of lead bricks 5.1 cm thick. The whole assembly is enclosed by 27.9 cm thick paraffin blocks acting as reflector for neutrons of energy less than 50 MeV produced in the near by objects. This reduces the effect of the surroundings on the counting rate in the monitor. The evaporation neutrons from the interactions of the secondary cosmic rays in the lead of the monitor, are detected in  $\text{BF}_3$  counters through the reaction  $\text{B}^{10} (n, \alpha) \text{Li}^7$ , after thermalization in the paraffin surrounding the counters. The monitor at Gulmarg is operated in a room about 20 feet above the ground and having a roof of tin sheets. Further, to avoid snow-accumulation in winter the



roof is provided with a slope of  $60^{\circ}$ .

The block diagram of the monitor and associated electronics is shown in figure 3.1. The  $\text{BF}_3$  counters are divided into five sections of four counters each. The millivolt pulses from each set of four counters are amplified by a factor  $\simeq 1000$ . The pulses due to neutrons are then discriminated against the low voltage pulses due to gamma ray photons produced in the  $\text{B}^{10} (n, \alpha) \text{Li}^7$  reaction. The neutron pulses after proper shaping (rectangular pulses) are scaled down by a factor of 64 and are finally registered by electromechanical recorders. The readings of the five recorders for the five sections are photographed every hour. The total counting rate of the monitor (five sections) is  $\simeq 260,000$  counts per hour. In comparison, at high latitudes and sea level, an IQSY super neutron monitor with six  $\text{BF}_3$  counters, has a counting rate 20 times greater than in an IGY monitor of the same number of counters at that place (Hatton, 1971). However, the advantage of high counting rate of an IQSY monitor is partly derived in the Gulmarg neutron monitor by the increase in the number of counters to twenty, whereas a standard IGY neutron monitor consists of either six or twelve counters. The station also has the advantage of high altitude, giving a higher counting rate. A microbarograph of the type Nagretta and Zambra is run in the neighbourhood of the neutron monitor. The microbarograph is very sensitive and can register a minimum change of 0.2

# GULMARG NEUTRON MONITOR

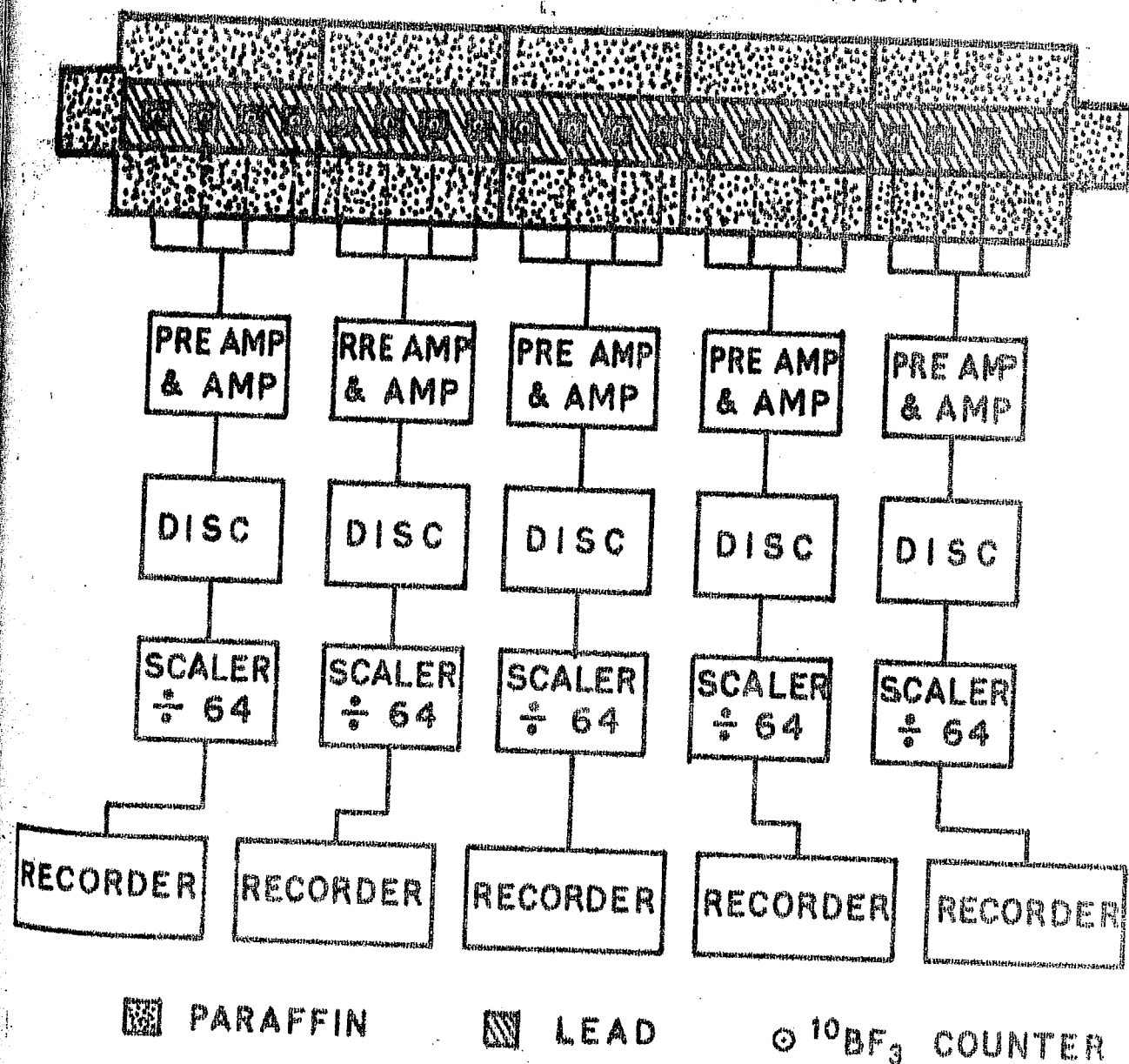
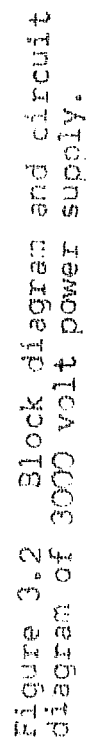


Figure 3.1 Schematic representation of Gulmarg neutron monitor and the block diagram of associated electronic circuits.

millibars and gives a deflection of one centimeter on the chart for a change of atmospheric pressure of 1 millibar. An electromagnet lifts the pen of the microbarograph, once in 30 minutes to remove the effect of friction between the pen and the paper chart. The uncertainty in the pressure correction of the monitor counting rates is then about 0.15%, while the standard error in the hourly counting rates is about 0.2% giving a total uncertainty of  $\approx 0.25\%$ . The complete power to the neutron monitor is provided by lead batteries since the mains supply has many breaks. The batteries are put on a floating charge and various voltages derived from them through DC-DC converters. The voltages needed are 2500V, 12V, -6V, -12V, -24V. The details of the power supplies giving these voltages are described below.

## II.2 3000 Volt Power Supply for the neutron monitor

For the continuous operation of the monitor, a battery operated transistorized power supply with output voltage varying between 1800 volts to 3000 volts at a maximum output current of 1 ma, has been designed and built by the author. Figure 3.2 shows the block diagram as well as circuit diagram of the high voltage power supply. A series voltage regulator (A) stabilizes the 24 volts from two accumulators to 18 volts. Another voltage regulator (B) in cascade to (A) drives the magnetically coupled multivibrator oscillating at a frequency  $\approx 5$  KHz and operating at a current



$\approx 0.7$  amp. The multivibrator produces square wave pulses in voltage, which are amplified to  $\approx 435$  volts r.m.s. by a transformer. This is followed by a full wave voltage multiplier consisting of rectifying diodes and gives a multiplication factor of 3. The multiplier has an efficiency of  $\approx 80\%$  at 1.5 ma current output. The output of the voltage multiplier is filtered through an RC inverted L type filter of three sections. A small factor of the output voltage of the power supply is derived from the bleeder at the output end and is sampled through an operational amplifier for self regulation against load changes by adjusting the input voltage to the magnetically coupled multivibrator.

The power supply has a ripple of less than one millivolt, a necessary condition to detect the millivolt neutron pulses from the  $\text{BF}_3$  counters in the neutron monitor. Temperature stability of the power supply is  $\approx 0.75$  volts per degree centigrade, which is attained by inserting compensating diodes of diffused junction type in series with the temperature sensitive components like zener diode in the voltage regulator (B) and in the emitter circuit of the operational amplifier.

A current limiter circuit is provided in the first voltage regulator (A) against short circuit protection. The two zener diodes connected in opposition across the tapping on the bleeder, inhibit very large changes in the

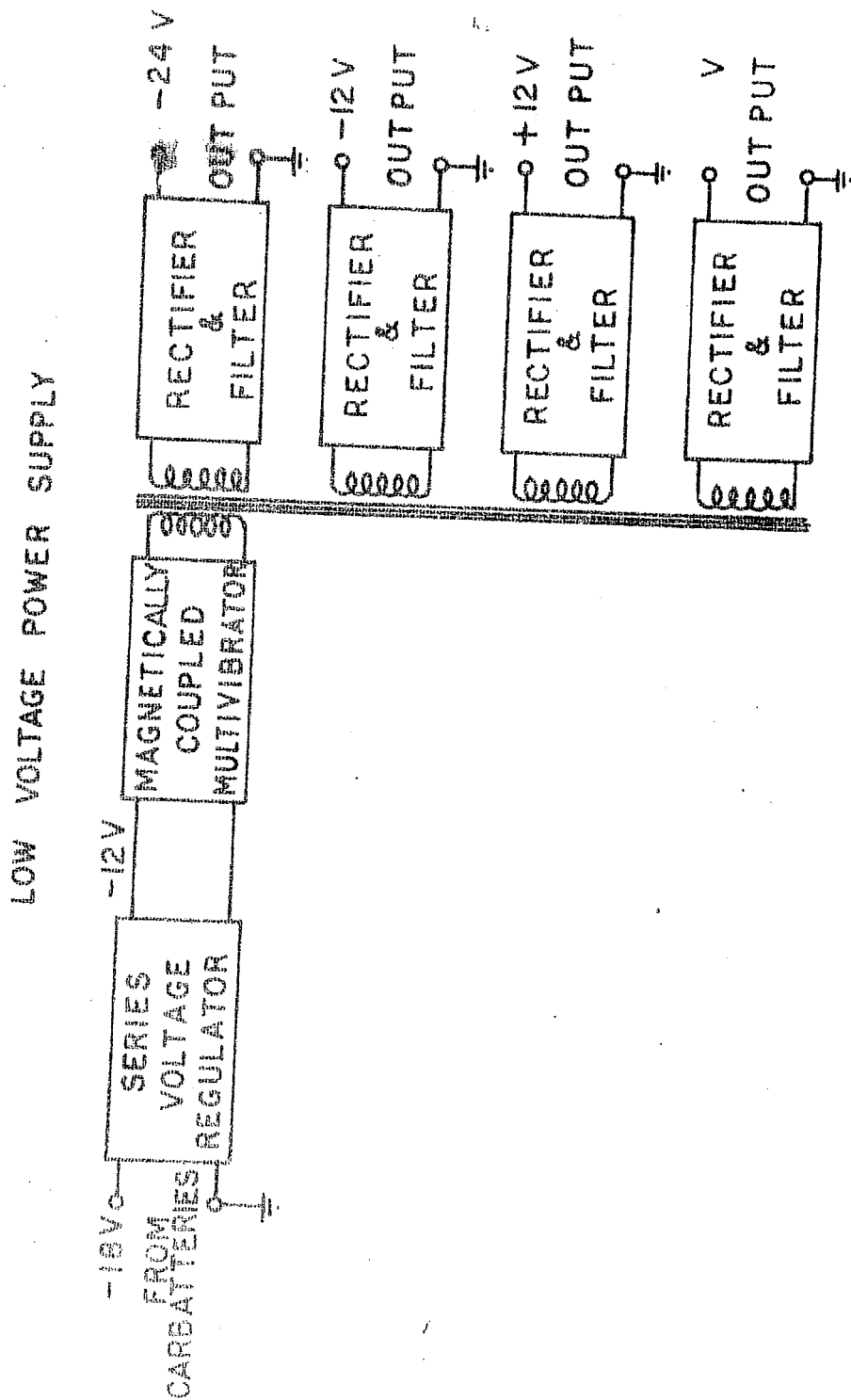
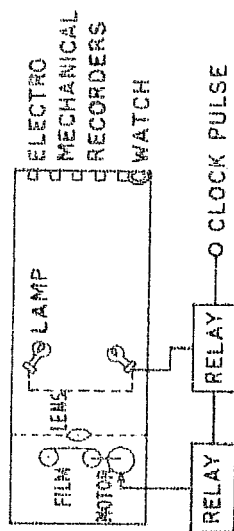


Figure 3.3 Low voltage power supply to derive -24V, -12V, -6V, +12V.

## CAMERA CONTROL CIRCUIT



## CLOCK CIRCUIT

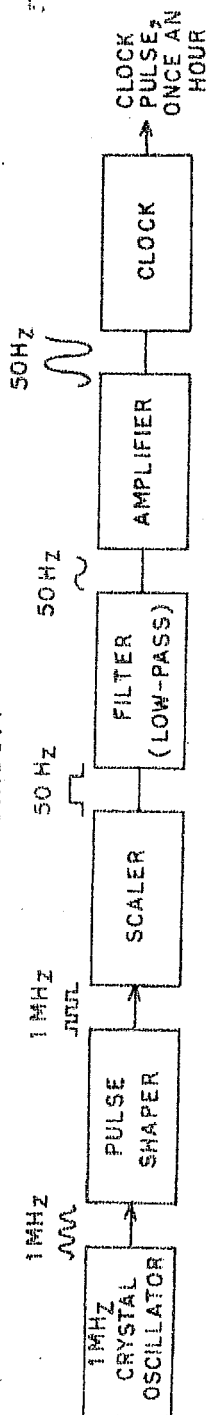


Figure 3.4a Relay operated camera to record neutron monitor counting rates on photographic film.

Figure 3.4b Block diagram of the clock circuit to operate the relay operated camera.

output voltage (like shorting of the output) through the fast feed back condenser from the output end of the bleeder to the tapping, being passed to the voltage regulator (B) and the magnetically coupled multivibrator through the operational amplifier. In addition to this, two other zener diodes of threshold voltages slightly higher than the maximum operating voltage of the magnetically coupled multivibrator, are connected in opposition across the input of the multivibrator, as a precaution against sudden large transients in the circuit, if any.

### III.3. Low Voltage power supplies

The various voltages (-12V, +12V, -6V, -24V) have been derived from a single DC-DC converter. The converter works on -12 volts derived from an electronic voltage regulator running on 18 volt batteries. The magnetically coupled multivibrator in this converter has various secondary AC outputs. The AC voltages at these terminals are rectified and filtered to obtain the various DC voltages. This is illustrated in the block diagram shown in figure 3.3.

### III.4. Camera Control and the clock circuit

The scaled down neutrons pulses are stored in the electromechanical recorders, which are photographed every hour. The camera control circuit employed for this purpose is shown in the figure 3.4 a. At the end of every hour,



a clock pulse triggers the relay circuit and puts the lights in the camera on for a predetermined period ( $\approx 1$  second). The photographic film is exposed during this interval to record the readings of the recorders. At the end of this period, another relay winds the film and keeps the camera ready for next operation. The block diagram of the clock which monitors the time, is shown in figure 3.4 b. An electronic crystal oscillator gives pulses at a frequency of 1 MHz. These are appropriately scaled down to square pulses at a frequency of 50 Hz. The shape of the pulses is then transformed into sine wave form, which is amplified to 220 volts AC by a transformer to run the electrical clock. The minute hand of the clock operates a relay at the end of every hour which sends a signal to the camera control circuit. The accuracy of the clock is of the order of a few seconds in a day.

## C H A P T E R    I V

### NEUTRON MULTIPLICITY MEASUREMENTS IN GULMARG NEUTRON MONITOR

#### IV.1. Introduction

A cosmic ray particle interacting in the lead of the monitor produces multiple evaporation neutrons, which are detected in the  $\text{BF}_3$  proportional counters after thermalization in the paraffin surrounding the counters. The rate  $N_i$  at which neutrons are detected by the monitor in response to a particular component of the secondary cosmic radiation is proportional to the product of the intensity  $I_i$  of the  $i^{\text{th}}$  component, the probability  $P_i$  that it will interact in the monitor,  $\nu_i$  the average number of neutrons produced in each interaction and  $\epsilon$  the efficiency of neutron detection by  $\text{BF}_3$  counters (Hughes and Marsden, 1966).

Thus

$$N_i = I_i \cdot P_i \cdot \nu_i \cdot \epsilon \cdot A \quad \dots(4.1)$$

where  $A$  is the horizontal surface area of the monitor.

Hughes and Marsden conclude that, in a standard IGY neutron monitor,  $31.3 \pm 2.4\%$  of the detected neutrons can be attributed to neutron interactions,  $11.2 \pm 1.1\%$  to proton interactions,  $6.8 \pm 1.2\%$  to captured muons and less than 1% to the combined effects of muons in flight, pions and the various components of extensive air showers.

Multiplicity of neutron production in a neutron monitor is a function of energy of the particle initiating

the interaction (Cocconi et al., 1950; Geiger, 1956; Hughes et al., 1964; Hughes and Marsden, 1966 and Schen, 1968). The multiplicity increases with energy of the interacting particle and hence the multiplicity spectrum is expected to be related to the energy spectrum of the secondary cosmic radiation in the atmosphere. An attempt is made here to investigate the possibility of using changes in the multiplicity spectrum measurements to study the secondary and hence primary cosmic ray spectrum during disturbed periods like Forbush decreases and solar flare increases, from a single station like Gulmarg. A multiplicity meter was therefore, incorporated in the monitor at Gulmarg for the period October 1967 - October 1971, to measure the neutron multiplicity in the pile. The experimental set up is described below. Eventhough the neutron monitor at Gulmarg has 20 Boron-tri-fluoride counters, the continuous multiplicity measurements are restricted to only 12 counters of the pile. The preliminary results of the multiplicity recordings at Gulmarg have been published earlier (Bemalkhedkar et al., 1967; Bemalkhedkar and Kaul, 1969).

#### IV.2. Neutron multiplicity meter

The block diagram of neutron multiplicity meter developed by the author is shown in figure 4.1. The multiplicity meter receives neutron pulses from twelve  $\text{BF}_3$  counters of the monitor, which appear as a train of pulses

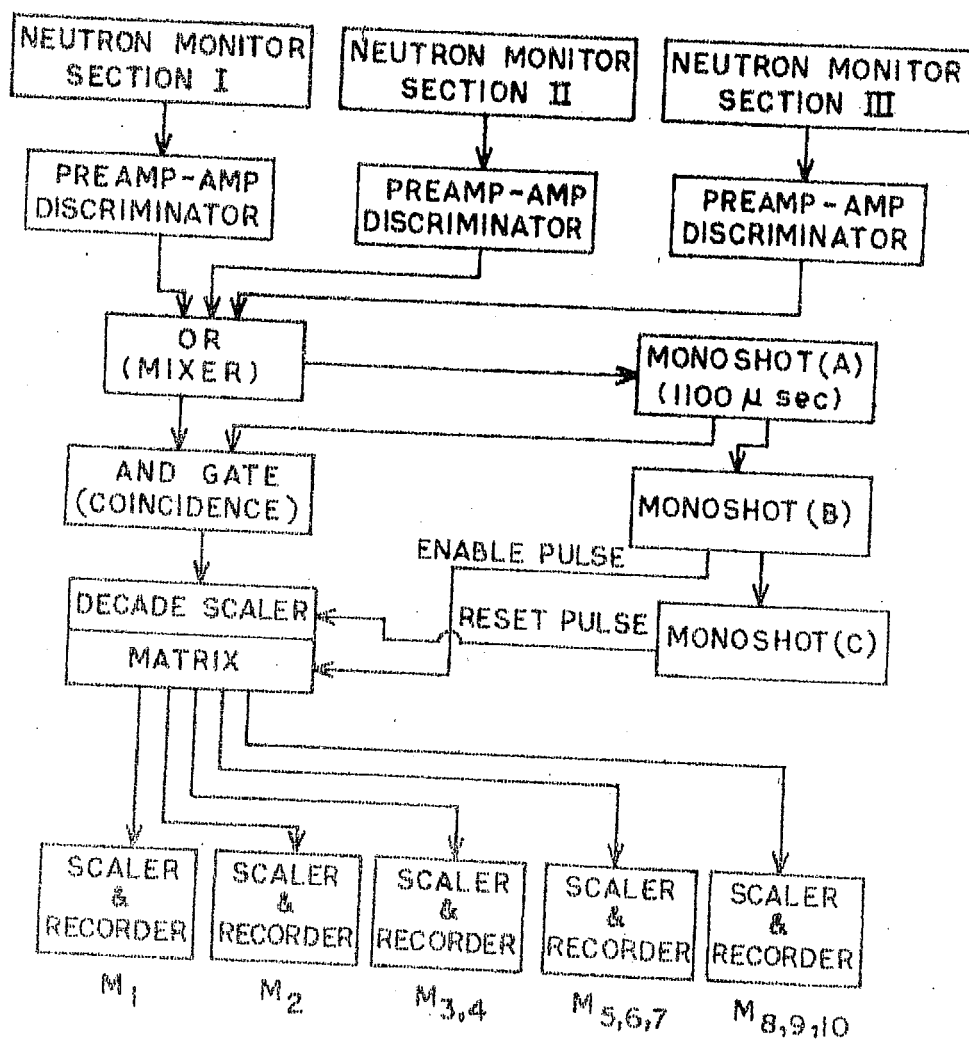


Figure 4.1 Block diagram of neutron multiplicity meter.

AMPLIFIED NEUTRON PULSES FROM THREE  
SECTIONS (I, II, III) IN THE MONITOR

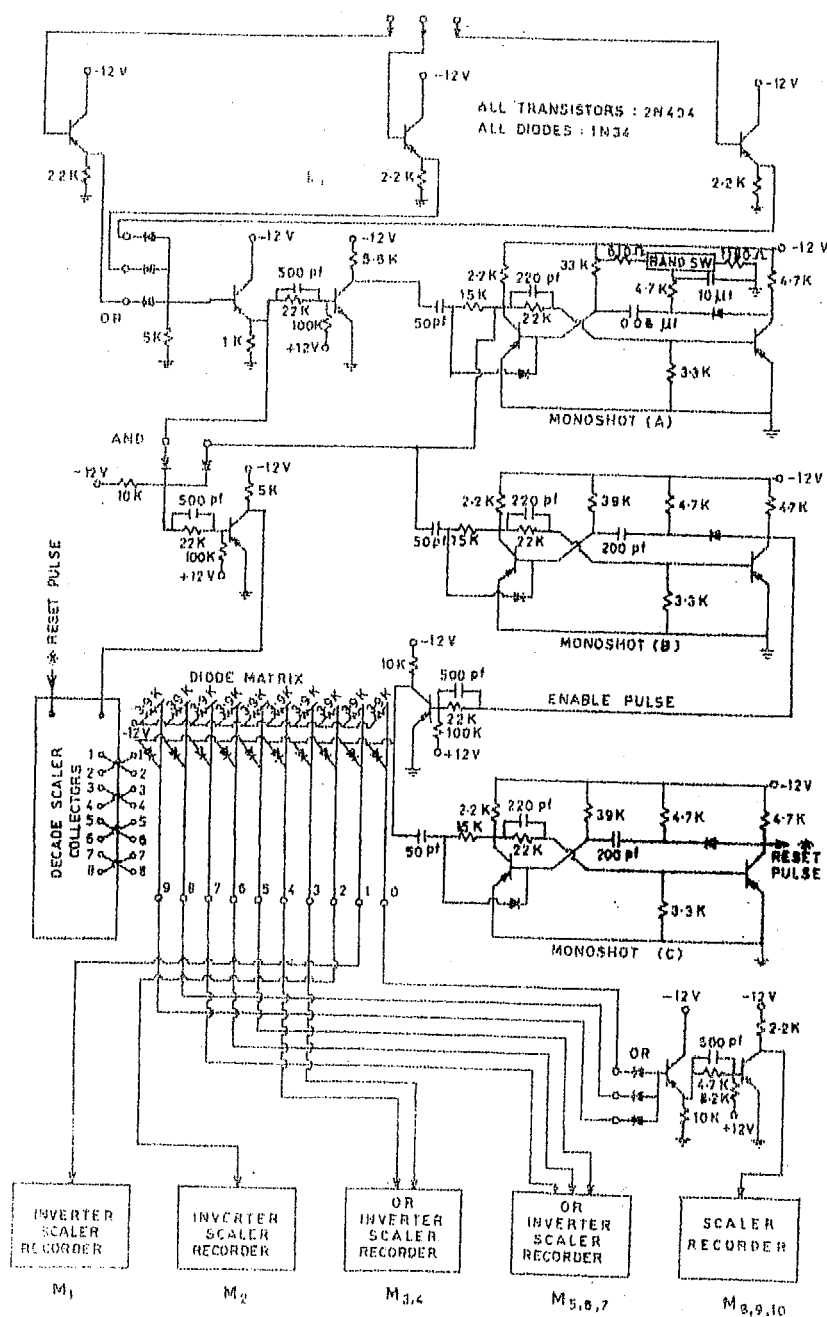


Figure 4.2 Circuit diagram of  
neutron multiplicity meter.

due to each individual interaction in the monitor. The pulses are amplified, shaped, and then fed to the input OR gate after discrimination against gammas. The first pulse in a group after passing through the OR gate triggers a monostable multivibrator (A) which opens an AND (coincidence) gate, hereafter referred to as 'Gate'. The subsequent pulses, as well as the Gate-opening pulse, are passed through the Gate, till it remains open. Selection of the appropriate Gate-width is discussed in the section (IV.4). The number of pulses received during the Gate-time is termed the multiplicity of the event. The pulses received in an event are then stored in a decade scaler, which are then identified in an associated diode matrix after the Gate is closed. This is achieved by an Enable pulse from the monostable multivibrator (B) triggered by the trailing edge of the Gate-pulse. Similarly, the trailing edge of the Enable pulse, triggers another monostable multivibrator (C), which resets the decade memory for the recording of the next event. The enable pulse transfers the information to a particular output channel in the matrix corresponding to the number of neutrons detected during the Gate-time. Though the circuit is able to record the multiplicities individually, they have been grouped, for the convenience of recording, as  $m_1$ ,  $m_2$ ,  $m_{3,4}$ ,  $m_{5,6,7}$  and  $m_{8,9,10}$ . The hourly counting rates in these groups, after proper scaling (256, 32, 16, 2, 2 respectively), are recorded in electromechanical recorders

and are photographed on the same photographic film that is used to record counting rates in the five sections of the neutron monitor. Actual circuit diagram of the neutron multiplicity meter is shown in figure 4.2.

#### IV.3. 'Bunch pulser' for continual checking of neutron multiplicity meter

The long term operation of the neutron multiplicity meter needs continual checking to ensure its proper functioning. The author has designed and built a 'Bunch pulser' (Bemalkhedkar, 1969) simulating the input pulses to the neutron multiplicity meter. In the present case, the Bunch pulser was designed to meet the following specifications: (i) output in the form of groups of pulses, (ii) number of pulses in a group to vary between one and ten, (iii) frequency of pulses between 10 KHz to 40 KHz, (iv) group repetition frequency between 200 Hz to 1000 Hz and (v) the first pulse in a group to be synchronized with the group repetition period. However, the design of the Bunch pulser has incorporated circuits whereby many of the characteristics can be altered beyond the limits specified, making the design general in character.

Figure 4.3 shows the block diagram of Bunch pulser. The astable multivibrator (A) generates square pulses at frequencies between 200 Hz to 1000 Hz. The monostable multivibrator (B) triggered by (A) feeds a pulse of duration

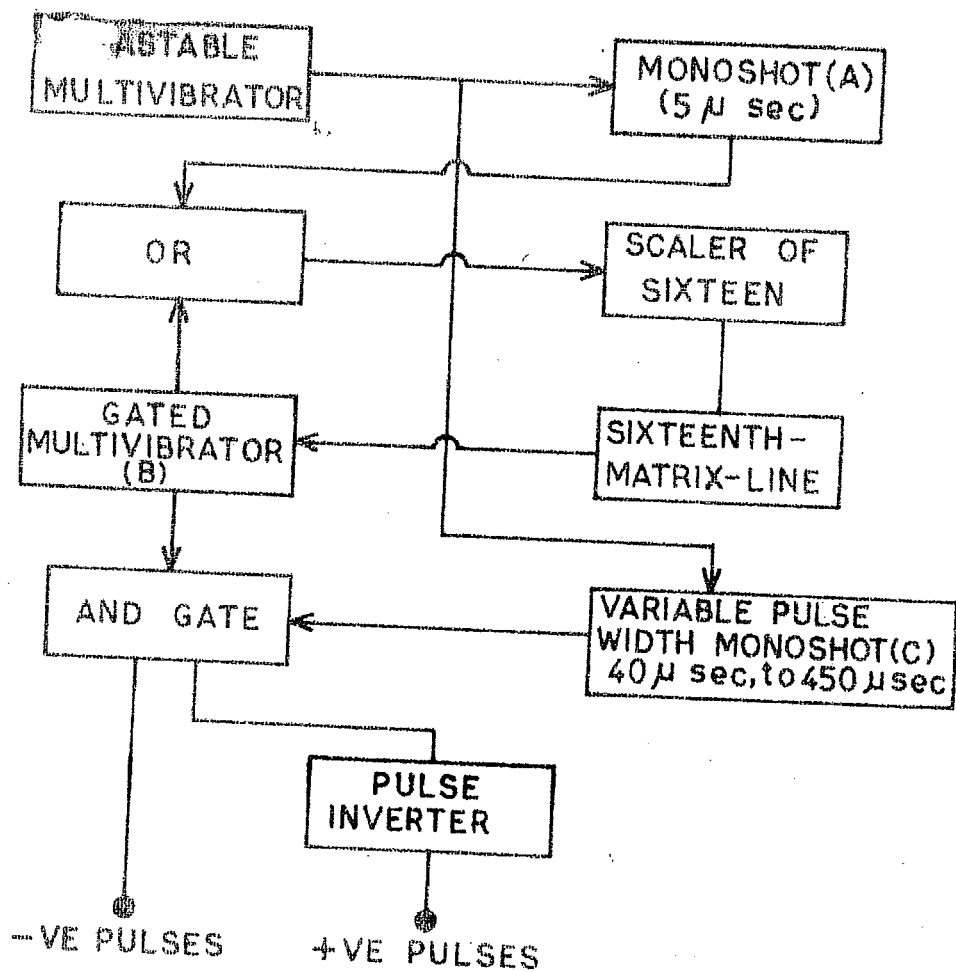


Figure 4.3 Block diagram of 'Bunch pulser'.



# BUNCH - PULSER

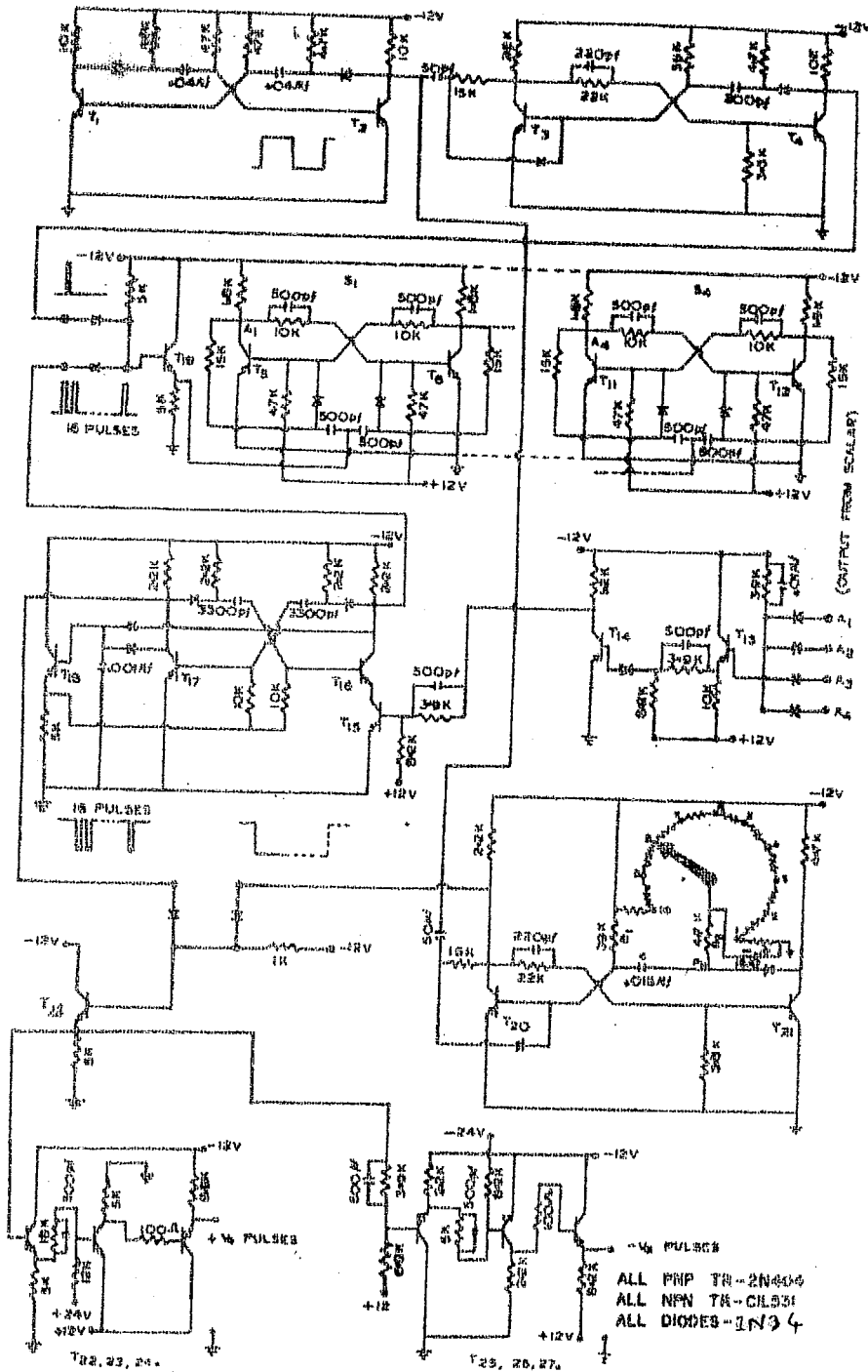


Figure 4.4a Circuit diagram of 'Bunch pulser'.

VARIABLE - PULSE - WIDTH - MONOSHOT (C)

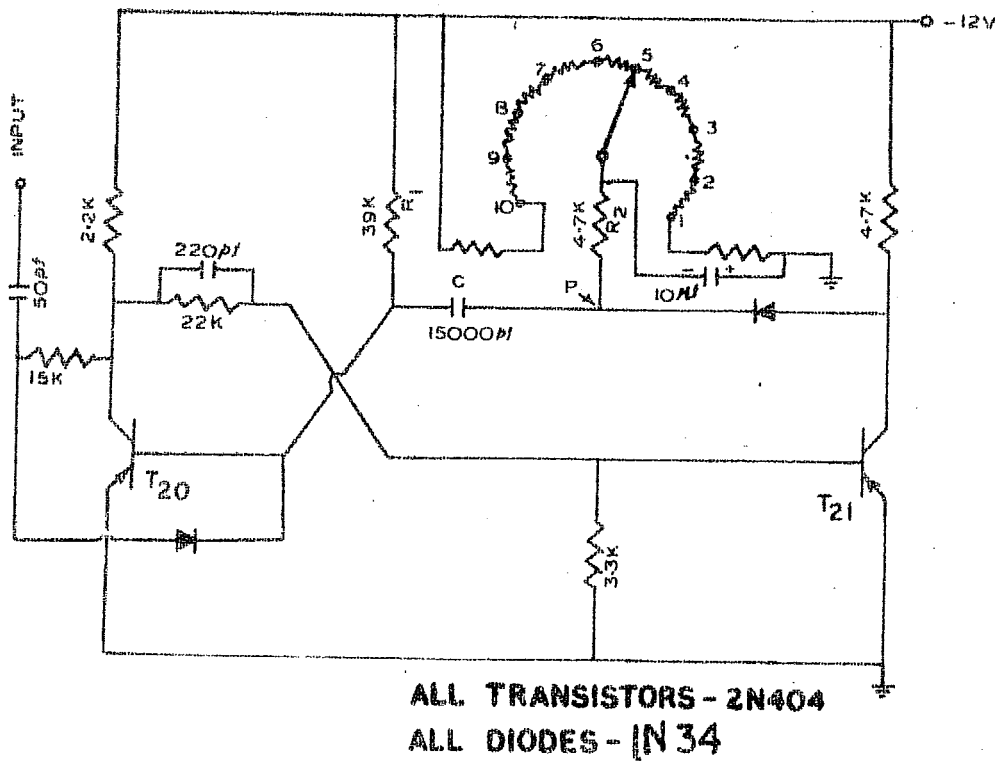


Figure 4.4b Variable pulse-width  
monoshot (c)

$\approx$  5 microseconds to a scaler of sixteen through an OR gate. The logic output corresponding to 0000 condition of the scaler controls the gated astable multivibrator (C). The change in 0000 condition of the scaler by a pulse from monostable multivibrator (B) starts the oscillations in the gated multivibrator (C) producing square wave pulses at a preselected frequency between 10 KHz to 40 KHz. These pulses are fed back to the scaler through the above mentioned OR gate. Thus the gated multivibrator oscillates 15 times, and stops when the scaler returns to 0000 condition and awaits for the scaler to be disturbed again from this condition by the next pulse from the astable multivibrator (A). To get a variability in the number of pulses in a group, the output of the gated multivibrator is further gated by a pulse of variable time width in synchronization with the pulse from the astable multivibrator (A). This is achieved by triggering another monostable multivibrator (D) whose pulse width is controlled by the height of the pulse fed to the base of the conducting transistor in it. Finally, the bunch pulser gives groups of pulses of either polarity, while the group repetition frequency can also be derived from an external source. The actual circuit diagram of 'Bunch pulser' is shown in figure 4.4.

#### IV.4. Corrections of the multiplicity counting rates for chance coincidence and life time of neutrons in the monitor

The neutron multiplicity spectrum measured by the multiplicity meter has to be corrected for two inherent effects, (1) the probability that the neutrons from different multiplicity events will overlap within the Gate-time (overlapping effect) and (2) the probability that some of the subsequent neutrons produced in an event pass over the Gate-time and are recorded as two or more events (Overpassing effect). Though both of these effects are important in an NM-64 superneutron monitor (Fujii et al., 1972), only the overlapping effect predominates in an IGY neutron monitor (Niemi, 1966 and Debrunner and Walther, 1968). Following the method due to Debrunner and Walther (1968), the corrected counting rates  $N_m^*$  in the various multiplicities can be expressed in terms of the uncorrected counting rates  $N_m$ , the corrected counting rates in the lower multiplicities, the gate time  $T$  and the average probabilities  $\bar{w}_l^k$  of detecting  $l$  neutrons out of the  $k$  produced as,

$$N_m^* = \left\{ 1 - T \sum_{i=1}^{\infty} N_i \right\} \cdot \left[ N_m - \sum_{n=1}^m N_n^* T \cdot \sum_{j=m-n}^{\infty} N_j \bar{w}_{(m-n)}^j \right. \\ \left. - N_1^* T^{(m-1)} \cdot \sum_{j=1}^{\infty} (N_j \bar{w}_1^j)^{m-1} \right. \\ \left. - \left\{ N_1^* T^{(m-1)} \right\} \cdot \prod_{i=1}^{(m-1)} \cdot \sum_{j=1}^{\infty} N_j \bar{w}_1^j \right] \dots (4.2)$$

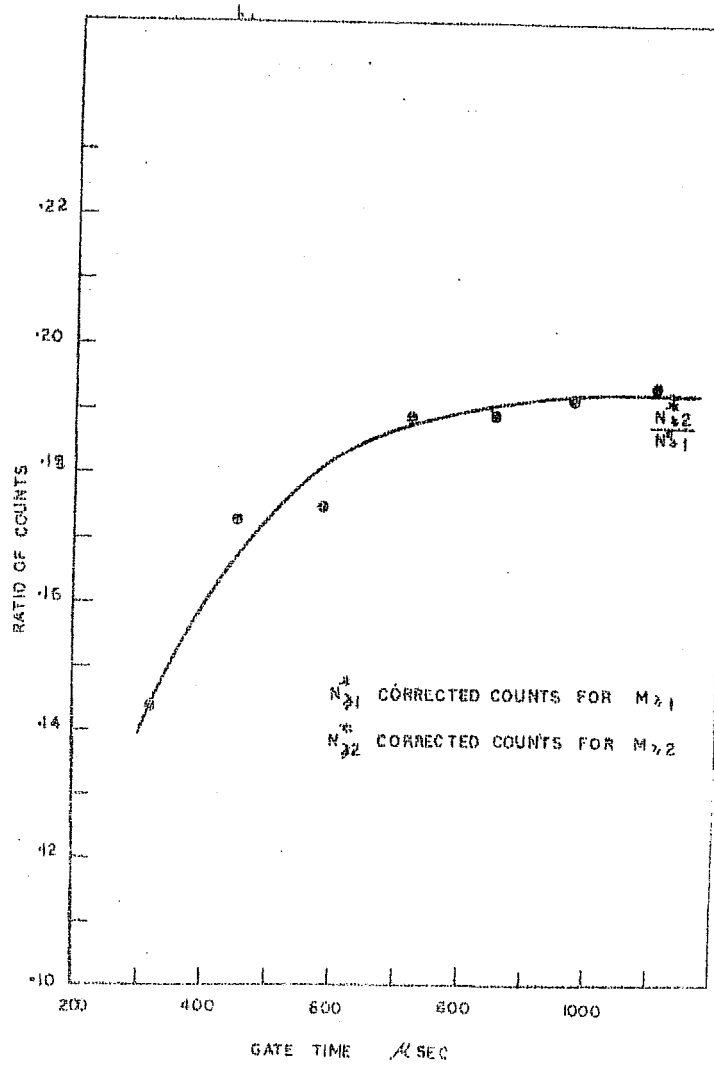


Figure 4.5 Plot of  $N_{\geq 2}/N_{\geq 1}$  against Gate-width of neutron multiplicity meter for selection of appropriate Gate-width.

In the present case, the summations involving infinite number of terms <sup>are carried</sup> out up to  $i, j = 10$  since the data are obtained only upto  $m = 10$ . The contribution due to higher multiplicities decreases continuously. Further, none of the summations in the larger bracket are applicable for  $m = 1$  but only for  $m \geq 2$ .

The above equation can also be used to estimate the proper Gatewidth  $T$  of the neutron multiplicity meter, which will not under estimate a high multiplicity event due to overpassing effect. Following Debrunner and Walther (1968), we have plotted, the ratio  $N_{\geq 2}^* / N_{\geq 1}^*$  against the Gate-width in figure 4.5, where  $N_{\geq 1}^*$  is the counting rate for multiplicity  $m_1$  and greater and  $N_{\geq 2}^*$  that for  $m_2$  and greater, which are corrected for chance coincidences and effects of neutron life time in the monitor. The ratio attains saturation after a Gate-width of about 1100 microseconds indicating it to be sufficient to count neutrons in a multiple event. Based on these experimental results, we have chosen 1100 microseconds as the Gate-width for all subsequent recordings. A period of about 10 microseconds lapses between the time of the closing of the Gate and the time when the circuit is set ready to record the next event. The probability of occurrence of next event during these 10 microseconds is very small and therefore does not introduce any significant error in our multiplicity recordings.

#### IV.5. Neutron multiplicity spectrum and the mean multiplicity

A typical neutron multiplicity spectrum at Gulmarg, corrected for chance coincidence and neutron life time effects, is presented in figure 4.6. The figure also shows for comparison the spectra obtained by Hughes and Marsden (1966), Kodama and Ishida (1967) and Agrawal et al. (1969). All these spectra have similar form and are curved on the semilogarithmic plot, which shows that the neutron production spectrum in the monitor is not of simple exponential form (Gieger, 1956).

The mean neutron multiplicity is derived from the relation,

$$\bar{m} = \frac{\sum_{m=1}^n m \cdot N_m^*}{\sum_{m=1}^n N_m^*} \quad \text{--- (4.3)}$$

where  $N_m^*$  is the corrected counting rate in the multiplicity  $m$ , and  $n$  is the highest multiplicity recorded. The typical multiplicity spectrum at Gulmarg shown in figure 4.6, yields the mean neutron multiplicity

$$m = 1.398 \pm .003$$

Hughes and Marsden (1966) have estimated theoretically the multiplicity rates  $N_m^*$  in Leeds IGY neutron monitor for a given secondary nucleonic energy spectrum divided into six energy intervals: 0.1 GeV, 0.1-.3 GeV, 0.3-1 GeV, 1-3 GeV, 3-10 GeV and  $>10$  GeV. From these spectra, they

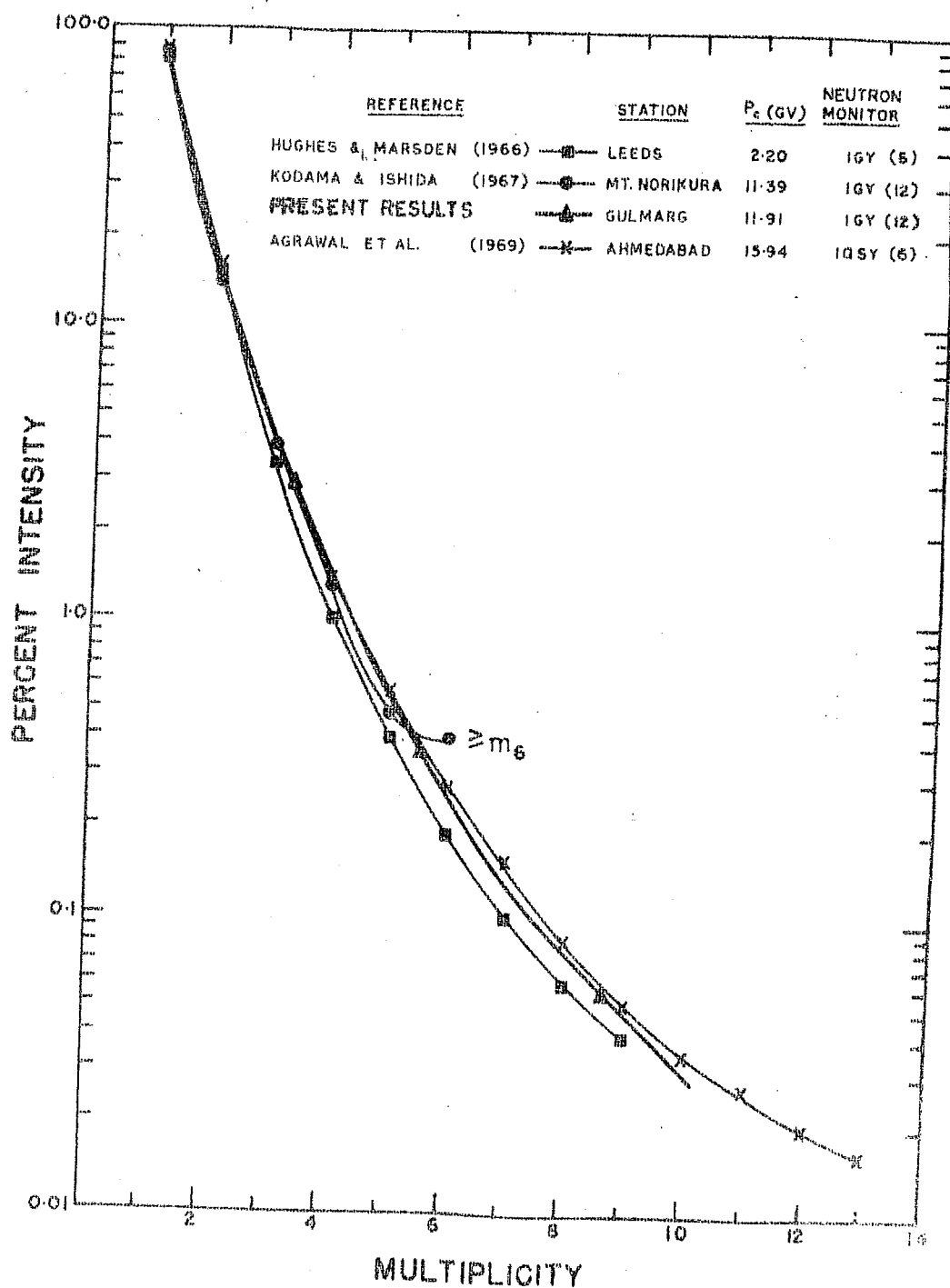


Figure 4.6 A typical neutron multiplicity spectrum in Gulmarg neutron monitor, corrected for chance coincidence and neutron life time effects. The figure also shows the spectra obtained by Hughes and Marsden (1966), Kodama and Ishida (1967) and Agrawal et al. (1969) and the number of  $\text{BF}_3$  counters used (numbers in bracket).



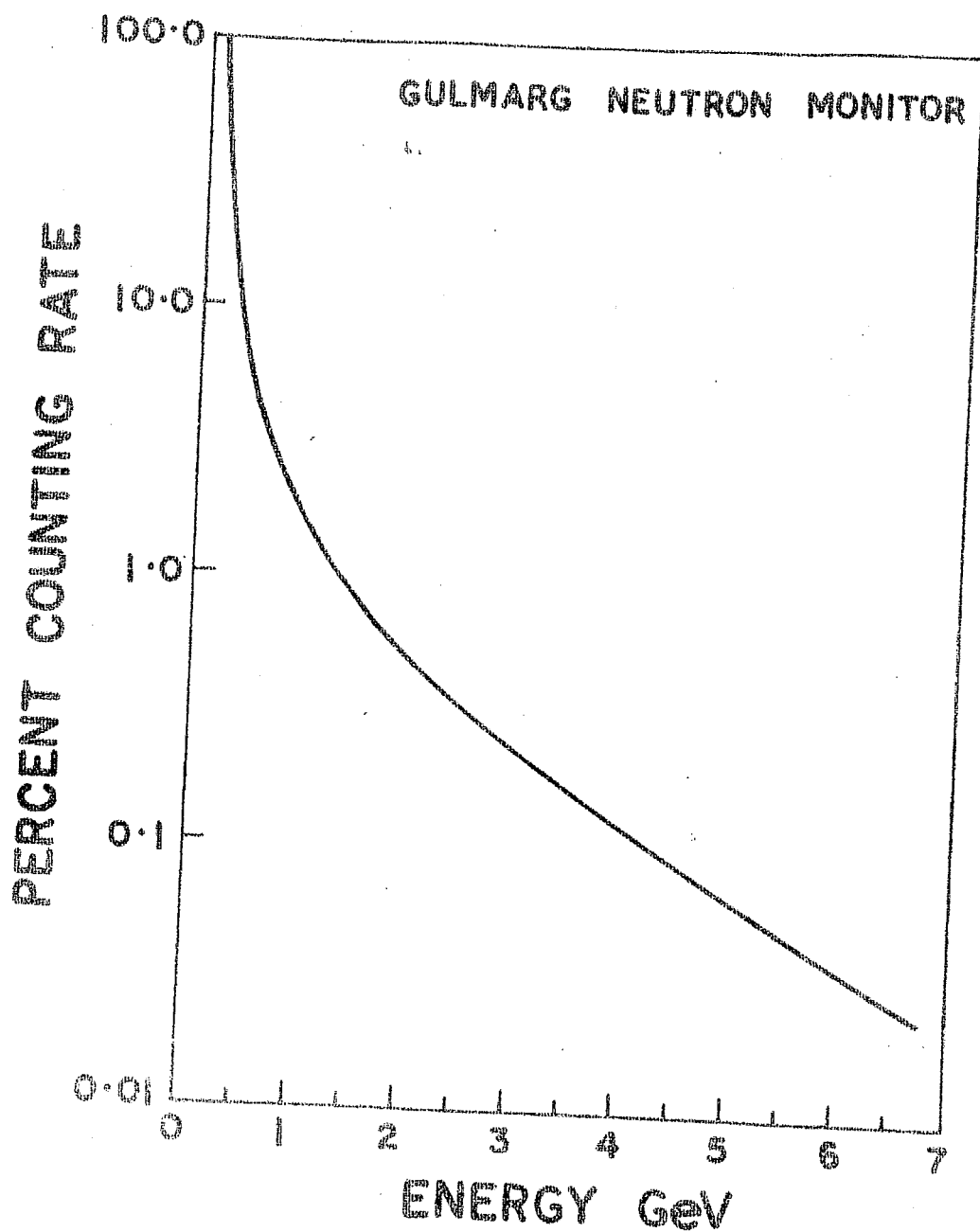


Figure 4.7 The energy spectrum of secondary cosmic ray nucleons recorded by Gulmarg neutron monitor.

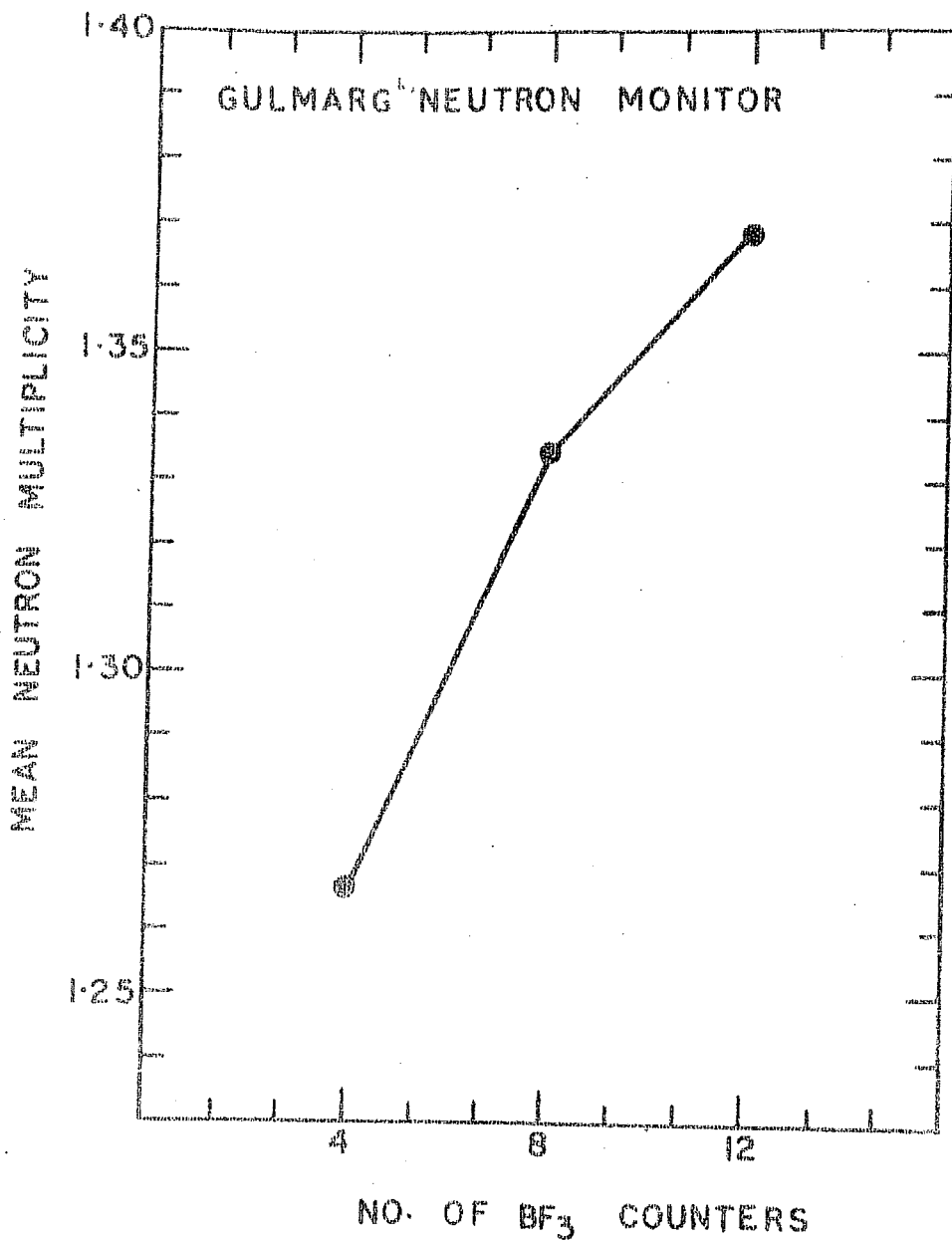


Figure 4.8 Variation of mean multiplicity with number of  $\text{BF}_3$  counters in Gulmarg neutron monitor.

have evaluated the median energies of secondary cosmic ray nucleons corresponding to various multiplicities upto  $m = 9$ . By using these results, the energy spectrum of secondary cosmic ray nucleons at Gulmarg is derived from the observed multiplicity spectrum. The energy spectrum is shown in figure 4.7 and has a form  $\sim E^{-2.3}$ . The exponent can be compared with the average energy spectrum of secondary cosmic rays  $E^{-2.5}$  measured in balloon experiments (Hess et al., 1959, Simpson and Hopper, 1971).

A study has also been made to investigate the mean multiplicity for different number of counters in the Gulmarg neutron pile. The mean multiplicity is found to increase with the number of counters as shown in figure 4.8. The increase in the mean multiplicity results from the enhanced probability of detecting neutrons, which are produced in a single interaction taking place in the total area presented by the lead surrounding the counters. The result is important in comparing the mean multiplicities from other monitors with different number of counters.

#### IV.6 Latitude and altitude variation of mean multiplicity

The mean multiplicity  $\bar{m}$ , being determined by the energy spectrum of secondary cosmic ray nucleons impinging upon the monitor, is known to be a function of the geomagnetic latitude. The latitude variation in the mean multiplicity at sea level has been studied through

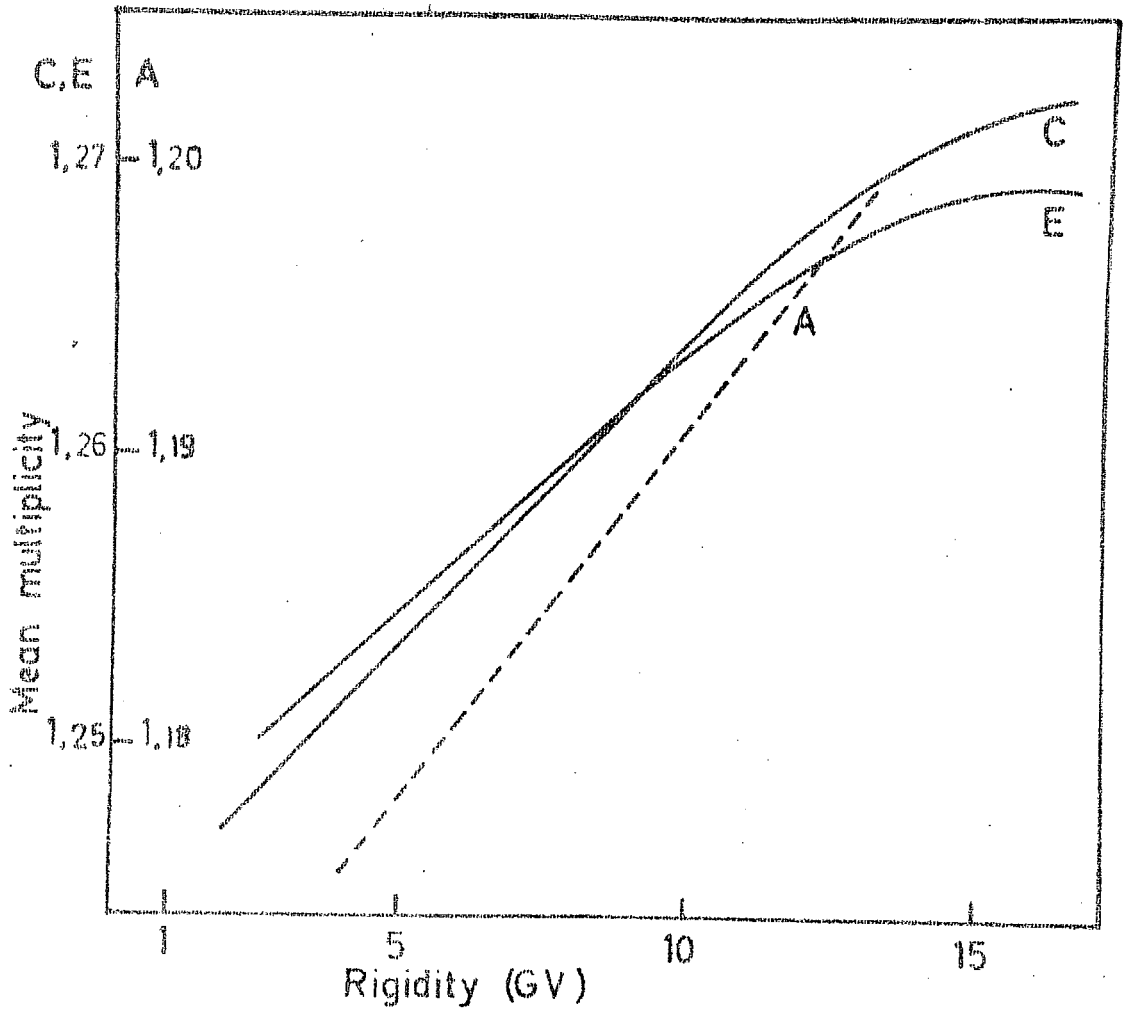


Figure 4.9 Latitude variation of the mean multiplicity in an IGV neutron monitor (Dyring and Sporre, 1966) in different surveys.

shipborne surveys by Dyring and Sporre (1966), Kodama and Ohuchi (1968), Kodama and Inoue (1970a) and Iucci et al. (1971). A similar survey at airplane altitudes has been conducted by Kent et al. (1968). Figure 4.9 shows an example of variation in the mean multiplicity in an IGY neutron monitor, as a function of geomagnetic cutoff-rigidity during the shipborne survey by Dyring and Sporre (1966); the mean multiplicity increasing with the cutoff-rigidity. The mean multiplicity is also known to be a function of the number of counters in the neutron pile as well as its geometry as shown in section IV.5 and also by Kodama and Ishida (1967) and Kodama and Inoue (1970).

Table 4.1 presents the mean multiplicities in different neutron monitors obtained by various authors [Hughes and Marsden, 1966; Kodama and Ishida, 1967; Bachelet et al., 1968; Debrunner and Walther, 1968; Kent et al., 1968; Agrawal et al., 1969; and Kodama and Inoue, 1970]. The table also lists relevant station parameters. In this section a normalized mean multiplicity value has been arrived at for individual IGY neutron monitors by correcting for the latitude effect and the number of counters used for studying the altitude variation in the mean multiplicity. Such normalizations have not been attempted for IQSY NM-64 monitors since the mean multiplicities in them are available only at sea level. The mean multiplicity ( $\bar{m}$ ) values in the various IGY neutron monitors have been normalized to

Table 4.1

Mean neutron multiplicity in various IGY neutron monitors. The last column ( $\bar{m}'$ ) indicates the value normalized to twelve BF<sub>3</sub> counters at the latitude of Gulmarg with cutoff rigidity 11.91 GV.

Reference	Station	Vertical cutoff rigidity (GV)	Geographic coordinates Lat. Long.	Altitude meters	No. of BF <sub>3</sub> counters	Mean neutron multiplicity $\bar{m}$	$\bar{m}'$
Bachellet et al. (1968)	Uppsala	1.43	59.85°N 17.58°E	25	6	1.215	1.299
Hughes and Marsden (1966)	Leeds	2.20	53.83°N 1.5°W	100	6	1.229	1.312
Debrunner and Walther (1968)	Jungfraujoeh	4.48	46.50°N 8.00°N	3550	12	1.321	1.406
Kodama and Ishida (1967)	Mt. Norikura	11.39	36.12°N 137.55°E	2770	12	1.360 ± 0.002	1.361
Kodama and Ishida (1967)	Itabashi	11.50	35.67°N 139.75°E	20	6	1.220 ± 0.002	1.286
Present result	Gulmarg	11.91	34.07°N 74.42°E	2743	12	1.398 ± 0.003	1.398

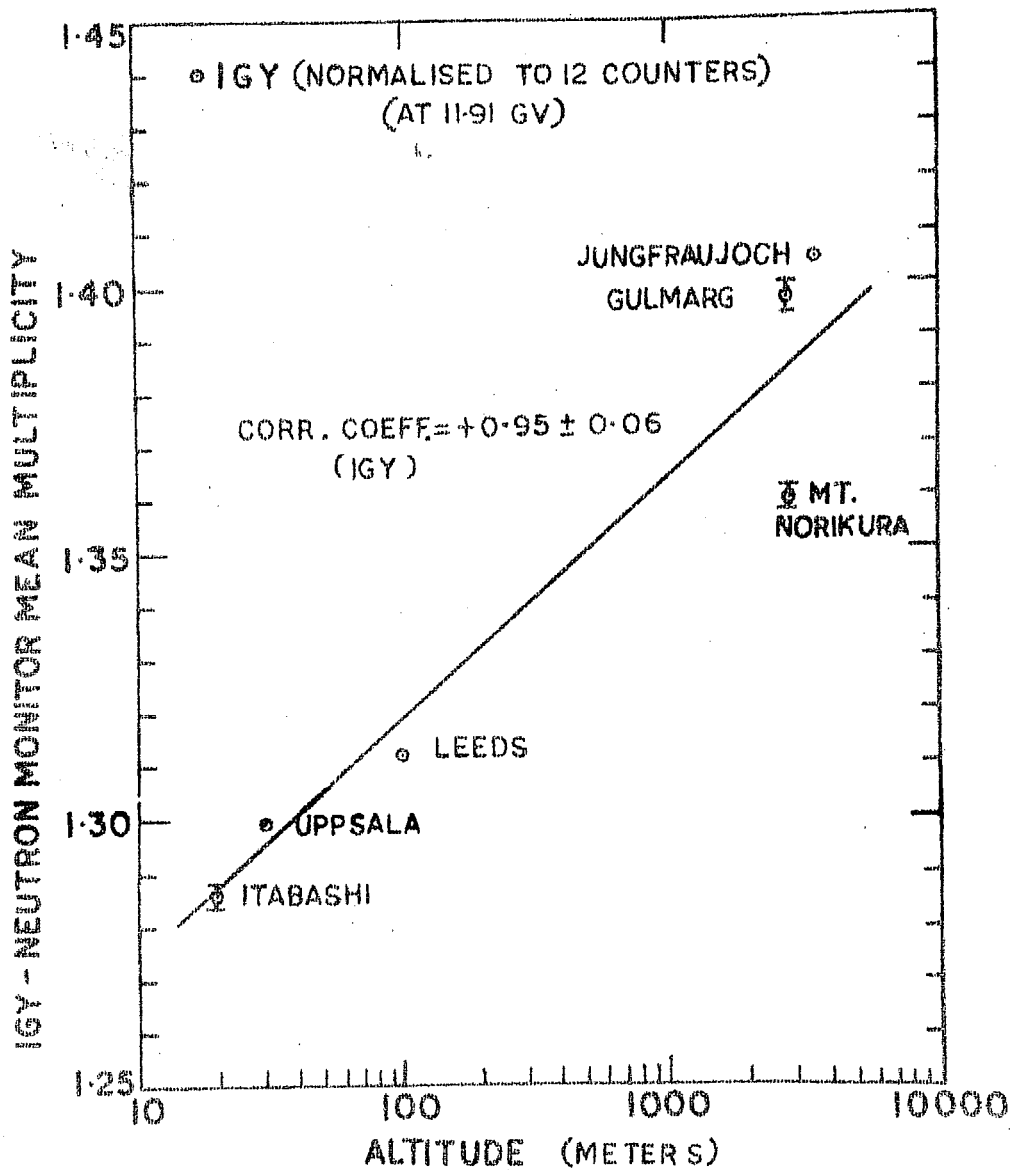


Figure 4.10 Altitude dependence of mean multiplicity in IGY neutron monitors.

Gulmarg latitude as well as to the number of counters used there i.e. 12. These normalized values are expected to be a function of only the altitude of the station now and in figure 4.10 are presented these normalized values ( $\bar{m}'$ ) as a function of altitude. The figure shows that the mean multiplicity  $\bar{m}$  increases linearly with logarithm of the altitude upto  $\simeq 3000$  meters above sea level. The regression analysis gives a correlation coefficient of  $0.95 \pm 0.06$ .

The regression equation is of the form,

$$\bar{m}' = (0.020 \pm 0.003) \cdot \log(h) + (1.23 \pm 0.02) \quad \text{---(4.4)}$$

where  $h$  is the altitude in meters.

Kodama and Ishida (1967) have also shown that the mean multiplicity in a 6 counter IGY neutron monitor increased from  $1.220 \pm 0.002$  at sea level (Itabashi) to  $1.324 \pm 0.002$  at 2770 meters altitude (Mt. Norikura) as indicated in table 4.1. The present quantitative analysis incorporating large number of neutron monitors has given the functional form of the variation.

The decrease in the mean multiplicity with an increase in the atmospheric depth indicates that the differential energy spectrum of the secondary cosmic ray nucleons steepens with an increase in the atmospheric depth. The actual balloon observations of the secondary nucleonic spectrum in the GeV range, show that the form of the spectrum is similar for neutrons as well as protons and that it also steepens with



the atmospheric depth in agreement with the above observations (Baradzei, 1951; Mylroi and Wilson, 1951; Meshkovskij and Sokolov, 1957; Kocharian et al., 1958; and Simpson and Hopper, 1971). The results may be explained as due to the preponderance of pions over the nucleons produced in nuclear interactions above 1 GeV energy of the interacting nucleon, causing reduction in the high energy secondary nucleon flux compared to that in the primary cosmic rays. The secondary nucleons above 1 GeV produce further interactions in the atmosphere and thus cause a continuous reduction in the high energy nucleonic flux all the way to sea level leading to steepening of the secondary nucleonic spectrum (Hayakawa, 1969).

#### IV.7 Multiplicity spectrum during Forbush decreases

A study of the multiplicity spectrum during Forbush decreases has been made for two Forbush decreases occurring on October 29, 1963 and November 7, 1970. The decreases in the Gulmarg neutron monitor were 6.5% and 4.5% respectively. Figures 4.11 and 4.12 show percent intensity plots during these two Forbush decreases in the total monitor counting rate as well as in the various multiplicities. The multiplicities have been grouped as  $m_1$ ,  $m_2$ ,  $m_{3,4}$  and  $m_{5-10}$  for reducing the statistical errors in the counting rates. Table 4.2 shows the regression coefficients obtained for the decrease in various  $m_i$  groups versus  $m_1$  for the two

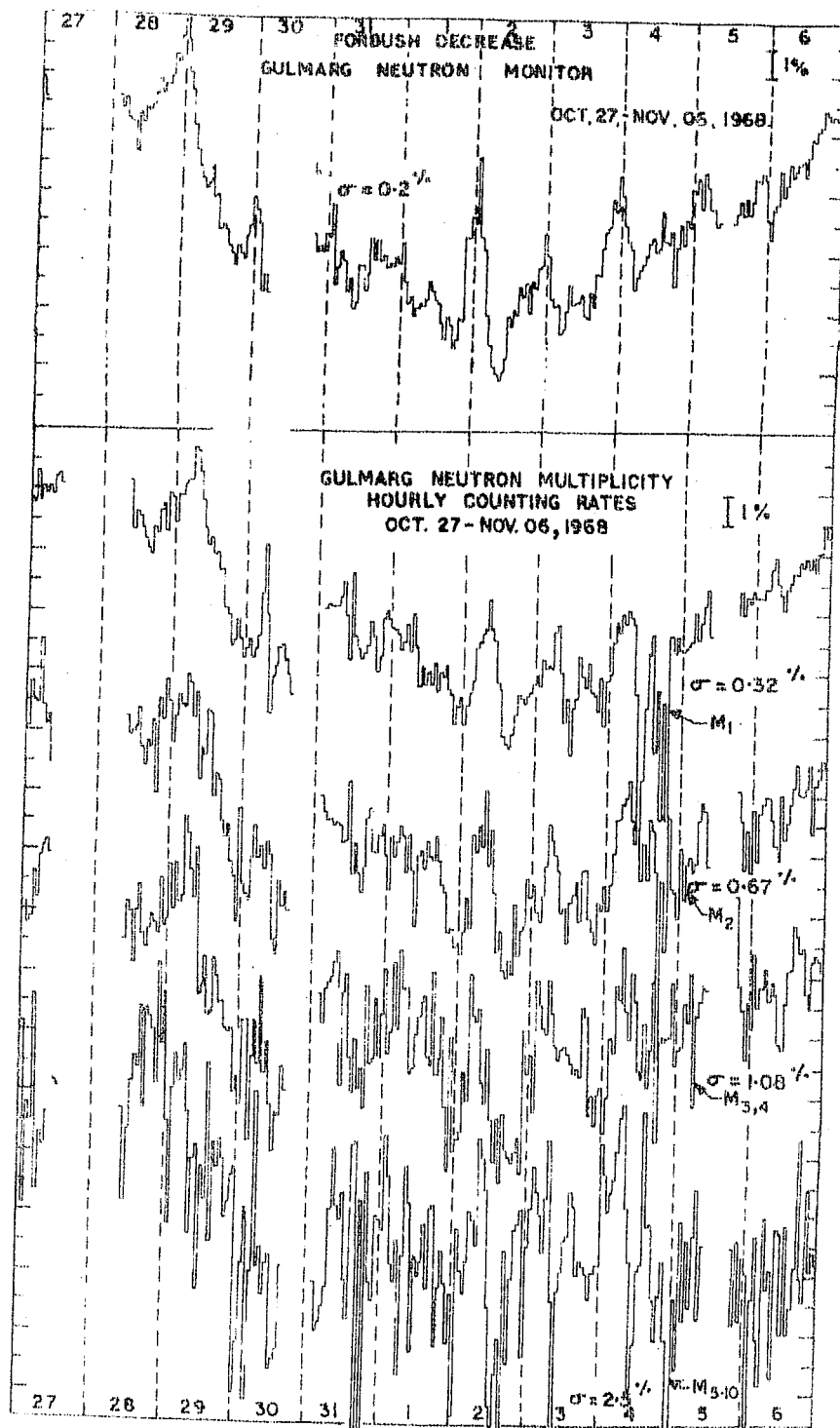


Figure 4.11 The hourly percent total intensity as well as in various multiplicity groups in Gulmarg neutron monitor during the Forbush decrease of October 29, 1968.

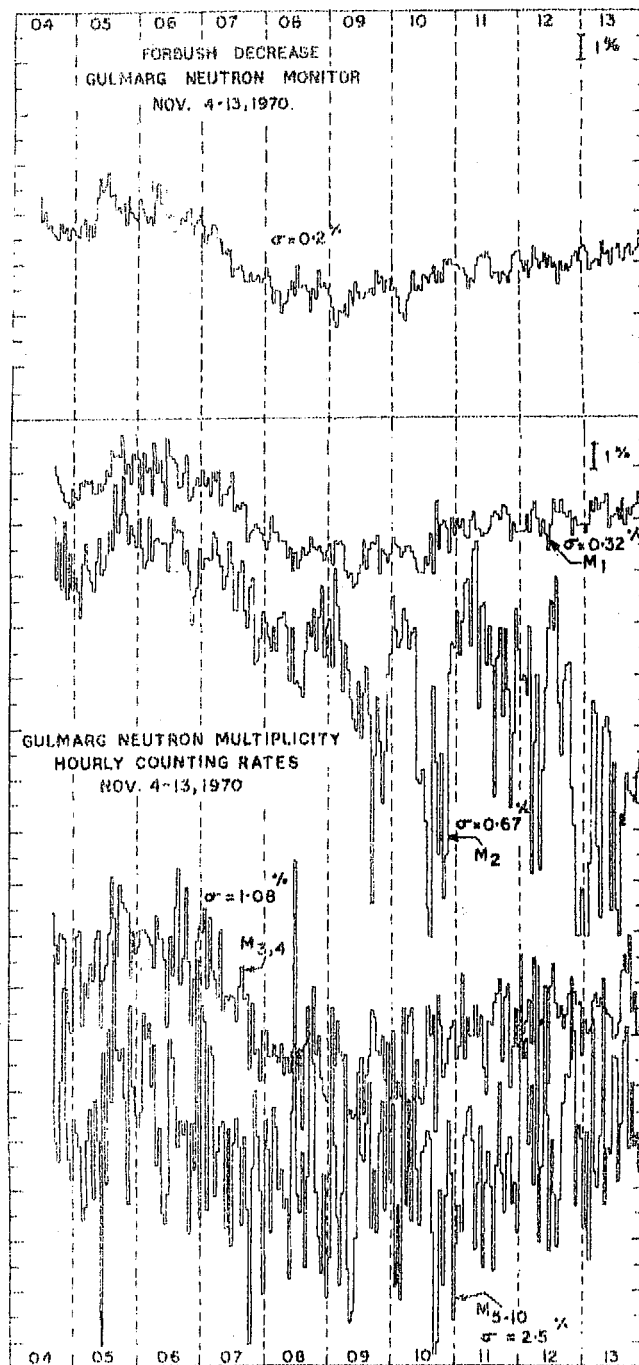


Figure 4.12 The hourly percent total intensity as well as in various multiplicity groups in Gulmarg neutron monitor during the Forbush decrease of November 7, 1970.

Forbush decreases. The regression plots are shown in figure 4.13 and 4.14. During the decrease of October 29, 1968 the regression coefficient between  $m_2$  and  $m_1$  is  $0.82 \pm 0.18$  while it is  $0.56 \pm 0.20$  and  $0.74 \pm 0.32$  for  $m_{3,4}$  versus  $m_1$  and  $m_{5-10}$  versus  $m_1$  respectively. The coefficients are not different from each other within the statistical errors. Nor are they significantly different from unity except in the case of  $m_{3,4}$  versus  $m_1$ . During the Forbush decrease of November 7, 1970, the regression coefficients are:  $1.04 \pm 0.23$  in the case of  $m_2$  versus  $m_1$ ,  $1.10 \pm 0.35$  for  $m_{3,4}$  versus  $m_1$  and  $0.71 \pm 0.63$  for  $m_{5-10}$  versus  $m_1$ . Again the three regression coefficients are not different from unity within the statistical errors.

Dyring and Sporre (1966) studied the multiplicity dependence of two small Forbush decreases of magnitude 1-2% in the Uppasala neutron monitor, which occurred on January 29, 1964 and February 9, 1965. Though the counting rate in multiplicities  $m \geq 2$  together, showed a smaller decrease than in  $m_1$ , the authors have concluded that the results are not convincing in view of the small magnitude of the decreases. Griffiths et al. (1968) have compared the intensity variations in the multiplicities  $m \geq 4$  and  $m \geq 6$  with total counting rates in the Leeds neutron monitor, during the Forbush decreases of October 27, December 15, 1966; January 9, February 9 and May 26, 1967. These decreases were of magnitude 4-7% in the Leeds neutron monitor. The mean

Table 4.2 Multiplicity dependence of Forbush decreases in different multiplicities in Gulgarg Neutron monitor (Linear regression analysis).

Forbush decrease	Regression between	Regression coefficient	Constant term	Correlation coefficient	Total of data	Number points
October 29 1968	$M_2 V_s M_1$	$0.82 \pm 0.18$	$17.50 \pm 17.08$	$0.70 \pm 0.11$		24
	$M_{3,4} V_s M_1$	$0.56 \pm 0.16$	$42.45 \pm 15.40$	$0.60 \pm 0.14$		24
	$M_{5-10} V_s M_1$	$0.74 \pm 0.32$	$22.68 \pm 31.42$	$0.44 \pm 0.17$		24
November 07 1970	$M_2 V_s M_1$	$1.04 \pm 0.26$	$-5.33 \pm 26.75$	$0.52 \pm 0.11$		45
	$M_{3,4} V_s M_1$	$1.10 \pm 0.35$	$-12.06 \pm 33.76$	$0.44 \pm 0.12$		45
	$M_{5-10} V_s M_1$	$0.71 \pm 0.62$	$27.59 \pm 60.98$	$0.17 \pm 0.15$		45

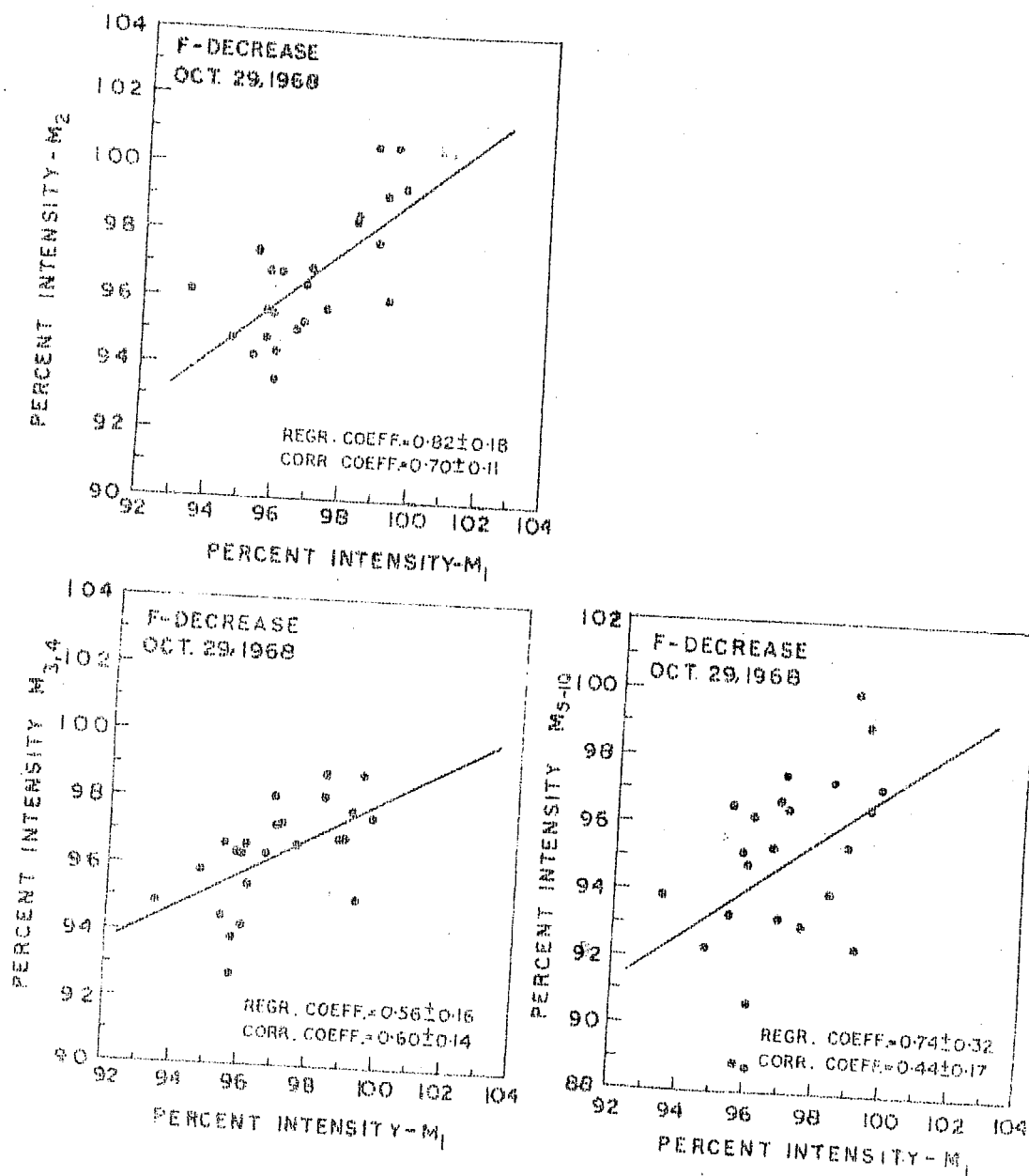


Figure 4.13 The regression plots of  $m_2$  vs  $m_1$ ;  $m_{3,4}$  vs  $m_1$  and  $m_{5-10}$  vs  $m_1$  during the Forbush decrease of October 29, 1968 in Gulgarg neutron monitor.

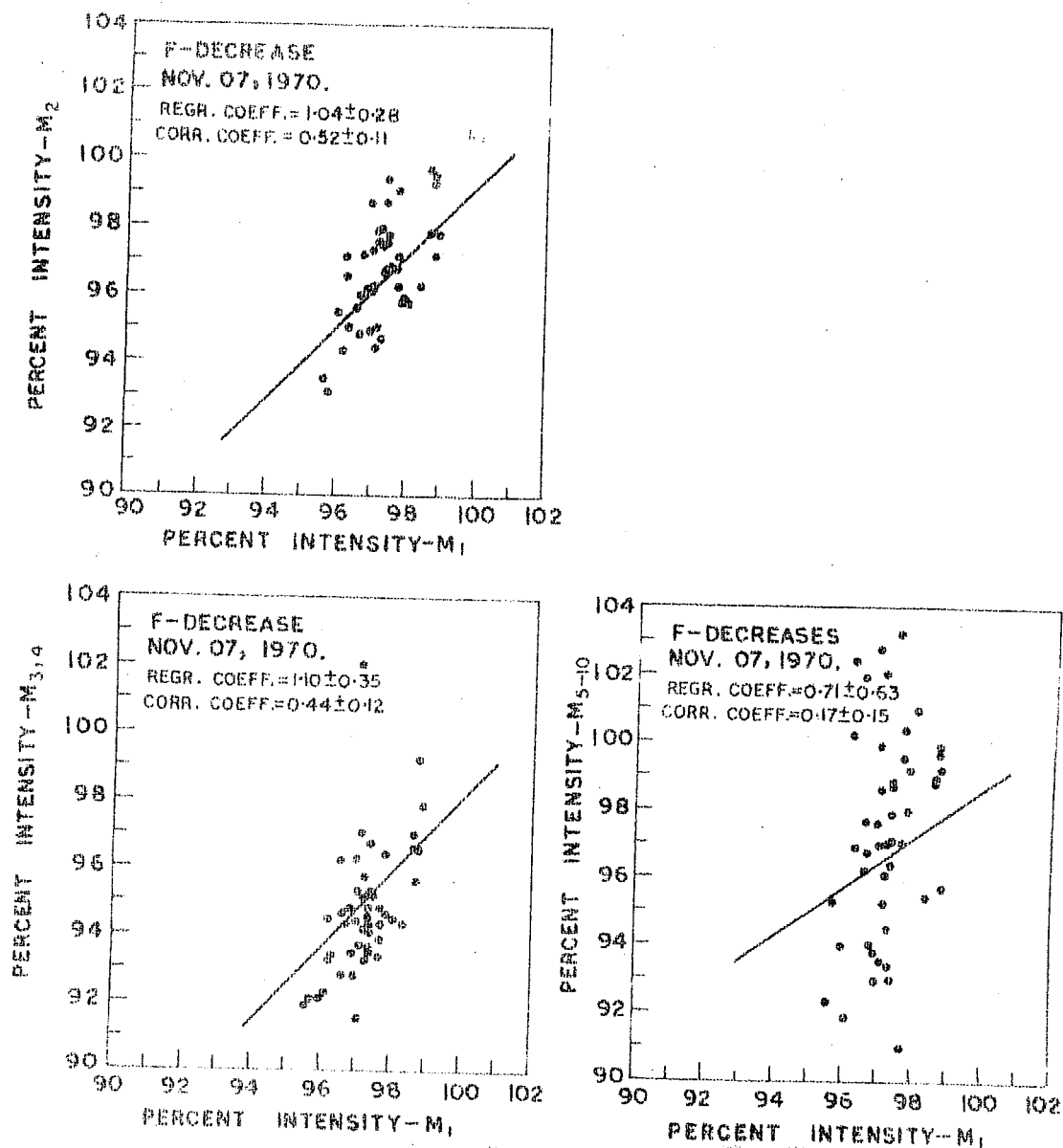


Figure 4.14 The regression plots of  $m_2$  vs  $m_1$ ;  $m_{3,4}$  vs  $m_1$  and  $m_{5-10}$  vs  $m_1$  during the Forbush decrease of November 7, 1970 in Gulmarg neutron monitor.

regression coefficients found by them are  $0.795 \pm 0.024$  for  $m \geq 4$  and  $0.549 \pm 0.025$  from  $m \geq 6$  versus the total counting rate. Also the regression coefficients for the individual Forbush decrease of May 26, 1967 were  $0.79 \pm 0.03$  for  $m \geq 4$  and  $0.56 \pm 0.07$  for  $m \geq 6$  versus the total counting rate. In comparison, Bachelet et al. (1968) did not find any significant multiplicity dependence in the Forbush decrease of May 26, 1967 in Rome neutron monitor.

Kodama and Inoue (1970 a) have investigated the multiplicity dependence in the neutron monitor at Syowa Base during the Forbush decreases of April 4, May 1, May 24, June 6, September 19, October 28 and December 30, 1967. They find the average regression coefficients between the multiplicity counting rates and the total to decrease from 0.99 for  $m_1$  to 0.6 for  $m \geq 6$ , with the exception that the coefficient for multiplicity  $m_2$  is larger than  $m_1$  and is 1.14. They have attributed this strange behaviour of  $m_2$  to less muon contribution than in  $m_1$ , in the superneutron monitor. Similar explanation is forwarded for larger solar flare increase in  $m_2$  than in  $m_1$  (Kodama, 1967). It should be noted that the same authors (Kodama and Inoue, 1970 b) report that the mean multiplicity during the Forbush decrease of October 23, 1967 did not change significantly, indicating practically zero multiplicity dependence of the decrease.



Lockwood and Singh (1969) have studied multiplicity dependence of Forbush decreases in Mt. Washington and Durham neutron monitors, occurring on June 11, July 11, September 30, October 25, 1968; and March 23, April 13, 1969. These authors find that the ratios of daily mean counting rates in the various multiplicities to the total counting rates during the decreases reduce continuously in magnitude from lower to higher multiplicities. They have estimated the mean rigidity spectrum of these Forbush decreases to have a form  $\exp[-K/P^{-0.7}]$  where  $P$  is the rigidity and  $0.2 < K < 0.9$ . Similar results have been obtained by Iucci et al. (1971).

The widely varying results in different Forbush decreases by different authors are probably due to:

- 1) different energy dependence of individual Forbush decreases, 2) large statistical errors particularly in the higher multiplicities and 3) not so prominent dependence of the form of the multiplicity spectrum on the primary cosmic ray spectral changes. The results indicate that the study of the multiplicity spectrum has not proved to be useful for studying the primary cosmic ray spectral changes during Forbush decreases. Nor have such studies shown any definite advantage over the conventional methods for studying other cosmic ray variations such as during solar flares (Kodama, 1967; Bachelet et al., 1968, Kodama and Inoue, 1970 a, b).

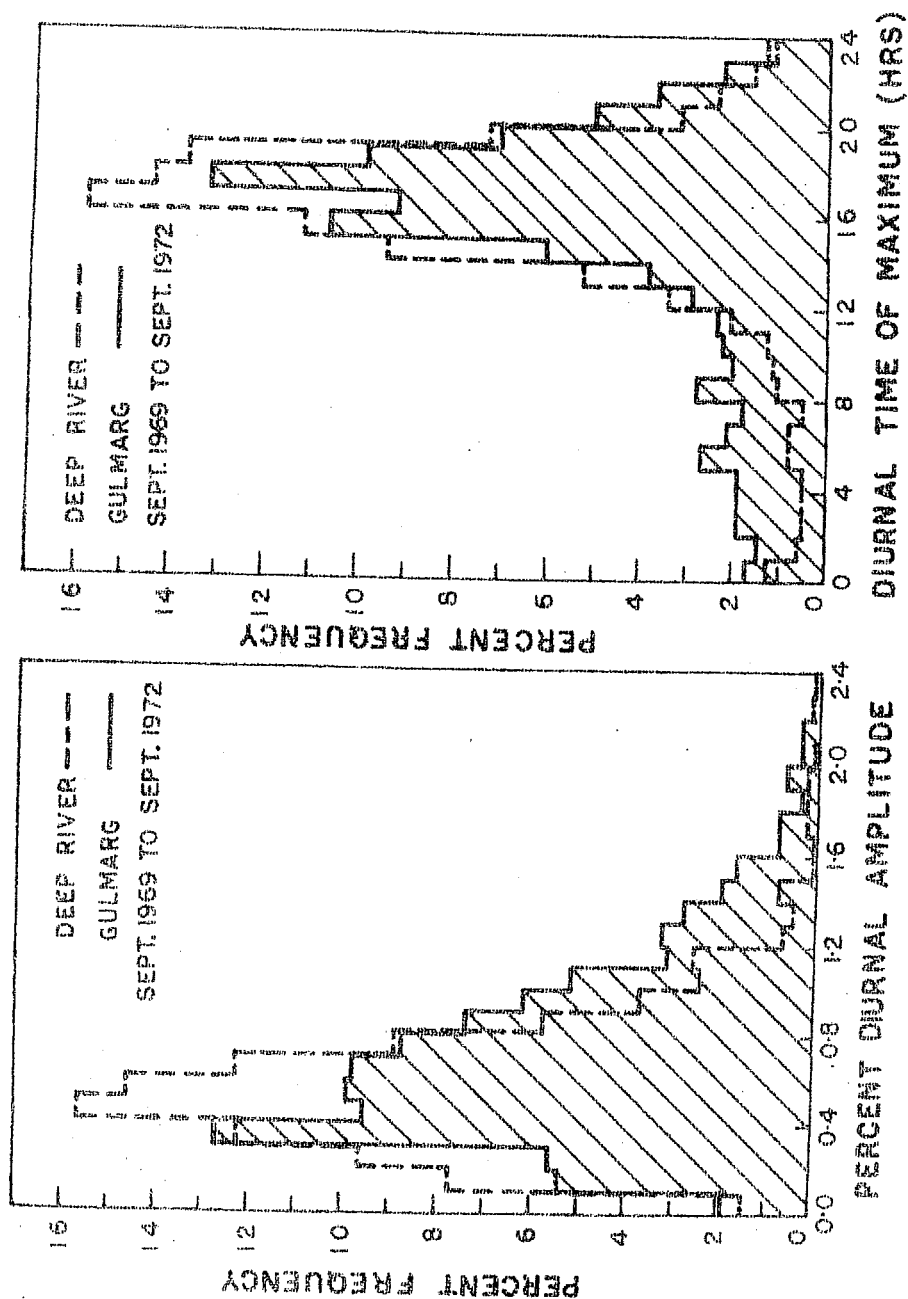


Figure 3.1 Histograms of amplitude and time of maximum of diurnal variation in the cosmic ray intensity in the interplanetary space, derived from Gulmarg neutron monitor. The figure also shows similar histograms derived from Deep River neutron monitor for comparison.

the diurnal amplitude and the time of maximum at Gulmarg compared to that at Deep River is probably due to larger statistical error ( $\approx 2.7$  times) in the counting rate in the Gulmarg neutron monitor.

Certain types of abnormal diurnal variations on the individual days have been already discussed in section I.4c, notable among them being the enhanced diurnal variation with maximum along 21 hour direction. However the periods of anomalous diurnal variation with maximum between 06-12 hours have not been discussed so far in literature, although Lockwood and Razdan (1963), Rao and Sarabhai (1964), and Lindgren (1968, 1969) have pointed out a few such instances. This chapter investigates the characteristics of the anomalous diurnal variation with maximum in morning hours (06-12 hours) and the various possible conditions in the interplanetary medium which can produce it. The study of such an infrequent phenomenon as revealed in figure 5.1, requires an extensive use of data for many years from a large number of neutron monitors. The monitors need to be spread in longitudes preferably in the latitude belt of  $40^{\circ}$ - $60^{\circ}$  geographic where asymptotic cones have small longitudinal width ( $30^{\circ}$ - $40^{\circ}$ ) and lie near the equatorial plane of the earth. The reasons have already been discussed in section II.3. Gulmarg neutron monitor data has not been used for this analysis because of non-availability of data from a large number of stations during the period of its operation.

In the first phase of the analysis, neutron monitor data for the years 1965-1967 from various stations listed in table 5.1, are used to understand the general characteristics of the anomalous diurnal variation in the cosmic ray intensity with maximum between 06-12 hours. In the second phase, the data from Deep River, Climax and Lindau neutron monitors have been analysed in pairs for the extended period 1960-1970, to understand further details of the anomalous diurnal variation. The data of Climax and Lindau have been used for the period 1960-62 and Deep River and Lindau for the period 1963-70. Simultaneous study of data from at least two stations at a time, at two widely spaced longitudes, have been felt necessary in order to be sure of the worldwide character of the anomalous diurnal variation. The choice of the pair of stations used at a time for the analysis, has been mainly governed by the availability of the data. The results of the investigation are discussed in terms of the model of the interplanetary conditions which can cause the anomalous diurnal variation with the time of maximum so widely different from the average. Finally, the anomalous diurnal variation with essentially low amplitudes compared to the average value of 0.4% and occurring during quiet periods, has been studied for the years 1960-1970. Most of the above investigations have been published (Razdan and Bemalkhedkar, 1971, 1972; Bemalkhedkar et al., 1973).

## V.2 Enhanced anomalous diurnal variation with morning maximum during the years 1965-1967

### V.2a General characteristics:

Harmonic analysis of Deep River neutron monitor data for the years 1965-1967 shows that on about 8% days, the diurnal variation in the cosmic ray intensity exhibits maximum between 06-12 hours in the interplanetary space. In comparison, the corresponding percentage of days during the period September 1969 to September 1972 is 10.5% for Gulmarg. The diurnal vectors in the interplanetary space on the days of anomalous diurnal variation have been obtained for rigidity independent spectrum up to 100 GV. This is in accord with the spectral exponent  $\approx 0.0$ , obtained for the enhanced anomalous diurnal variation, (section V.2b). The histograms of diurnal amplitude and time of maximum in the interplanetary space on these days are shown in figure 5.2a, b. The time of maximum has a peak around 8-10 hours. The diurnal amplitudes are peaked around 0.2-0.4%, but the histogram has also a long tail with amplitudes greater than 0.5%. A scan of neutron monitor data shows that while most of the low amplitude days occur during undisturbed cosmic ray intensity conditions, the anomalous diurnal variation shows enhanced amplitudes essentially during the recovery phase of Forbush decreases. In both the cases, the anomalous diurnal variation occurs either on single isolated days or in groups of days ranging from 2-4 days.

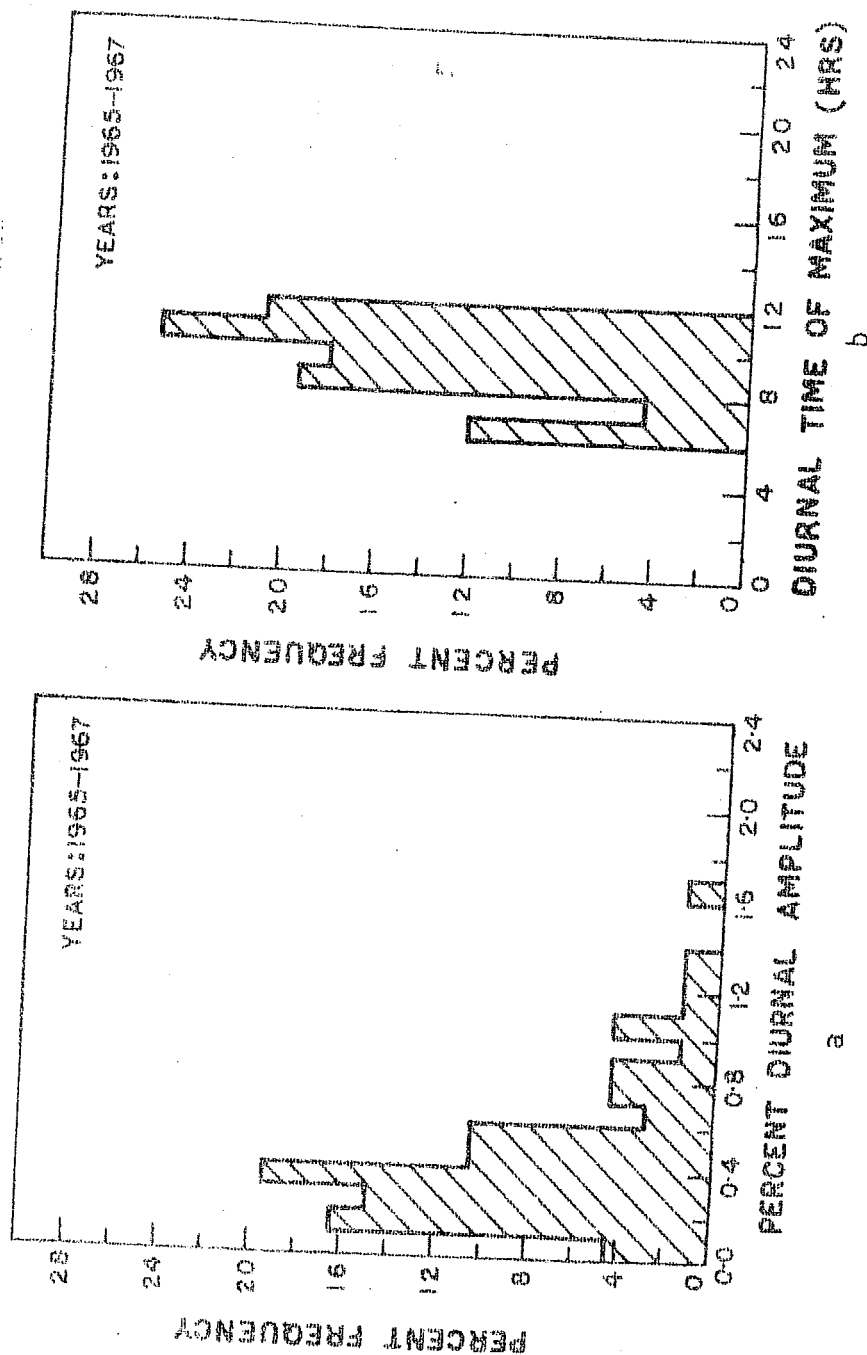


Figure 5.2a,b Histograms of amplitude and time of maximum in cosmic ray intensity in the interplanetary space on the days of anomalous diurnal variation with morning maximum derived from Deep River neutron monitor during the years 1965-1967.

Figure 5.3 shows three examples of the Forbush decreases with the large amplitude anomalous diurnal variation occurring on consecutive days during its recovery. The data presented in the figure are the three hourly moving averages of the neutron intensity at Deep River. The list of all Forbush decreases during the years 1965-1967 exhibiting enhanced anomalous diurnal variation during their recovery phase is given in table 5.2 along with the details of the Forbush decreases. The decreases occurred on June 15, 1965; December 13, 1966; January 7, 1967; May 25, 1967; and June 25, 1967. The table 5.2 also lists two more such earlier Forbush decreases quoted in the literature (Lockwood and Razdan, 1963; Rao and Sarabhai, 1964), though no detailed investigations were carried out regarding the anomalous diurnal variation during their recovery phase.

To confirm the existence of the enhanced anomalous diurnal variation, the hourly cosmic ray data at a large number of stations listed in table 5.1, have been harmonically analysed. The stations are well spread in longitude and have their asymptotic cones of acceptance within  $\pm 40^\circ$  of the earth's equatorial plane. Even when the effect of the long term variation in the intensity on the harmonic coefficients is removed by subtracting the 24 hour moving average values from the corresponding hourly intensities during the day, the method of harmonic analysis is known to give erroneous results for the diurnal variation when the cosmic ray

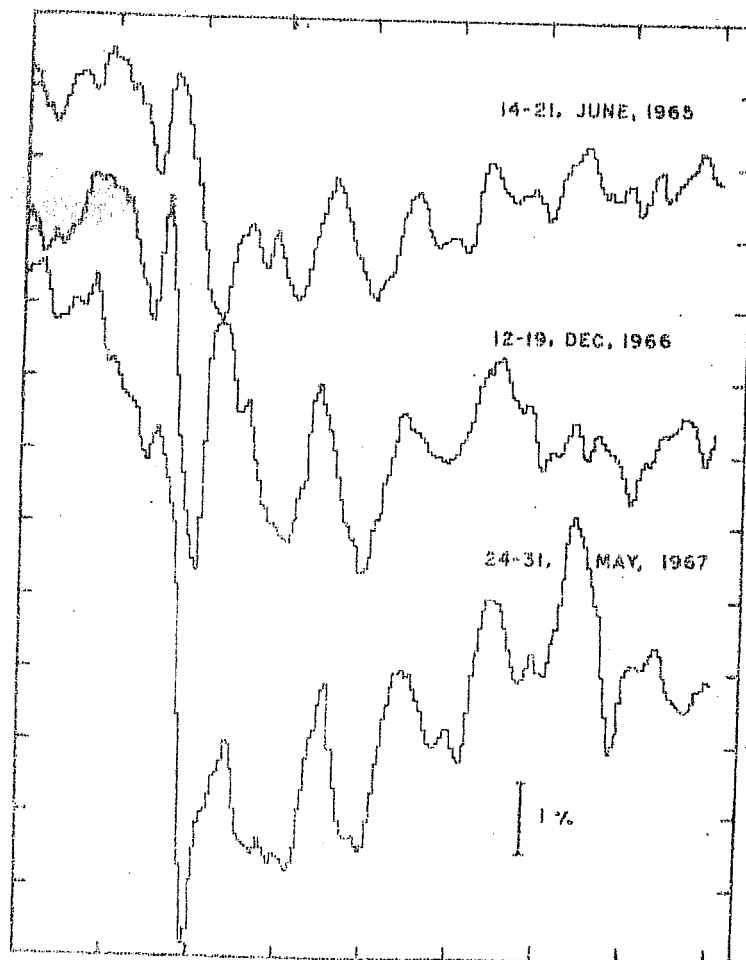


Figure 5.3 Three hourly moving average intensity profiles in the Deep River neutron monitor during three Forbush decreases producing enhanced anomalous diurnal variation in their recovery phases.

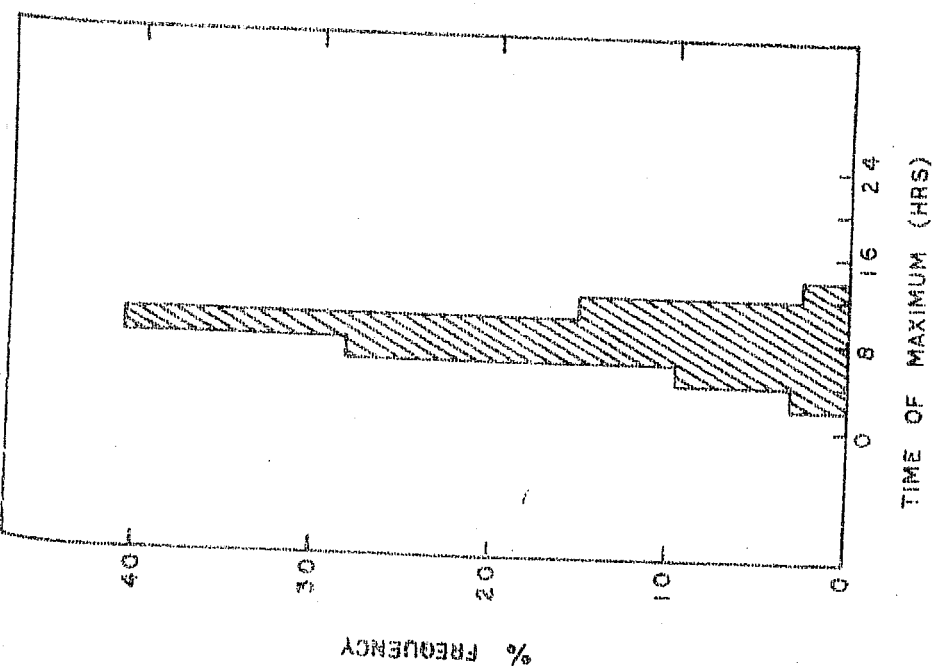


Table 5.1 A list of neutron monitors used in the present study

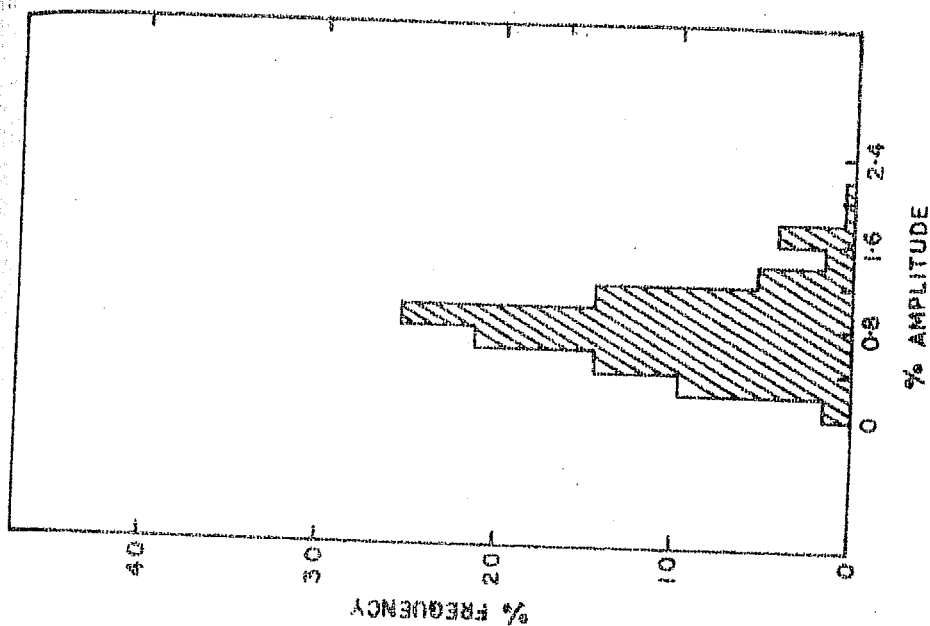
Sr. No.	Station	Altitude meters	<u>Geographic</u>		Cutoff rigidity GV
			Lat. degrees	Long. degrees	
1	Inuvik	21	68.35	226.27	0.18
2	Churchill	39	58.75	265.91	0.21
3	Goosebay	46	53.33	299.58	0.52
4	Calgary	1110	51.08	245.91	1.09
5	Deep River	145	46.10	282.50	1.02
6	Mt. Washington	1917	44.30	288.70	1.24
7	Leeds	100	53.80	358.45	2.20
8	Kiel	54	54.33	10.13	2.29
9	Lindau	140	51.60	10.10	3.00
10	Climax	3400	39.37	253.82	3.43
11	Dallas	208	32.78	263.20	4.35
12	Pic du Midi	2860	42.93	0.25	5.36
13	Mina Aguilar	4000	-23.10	294.30	12.51
14	Chacaltaya	5220	-16.31	291.85	13.10
15	Kula	915	-20.71	203.74	13.30

intensity changes are abrupt such as during Forbush decreases. Therefore, in the presentation of the results from harmonic analysis, those days are excluded which fall within 24 hours of the maximum of the decrease. The present investigation includes only the first harmonic of diurnal variation since the diurnal variation on the days under the consideration is dominant over the second harmonic.

The histograms of the time of diurnal maximum and the amplitude on the days under consideration are shown in figure 5.4 for all the stations combined. The histograms reveal that most of these days have a time of maximum around 8-10 hours and the median of the amplitude  $\approx 0.8\%$  in the interplanetary space as was also observed at Deep River. To check further the consistency at various stations in regard to the above results, the diurnal vectors averaged over all the enhanced diurnal variation days are plotted for each station individually on a harmonic dial in figure 5.5. The vectors once again reveal a time of maximum varying between 6.6 hours to 9.4 hours and an amplitude varying between 0.50% to 0.97%. The scatter in the vectors at various stations is understandable as due to a finite width of the asymptotic cones of acceptance of the neutron monitors and partly due to spurious effects caused by superimposed worldwide time dependent fluctuations in the cosmic ray intensity, which are not unlikely to occur during such disturbed periods.



a



b

Figure 5.4a,b Histograms of amplitude and time of maximum on the days of anomalous diurnal variation during the recovery phase of the five Forbush decreases during the years 1955-1967 (Table 5.2) utilizing data from various neutron monitors listed in table 5.1.

Further credence to the results from harmonic analysis is added by noting the time of maximum intensity on each day of anomalous diurnal variation under consideration from the three hourly moving average curves of cosmic ray intensity plotted for each of the stations. Eventhough such an analysis has a subjective element, it does not have the drawback inherent in the harmonic analysis discussed above. Moreover, most of the days under study are single humped and the rate of recovery per day in the cosmic ray intensity during these periods is small compared to the amplitude of the anomalous diurnal variation. Therefore, the time of maximum intensity on these days can be pinpointed without much ambiguity. The analysis includes about 78% of the anomalous diurnal variation days at all the stations. On other days, the time of diurnal maximum could not be derived unambiguously. The histogram of time of maximum in the interplanetary space, obtained by this method, is shown in figure 5.6. The histogram once again reveals a peak around 3-10 hours confirming the results obtained from the harmonic analysis.

#### V.2b Rigidity spectrum of the enhanced anomalous diurnal variation:

The rigidity spectrum of the enhanced anomalous diurnal variation has been determined with a view to compare it with the average diurnal variation, to get a possible clue to the mechanism. The rigidity spectra for the groups of anomalous diurnal variation days occurring in the recovery phase of

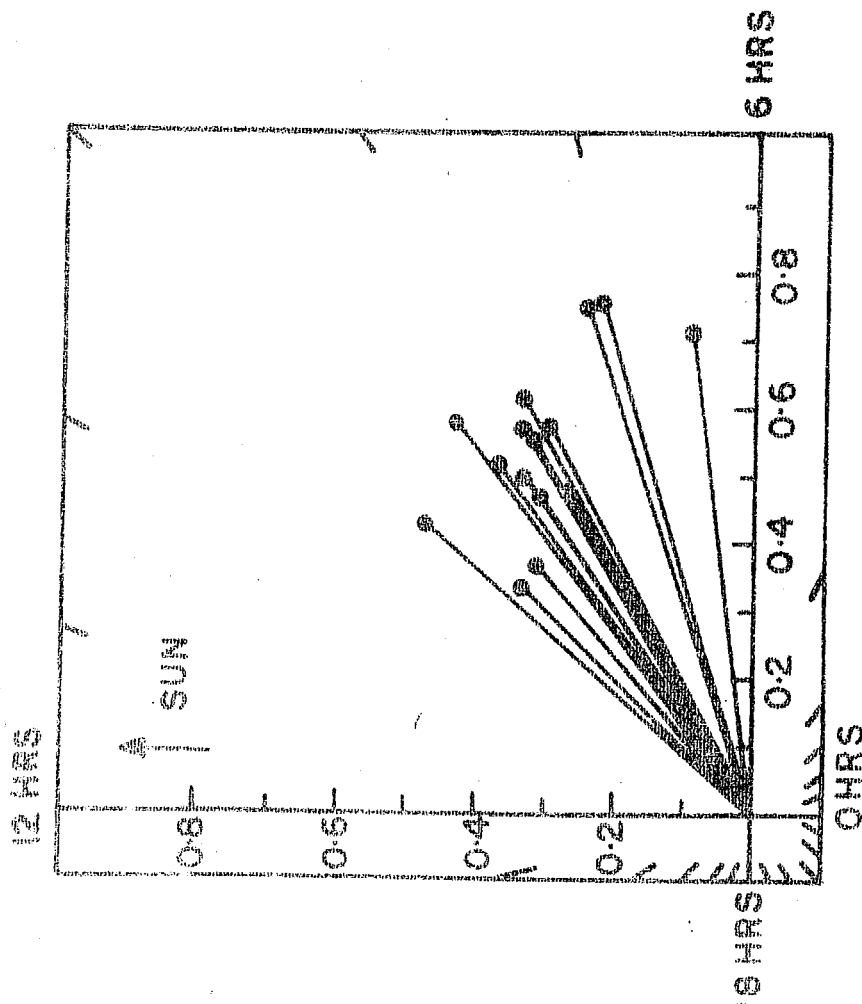


Figure 5.5 Diurnal vectors in the cosmic ray intensity in the interplanetary space averaged over all the days of anomalous diurnal variation during the recovery phase of the five Forbush decreases during the years 1965-1967 (table 5.2), as derived from the various neutron monitors.

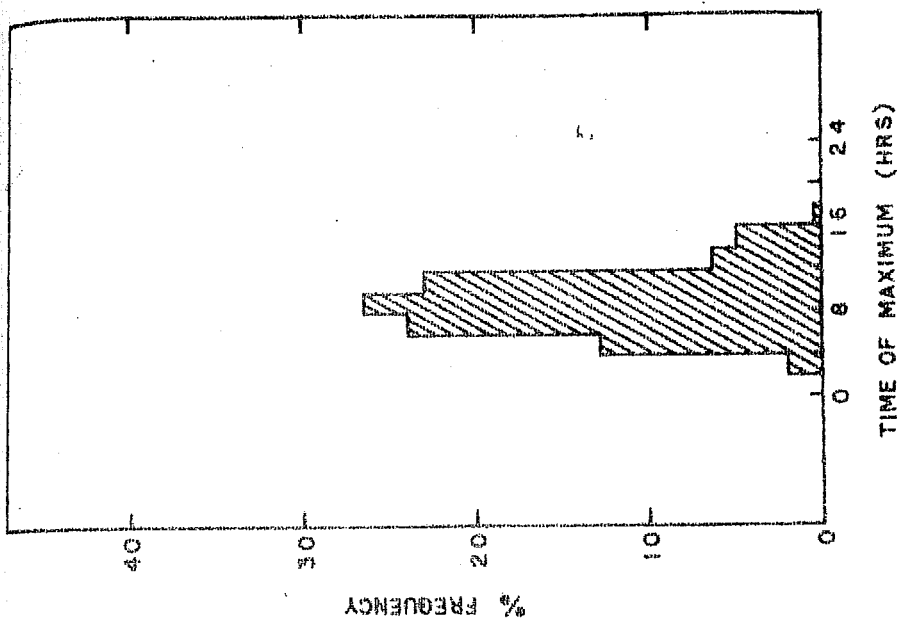


Figure 5.6 Histogram of diurnal time of maximum in the cosmic ray intensity in the interplanetary space on the days of anomalous diurnal variation used in figures 5.4 a,b and 5.5, by noting the time of maximum in the three hourly moving average intensity profiles at various stations.

the five Forbush decreases (table 5.2) have been obtained separately, as well as the mean found for all the events. The differential rigidity spectrum of variation  $\delta D(P)/D(P)$  is assumed to have a form  $KP^{\gamma}$  where  $P$  is the particle rigidity,  $D(P)$  the differential rigidity spectrum and  $\delta D(P)$  the observed change in it. Further the spatial anisotropy causing the anomalous diurnal variation is assumed to be zero for rigidities above 100 GV. For various presumed values of  $\gamma$ , the mean diurnal amplitude in the interplanetary space is derived from different stations, and a parameter,  $S^2$  proportional to variance is calculated for each  $\gamma$  from the relation

$$S^2 = \sum_{i=1}^N (r_i - \bar{r})^2 / \bar{r}^2$$

where  $r_i$  is the diurnal amplitude in the interplanetary space as observed by the  $i^{\text{th}}$  station,  $\bar{r}$  the mean of the amplitudes in the interplanetary space observed by all the stations and  $N$  the total number of independent observations used in the analysis. The  $S^2$  values are plotted in figure 5.7 and for all the events combined the curve has a minimum for

$\gamma = +0.2$ . For individual events the minimum value of  $S^2$  is attained for the spectral exponent varying from  $-0.6$  to  $+0.4$ .

As the size of the statistical sample in each event is small, it has been felt necessary to apply the significance test to the minimum variance. The standard error in the value

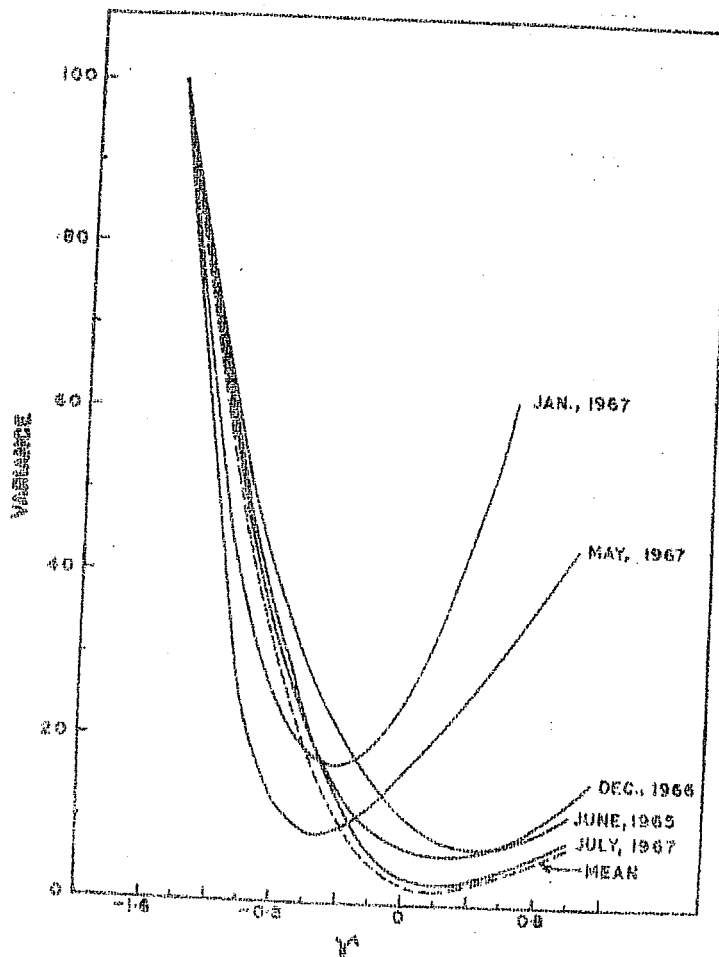


Figure 5.7 Variance versus spectral index of the rigidity spectrum of the anomalous cosmic ray diurnal variation. The dashed curve represents the average behaviour of all the five events.

of  $S^2$  for each value of  $\gamma$  is found to be given approximately by

$$\sigma_{S^2} = \sqrt{2/N} \cdot S^2$$

With this standard error, the minimum values of  $S^2$  are not found to be significantly different from the respective values at  $\gamma = 0$  in each event. It is, therefore, concluded that the rigidity spectrum of the enhanced anomalous diurnal variation is not significantly different from that of the average diurnal variation for which  $\gamma = 0$ . The above analysis further suggests that the anomalous diurnal variation in the cosmic ray intensity might also be predominantly caused by the same processes producing the average diurnal variation with maximum at 18 hours, namely the radially outward convection by the magnetic field irregularities in the solar wind and field parallel and perpendicular diffusion of cosmic rays essentially in the plane of ecliptic.

V.2c The solar and geomagnetic phenomena preceding the Forbush decreases associated with the anomalous diurnal variation:

Since the enhanced anomalous diurnal variation days during the years 1965-1967, occur in groups in the recovery phase of the five Forbush decreases, it appears reasonable to associate the mechanism to the solar interplanetary conditions causing the decreases. The solar and associated geomagnetic phenomena preceding the decreases have been tabulated in table 5.2 and are discussed below.



The onset of the 4% decrease of June 15, 1965 is associated with a geomagnetic storm with an SC at 1100 UT. The CRPL report indicates that only the Tachkent observatory has reported a solar flare of importance 2, 56 hours prior to the SC which may be associated with this Forbush decrease. The flare occurred on June 13, at 0258 UT at the location N24E00 on the solar disc. The decrease is further followed 27 days later by a well defined worldwide Forbush decrease of magnitude 2.5% at Deep River on July 12, 1965 which is associated with an SC at 1700 UT. However, this decrease is not preceded by any solar flare of importance greater than 1 within 100 hours prior to the decrease. During the recovery phase of this decrease, the cosmic ray diurnal variation again exhibits maximum in the morning hours. Figure 5.8a, shows the mean diurnal vectors on July 14, 15 at various stations. The diurnal vectors at different stations lie between  $\simeq 06$  hours and  $\simeq 12$  hours in the interplanetary space. The reason for the wide spread in the time of maximum could be partly due to the small diurnal amplitude itself with relatively larger statistical error associated with it and partly to the occurrence of small time dependent changes in the cosmic ray intensity. In figure 5.8b, is plotted the asymptotic longitude of each station versus the diurnal time of maximum intensity in the interplanetary space. The time of maximum shows no dependence on the asymptotic longitude, which ascertains that the observed diurnal variation is predominantly due to a spatial anisotropy.

Table 5.2 Characteristics of the worldwide cosmic ray intensity decreases associated with the anomalous diurnal variation with maximum along the geomagnetic axis direction in the interplanetary space. The table also lists the likely associated polar flares and geomagnetic storms.

Sr. No.	Day of Forbush decrease	Onset time in Deep River BH	Decrease in Deep River BH	Days of anomalous d.v.	Associated Geomagnetic storm (SC)	Likely associated solar flare		27 day recurrence of Forbush decreases and SC's					
						Time	Importance	Location	McMath plage region	Preceding Forbush decrease	Preceding SC	Succeeding Forbush decrease	Succeeding SC
1.	June 15, 1965	18 UT	4%	June 17, 18, 19, 20	June 15, 1100 UT	Dec. 12, 1430 UT	2N/2E	N 23 E 35	5610	Nov. 17, 20 UT	Nov. 17, 0000 UT	July 12, 22 UT	July 12, 1700 UT
2.	Dec. 13, 1966	16 UT	6%	Dec. 14, 15, 16, 17		May 23, 1935 UT	3E	N 25 E 25	8816				
3.	Jan. 7, 1967	13 UT	5%	Jan. 10, 11, 12	Jan. 7, 0759 UT	June 23, 1032 UT	3N	N 30 E 45	8863	Dec. 13, 16 UT		June 25, 20 UT	June 25, 0221 UT
4.	May 25, 1967	14 UT	9%	May 26, 27, 28, 29	May 25, 1235 UT	July 11, 1620 UT	3	N 07 E 32	6235	May 25, 14 UT	May 25, 1235 UT		
5.	June 25, 1967	00 UT	4%	July 1, 2, 3, 4	June 25, 0221 UT	Sept. 28, 2202 UT	3	N 15 E 29	6235			Oct. 26, 2200 UT	Oct. 26, 2200 UT
6.	July 13, 1961	12 UT	12%	July 14, 15	July 13, 1130 UT								
7.	Sept. 30, 1961	18 UT	5%	Oct. 2, 3, 4	Sept. 30, 2108 UT								

JULY 14, 15, 1965.

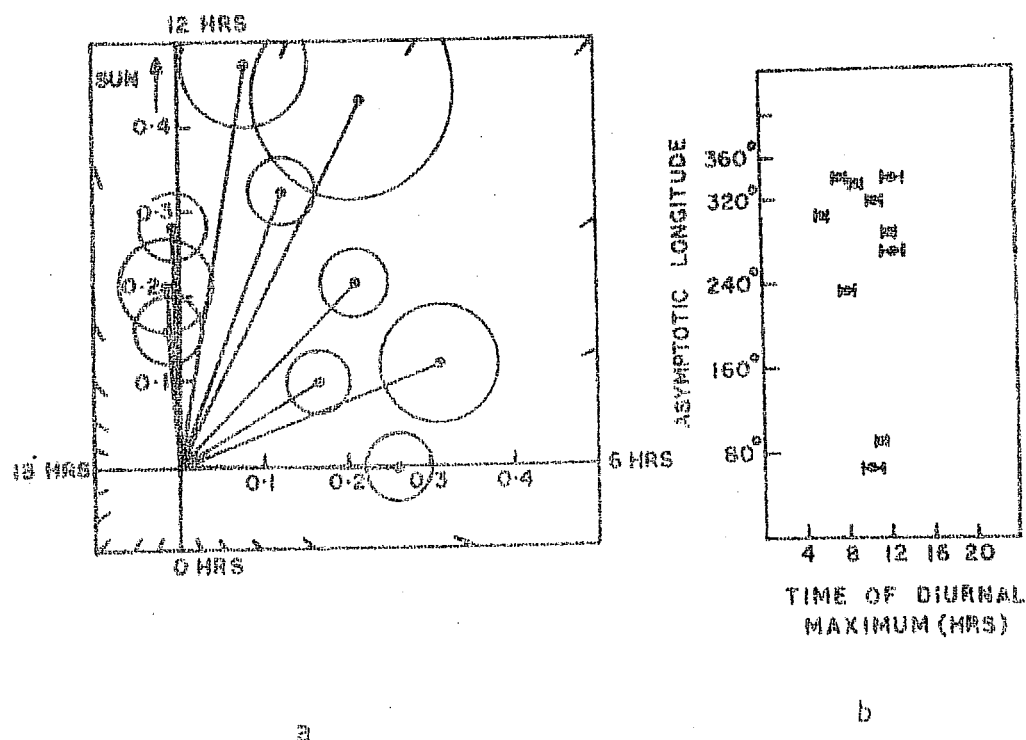


Figure 5.8a,b a) Mean cosmic ray diurnal vectors in the interplanetary space at various stations, averaged over July 14, 15, 1965. b) Asymptotic longitude of the station versus the time of diurnal maximum in cosmic ray intensity in the interplanetary space for July 14, 15, 1965.

NOV. 19, 1966

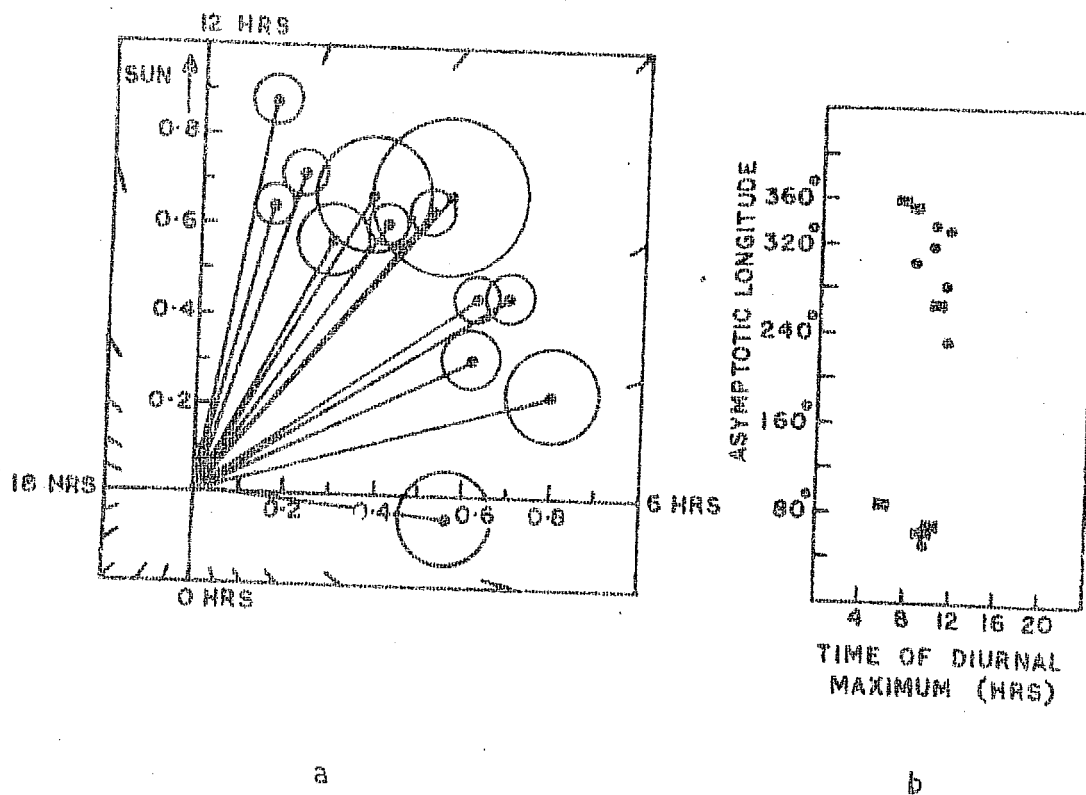


Figure 5.9a,b a) Cosmic ray diurnal vectors in the interplanetary space at various stations on November 19, 1966. b) Asymptotic longitude of the station versus the time of diurnal maximum in cosmic ray intensity in the interplanetary space on November 19, 1966.

The Forbush decrease of December 13, 1966 is not associated with any SC, though the daily geomagnetic index  $K_p$  is high at the time of decrease ( $\sum K_p > 40$ ). The period of high  $K_p$  is preceded by an SC 26 days before and an SC 25 days after. The Forbush decrease of December 13, 1966 is preceded by a solar flare of importance 2N/2B on December 10 at 1430 UT with coordinates N23 E38. Bukata et al.(1968) have intercompared the cosmic ray intensity at the time of this decrease in two space-crafts, Pioneers VI and VII, which were  $62^\circ$  apart in heliolongitude. Pioneer VI observed a small decrease of about 3% which was far to the west of the earth sun line, as compared to a 12% decrease at Pioneer VII. Further, the decrease at Pioneer VI was recorded one day earlier than expected from a solar corotating stream. They have thus concluded that the decrease was caused by the transient plasma cloud from a solar flare.

It is already mentioned in section V.2a that the decrease of December 13, 1966 is followed 25 days after by another worldwide gradual commencement type decrease of January 7, 1967. The cosmic ray diurnal variation again exhibits maximum in the morning hours on January 10, 11, 12 during the recovery phase of this decrease. The decrease is associated with an SC and a 27 day recurrent high  $K_p$ . However, no solar flare of importance greater than or equal to 2 B/3 N occurred upto 100 hours prior to the decrease.

The decrease of December 13, 1966 is further preceded 26 days before by a Forbush decrease (3.5% at Deep River) on November 17, 1966 with onset at 2000 UT. This decrease is associated with an SC at 0000 UT on November 17 and is further preceded by a solar flare of importance 2B on November 14 at 1215 UT in the region N25 E70. A plasma cloud of sufficient angular width from this flare might be associated with this decrease. During the recovery phase of this decrease, cosmic ray intensity again exhibits diurnal variation with maximum in the morning hours on November 19. This is shown in figure 5.9a, wherein diurnal vectors in space derived from various stations are plotted. The independence of the time of diurnal maximum for the stations with various asymptotic longitudes (figure 5.9b), again brings out the predominance of the spatial anisotropy over temporal fluctuations in the intensity on November 19, 1966. All the three Forbush decreases form a 27 day recurrent series and further two of them appear to have an association with an east limb flare.

The May 25, 1967 decrease likewise shows a definite association with an SC recurring for three solar rotations and is associated with a solar flare of importance 3B in the region N28 E25 (Lindgren, 1968). Thirty days after on June 25, 1967, there occurred another Forbush decrease, which is preceded by a solar flare of importance 3N on June 23, 1967 at 1032 UT, at the location N30 E48 on the solar disc.

The decrease is further associated with an SC, recurrent with the one on May 25, 1967. Both the decreases show anomalous diurnal variation with maximum in the morning hours and form a 27 day recurrent pair.

The last two Forbush decreases, mentioned in table 5.2, occurred on July 13, 1961 and September 30, 1961, which exhibited anomalous diurnal variation in their recovery phases, immediately following the decrease phase (Lockwood and Razdan, 1963; Rao and Sarabhai, 1964), although the results were not then pinpointed by the authors clearly. The Forbush decrease of July 13, 1961 is preceded by a solar flare of importance 3 occurring in the region S07 E32 on July 11 at 1620 UT. The other Forbush decrease of September 30, 1961 has a preceding solar flare of importance 3 in the region N15 E29, at 2200 UT on September 28. It is interesting to note that they are also preceded by 27 day recurrent SC's and/or Forbush decreases.

The 27 day recurrence tendency of all the Forbush decreases discussed above, is shown in the form of Bartel's diagram in figure 5.10 along with the days of anomalous diurnal variation. The fact that the Forbush decreases discussed above are recurrent is also demonstrated by their association with high solar wind velocity. The solar wind velocity data has been obtained from Explorer 35 (S.J. Bames, 1972, private communication), for the period 1966-1967, and has been subjected to Chree analysis with the days of the

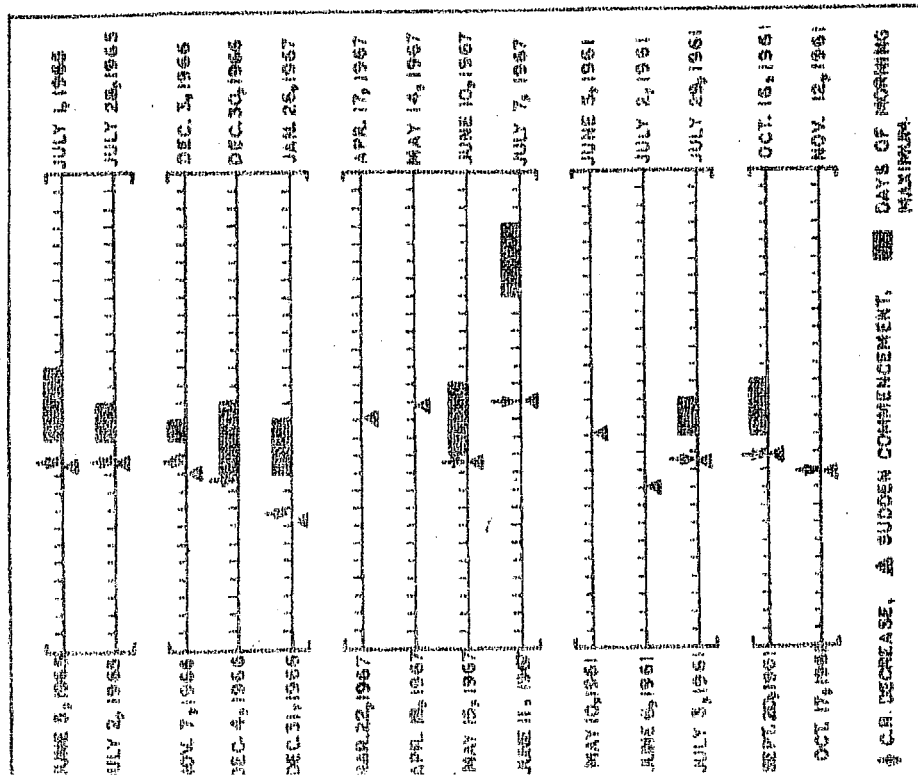


Figure 5.10 Bartlett diagram showing 27 day recurrence tendency in the Forbush decreases associated with anomalous diurnal variation. The decreases also associated with recurrent SC's.

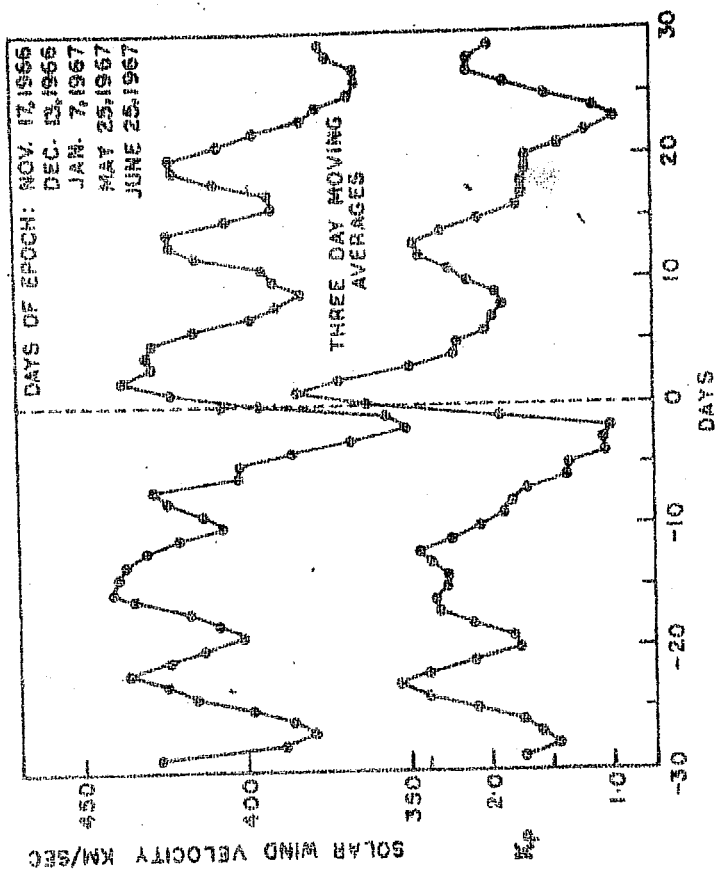


Figure 5.11 Three day moving averages of three analysis of solar wind velocity and geomagnetic index  $K_p$  with onset of the Forbush decreases associated with anomalous diurnal variation as epochs.



onset of Forbush decreases as epochs. The three day moving average of the results of Chree analysis is shown in figure 5.11. In the same figure is also presented, the Chree analysis of the geomagnetic index  $K_p$ . It is observed that around the day of the epoch, the solar wind velocity has increased by about  $50-60 \text{ km sec}^{-1}$  from about  $350 \text{ km sec}^{-1}$  prior to the decrease. It should be noted that the peak value of solar wind velocity during the individual Forbush decreases is  $\geq 550 \text{ km sec}^{-1}$ . Figure 5.11 gives only the average picture of the variation in the solar wind velocity. The solar wind velocity is further seen to exhibit a regular 7 day variation which is in accord with sector structure of interplanetary magnetic field and the solar wind velocity (Wilcox and Ness, 1964). The geomagnetic activity  $K_p$  also exhibits large increase on the epoch day indicating a 27 day recurrence of the geomagnetic disturbance associated with the onset of the Forbush decrease. Since, the days of epoch are selected only on the basis of onset of the Forbush decreases, the sector structure type variation in the solar wind velocity revealed by the Chree analysis, is possible only if these Forbush decreases are associated with solar corotating streams. However, the corotating streams in the interplanetary space associated with these decreases, cannot be identified with the conventional sectors in the interplanetary space discussed by Wilcox and Ness (1964), since every consecutive sector does not give rise to a Forbush decrease and the anomalous diurnal variation.

The interplanetary magnetic field data has not been available for the whole period. However, during the Forbush decrease periods and on the days of anomalous diurnal variation, the magnetic field data (C.P.Sonnet, 1972, private communication) shows no significant change in the average direction of the interplanetary magnetic field from garden hose direction, while the magnitude of the field lies in the range 5-10 gamma.

From the above study for the period 1965-1967, it is therefore concluded that the enhanced anomalous diurnal variation in the cosmic ray intensity occurs during the recovery phase of Forbush decreases for a successive period of 2-5 days. The decreases are found to be associated with corotating solar streams and in many cases, are preceded by east limb solar flares of importance  $> 2B/3N$ .

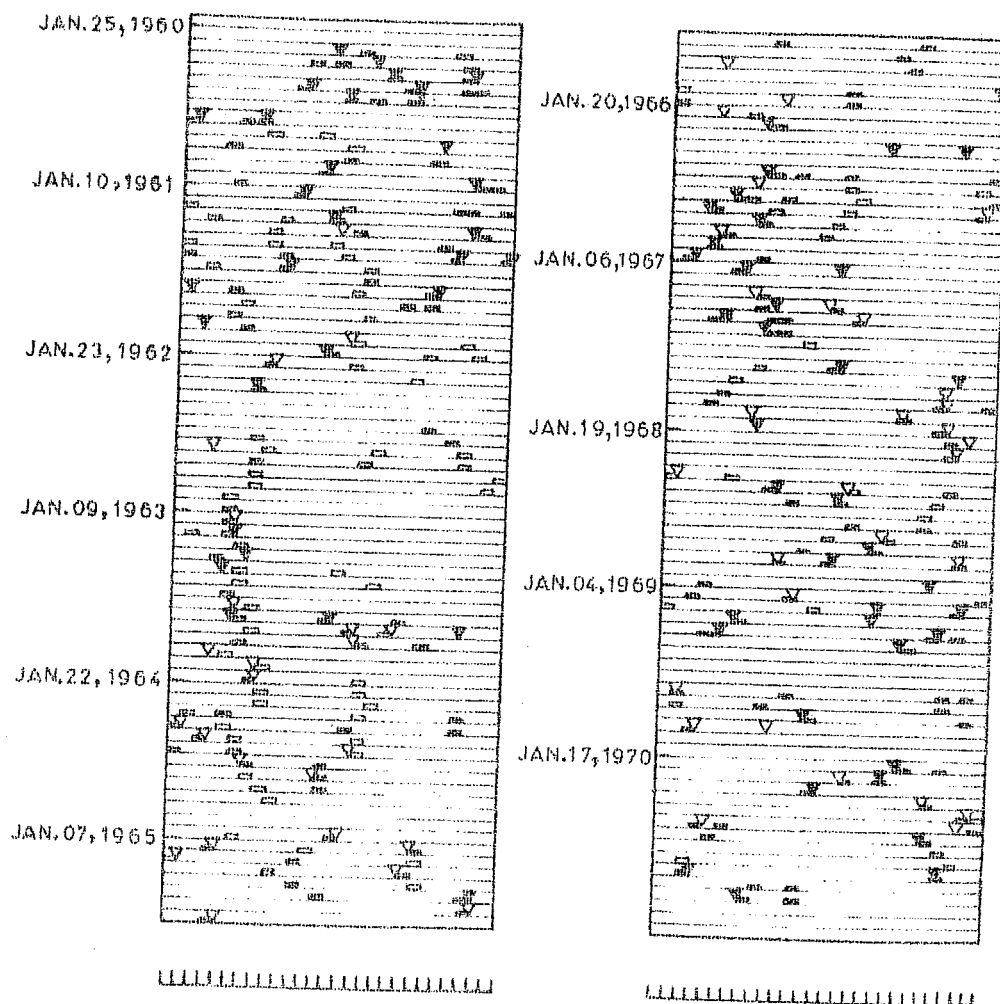
### V.3 Statistical analysis of anomalous diurnal variation in the recovery phase of Forbush decreases during the years 1960-1970

The scan of the cosmic ray data for the period 1965-1967 also shows that there are Forbush decreases which are 27 day recurrent, but do not exhibit anomalous diurnal variation in their recovery phases. This has indicated that the 27 day recurrence of Forbush decreases is probably not the sufficient condition for the occurrence of the anomalous diurnal variation. In this section, an analysis of diurnal variation during the recovery phases of a large number of

Forbush decreases occurring during the years 1960-1970 is undertaken to clarify these points as well as to find further characteristics of the interplanetary medium during the recovery phase of the Forbush decreases, causing morning maximum in the diurnal variation.

Figure 5.12 presents, on Bartels diagram, the Forbush decreases of magnitude  $\geq 2\%$  recorded at Deep River during the years 1960-1970, along with the associated SC's and/or periods of high  $K_p$ , high  $K_p$  being defined as daily

$\sum K_p > 40$ . The Forbush decreases of so small an amplitude are identified by a sharp decrease and a slow recovery observed by at least two far off stations at the same universal time. The definition of the periodicity is restricted here to  $27 \pm 3$  days. On the basis of random distribution, the probability of two Forbush decreases occurring in recurrence within  $27 \pm 3$  days is  $\simeq 0.6\%$ , whileas the probability is much smaller for three or more Forbush decreases to recur in succession every  $27 \pm 3$  days. It is observed that out of the total 123 Forbush decreases, 80% decreases are preceded or followed by either a Forbush decrease, an SC or a period of high  $K_p$  within  $27 \pm 3$  days. Further, 50% of the total Forbush decreases are found to be recurrent within  $27 \pm 3$  days. The further analysis of diurnal variation is restricted to these clear-cut recurrent Forbush decreases with the added condition that the decreases have a magnitude  $\geq 4\%$ .



▽ FORBUSH DECREASE  $\geq 2\% \rightarrow 4\%$   
 ■ FORBUSH DECREASE  $\geq 4\%$   
 SC HIGH K<sub>p</sub>

Figure 5.12 Bartels diagram showing all the Forbush decreases of magnitude  $\geq 2\%$  in Deep River neutron monitor during the years 1960-1970. The figure also shows associated SC's.

This helps in identifying unambiguously the recovery period of the decrease. As in the analysis presented in section V.2a, the first day in the recovery phase is excluded from the analysis to avoid the ambiguity in the harmonic coefficients on such days. The analysis includes the next five days or less in every case, depending on the length of the recovery phase.

There have been 34 recurrent Forbush decreases of magnitude  $\geq 4\%$  during the years 1960-1970. These Forbush decreases have been classified on the basis of the longitude of the associated solar flare of importance  $\geq 2B/3N$  occurring upto 100 hours prior to the decrease, the longitude groups being: 1)  $90^{\circ}E-20^{\circ}E$ , (2)  $20^{\circ}E-20^{\circ}W$ , (3)  $20^{\circ}W-90^{\circ}W$  and (4) No solar flare. A solar flare preceded by less than 30 hours from the onset of the decrease is not considered for association, because it involves excessively large value of the solar wind velocity of greater than  $1400 \text{ km sec}^{-1}$ . Such higher values of the solar wind velocity are extremely rare. Likewise, flares preceding the onset by more than 100 hours are not considered to be associated because of the low solar wind velocity ( $< 400 \text{ km sec}^{-1}$ ). So the flares occurring between 30-100 hours prior to the decrease are considered for association. With this criterion it has turned out that in 28 decreases, the flares preceding the decrease lie within one of the three longitude groups mentioned, whereas in the remaining 6 decreases they spread

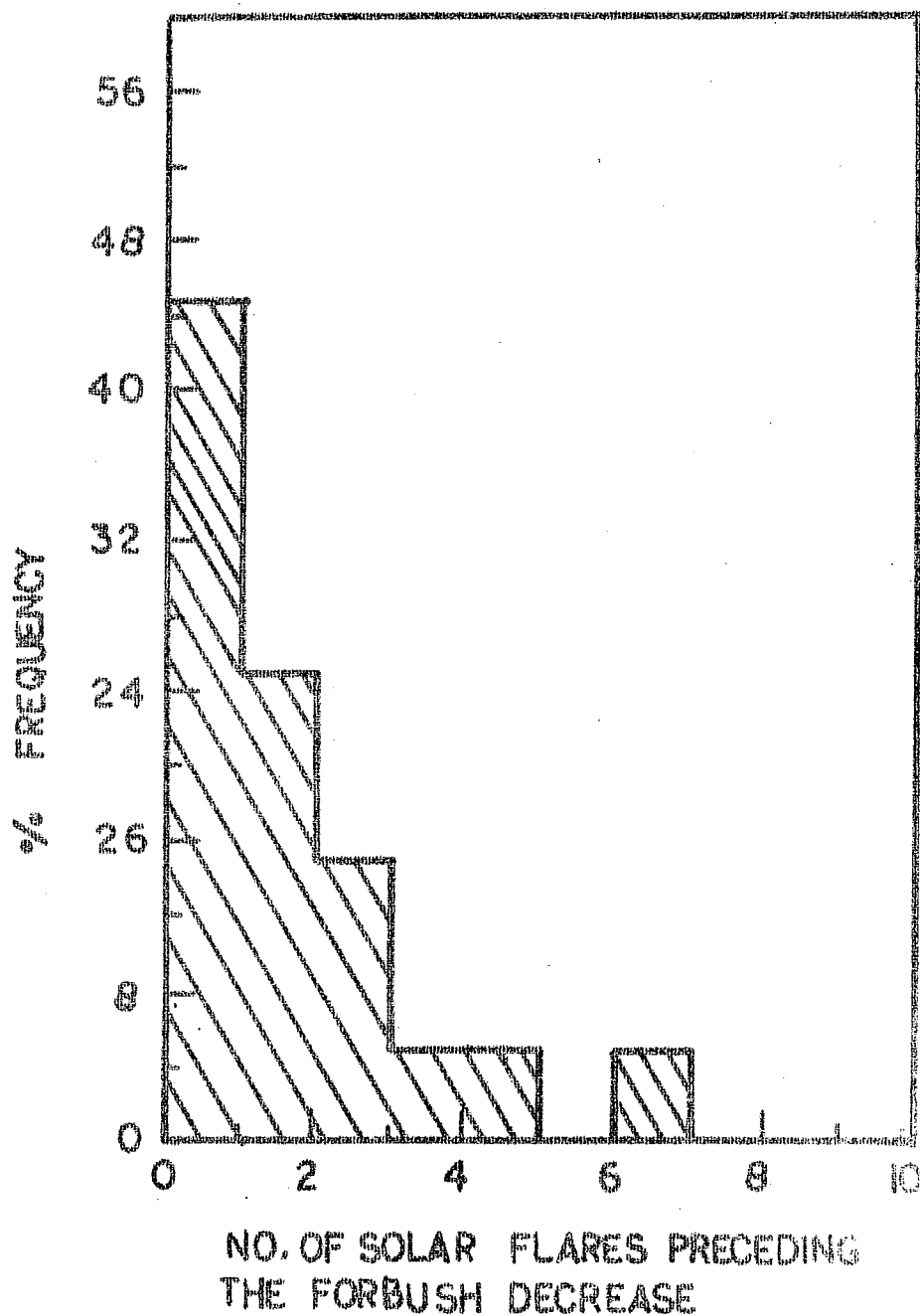


Figure 5.13 Histogram of number of solar flares of importance  $\geq 2B/3N$  occurring upto 100 hours prior to the onset of the recurrent Forbush decreases of magnitude  $\geq 4.0\%$  under study.

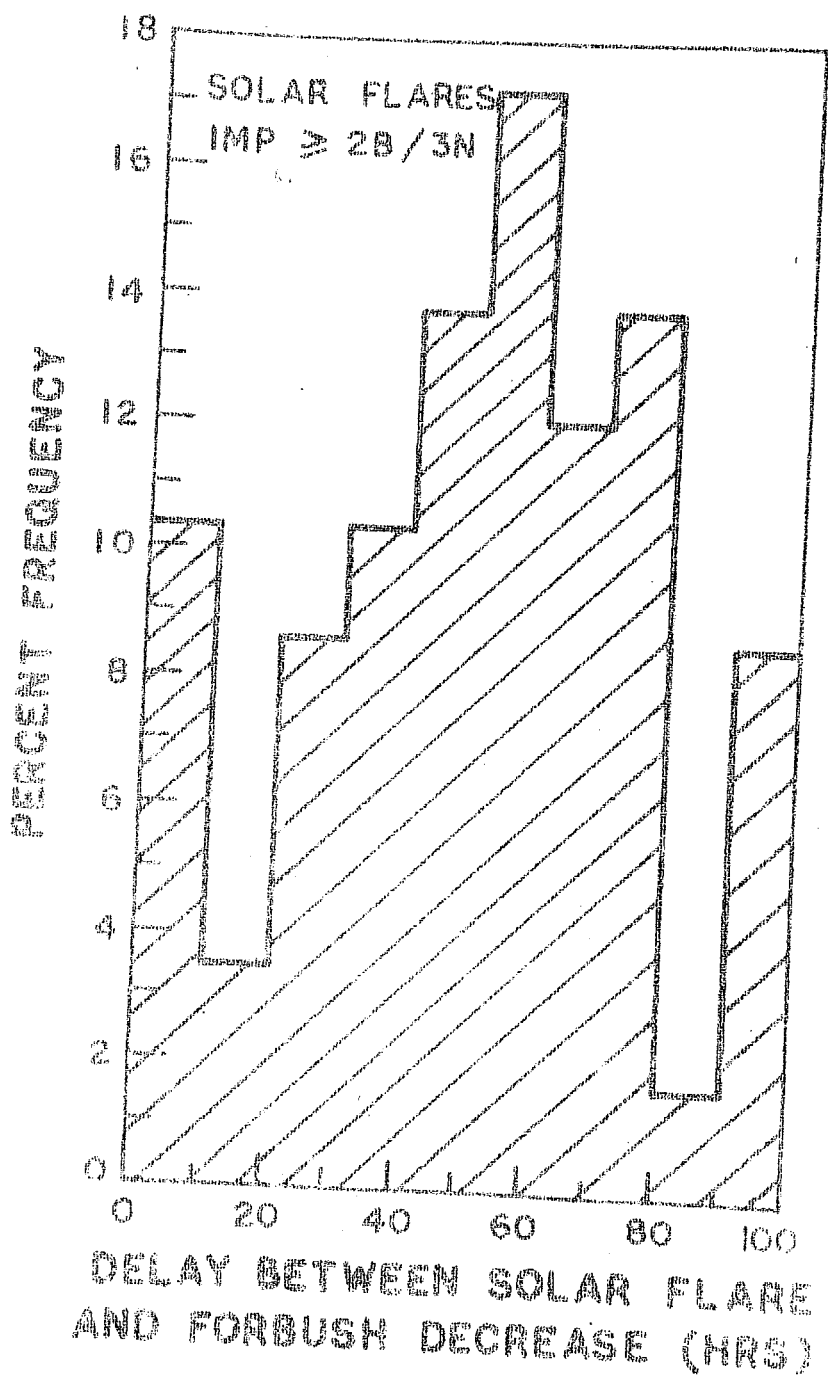


Figure 5.14 Histogram of time delay between the occurrence of a solar flare and onset of the Forbush decrease.

over all the three longitude groups. These six decreases, which cannot be uniquely associated with flares in one of the three longitude groups have been excluded from the analysis. It is further shown from figure 5.13 that in 42% decreases, only one flare occurs within 30-100 hours preceding the decrease so that the association of a flare with these decreases is unique. The next 26% of the decreases are preceded by two solar flares, whileas in the remaining cases, the frequency for association with more than two flares drops fast. To identify the flare having maximum probability of association in such cases, in figure 5.14 is presented the histogram of time delay between all the flares preceding the 28 Forbush decreases under consideration. The histogram reveals a peak around 40-60 hours. It is therefore assumed that a flare with a time delay of 40-60 hours is the most probable flare associated with the decrease. Further it is assumed in such cases, that the flares with coordinates closer to the central meridian are most probable in producing the cosmic ray decrease. These criteria have been used to associate a particular flare with a decrease. Table 5.3 presents details of these 28 Forbush decreases with the associated flares along with the Forbush decreases not preceded by any flare.

Based on the above criterion of flare association, figure 5.15 shows the histograms of time of diurnal maximum in the recovery phase of the recurrent Forbush decreases of magnitude  $\geq 4\%$  and associated with solar flares in the three



different longitude regions;  $90^{\circ}\text{E}$ - $20^{\circ}\text{E}$ ,  $20^{\circ}\text{E}$ - $20^{\circ}\text{W}$  and  $20^{\circ}\text{W}$ - $90^{\circ}\text{W}$ . The fourth histogram in the same figure corresponds to recurrent Forbush decreases not preceded by any solar flare. To reduce the uncertainties in the time of diurnal maximum on low amplitude days, the days exhibiting diurnal amplitudes  $\geq 0.2\%$  only have been included in the histogram. Details of diurnal amplitudes and times of maximum on these days along with the related solar and geomagnetic parameters are mentioned in table 5.3. For the Forbush decreases associated with flares in the longitude region  $90^{\circ}\text{E}$  to  $20^{\circ}\text{E}$ , the histogram reveals that more than 60% of days exhibit diurnal time of maximum between 06-12 hours during the recovery phase. Figure 5.15b, corresponding to Forbush decreases preceded by solar flares occurring in the longitudes  $20^{\circ}\text{E}$  to  $20^{\circ}\text{W}$ , shows that the percentage of days with diurnal morning maximum (06-12 hours) drops to 45% in this group. In the third histogram, figure 5.15c, the Forbush decreases preceded by west limb solar flares ( $20^{\circ}\text{W}$  to  $90^{\circ}\text{W}$ ), do not at all exhibit diurnal variation with morning maximum in their recovery phase but reveal the persistence of the average 18 hour component alone. The analysis therefore shows a systematic change in the frequency of occurrence of the anomalous diurnal variation in the recovery phase of recurrent Forbush decreases associated with the solar flares at various longitudes. The recurrent Forbush decreases not preceded by any solar flare (5.15d), also show a moderate probability ( $\approx 23\%$ ) for producing the

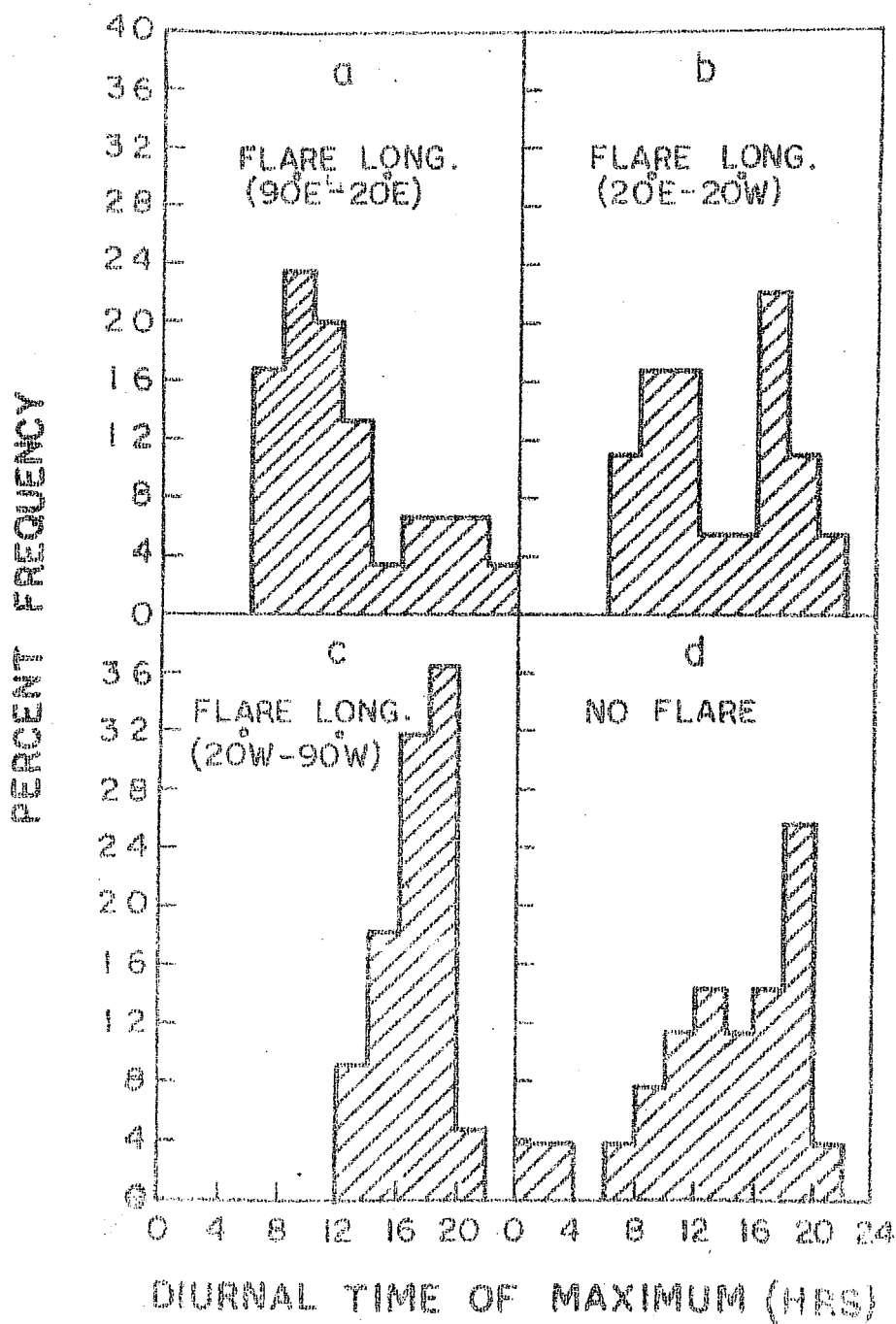


Figure 5.15a,b,c,d Histograms of time of diurnal maximum in cosmic ray intensity during the recovery phase 27 day recurrent Forbush decreases of magnitude 4.0% in Deep River neutron monitor during the years 1960-1970. a) associated with solar flares between 90°E-20°E, b) between 20°E-20°W, c) between 20°W-90°W and d) no solar flare.

morning maximum in the diurnal variation. It should be again emphasized that in certain Forbush decreases the non-rigorous criterion of associating with one particular flare does not introduce any error in the conclusions above since, as already pointed out, each Forbush decrease is at least uniquely associated with a flare or flares in one of the three longitude belts. Also, the  $\chi^2$  test applied to these histograms has shown them to be significantly different from random distribution.

A study has also been made of the Forbush decreases which are nonrecurrent and are not even associated with a recurrent SC and/or a period of high  $K_p$ . Such decreases have again been found to exhibit predominantly the diurnal variation with 18 hour maximum in their recovery phase (figure 5.16). The predominance of the diurnal variation with maximum at 18 hours in the recovery phase of the nonrecurrent Forbush decreases as well as the recurrent decreases with apparent association with west limb flares is conspicuous.

There has been only one nonrecurrent Forbush decrease of magnitude  $\gg 4\%$  occurring on May 31, 1966 having an apparent association with a west limb flare of importance 2B, coordinates N15 W47, which shows anomalous diurnal variation with morning maximum for four successive days during its recovery phase. This decrease is included in the histogram for the diurnal time of maximum in the recovery phase of the nonrecurrent Forbush decreases (figure 5.16). Another

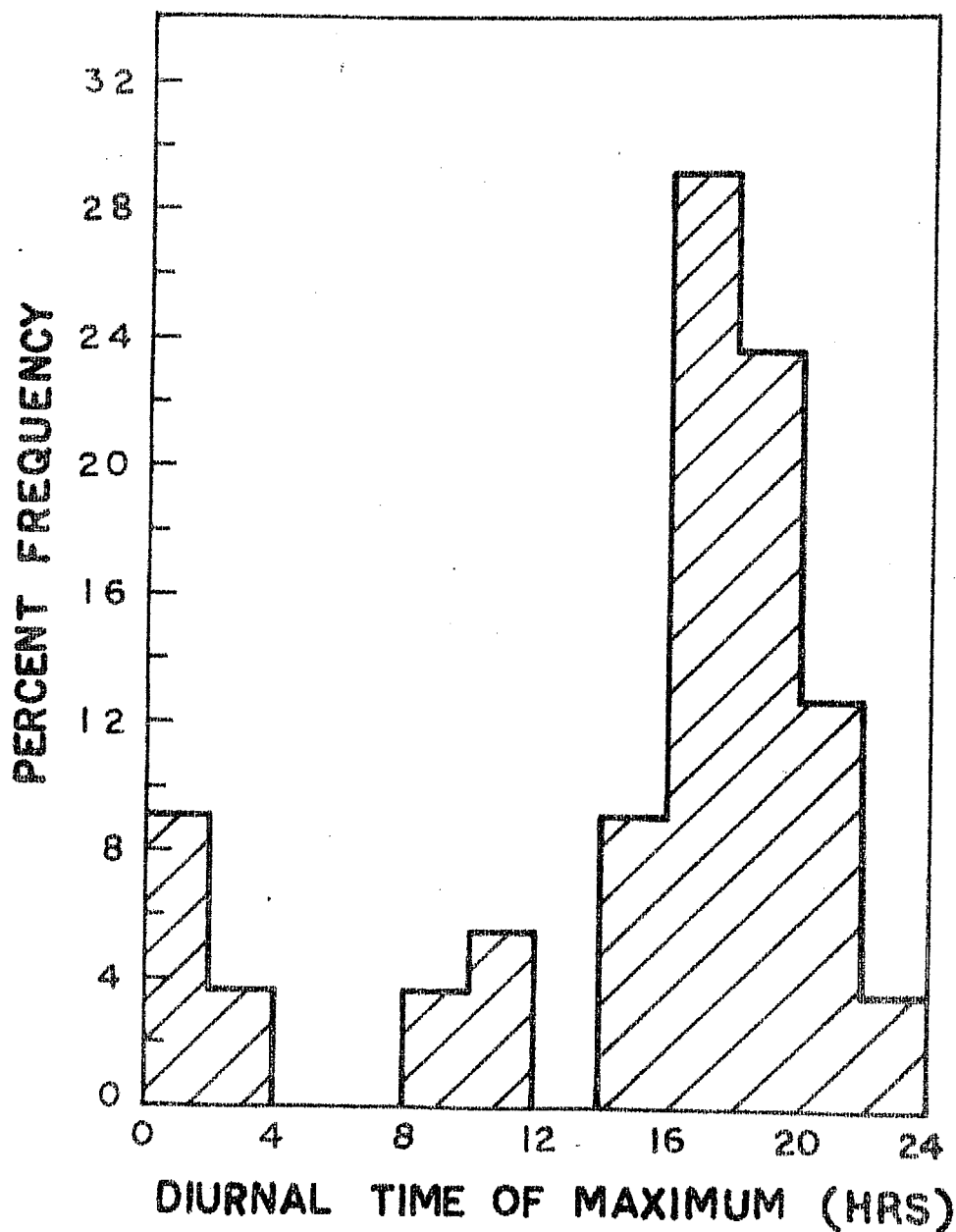


Figure 5.16 Histogram of time of diurnal maximum in cosmic ray intensity during the recovery phase of 27 day nonrecurrent Forbush decreases of magnitude  $\geq 4.0\%$  in Deep River neutron monitor during the years 1960-1970.

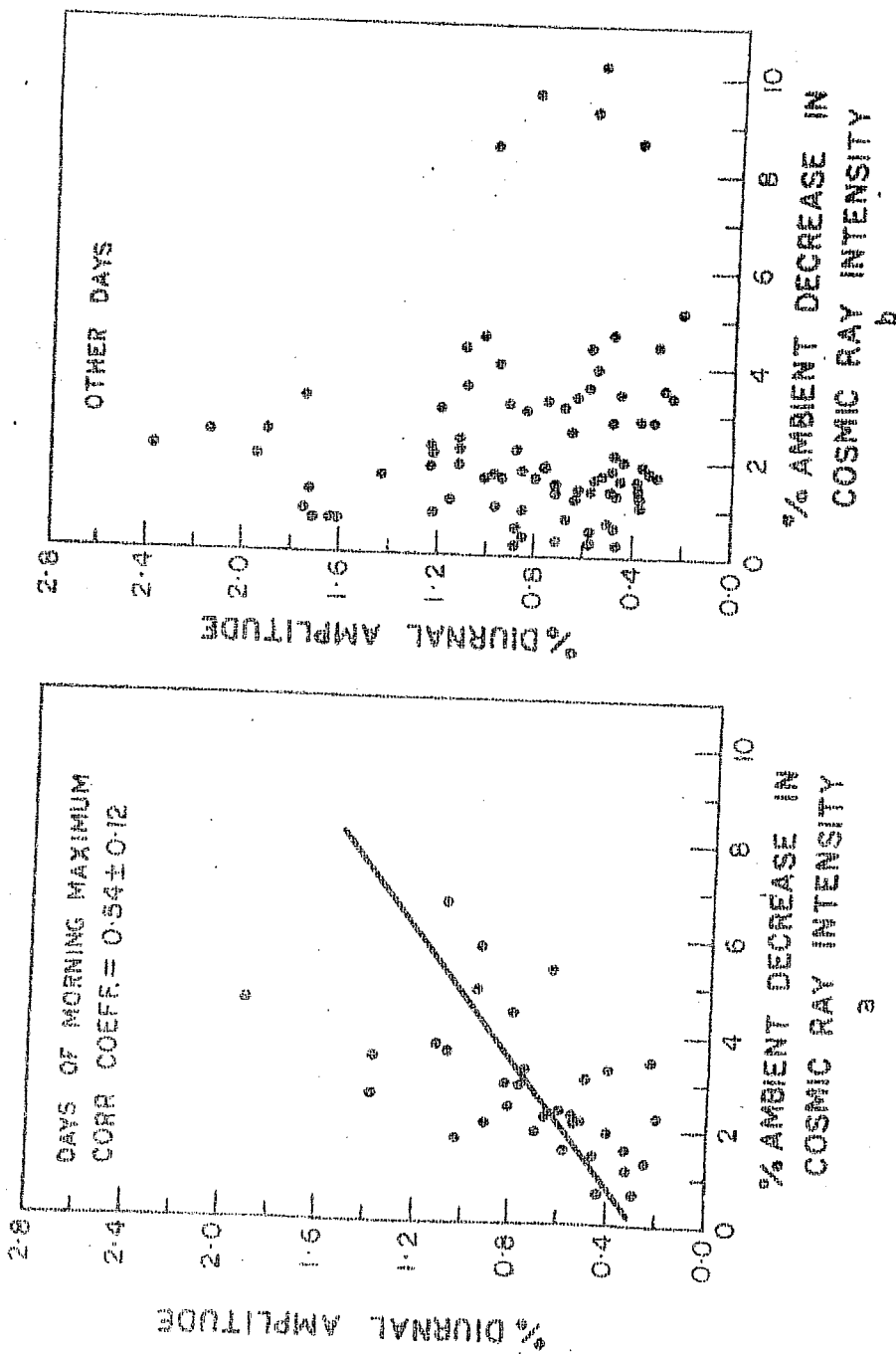


Figure 5.17a, b Dependence of percent diurnal amplitude in cosmic ray intensity on the percent decrease in the mean intensity level in the recovery phase of 27 day recurrent Forbush decreases of magnitude 4.0% in Deep River neutron monitor during the years 1960-1970.  
 a) anomalous diurnal variation days,  
 b) other days.

1200-1300

the diurnal variation characteristics in the interplanetary space during the recovery phase of recurrent Forbush decreases of magnitude  $\geq 4.0\%$  during the years 1960-1970, associated with a solar flare between longitudes 90E-20E.

Year	Day of Forbush decrease	Hour of onset	Decrease in Deep River NM	Coordinates of the associated flare			Time of flare	Importance of the flare	Diurnal variation		
				Lat.	Long.	Mcmnath region			Day	Amplitude (%)	Time of maximum (hrs)
1963	May 03	00 UT	5.5%	N18	E47	6790	May 01, 0548 UT	3+	May 05	0.24	11.03
									06	0.20	10.95
									07	0.48	12.62
									08	0.43	6.36
									09	0.29	11.51
1966	Aug. 29	18 UT	8.0%	N23	E26	8461	Aug. 26, 1806 UT	2B	Sept.01	0.64	8.10
1966	Dec. 13	18 UT	5.0%	N23	E38	8610	Dec. 10, 1430 UT	2B	Dec. 15	1.38	8.20
									16	0.75	7.72
									17	0.60	7.79
									18	0.50	11.94
1967	Feb. 07	18 UT	4.0%	N11	E40	8682	Feb. 04, 1640 UT	2B	Feb. 10	0.44	13.60
									11	0.47	14.73
1967	May 25	18 UT	8.0%	N28	E24	8818	May 23, 1835 UT	3B	May 27	1.09	9.71
									28	0.94	8.18
									29	0.96	10.01
1967	June 25	00 UT	4.0%	N13	E74	8863	June 23, 1032 UT	3N	July 01	1.38	10.96
									02	0.76	7.89
									03	1.03	8.35
									04	0.58	9.30
1969	June 08	06 UT	5.0%	S13	E61	10135	June 05, 2308 UT	3B	June 11	1.09	21.39
									12	0.96	23.24
									15	0.91	20.45
1969	Nov. 09	00 UT	5.0%	N29	E31	10412	Nov. 07, 1804 UT	3B	Nov. 11	1.90	12.33
									12	1.11	13.14
									13	0.49	18.29
1970	July 23	06 UT	7.0%	N08	E55	10845	July 20, 1109 UT	2B	July 26	1.91	8.69
									27	1.07	6.68
									28	0.45	18.45
									29	1.19	16.69
									30	1.75	17.10

Table 5.3b.

The characteristics of the diurnal variation in the cosmic ray intensity in the interplanetary space during the recovery phase of recurrent Forbush decreases of magnitude  $> 4.0\%$  during the years 1960-1970, associated with a solar flare between longitudes  $20^{\circ}\text{E}-20^{\circ}\text{W}$ .

Year	Day of Forbush decrease	Hour of the onset	Decrease in Deep River NM	Coordinates of the associated flare		Time of flare	Importance of the flare	Diurnal variation		
				Lat.	Long.			Day	Amplitude (%)	Time of maximum (hrs)
1960	May 29	00 UT	5.0%	N16	W15	5669	2+	May 31	0.41	8.48
								June 01	0.35	15.10
1960	June 27	02 UT	7.0%	N20	E06	5713	3	June 29	0.81	11.59
								June 30	0.21	0.19
1963	Sept. 22	00 UT	9.0%	N15	E05	6964	2+	July 01	1.12	21.99
								July 02	0.31	18.60
1965	June 15	22 UT	4.0%	N24	E00	7847	2	Sept. 25	1.10	17.38
								Sept. 26	0.84	17.94
1969	May 14	18 UT	7.0%	N17	E20	10084	2B	June 17	0.91	11.66
								June 18	0.70	9.30
1969	May 14	18 UT	7.0%	N17	E20	10084	2B	June 19	0.47	6.70
								June 20	0.32	6.42
								May 17	1.12	9.62
1969	May 14	18 UT	7.0%	N17	E20	10084	2B	May 18	1.11	13.86
								May 19	1.11	18.86
								May 20	0.97	17.30
1969	May 14	18 UT	7.0%	N17	E20	10084	2B	May 21	1.22	16.58

Table 5.3c. The characteristics of the diurnal variation in the cosmic ray intensity in the interplanetary space during the recovery phase of recurrent Forbush decreases  $> 4.0\%$  during the years 1960-1970, associated with a solar flare between longitudes  $20^{\circ}\text{W}-90^{\circ}\text{W}$ .

Year	Day of Forbush decrease	Hour of onset	Decrease in Deep River NM	Coordinates of the associated flare Lat. Long. McMath region	Time of flare	Importance of the flare	Diurnal variation Day	Amplitude (%)	Time of maximum (hrs)
1963	May 27	22 UT	4.0%	N05 W80 6805	May 25 1627 UT	2	June 01 02 03 04 05	0.65 0.48 0.49 0.47 0.46	17.21 19.41 17.48 19.15 21.54
1966	July 08	18 UT	5.0%	N34 W45 8362	July 7 0022 UT	2B	July 11 12 14 15	0.55 1.23 0.95 0.71	17.70 18.10 17.22 17.40
1969	March 16	22 UT	4.0%	N12 W78 9966	March 12 1739 UT	3B	March 18 19	1.73 1.24	19.16 17.30
1969	April 27	00 UT	6.0%	N22 W63 10035	April 24 0304 UT	2B	April 30 May 01 02 03 04	1.75 0.97 1.23 0.89 1.44	18.57 18.72 13.95 14.96 18.50
1970	March 31	04 UT	5.0%	N15 W38 10641	March 29 0140 UT	2B	April 02 03 04 05 06	0.85 1.64 1.72 0.86 1.64	13.13 15.08 15.69 17.57 18.11
1970	April 20	18 UT	4.0%	N20 W70 10675	April 18 2235 UT	2B	April 22	1.60	15.79



interplanetary space during the recovery phase of recurrent Forbush decreases of magnitude  $\geq 4\%$  during the years 1960-1970, not preceded by any solar flare of importance  $\geq 2B/3N$  upto 100 hours prior to the decrease

Year	Day of Forbush decrease	Hour of the onset	Decrease in Deep River NM	Diurnal variation		Time of maximum (hrs.)
				Day	Amplitude (%)	
1961	February 03	00 UT	5.0%	February	07 0.57	16.70
					08 0.58	17.70
					09 0.88	18.10
					10 0.88	17.79
1961	April 13	18 UT	7.0%	April	15 0.77	17.78
					16 0.81	18.25
					17 0.49	13.98
1963	March 08	20 UT	4.0%	March	13 0.45	17.22
					14 0.54	18.96
					15 0.53	14.61
					16 0.39	15.35
1963	September 14	00 UT	4.0%	September	19 0.69	18.15
					20 0.51	8.27
1966	October 24	00 UT	5.0%	October	28 0.23	11.06
					29 0.56	7.14
1967	January 07	20 UT	5.0%	January	11 0.81	10.20
					12 0.53	8.86
1967	October 27	00 UT	6.0%	October	31 0.50	12.40
				November	01 0.32	12.25
					02 0.56	3.90
					03 0.59	21.30
1968	January 26	16 UT	5.0%	January	28 0.66	10.59
					29 0.31	15.19
					30 0.39	18.11
				February	01 0.57	13.92
1969	April 01	02 UT	4.0%	April	04 1.02	18.14
					05 1.16	18.36
					06 0.86	17.43
1969	April 12	20 UT	6.0%	April	15 0.28	0.11
					16 0.76	18.93
					17 0.05	16.16

The characteristics of the diurnal variation in the cosmic ray intensity in the interplanetary space during the recovery phase of nonrecurrent Forbush decreases of magnitude  $\gg 4\%$  during the years 1960-1970.

Year	Day of Forbush decrease	Hour of the onset	Decrease in Deep River NM	Coordinates of the associated solar flare	Lat. Long. McMath region	Time of flare	Import- ance of the flare	Diurnal Day	Ampli- tude %	Time of maximum (hrs.)
1960	Aug. 14	10 UT	4.0%	N22 E27	5794	Aug. 11 1924 UT	3+	Aug. 16	0.52	0.66
								17	0.72	10.46
								18	0.41	21.92
1966	Jan. 19	20 UT	4.0%	N19 E27	8131	Jan. 17 1046 UT	3B	Jan. 23	0.78	17.36
								24	0.90	16.67
								25	0.66	17.35
								26	1.05	19.00
								27	0.90	17.10
1967	Sept. 19	22 UT	4.0%	N15 E61	8985	Sept. 17 0353 UT	2B	Sept. 22	0.96	15.57
								23	0.51	17.01
								24	0.77	18.24
1961	July 18	00 UT	5.0%	N14 E14	6172	July 15 1434 UT	3+	July. 20	1.32	2.10
								21	0.40	1.10
								22	0.69	0.30
								23	0.74	22.90
1962	April 20	22 UT	5.0%	N09 E03	6393	April 18 1734 UT	3	April 22	0.53	12.82
								26	0.35	0.68
1963	Oct. 29	20 UT	5.0%	N12 W20	7003	Oct. 28 0158 UT	3	Oct. 31	0.46	19.19
								Nov. 01	0.77	18.30
1967	Feb. 15	22 UT	5.0%	N22 W10	8687	Feb. 13 1746 UT	4B	Feb. 17	0.38	14.83
								18	0.75	14.93
								19	0.44	16.82
								20	0.87	16.21
								21	0.29	14.63
1969	Jan. 26	04 UT	5.0%	N20 W09	9879	Jan. 24 0803 UT	2B	Feb. 02	1.27	16.17

exception is the recurrent Forbush decrease of June 8, 1969 of magnitude 5%, associated with the east limb flare having coordinates S13 E61 but showing diurnal variation with maximum around 21 hours for three consecutive days in the recovery phase. This behaviour of diurnal variation during the recovery phase of these two individual Forbush decreases is contradictory to the results presented in figure 5.15 and is not yet understood.

Another property of the diurnal variation with maximum in the morning hours is revealed in figure 5.17, wherein the percent diurnal amplitudes are plotted against percent decrease in the mean intensity on individual days. It is found that on the days of morning maximum, the percent diurnal amplitude indicates a linear relation with the percent decrease in the mean intensity, though the correlation coefficient is only  $0.54 \pm 0.12$ . Such a relation is totally absent on the days when diurnal vectors lie in the other three quadrants in the interplanetary space. The dependence of the percent amplitude of the anomalous diurnal variation on the percent decrease in the mean intensity, though not confirmative, suggests a different character of these Forbush decreases. The implication of this dependence, if true, is not yet fully understood.

From the analysis presented above and that in section V.2, the following conclusions are drawn about the enhanced anomalous diurnal variation with maximum between 06-12 hours.

- (1) The days of enhanced anomalous diurnal variation with maximum in the morning hours occur in bunches, ranging from 1-5 days, during the recovery phase of recurrent Forbush decreases, just after the decrease phase is over.
- (2) The probability of occurrence of the anomalous diurnal variation is enhanced in the case of recurrent Forbush decreases associated with east limb solar flares.
- (3) Recurrent Forbush decreases preceded by west limb solar flares do not produce the anomalous diurnal variation, but only the diurnal variation with maximum in the 13 hour direction.
- (4) The nonrecurrent Forbush decreases also exhibit only the 13 hour diurnal variation in their recovery phase and not the anomalous diurnal variation.
- (5) The rigidity spectrum of the anomalous diurnal variation is not significantly different from that of the average diurnal variation with spectral exponent  $\approx 0.0$ .

#### V.4 Recurrent Forbush decreases and solar flares

In this section an attempt is made to understand the relationship between the recurrent Forbush decreases and the preceding solar flares.

Figure 5.18 shows the histogram of longitudes of the solar flares preceding the recurrent Forbush decreases under study. The histogram corresponds to only those decreases which are preceded by flares in only one of the three groups:

(1)  $90^{\circ}\text{E}-20^{\circ}\text{E}$ , (2)  $20^{\circ}\text{E}-20^{\circ}\text{W}$  and (3)  $20^{\circ}\text{W}-90^{\circ}\text{W}$ . The figure reveals that the east limb flares peak around  $30^{\circ}\text{E}-40^{\circ}\text{E}$  indicating their association with the decreases. On the other hand, the west limb flares reveal a flat distribution, so apparently no association with the recurrent Forbush decreases.

In figure 5.19 is presented a Chree analysis of neutron intensity at Deep River during the Forbush decreases having apparent association with flares in the three longitude groups separately as well as for the Forbush decreases which are not preceded by any flare. The hourly intensity profiles at Deep River during the decreases have been superposed upon each other with the hour of onset of the decrease as epoch. It is observed that the average magnitude of the decrease in the case of Forbush decreases preceded by west limb flares ( $20^{\circ}\text{W}-90^{\circ}\text{W}$ ) and those not preceded by any flare, are  $\approx 2.4\%$  each, while it is  $\approx 4.2\%$  if the associated flare lies between  $20^{\circ}\text{E}-20^{\circ}\text{W}$ , and  $\approx 3.4\%$  for flares between  $90^{\circ}\text{E}-20^{\circ}\text{E}$ . This indicates that the fresh plasma from an east limb or central meridian flare enhances the depression in the intensity during the recurrent decreases. The decrease in the intensity being smaller for Forbush decreases associated with west limb flares as well as for those not preceded by any flare, suggests that the plasma from the west limb flare does not affect the corotating stream causing the recurrent Forbush decrease.

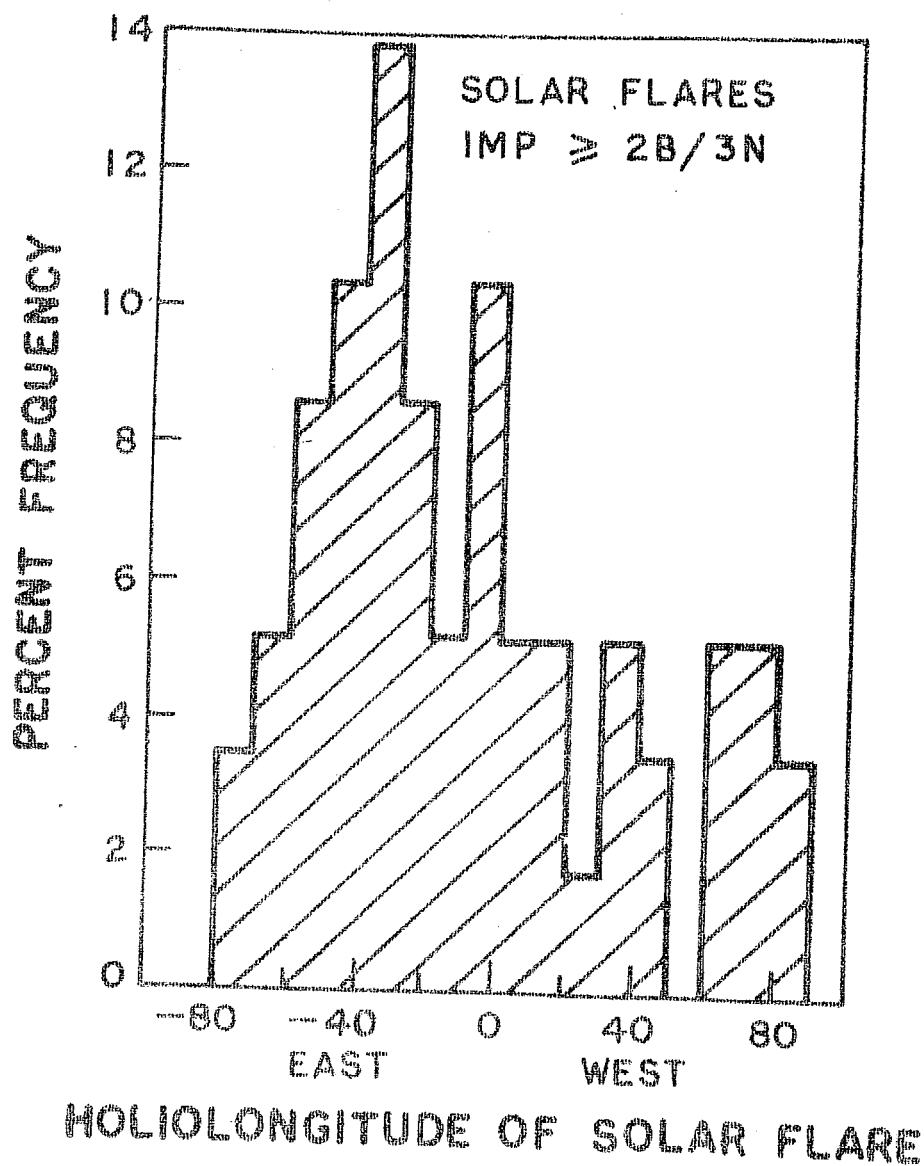


Figure 5.18 Histogram of longitudes of the solar flares associated with 27 day recurrent Forbush decreases during the years 1960-1970.

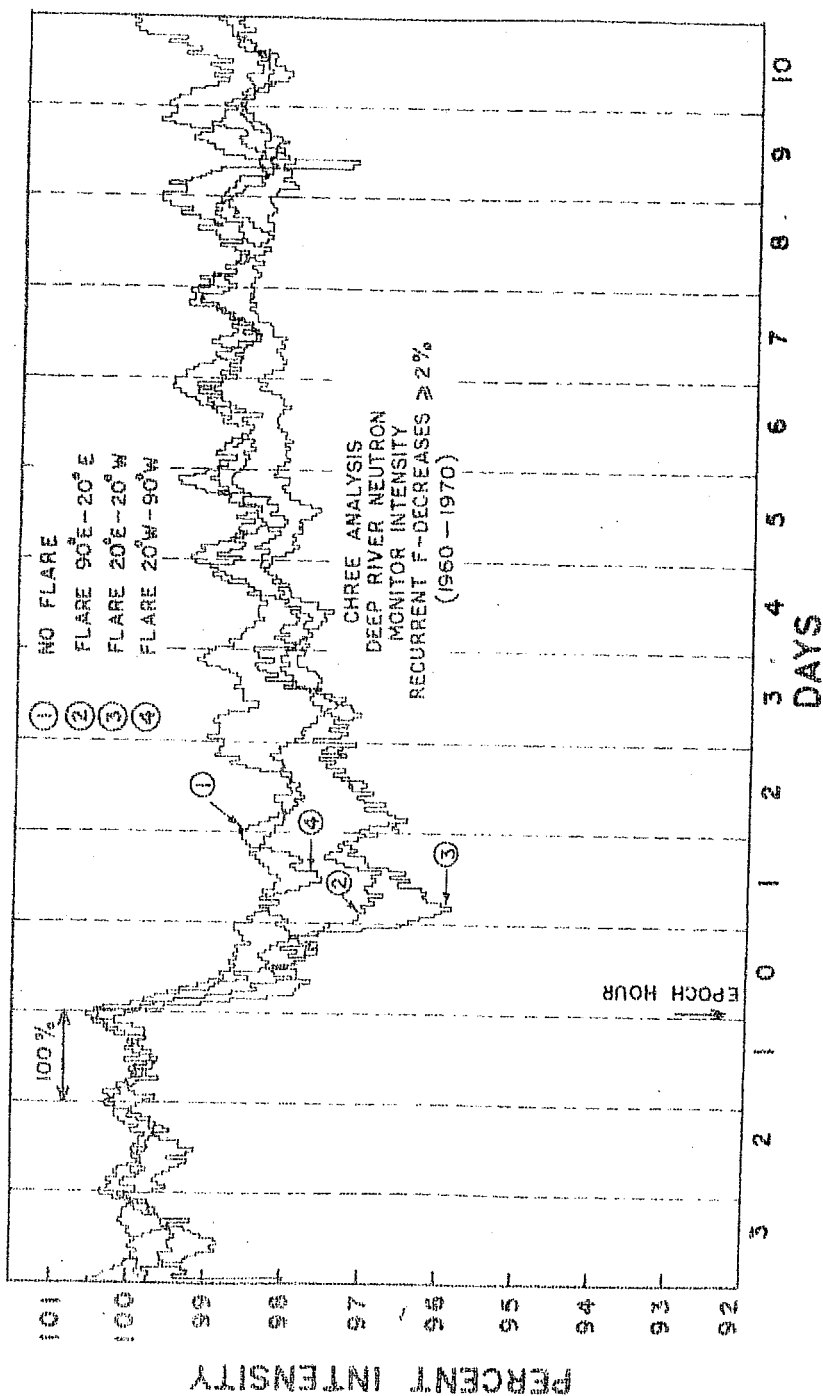


Figure 5.19 Chree analysis of percent intensity in Deep River neutron monitor during the 27 day recurrent Forbush decreases during the years 1960-1970, associated with solar flares in various longitude groups as well as without an association with a flare.

This is also understandable since the plasma cloud from the west limb flare emitted about 30-100 hours prior to the decrease will not, in general, engulf the earth unless the angular dimension of the plasma cloud is excessively large.

A check has been made of the effect of plasma cloud from an east limb flare on the periodicity of the 27 day recurrent Forbush decrease. For example if the flare occurs in the same solar active region producing the corotating stream of enhanced solar wind velocity associated with the decrease, it may widen the angular extent of the stream. In such a case the time interval between two Forbush decreases will be smaller than 27 days if the earlier decrease is not preceded by any flare while the latter one is associated with an east limb flare and vice versa. An investigation along these lines has not, however, yielded any conclusive results.

A variety of other analyses were also undertaken to explore the relationship between the recurrent Forbush decreases causing the anomalous diurnal variation in the recovery phase and the preceding flares. A few examples of these are: (1) correlation with the flare importance, (2) area of the solar flare, (3) frequency of solar flares in the active region on the visible side of the solar disc, (4) number of solar rotations for which the McMath region was active and (5) area and intensity of the calcium plage. None of these investigations have yielded any conclusive results.



## V.5 Corotating corpuscular streams and the anomalous diurnal variation in the cosmic ray intensity

An M region on the solar disc has been defined as the region of prolonged activity causing 27 day recurrent geomagnetic disturbances (Bartels, 1934). Snyder et al.(1963) have indicated that these regions produce corotating streams of enhanced solar wind velocity; a conclusion also arrived at by Sarabhai (1963), Mustel (1963) and Razdan et al.(1965). Such regions have been sometimes identified with sunspots having elevated coronal temperatures, while in many cases they are found to exist independently for many solar rotations (Chapman and Bartels, 1940). A number of authors, Billigs and Roberts (1964), Davis (1965), Pneuman and Kopp (1971), Gosling et al.(1972) and Pneuman (1972) have, however, suggested that the corotating streams might originate from magnetically open regions in the corona rather than from the regions of elevated coronal temperatures. From the X-ray images of the sun taken on November 24, 1970, Krieger et al. (1972) have reported observations of such a 'coronal hole', giving high velocity solar wind. Similar idea is also advocated by Parker (1973) namely, that the M region on the sun can be identified as the regions producing high velocity solar wind on either side of an active region with high localized magnetic fields which oppose the flow of solar wind there and thus reduce the wind velocity.

The corotating streams of enhanced solar wind velocity have been earlier shown to be associated with 27 day recurrent Forbush decreases (section V.3). It is expected that the solar wind with enhanced velocity, sweeping out solar magnetic field irregularities in the stream, causes larger outward convection of cosmic ray particles. In an equilibrium state, the enhanced outward convection coupled with the simultaneous inward diffusion of particles from all sides, gives rise to the quasi-permanent depressed cosmic ray intensity inside the stream for many solar rotations, producing the 27 day recurrent Forbush decreases.

Some of the 27 day recurrent Forbush decreases have been shown to be followed by anomalous diurnal variation with morning maximum during the recovery phase and in many instances they are also associated with east limb solar flares. Further the anomalous diurnal variation is rigidity independent upto 100 GV as in the case of the average diurnal variation with 18 hour maximum. This is taken as an indication of similar interplanetary processes responsible for both the types of diurnal variations namely the radially outward convection of cosmic ray particles by the interplanetary magnetic field irregularities moving with the solar wind and the simultaneous field parallel and perpendicular diffusion of cosmic rays.

During the course of solar rotation a corotating stream engulfs the earth from east of the earth-sun line. In such a case, the transient modulating region offers larger modulation depth on east of earth-sun line than on west for at least a few days after the earth enters the stream (figure 5.21). The asymmetry of modulating region with respect to the specialized location of the earth in the stream causes a larger inward diffusion of cosmic ray particles at earth from west of the earth-sun line than from the east. In other words, the diffusion parallel to the interplanetary magnetic field line from the garden hose direction is greater than the diffusion from the antigarden hose direction (figure 5.21). In the specialized geometry inside the corotating stream, the field perpendicular diffusion from the 03 hour direction (west of the earth-sun line) is also expected to be large because of smaller extent of the transient modulating region while there is practically negligible diffusion from the 15 hour direction. The anomalous diurnal variation is then the combined effect of the enhanced radially outward convection and the field parallel and perpendicular diffusions from west of the earth sun line in a solar corotating stream.

The effect of the east limb flares preceding the recurrent Forbush decreases seems to be very conspicuous on the occurrence of the anomalous diurnal anisotropy. An east limb flare preceding the recurrent decrease indicates that the flare takes place either in the solar active region

producing the corotating stream or in the nearby region on the solar disc. The three possible configurations of the corotating stream and the plasma cloud from an east limb flare are shown in the figure 5.20 a,b,c. The plasma cloud has been shown to have larger angular width, since the M-region streams often have an angular width  $\simeq 20^\circ - 30^\circ$  (Chapman, 1929) while plasma clouds of angular width  $\gg 90^\circ$  from solar flares are not uncommon. In all the three cases, modulation depth increases further on the east of the earth sun line than on west, enhancing the probability of getting anomalous diurnal variation during the recovery phase of the Forbush decrease.

In figure 5.20d, is presented the possible configuration of the electromagnetic state of the interplanetary medium when a corotating stream producing the decrease and the plasma cloud from a west limb flare exist simultaneously in the interplanetary space. The plasma cloud from such a flare does not interact with corotating stream, but it produces a region of depressed intensity on the west of the earth-sun line. As viewed from the earth, the combined effect of the corotating stream and the plasma cloud from the west limb flare is to produce a larger modulating depth on west than on east of the earth sun line. This causes now a greater diffusion of cosmic ray particles from east of the earth-sun line than from west, mostly along the field lines, in the 21 hour direction as in the case of average diurnal variation model. Thus, while a corotating stream above can possibly

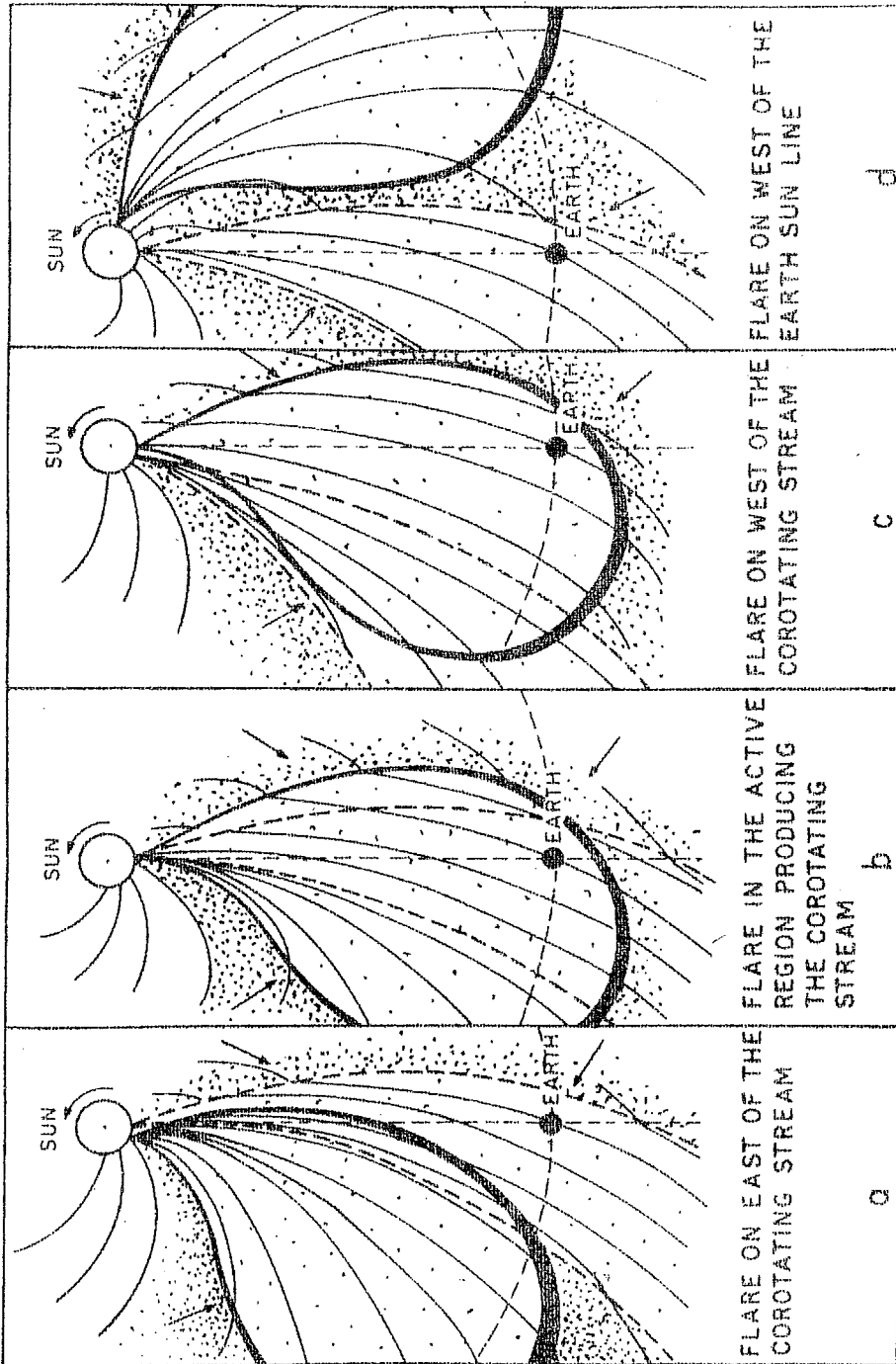


Figure 3.20a, b, c, d. Schematic representation of interplanetary magnetic field conditions in the interplanetary space for various positions of occurrence of a solar flare relative to the active region producing the corotating corpuscular stream. The figure also indicates cosmic ray diffusion inside the transient modulation region of the plasma cloud from the solar flare and the corotating stream.

produce anomalous diurnal variation, it cannot do so when a plasma cloud from a west limb flare exists simultaneously.

A simplified picture of the convection and diffusion of cosmic rays in a corotating stream is presented in figure 5.21, which leads to the anomalous diurnal variation with maximum in the garden hose direction (09 hours) inside the stream. The total streaming equation of cosmic rays (equation 1.19) is again stated below (for quick reference).

$$\begin{aligned} \tilde{S}(\tilde{r}, T) = CUV_{\tilde{s}} - K_{\parallel} \left[ \frac{\partial \tilde{U}}{\partial \tilde{r}} \right]_{\parallel} - K_{\perp} \left[ \frac{\partial \tilde{U}}{\partial \tilde{r}} \right]_{\perp} \\ - \frac{v^2}{3c} \cdot \frac{(\omega \tilde{r})^2}{[1 + (\omega^2 \gamma^2)]} \cdot \frac{\left[ \frac{\partial \tilde{U}}{\partial \tilde{r}} \times \tilde{B} \right]}{B} \dots (5.1) \end{aligned}$$

In the absence of north-south cosmic ray particle density gradients (as in the case of average cosmic ray diurnal variation, Subramanian, 1971), the last term in the above equation can be omitted for simplicity in the following calculations. The effects of such temporary heliolatitudinal density gradients are described later.

The various components of the streaming  $\tilde{S}$  inside a solar corotating stream are shown in figure 5.21. Consider cosmic ray particles of rigidity 9 GV corresponding to the mean rigidity response of high latitude neutron monitors. For a solar wind velocity of  $400 \text{ km sec}^{-1}$ , the anisotropy  $\tilde{\alpha} = 3\tilde{S}/vU$  in the radial direction due to convective streaming ( $CUV_{\tilde{s}}$ ), turns out to be 0.56%. Resolving it along and

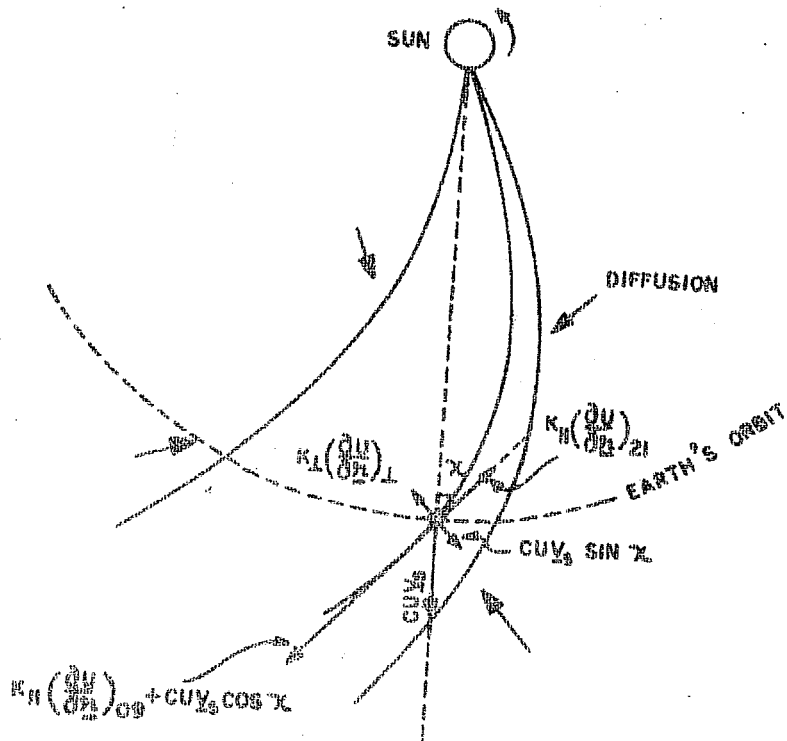


Figure 5.21 Cosmic ray streaming vectors inside a simple corotating solar corpuscular stream.

perpendicular to the interplanetary magnetic field line having garden hose angle of  $45^\circ$ , both the components are found to be of 0.4% amplitude. In order to explain the observed enhanced diurnal amplitude of 0.8%, along the garden hose direction, the field perpendicular convective component in the 15 hour direction should be cancelled by the field perpendicular diffusion from the 03 hour direction, while the field parallel diffusion from the 09 hour direction should add 0.4% anisotropy to the component of convective anisotropy in that direction. The field perpendicular convective component in 15 hour direction can be cancelled if there is a net diffusion streaming

$K_{\perp} \left[ \frac{\partial U}{\partial r} \right]_{\perp}$  perpendicular to the field lines from the west of the earth-sun line (03 hour direction) having magnitude  $CUV_s \cdot \sin \chi$ , where  $\chi$  is the garden hose angle. For a 5% difference in the intensity at earth and outside the transient modulating region, and a modulating depth of about 0.13 AU in the 03 hour direction (estimated approximately from the geometry of the stream), the percent gradient

$\frac{1}{U} \cdot \left[ \frac{\partial U}{\partial r} \right]_{\perp}$  turns out to be  $2.6 \times 10^{-12} \text{ cm}^{-1}$ . Equating  $K_{\perp} \left[ \frac{\partial U}{\partial r} \right]_{\perp}$  with  $CUV_s \cdot \sin \chi$ , we get  $K_{\perp} = 1.56 \times 10^{21} \text{ cm}^2 \text{ sec}^{-1}$ . The value of  $K_{\perp}$  derived in this case is of comparable magnitude with the value  $2 \times 10^{21} \text{ cm}^2 \text{ sec}^{-1}$  quoted by Jokipii and Coleman (1968) and Jokipii (1971), from the power spectrum of the interplanetary magnetic field measured by Mariner IV, for the period November 1964-May 1965, although the two are not strictly comparable.



In the case of field parallel diffusion of cosmic rays, adding 0.4% anisotropy along the garden hose direction to the convective anisotropy, there could be two possibilities. First, that the transient corotating stream imposes a very large modulation depth in the antigarden hose direction, so that only the diffusion along the garden hose direction contributes significantly to the observed diurnal anisotropy. In this case, again assuming a 5% reduction in the cosmic ray density inside the modulating region at earth compared to the region outside the stream, and a modulating depth of 0.5 AU in the garden hose direction (derived approximately from geometry of the stream), the gradient  $\frac{1}{U} \left[ \frac{\partial U}{\partial r} \right]_{\parallel}$  in the particle density turns out to be  $6.7 \times 10^{-13} \% \text{ cm}^{-1}$ . The required diffusive anisotropy of 0.4% in the garden hose direction then gives the field parallel diffusion coefficient  $K_{\parallel}$  to be  $0.6 \times 10^{22} \text{ cm}^2 \text{ sec}^{-1}$ . Jokipii and Coleman (1968) and Jokipii (1971) have arrived at the following empirical relation for the field parallel diffusion coefficient  $K_{\parallel}$  as a function of the particle rigidity  $P$  and the particle velocity  $\beta$  ( $\beta = v/c$ ). For rigidities greater than 1 GV, the relation is

$$K_{\parallel} = 1.5 \times 10^{21} P \beta \text{ cm}^2 \text{ sec}^{-1} \quad \dots(5.2)$$

This leads to a  $K_{\parallel}$  value of  $1.35 \times 10^{22} \text{ cm}^2 \text{ sec}^{-1}$  for the representative particle rigidity of 9 GV. The presently derived value is therefore smaller than the average magnitude.

Alternatively, taking  $K_{\parallel} = 1.35 \times 10^{22} \text{ cm}^2 \text{ sec}^{-1}$  as derived by Jokipii and Coleman (1968) and Jokipii (1971), the required diffusive anisotropy of 0.4% in the garden hose direction can still be obtained by assuming substantial diffusion along the antigarden hose direction as well to partly cancel the streaming from the garden hose direction. In this case the transient modulation depth in the antigarden hose direction has to be limited although still much larger than in the garden hose direction.

The ratio of field perpendicular to field parallel diffusion coefficient  $K_{\perp}/K_{\parallel}$  is 0.26 when the field parallel diffusive streaming is only in the garden hose direction. In the later case of partial streaming from the antigarden hose direction when the average value of  $K_{\parallel}$  (Jokipii and Coleman, 1968) is used, the ratio  $K_{\perp}/K_{\parallel}$  turns out to be 0.12. A unique value of  $K_{\parallel}$  is therefore not possible to obtain since it also depends upon the extent of modulating solar stream beyond the earth's orbit, which is uncertain.

It should be mentioned that the recent experiments on Pioneer 10 for measuring the cosmic ray density (Lentz et al. 1973; Teegarden et al., 1973, and Van Allen, 1973) have shown that the cosmic ray density gradient between the earth and Jupiter is only  $\lesssim 1\% \text{ AU}^{-1}$ . This gives extremely large value for the diffusion coefficient  $K_{\parallel}$ , which cannot be accommodated within the ranges given by Jokipii and Coleman (1968).

However, the presently derived smaller value of the field parallel coefficient  $K_{\parallel}$  inside the corotating stream can probably arise from larger turbulence in the magnetic field due to enhanced solar wind velocity inside the stream.

The treatment so far excludes any contribution to the cosmic ray streaming in the plane of ecliptic, from the heliolatitudinal particle density gradients, since such gradients are found to be negligible on an average basis (Subramanian, 1971). However, at heliolongitudes covered by solar corotating streams, such temporary gradients are not unlikely to occur particularly in view of the enhanced convection inside the transient modulating region compared to the one outside the stream. The streaming due to such heliolatitudinal gradient is dependent on the direction of the interplanetary magnetic field lines as well as that of the particle density gradient, given by  $\left[ \frac{\partial U}{\partial r} \times \hat{B} \right]$  term in equation of cosmic ray streaming (1.19). For magnetic field pointing away from the sun and the positive density gradient in the direction of solar north pole, the streaming would be from 03 hour direction. If any one of the two parameters changes sign, the direction of streaming would be reversed and will be from 15 hour direction. In fact, to get a net streaming of 0.4% from the 03 hour direction to explain anomalous diurnal variation, the streaming

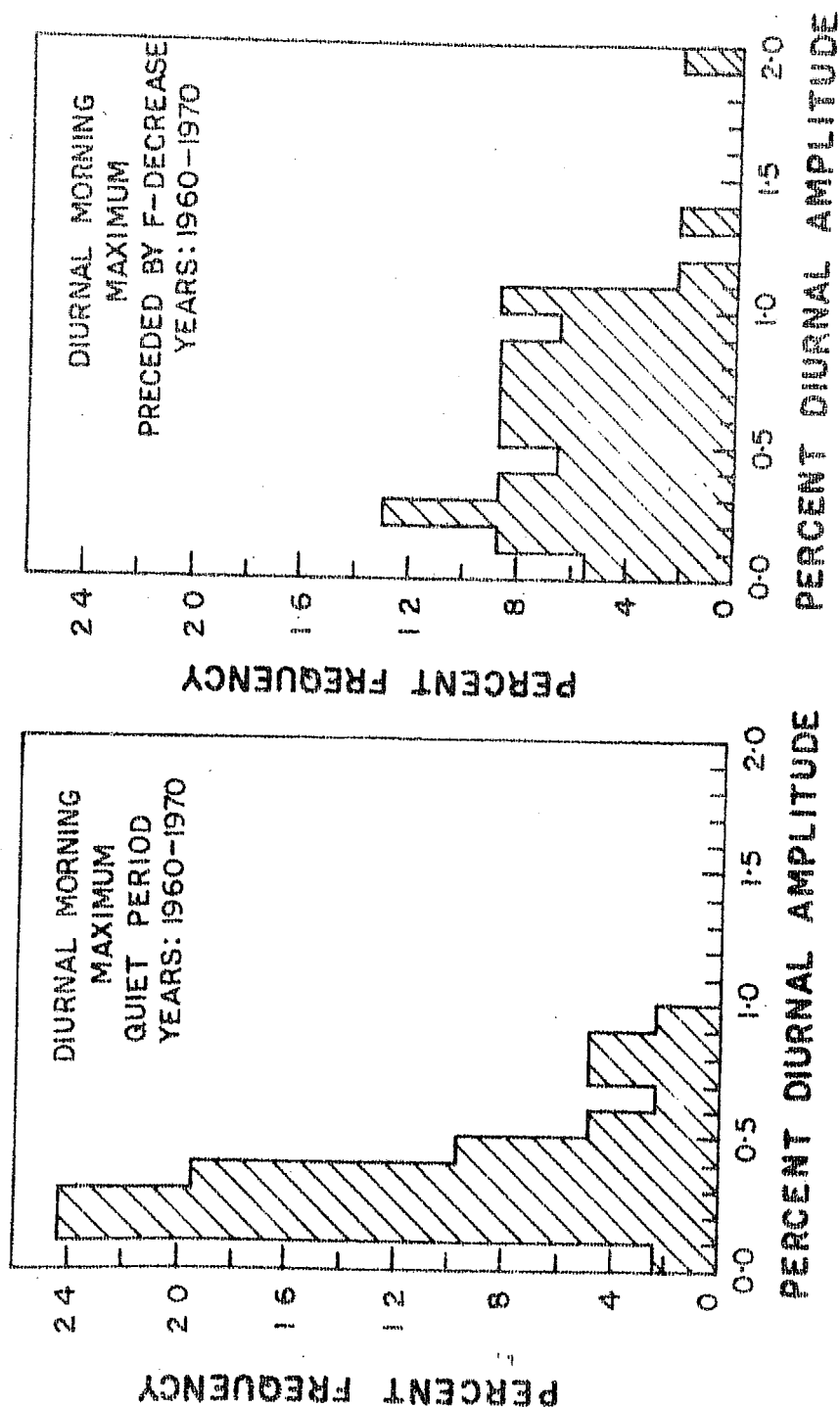
$K_{\perp} \left[ \frac{\partial U}{\partial r} \right]_{\perp}$  in the plane of ecliptic would be reduced to

accommodate the  $\left[ \frac{\partial U}{\partial r} \times B \right]$  streaming from 03 hour direction and vice versa. Quantitative calculations are, however, not possible at present because of the nonavailability of the north-south gradient values.

#### V.6 Quiet time anomalous diurnal variation

There are a number of instances when the anomalous diurnal variation with the time of maximum between 06-12 hours in the interplanetary space, occur during quiet periods and are not preceded by any Forbush type decrease of magnitude  $> 1\%$  in Deep River neutron monitor. Such events occur as frequently as the anomalous diurnal variation events preceded by Forbush decreases, i.e.  $\simeq 2\%$  days.

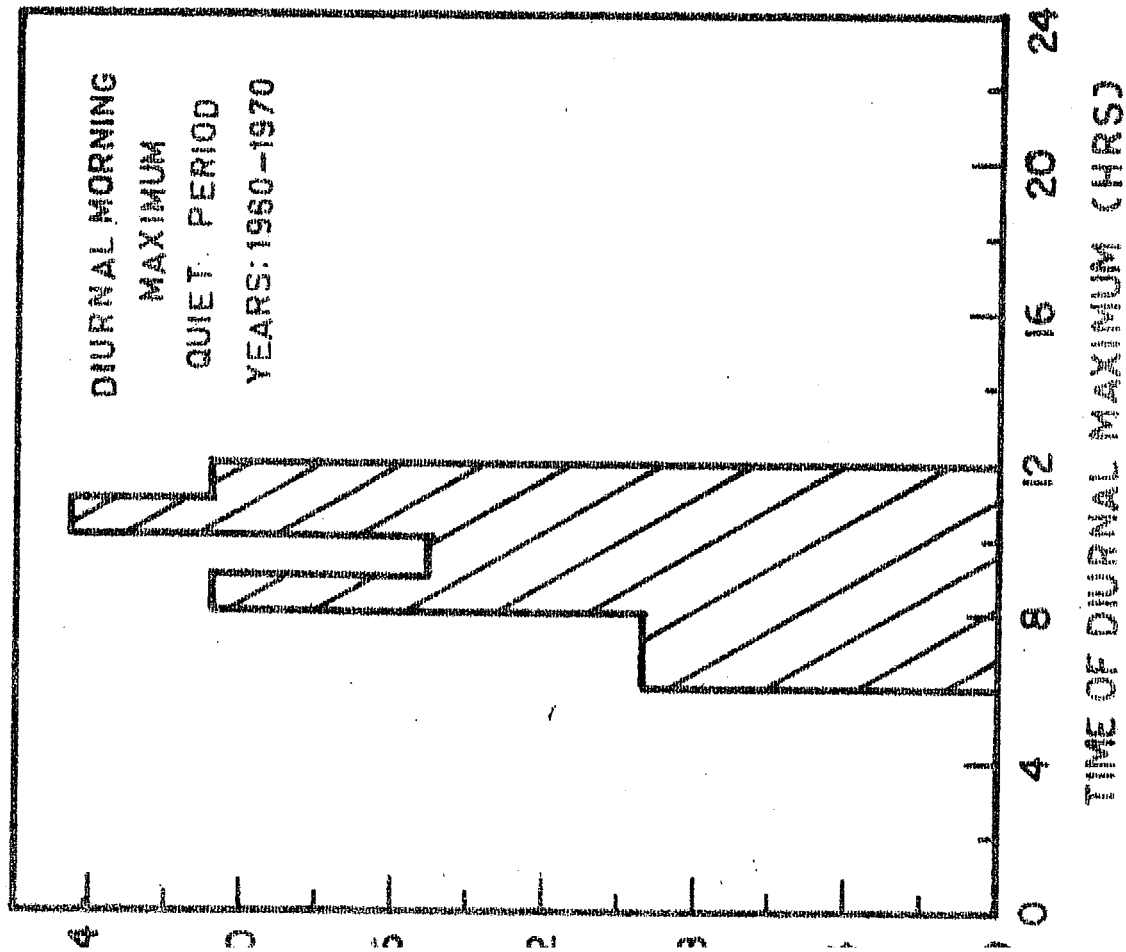
In figure 5.22 are shown the histograms of diurnal amplitude and time of maximum on such days corresponding to quiet time anomalous diurnal variation, during the years 1960-1970. The figure also shows for comparison, similar histograms for the days of anomalous diurnal variation preceded by Forbush decreases of amplitude  $> 2\%$  at Deep River. The diurnal vectors on these days are the averages derived from neutron monitors at Climax and Lindau during the years 1960-1962, while for the latter period, data from Deep River and Lindau are used. The figure reveals that, on the quiet days, the amplitude histogram shows a peak around 0.2-0.4% while those days preceded by Forbush decreases reveal a flat distribution for amplitudes upto  $\simeq 1.0\%$ , showing higher probability of getting enhanced amplitudes during such periods.



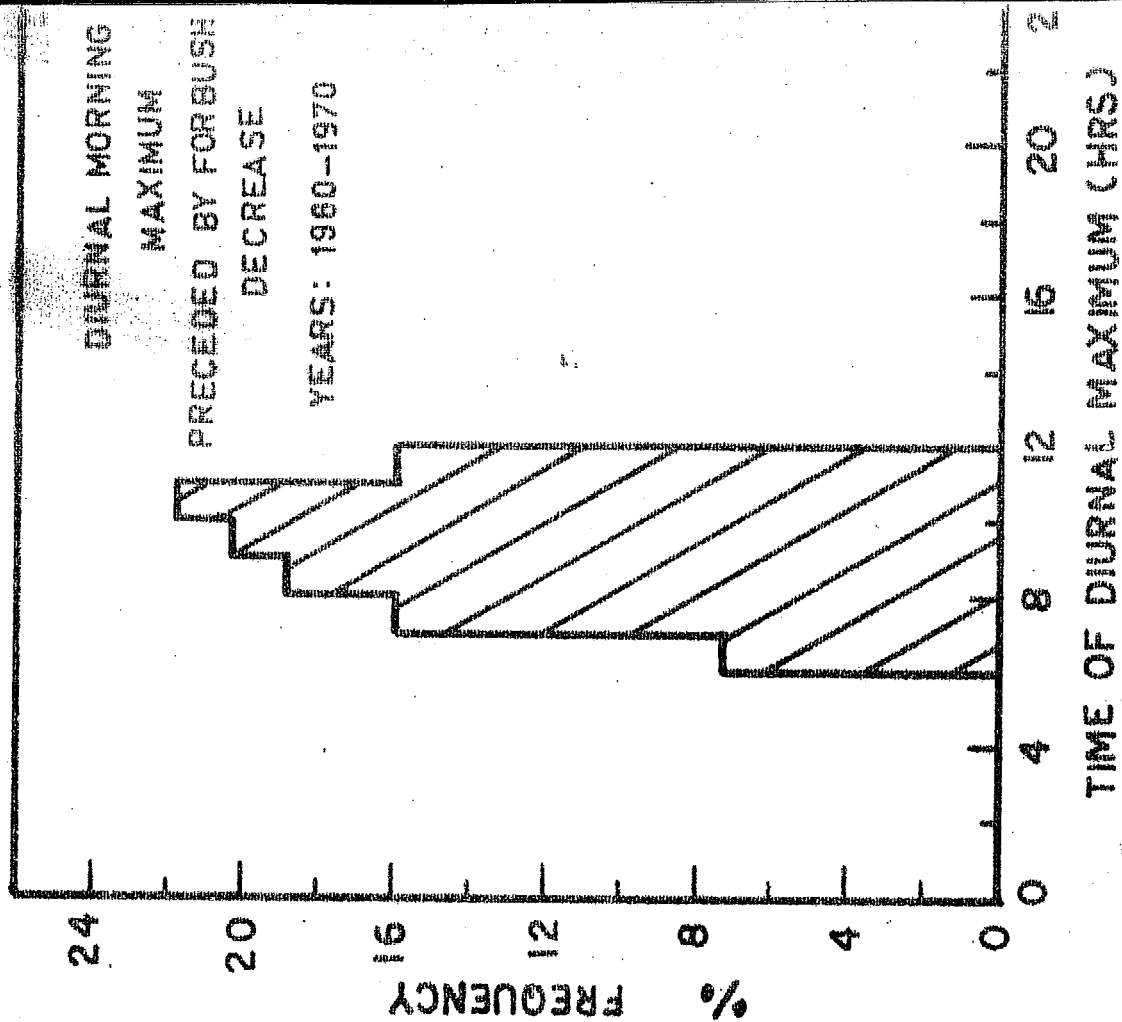
a1

a2

Figure 5.22a Histogram of diurnal amplitudes on the anomalous diurnal variation days during the years 1960-1970. a1) quiet periods a2) during the recovery periods of Forbush decreases.



b1



b2

Figure 5.22b Histogram of diurnal time of maximum on the anomalous diurnal variation days during the years 1960-1970. b1) quiet periods b2) during the recovery periods of

The necessity of using a large number of neutron monitors spread over the globe, for studying detailed characteristics of the quiet time anomalous diurnal variation, has restricted the further analysis to the years 1965-1967. In figure 5.23 is shown the Chree analysis of the hourly intensity in the Deep River neutron monitor using the day of quiet time anomalous diurnal variation as the day of epoch. When such days occur in a group, the first day is taken as the day of epoch. In the same figure are shown the diurnal amplitude and the time of maximum in the interplanetary space, as derived from the intensity profile obtained by Chree analysis. The amplitude on the day of epoch is  $\approx 0.35\%$  while the time of maximum lies around 10-11 hours. The figure reveals that the changes in the neutron intensity are less than 1% for at least four days prior to the day or days of anomalous diurnal variation.

The existence of the anomalous diurnal variation on these days is further confirmed from the diurnal variation analysis of neutron data from a large number of stations listed in table 5.1. In figure 5.24a are presented the average diurnal vectors on these days as derived from individual monitors. The vectors have an average amplitude 0.2-0.3%, while they show a spread in the time of maximum between 07-13 hours. The spread cannot be explained as due to statistical errors in the vectors (shown as the circles at the tip of the vectors). However, the possibility that

the spread is due to any universal time variation in the intensity is ruled out since the time of maximum is independent of the asymptotic longitudes of the stations (figure 5.24 b).

A Chree analysis of the solar wind velocity with the day of quiet time anomalous diurnal variation as epoch, is shown in figure 5.25 in the form of three day moving averages. The solar wind velocity is low ( $\simeq 350 \text{ km sec}^{-1}$ ) on the day of epoch, while it increases on the previous as well as following days. However, geomagnetic index  $K_p$  on the days of quiet time anomalous diurnal variation, is larger than the value on previous days and then decreases slowly. In comparison, the anomalous diurnal variation preceded by Forbush decreases is associated with the enhanced solar wind velocity (figure 5.13).

An interesting feature about the anomalous diurnal variation during the quiet periods is that they also show a 27 day recurrence tendency as revealed in figure 5.26 where the anomalous diurnal variation days are presented on a Bartels diagram along with other associated geomagnetic indices. The days are either recurrent and/or associated with recurrent SC's or periods of high  $K_p$ . In one instance (July 24, 1967) the day of quiet time anomalous diurnal variation also belongs to the 27 day recurrent series of enhanced anomalous diurnal variation preceded by Forbush decreases.



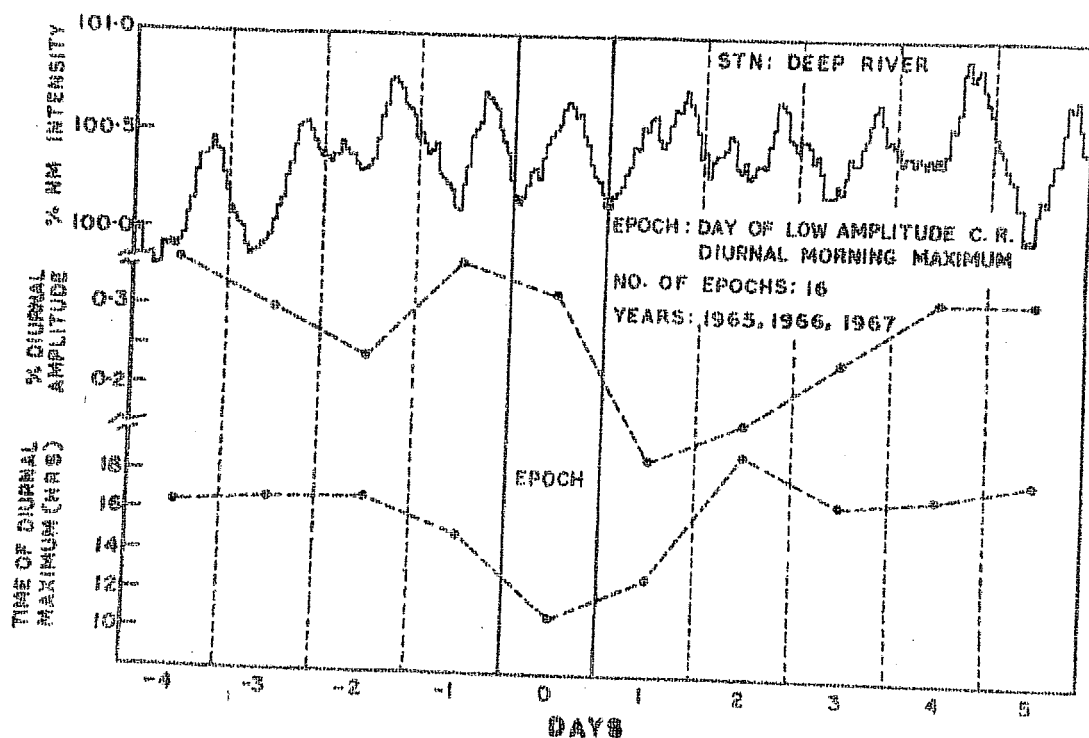


Figure 5.23 Chree analysis of neutron monitor intensity at Deep River with the day of quiet time anomalous diurnal variation (or first day in a group) as the epoch during the years 1965-1967. The figure also shows the diurnal amplitudes and times of maximum in the interplanetary space, derived from the above intensity profile.

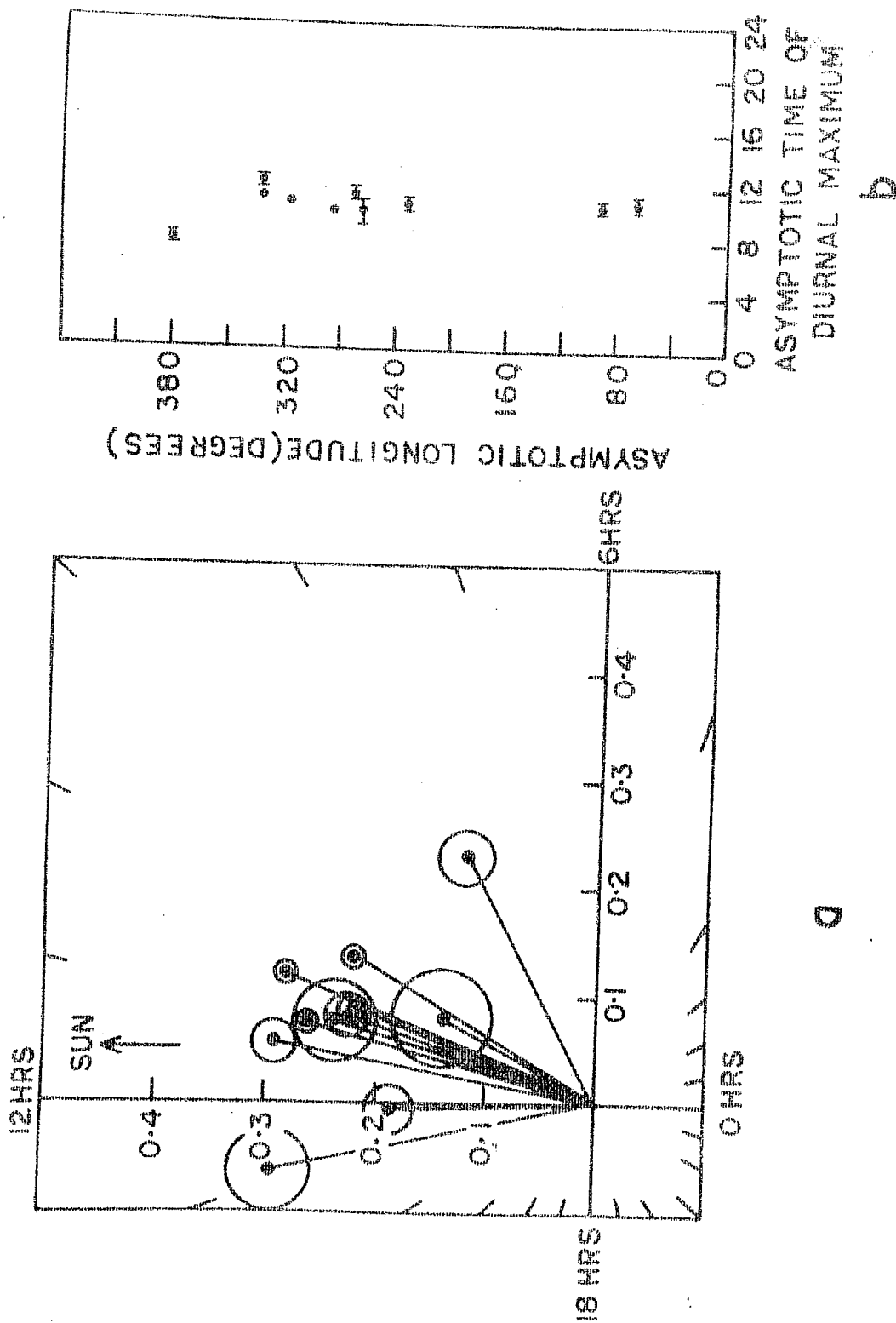


Figure 5.24a, b a) Vector diagram of diurnal vectors in the cosmic ray intensity derived from various stations listed in table 5.1 on the days of quiet time anomalous diurnal variation during the years 1965-1967 b) Asymptotic longitudes of the station versus the time of diurnal maximum on these days

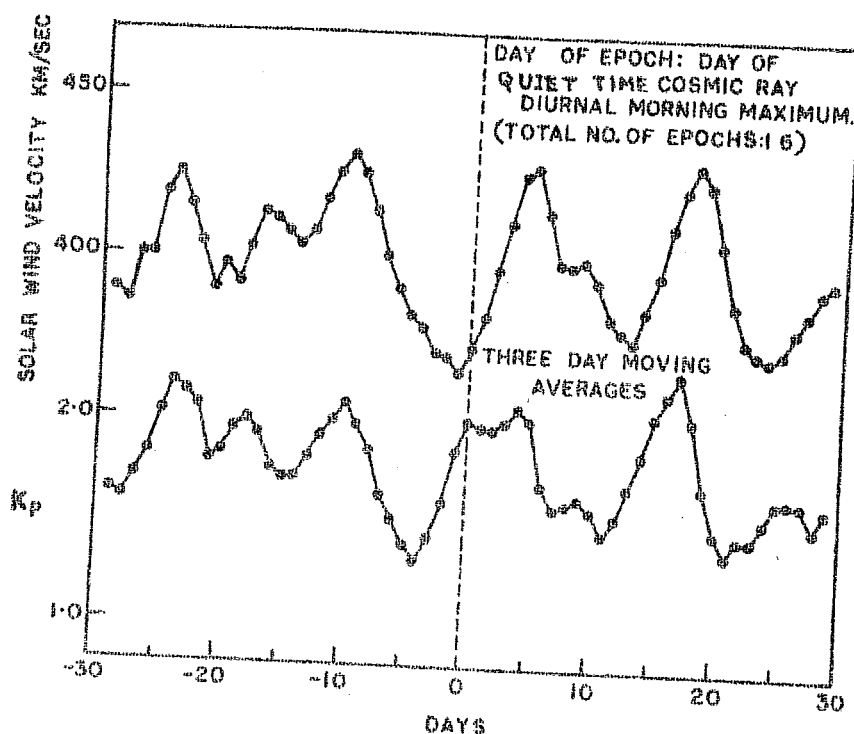


Figure 5.25 Three day moving averages of Chree analysis of solar wind velocity and geomagnetic index  $K_p$  with day of quiet time (or first day in a group) as the epoch during the years 1965-1967.

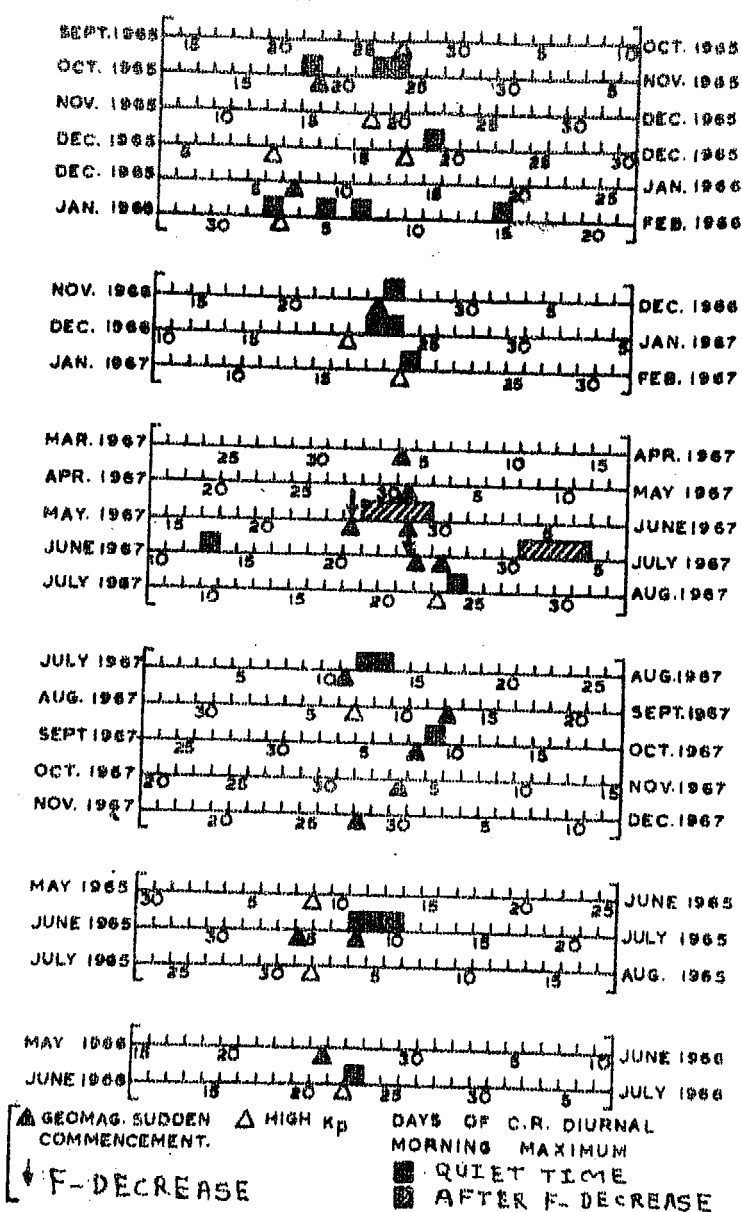


Figure 5.26 Bartels diagram showing 27 day recurrence of days of quiet time anomalous diurnal variation during the years 1965-1967.

In figure 5.27 is finally shown the plot of low energy protons ( $> 175$  MeV) from Pioneer VI and VII (published in CRPL reports) corresponding to three instances of the anomalous diurnal variation on quiet days during the months of June, July and September 1969. The intensity does not reveal any significant changes around the days of the anomalous diurnal variation. This excludes the possibility that these days might have been associated with 27 day recurrent decreases of small magnitude which were not observable in Deep River neutron monitor.

Since the anomalous diurnal variation during quiet periods, though recurrent, is not associated with any Forbush decrease, the model of corotating solar stream of enhanced solar wind velocity cannot be used to explain the phenomenon. We therefore present below, another possible mechanism.

Sarabhai and Subramanian (1966) and Subramanian and Sarabhai (1967) have discussed the possibility of the existence of a north-south cosmic ray density gradient symmetric with respect to the solar equatorial plane which arises as a result of larger convection of cosmic ray particles near the solar equatorial plane compared to the convection at higher heliolatitudes. The conclusion is based on the experimental observation of the sunspot distribution over the heliolatitudes and is supported by observations of coronal green line intensity at wavelength

5303  $\text{\AA}^0$  (Pathak and Sarabhai, 1970). Such a particle density gradient would result in the diffusion of particles from the north and south directions towards the solar equatorial plane. If these particles encounter irregularities in the interplanetary magnetic field, they will get scattered and would then be moving away from the sun along the field lines. If the scattering field irregularities are in the sun earth region, this will produce an extra cosmic ray flux in the garden hose direction. It should be noted that such a possible streaming in cosmic ray intensity is in addition to the  $\left\{ \frac{\partial U}{\partial r} \times \tilde{B} \right\}$  streaming (equation 5.1), perpendicular to the field lines whose magnitude is shown to be small in general (Subramanian, 1971). The mechanism is presented schematically in figure 5.28 along with the various components of cosmic ray streaming in such a configuration. The morning time of maximum ( $\simeq$  the garden hose direction) would then be caused by the compensation of the field aligned inward diffusion by excess particle flow from 09 hour direction. The exact magnitude and direction of the anisotropy will be determined by the existing radially outward convection and field perpendicular inward diffusion of cosmic rays. If the mechanism is true, then the 27 day recurrence of the quiet time anomalous diurnal variation indicates the existence of quasi-permanent regions on the solar disc causing larger number of irregularities in the interplanetary magnetic field, but not leading to any 27 day

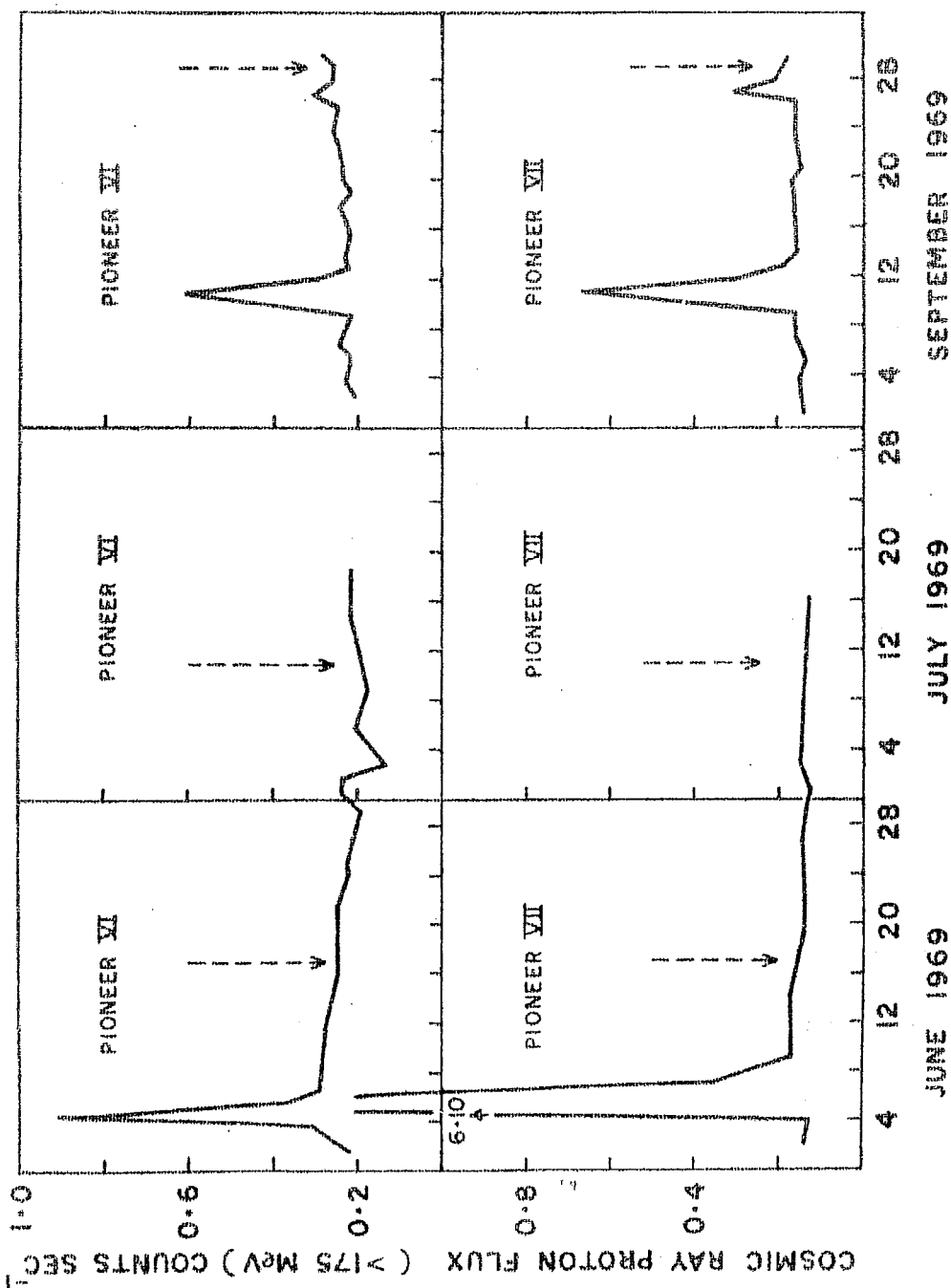


Figure 5.27 Low energy proton flux (> 175 MeV) measured by instruments aboard spacecrafts Pioneer VI and VII around the three days of quiet time around the anomalous diurnal variation (shown by dashed arrows) in the year 1969.

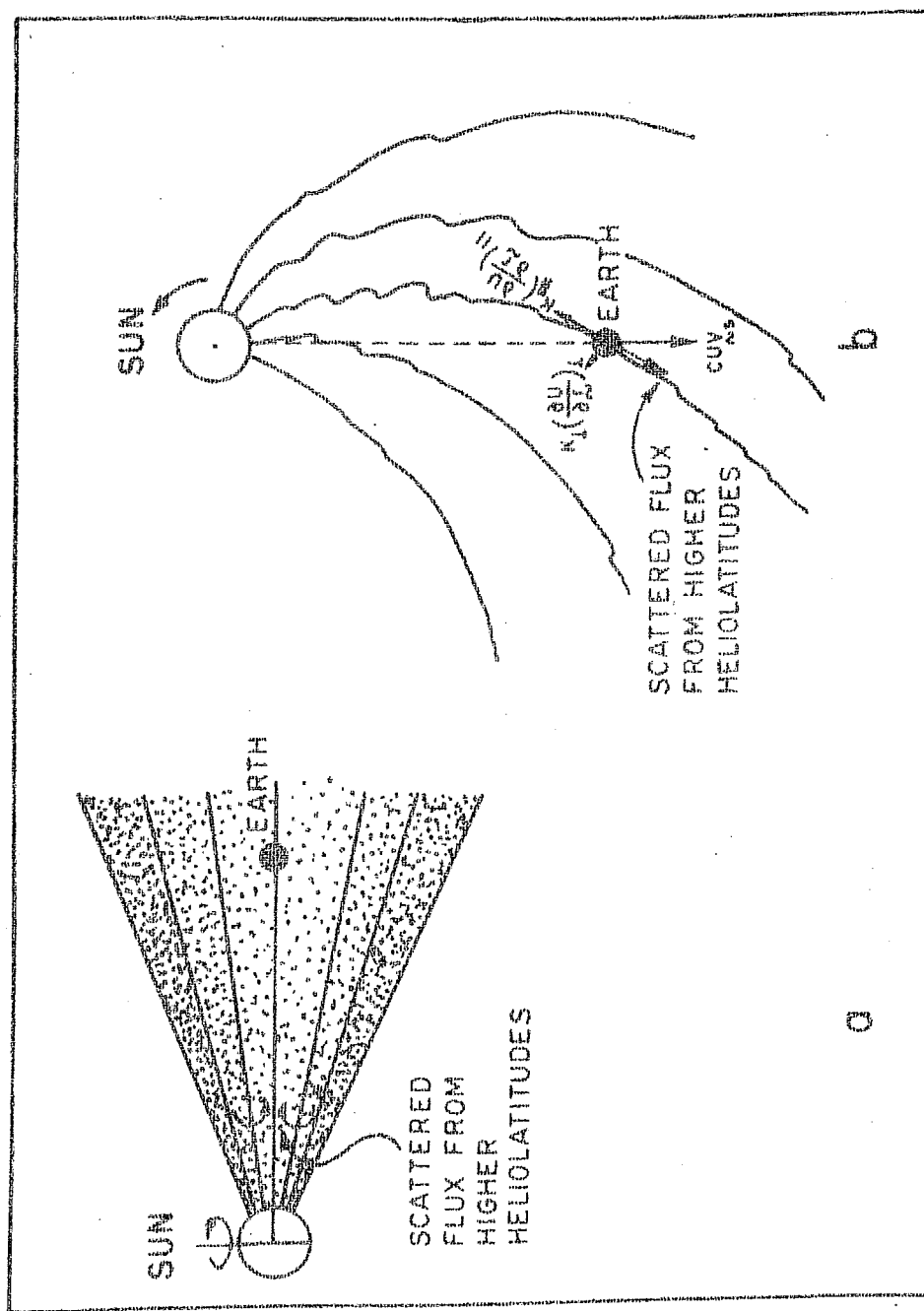


Figure 5.28a, b Schematic representation of mechanism of quiet time anomalous diurnal variation in cosmic ray intensity resulting from short circuiting of heliolatitudinal cosmic ray particle density gradients (symmetric with respect to solar equatorial plane) by interplanetary magnetic field irregularities.



recurrent type decreases in the cosmic ray intensity. The high geomagnetic index  $K_p$  on such days (figure 5.25) corroborates this view (Dessler and Fejer, 1963).

#### V.7 Concluding remarks

The anomalous diurnal variation in the cosmic ray intensity with maximum between 06-12 hours in the interplanetary space, is shown to be a major systematic deviation from the average diurnal variation with maximum in the 18 hour direction. The class of anomalous diurnal variation associated with Forbush decreases reveal on an average much higher amplitudes than the anomalous diurnal variation during quiet periods, but both indicate 27 day recurrence tendency. The study of this phenomenon, utilizing the basic Parker-Axford model, points the varying conditions of cosmic ray particle convection and diffusion in quasi-equilibrium state in a corotating solar stream with or without an added interaction with a transient plasma cloud from a flare. The study further shows that the interaction between a corotating high velocity solar stream, arising from a long lasting solar active region, and the high velocity, high density plasma cloud from an east or central limb solar flare, is also important in understanding in detail the majority of Forbush decreases. That a certain class of recurrent Forbush decreases are not associated with any flare, and apparently caused by solar corotating streams alone, raises, further, an important

issue of why the recovery of the intensity is such long lived phenomenon (of greater than 15 days in many instances) compared to the sweeping period of the stream past the earth. The simple concept of a depressed cosmic ray intensity, being in a quasi-equilibrium state in a corotating stream, needs modification in view of this observation. The in-situ spacecraft measurements of the interplanetary plasma, the magnetic field and the cosmic ray flux over extended energy ranges would be of great assistance in understanding these phenomena.

# REFERENCES

- |  |      |  |
|--|------|--|
| Ables J.G., Barouch E. and<br>McCracken K.G.   | 1967 | Planet. Space Sci., <u>15</u> , 547.   |
| Agrawal S.P., Ray S.K. and<br>Rao U.R.   | 1970 | Acta Physica Academiae<br>Scientiarum Hungariae,<br><u>29</u> , Suppl. 2, 597. |
| Agrawal S.P., Ananth A.G.<br>Bemalkhedkar M.M.,<br>Kargathra L.V., Rao U.R.<br>and Razdan H. | 1973 | J. Geophys. Res., Accepted<br>for publication, 1973.                           |
| Ahluwalia H.S. and<br>Dessler A.J.   | 1962 | Planet. Space Sci., <u>9</u> , 195.  |
| Ahluwalia H.S. and<br>McCracken K.G.   | 1965 | Proc. Int. Conf. Cosmic<br>Rays, London, <u>1</u> , 568.                       |
| Alpher R.A.  | 1950 | J. Geophys. Res., <u>55</u> , 437.   |
| Anand K.C., Daniel R.R.<br>and Stephens S.A.   | 1968 | Can. J. Phys., <u>46</u> , S484.   |
| Anderson K.A.  | 1969 | Solar Phys., <u>6</u> , 111.   |
| Angle J.R.P. and<br>Landstreet J.D.  | 1970 | Astrophys. J., <u>162</u> , L61.   |
| Antonucci E., Castagnoli G.C.<br>and Doderio M.A.  | 1971 | Solar Physics, <u>20</u> , 497.  |
| Arnold J.R., Honda M. and<br>Lal D.  | 1961 | J. Geophys. Res., <u>10</u> , 3519.  |
| Axford W.I., Dessler A.J.<br>and Gottlieb B.   | 1963 | Astrophys. J., <u>137</u> , 1268.  |
| Axford W.I.  | 1965 | Planet. Space Sci., <u>13</u> , 115.   |
| Bachelet F.P., Conforto A.M.<br>and Iucci N.   | 1960 | Proc. First Space Sci.<br>Symp., 662, Nice.                                    |
| Bachelet F., Balata P.<br>Dyring E. and Iucci N.   | 1965 | Nuovo Cimento, <u>35</u> , 23.   |
| Bachelet F., Dyring E.<br>and Iucci N.   | 1968 | Can. J. Phys., <u>46</u> , S1057.  |
| Ballif J.R. and Jones D.E.   | 1969 | J. Geophys. Res., <u>74</u> , 3499.  |
| Ballif J.R., Jones D.E.<br>Skousen E.N. and Smith D.T.                                       | 1971 | J. Geophys. Res., <u>76</u> , 8401   |

- |  |       |   |
|--|-------|---|
| Balsubrahmanyam V.K. and Venkatesan D.                 | 1969  | Acta Physica Academiae Scientiarum Hungaricae, <u>29</u> , Supl.2, 319.   |
| Baradzei L.I.  | 1951  | J. Exp. Theor. Phys. USSR, <u>36</u> , 1151.  |
| Barnden L.R.   | 1973a | Proc. 13th Int. Cosmic Ray Conf., Hobart, <u>2</u> , 680.   |
| Barnden L.R.   | 1973b | Proc. 13th Int. Cosmic Ray Conf., Hobart, <u>2</u> , 686.   |
| Barnden L.R.   | 1973c | Proc. 13th Int. Cosmic Ray Conf., Hobart, <u>2</u> , 1271.  |
| Bartels J.   | 1934  | Terr. Magn. <u>39</u> , 201.  |
| Bemalkhedkar M.M., Nerurkar N.W. and Razdan H.         | 1967  | Proc. 10th Symposium on Cosmic Rays, Elementary Particle Physics and Astrophysics, India, 162.                        |
| Bemalkhedkar M.M.                                      | 1969  | J. Inst. Telcom. Engrs. 15, 676.  |
| Bemalkhedkar M.M. and Kaul R.K.                        | 1969  | Proc. 11th Symposium on Cosmic Rays, Astrophysics, Geophysics and Elementary Particle Physics, India, <u>2</u> , 339. |
| Bemalkhedkar M.M. Subramanian G. and Razdan H.         | 1973  | Proc. 13th Int. Cosmic Ray Conf., Denver, <u>2</u> , 1293.  |
| Bercovitch M.  | 1963  | J. Geophys. Res., <u>68</u> , 4366.   |
| Billings D.E. and Roberts W.O.                         | 1964  | Astrophys. Norveg. <u>2</u> , 147.  |
| Biswas S., Fichtel C.E. and Guss D.E.                  | 1962a | Phys. Rev., <u>128</u> , 2756.  |
| Biswas S., Frier P.S. and Stein W.                     | 1962b | J. Geophys. Res., <u>67</u> , 13.   |
| Biswas S., Fichtel C.E., Guss D.E. and Waddington C.J. | 1963  | J. Geophys. Res., <u>68</u> , 3179.   |
| Biswas S. and Fichtel C.E.                             | 1964  | Astrophys. J., <u>139</u> , 941.  |

- |  |      |   |
|--|------|---|
| Biswas S. and Fichtel C.E.   | 1965 | Space Sci. Rev., <u>4</u> , 709.  |
| Biswas S. Ramadurai S. and Sreenivasan N.  | 1968 | Can. J. Phys., <u>46</u> , S593.  |
| Biswas S. and Ramadurai S.   | 1971 | Proc. 12th Int. Conf. Cosmic Rays, Hobart, <u>1</u> , 162.                                  |
| Bryant D.A., Cline T.L. Desai U.D. and McDonald E.B.                             | 1965 | Astrophys. J., <u>141</u> , 478.  |
| Bukata R.P., McCracken K.G. and Rao U.R.   | 1968 | Can. J. Phys., <u>46</u> , S994.  |
| Burlaga L.F.   | 1967 | J. Geophys. Res., <u>72</u> , 4449.   |
| Carmichael H.  | 1964 | Cosmic Rays, IQSY Instruction Manual No.7.  |
| Carmichael H., Bercovitch M. Steljes J.F. and Magidin M.                         | 1965 | Proc. 9th Int. Conf. on Cosmic Rays, London, <u>1</u> , 553.                                |
| Carmichael H., Bercovitch M. Shea, M.A., Magidin M. and Peterson R.W.            | 1968 | Can. J. Phys. <u>46</u> , S1006.  |
| Carmichael H. and Bercovitch M.  | 1969 | Can. J. Phys. <u>47</u> , 2073.   |
| Carmichael H. and Katzman J.   | 1971 | Proc. 12th Int. Conf. on Cosmic Rays, Hobart, <u>2</u> , 744.                               |
| Carmichael H. and Stoker P.H.  | 1970 | EOS Trans. AGU, <u>51</u> , 802.  |
| Chapman S. and Bartels J.  | 1940 | Geomagnetism, Oxford at the Clarendon Press, <u>1</u> , 414.                                |
| Chatterjee B.K., Murthy G.T. Ramana Murthy P.V., Sreekantan B.V. and Tonwar S.C. | 1969 | Presented in 11th Int. Conf. Cosmic Rays, paper No. OG14, Budapest.                         |
| Chapman S.   | 1929 | Monthly Notices Roy. Astron. Soc. London, <u>89</u> , 456.                                  |
| Clark G.W., Garmire G.P. and Kraushaar W.L.                                      | 1968 | Astrophys. J. <u>153</u> , L203.  |
| Clark G.W., Garmire G.P. and Kraushaar W.L.                                      | 1970 | Non-solar X and Gamma Ray Astronomy, L. Gratton, Ed., (Dordrecht, Holland; D. Riedel), 269. |

- |  |       |  |
|--|-------|--|
| Clark G.W., Garmire G.P.<br>and Kraushaar W.L.             | 1971  | Proc. 12th Int. Conf.<br>Cosmic Rays, Hobart, <u>1</u> , 91.   |
| Cline T.L. and McDonald F.B.                               | 1968  | Solar Phys., <u>5</u> , 507.   |
| Cocconi G., Cocconi V.,<br>Tongiorji V. and<br>Windgoff M. | 1950  | Phys. Rev., <u>79</u> , 768.   |
| Compton A.H. and Getting I.A.                              | 1935  | Phys. Rev., <u>47</u> , 817.   |
| Conforto A.M. and<br>Simpson J.A.                          | 1957  | Nuovo Cimento, <u>6</u> , 1052.  |
| Cowsik R.  | 1971a | Proc. 12th Int. Conf.<br>Cosmic Rays, Hobart,<br><u>1</u> , 329.                                     |
| Cowsik R.  | 1971b | Proc. 12th Int. Conf.<br>Cosmic Rays, Hobart,<br><u>1</u> , 334.                                     |
| Cowsik R. and Hutcheon I.D.                                | 1971  | Proc. 12th Int. Conf.<br>Cosmic Rays, Hobart,<br><u>1</u> , 102.                                     |
| Critchfield C.L., Ney E.P.<br>and Oleska S.                | 1950  | Phys. Rev. <u>79</u> , 402.  |
| Daniel R.R. and<br>Stephens S.A.                           | 1970  | Acta Physica Academiae<br>Scientiarum Hungaricae,<br><u>29</u> , Suppl. 1, 531.                      |
| Davis L.   | 1965  | Stellar and Solar<br>Magnetic Fields, North<br>Holland Publishing Co.,<br>Amsterdam, 204.            |
| Debrunner H. and Walther U.                                | 1968  | Can. J. Phys., <u>46</u> , S1140.  |
| Dessler A.J. and Fejer J.A.                                | 1963  | Planet. Space Sci., <u>11</u> , 505.   |
| Dessler A.J.   | 1967  | Rev. Geophys., <u>5</u> , 1.   |
| Dorman L.I.  | 1957  | Cosmic Ray Variations,<br>State Publishing House<br>Technical and Theoretical<br>Literature, Moscow. |
| Dorman L.I.  | 1963  | Prog. in Elementary<br>Particle and Cosmic Ray<br>Phys. <u>7</u> , 1.                                |

- Dorman L.I. 1969 Annals IQSY 4, 217.
- Duggal S.P. and Pomerantz M.A. 1962 Phys. Rev. Lett., 8, 215.
- Duggal S.P., Forbush S.E. and Pomerantz M.A. 1967 Nature, 214, 154.
- Duggal S.P. and Pomerantz M.A. 1970 Acta Phys. Acad. Sci. Hung. 29, Suppl.2, 351.
- Durgaprasad N., Fichtel C.E. Guss D.E. and Reames D.V. 1968 Astrophys. J. 154, 307.
- Dyring E. and Sporre B. 1966a Arkiv for Geophysik, Band 5, nr 9, 67.
- Dyring E. and Sporre B. 1966b Arkiv for Geofysik, Band 5, nr 10, 79.
- Elliot H. and Dolbear D.W.N. 1950 Proc. Phys.Soc., 63, 137.
- Elliot H. and Dolbear D.W.N. 1951 J. Atmospheric and Terrestrial Phys.,1, 205.
- Elliot H. 1952 Prog. in Cosmic Ray Phys. 1, 455.
- Fan C.Y., Gloeckler G., McKibben B., Pyle K.B. and Simpson J.A. 1968 Can J. Phys., 46, 5498.
- Fenton A.G., McCracken K.G., Rose D.C. and Wilson B.G. 1959 Can J. Phys., 37, 970.
- Fermi E. 1949 Phys. Rev. 75, 1169.
- Fichtel C.E. and Guss D.E. 1965 Phys. Rev. Lett. 6, 495.
- Fisk L.A. and Axford W.I. 1970 Solar Physics, 12, 304.
- Fonger W.H. 1953 Phys. Rev., 91, 351.
- Forbush S.E. 1958 J. Geophys. Res. 63, 651.
- Forbush S.E. and Venkatesan D. 1960 J.Geophys.Res., 65, 2213.
- Forbush S.E. 1966 Handbuch der Physik, 49, 1, 159.

- |  |      |   |
|--|------|---|
| Forbush S.E.   | 1967 | J. Geophys. Res., <u>72</u> , 4937.                                     |
| Forbush S.E.   | 1969 | J. Geophys. Res., <u>74</u> , 3451.                                     |
| Forman M.A. and Gleeson L.J.   | 1970 | Preprint.   |
| Friis-Christensen E.,<br>Lassen K., Wilcox J.M.,<br>Gonzalez W. and Colburn D.S. | 1971 | Nat. Phys.Sci., <u>233</u> , 48.  |
| Fujii Z., Kodama M. and<br>Wada M.   | 1972 | Sci. Papers IPCR., <u>66</u> , 1.                                       |
| Garmire G.P.   | 1970 | Bull. Am. Phys. Soc. <u>15</u> ,<br>564.                                |
| Geiger K.W.  | 1956 | Can. J. Phys., <u>34</u> , 288.   |
| Geiss J.   | 1963 | Proc. Int. Conf. on<br>Cosmic Rays, Jaipur, <u>3</u> ,<br>434.          |
| Gleeson L.J. and Axford W.I.   | 1967 | Astrophys. J., <u>149</u> , 115.  |
| Gleeson L.J. and Axford W.I.   | 1968 | Astrophys. J., <u>154</u> , 1011.                                       |
| Gleeson L.J.   | 1969 | Planet.Space Sci., <u>17</u> , 31.                                      |
| Ginzburg V.L.  | 1958 | Prog. in Elementary<br>Particle and Cosmic Ray<br>Phys. <u>4</u> , 337. |
| Gold T.  | 1959 | J. Geophys.Res., <u>64</u> , 1665.                                      |
| Gold T.  | 1969 | Nature, <u>221</u> , 25.  |
| Gosling J.T.,<br>Hundausen A.J., Pizzo V.<br>and Asbridge J.R.                   | 1972 | J. Geophys.Res., <u>77</u> , 5442.                                      |
| Griffiths W.K., Hatton C.J.,<br>Ryder P. and Harman C.V.                         | 1966 | J.Geophys.Res., <u>71</u> , 1895.                                       |
| Griffiths W.K., Harman C.V.,<br>Hatton C.J., Marsden P.L. and<br>Ryder P.        | 1968 | Can.J.Phys., <u>46</u> , S1044.   |
| Gruenwaldt H.,<br>Montgomery M.D. and<br>Rosenbauer H.                           | 1972 | EOS, Trans.AGU, <u>53</u> , 1053.                                       |



- |   |      |   |
|---|------|---|
| Hashim A. and<br>Thambyahpillai T.            | 1969 | Planet.Space Sci., <u>7</u> , 1879.                                       |
| Hashim A., Bercovitch M.<br>and Steljes J.F.  | 1972 | Solar Phys., <u>22</u> , 220.   |
| Hatton C.J.                                   | 1971 | Progress in Elementary<br>Particle and Cosmic Ray<br>Phys. <u>10</u> , 1. |
| Hayakawa S., Ito K. and<br>Terashima Y.       | 1958 | Prog. Theor. Phys. Suppl.<br>No.6, 1.                                     |
| Hayakawa S.                                   | 1969 | John Wiley and Sons,<br>New York, London,<br>Sydney, Toronto.             |
| Hedgecock P.C., Quenby J.J.<br>and Webb S.    | 1972 | Nature (Physical Sci.),<br><u>240</u> , 173.                              |
| Hess W.N., Patterson H.W.<br>and Wallace R.   | 1959 | Phys. Rev., <u>116</u> , 445.   |
| Hofmann D.J. and<br>Sauer H.J.                | 1968 | Space Sci. Rev. <u>8</u> , 750.   |
| Honda M., Shedolovsky J.P.<br>and Arnold J.R. | 1969 | Geochim. Acta, <u>22</u> , 133.   |
| Hughes E.B. and<br>Marsden P.L.               | 1966 | J.Geophys.Res. <u>71</u> , 1435.  |
| Hulsizer R.                                   | 1949 | Phys. Rev. <u>76</u> , 164.   |
| Hundhausen A.J.                               | 1970 | Rev. Geophys. and Space<br>Sci., <u>8</u> , 729.                          |
| Iucci N., Storini M. and<br>Villoresi G.      | 1971 | Nuovo Cimento, <u>6B</u> , 111.   |
| Jokipii J.R. and<br>Coleman P.J.              | 1968 | J. Geophys.Res., <u>73</u> , 5495.  |
| Jokipii J.R. and Parker E.N.                  | 1969 | Astrophys. J., <u>155</u> , 777.  |
| Jokipii J.R.                                  | 1971 | Rev. Geophys. and Space<br>Phys. <u>9</u> , 27.                           |
| Kahler S.W.                                   | 1969 | Solar Phys., <u>8</u> , 166.  |

- |  |       |   |
|--|-------|---|
| Kane R.P.  | 1966  | Nuovo Cimento, Ser.B,<br><u>45</u> , 132.             |
| Kane R.P.  | 1972  | J.Geophys.Res., <u>77</u> , 5573.                     |
| Kane S.R. and<br>Winckler J.R.                                   | 1969  | J.Geophys.Res., <u>74</u> , 6247.                     |
| Katz L., Meyer P. and<br>Simpson J.A.                            | 1958  | Nuovo Cimento, <u>8</u> , Suppl.<br>2, 277.           |
| Kellogg P.J. and<br>Schwartz M.                                  | 1959  | Nuovo Cimento, <u>13</u> , 761.                       |
| Kemp J.C., Swedlund J.B.,<br>Landstreet J.D. and<br>Angle J.R.P. | 1970  | Astrophys.J.Lett. <u>161</u> ,L77.                    |
| Kocharian N.M.,<br>Saakian G.S. and<br>Kirakosian Z.A.           | 1958  | J. Exp. Theor. Phys.<br>USSR, <u>35</u> , 1335.       |
| Kodama M. and Ishida Y.  | 1967  | Report Inosphere and<br>Space Res., <u>21</u> , 55.   |
| Kodama M.  | 1967  | Report Inosphere and<br>Space Res., <u>21</u> , 59    |
| Kodama M. and Ohuchi T.  | 1968  | Can.J.Phys., <u>46</u> , S1090.                       |
| Kodama M. and Inoue A.   | 1970a | JARE Scientific Reports,<br>Series A, No.9.           |
| Kodama M. and Inoue A.   | 1970b | Report Ionosphere and<br>Space Res., <u>24</u> , 281. |
| Kent D.W., Coxell H. and<br>Pomerantz M.A.                       | 1968  | Can.J.Phys., <u>46</u> , S1082.                       |
| Krieger A.S., Timothy A.F.<br>and Roelof E.C.                    | 1973  | Solar Phys. <u>28</u> , 505.                          |
| Landstreet J.D. and<br>Angle J.R.P.                              | 1971  | Astrophys.J.lett. <u>165</u> ,L67.                    |
| Lapointe S.M. and Rose D.C.                                      | 1961  | Can.J.Phys. <u>39</u> , 668.                          |
| Lapointe S.M. and Rose D.C.                                      | 1962  | Can.J.Phys. <u>40</u> , 687.                          |

- Laster H., Lenchek A.M.  
and Singer S.F. 1962 J.Geophys.Res., 67, 2639.
- Lemaitre G. and  
Vallarta M.S. 1936a Phys. Rev. 49, 719.
- Lemaitre G. and  
Vallarta M.S. 1936b Phys. Rev. 50, 493.
- Lentz G.A., McKibben R.B.,  
O'Gallagher J.J., Perkins M.,  
Simpson J.A. and  
Tuzzolino A.J. 1973 Proc. 13th Int. Cosmic  
Ray Conf., Denver, 2, 743.
- Lietti B. and Quenby J.J. 1968 Can.J.Phys., 46, S942.
- Lin R.P. and Anderson K.A. 1967 Solar Phys., 1, 446.
- Lin R.P., Kahler S.W. and  
Roclof E.C. 1968 Solar Phys., 4, 338.
- Lin R.P. 1970 Solar Phys., 12, 209.
- Lindgren S. 1962 Tellus, 14, 44.
- Lindgren S.T. 1968 Solar Phys., 5, 382.
- Lindgren S. 1969 Acta Physica Academiae  
Scientiarum Hungaricae,  
29, Suppl. 2, 319.
- Lockwood J.A. 1958 Phys.Rev., 112, 1750.
- Lockwood J.A. 1960 J.Geophys.Res., 65, 3359.
- Lockwood J.A. and  
Razdan H. 1963a J.Geophys.Res., 68, 1581.
- Lockwood J.A. and Razdan H. 1963b J.Geophys.Res., 68, 1593.
- Lockwood J.A. and Webber W.R. 1967 J.Geophys.Res., 72, 3395.
- Lockwood J.A. and Webber W.R. 1968 Can.J.Phys., 46, S903.
- Lockwood J.A. and Webber W.R. 1969 J.Geophys.Res., 74, 5599.
- Lockwood J.A., Lenzniak J.,  
Singh P. and Webber W.P. 1970 J.Geophys.Res., 75, 6385.

- |   |       |  |
|---|-------|--|
| Lockwood J.A. and Singh P.                            | 1970  | Acta Physica Academiae<br>Scientiarum Hungaricae,<br><u>29</u> , Suppl.2, 319. |
| Lockwood J.A.   | 1971  | Space Sci.Rev., <u>12</u> , 658.   |
| Marsden P.L. and Begum Q.N.                           | 1959  | Phil.Mag., <u>4</u> , 1247.  |
| Mathews P.M.  | 1959  | Can.J.Phys., <u>37</u> , 85.   |
| Mathews T., Mercer J.B.<br>and Venkatesan D.K.        | 1968  | Can.J.Phys., <u>46</u> , 854.  |
| Mathews T., Venkatesan D.<br>and Wilson B.G.          | 1969  | J.Geophys.Res., <u>74</u> , 1218.  |
| Mathews T., Quenby J.J. and<br>Sear J.                | 1971a | Nature, <u>229</u> , 246.  |
| Mathews T., Stoker P.H. and<br>Wilson B.G.            | 1971b | Planet.Space.Sci., <u>19</u> , 981.  |
| McCracken K.G. and<br>Johns D.H.                      | 1959  | Nuovo Cimento, <u>13</u> , 96.   |
| McCracken K.G.  | 1960  | Phys.Rev., <u>117</u> , 1570.  |
| McCracken K.G.  | 1962  | J.Geophys.Res., <u>67</u> , 447.   |
| McCracken K.G., Rao U.R.<br>and Bukata R.P.           | 1967  | J.Geophys.Res., <u>72</u> , 4293.  |
| McCracken K.G. and Rao U.R.                           | 1970  | Space Sci.Rev., <u>11</u> , 155.   |
| McCracken K.G., Rao U.R.,<br>Bukata R.P. and Keath E. | 1971  | Solar Phys., <u>18</u> , 100.  |
| McDonald F.B. and<br>Webber W.R.                      | 1960  | J.Geophys.Res., <u>65</u> , 767.   |
| McDonald F.B. and Desai U.D.                          | 1971  | J.Geophys.Res., <u>76</u> , 808.   |
| Meshkovskij A.G. and<br>Sokolov L.I.                  | 1957  | J. Exp. Theor. Phys.,<br>USSR, <u>33</u> , 542.                                |
| Mercer J.B. and Wilson B.C.                           | 1968  | Can.J.Phys., <u>46</u> , S849.   |
| Mori S., Ueno, H.,<br>Nagashima K. and Sagisaka S.    | 1964  | J.Geomag.Geolect., <u>16</u> , 68.   |

- |   |      |   |
|---|------|---|
| Mori S.   | 1968 | Nuovo Cimento, <u>B58</u> , 1.  |
| Mustel E.   | 1964 | Astron. Zh. <u>41</u> (5), 777.   |
| Myldoi M.G. and Wilson J.G.                                     | 1951 | Proc. Phys. Soc.(London),<br><u>A64</u> , 404.                                |
| Nagashima K., Fujimoto K.,<br>Fujii Z., Ueno H. and<br>Kondo I. | 1971 | Proc. 12th Int. Conf.<br>Cosmic Rays, <u>2</u> , 661.                         |
| Nerurker N. and<br>Webber W.R.                                  | 1964 | J.Geophys.Res., <u>69</u> , 815.  |
| Ness N.F., Searce C.S.<br>and Seek J.B.                         | 1964 | J.Geophys.Res., <u>69</u> , 3531.   |
| Nicolson P. and<br>Sarabhai V.A.                                | 1948 | Proc.Phys.Soc., <u>60</u> , 509.  |
| Niemi S.P.A.  | 1966 | Ann.Acad. Sci., Fennicae,<br>Series A, <u>VI</u> , 214.                       |
| Obayashi T.   | 1964 | Space Sci. Rev., <u>3</u> , 79.   |
| O'Gallagher J.J.  | 1967 | Astrophys.J., <u>150</u> , 675.   |
| O'Gallagher J.J.  | 1968 | Can. J. Phys., <u>46</u> , S943.  |
| O'Gallagher J.J.  | 1969 | J.Geophys.Res., <u>74</u> , 43.   |
| O'Gallagher J.J.  | 1972 | Rev.Geophys.Space Sci.,<br><u>10</u> , 821.                                   |
| Ormes J.F. and Webber W.R.                                      | 1968 | Can.J.Phys. <u>46</u> , S883.   |
| Ostriker J.P.   | 1970 | Acta Physica Academiae<br>Scientiarum Hungaricae,<br><u>29</u> , Suppl.1, 69. |
| Parker E.N.   | 1958 | Astrophys.J., <u>128</u> , 664.   |
| Parker E.N.   | 1961 | Astrophys.J., <u>133</u> , 1014.  |
| Parker E.N.   | 1963 | Interscience Publishers,<br>John Willy and Sons,<br>New York, London.         |
| Parker E.N.   | 1964 | Planet.Space Sci., <u>12</u> , 735.   |

Parker E.N.	1965	Planet.Space Sci., <u>13</u> , 9.
Parker E.N.	1969	Space Sci. Rev., <u>9</u> , 325.
Parker G.D.	1973	Proc. 13th Int. Cosmic Ray Conf. Denver, <u>2</u> ,1196.
Patel D., Sarabhai V. and Subramanian G.	1968	Planet.Space Sci., <u>16</u> ,1131.
Pathak P.N.	1969	Ph.D.thesis, Gujarat University, India.
Pathak P.N. and Sarabhai V.	1970	Planet Space Sci., <u>18</u> , 81.
Pomerantz M.A. and Duggal S.P.	1971	Space Sci.Rev., <u>12</u> , 75.
Pneuman G.W. and Kopp R.A.	1971	Solar Phys. <u>18</u> , 258.
Pneuman G.W.	1972	Submitted to Solar Phys.
Quenby J.J. and Webber W.R.	1959	Phil. Mag., <u>4</u> , 90.
Quenby J.J.	1965	Proc. 9th Int. Conf. Cosmic Rays, London, <u>1</u> , 180.
Quenby J.J.	1967	Handbuch der Physik, <u>46</u> , 2, 310.
Rao U.R., McCracken K.G. and Venkatesan D.	1963	J.Geophys.Res., <u>68</u> , 345.
Rao U.R. and Sarabhai V.	1964	Planet Space Sci., <u>12</u> ,1055.
Rao U.R.	1965	J.Geophys.Res., <u>70</u> , 3765.
Rao U.R., McCracken K.G., Allum F.R., Palmeira R.A.R. and Palmer I.	1971	Solar Phys., <u>19</u> , 209.
Rao U.R., Ananth A.G. and Agrawal S.P.	1972	Planet. Space Sci., <u>20</u> ,1799.
Rao U.R.	1972	Space Sci. Rev., <u>12</u> , 719.
Razdan H.	1960	Ph.D.Thesis, Gujarat University, India.
Razdan H. and Summers A.L.	1965	J. Geophys. Res., <u>70</u> , 719.

- |   |      |   |
|---|------|---|
| Razdan H. and Bemalkhedkar M.M.                     | 1971 | Proc. 12th Int. Conf. Cosmic Rays, Hobart, <u>2</u> , 697.                |
| Razdan H. and Bemalkhedkar M.M.                     | 1972 | Cosmic Electrodynamics, <u>3</u> , 297.                                   |
| Roelof E.C.   | 1971 | Proc. 12th Int. Conf. Cosmic Rays, Hobart, <u>2</u> , 764.                |
| Rose D.C., Fenton K.B., Katzman J. and Simpson J.A. | 1956 | Can. J. Phys. <u>34</u> , 968.  |
| Sarabhai V.   | 1963 | J. Geophys. Res., <u>68</u> , 1555.                                       |
| Sarabhai V. and Subramanian G.                      | 1965 | Proc. Int. Conf. Cosmic Rays, London, <u>1</u> , 170.                     |
| Sarabhai V. and Subramanian G.                      | 1966 | Astrophys. J. <u>145</u> , 206.   |
| Scarborough J.B.                                    | 1962 | Numerical Mathematical Analysis, The Johns Hopkins Press.                 |
| Schen M.  | 1968 | Supp. Nuovo Cimento, Series I, <u>6</u> , 1177.                           |
| Simpson J.A., Fonger W. and Trieman S.B.            | 1953 | Phys. Rev., <u>90</u> , 934.  |
| Simpson J.A.  | 1954 | Phys. Rev., <u>94</u> , 426.  |
| Simpson J.A. and Wang J.R.                          | 1970 | Astrophys. J., <u>161</u> , 265.  |
| Simpson N.G. and Hopper V.D.                        | 1971 | Proc. 12th Int. Conf. Cosmic Rays, Hobart, <u>3</u> , 917.                |
| Singer S.F.   | 1958 | Prog. in Elementary Particle and Cosmic Ray Phys., <u>IV</u> , 203, 1958. |
| Singh P., Lockwood J.A. and Razdan H.               | 1970 | J. Geophys. Res., <u>75</u> , 4354.                                       |
| Smart D.F., Shea M.A. and Gall R.                   | 1969 | J. Geophys. Res., <u>74</u> , 4731.                                       |
| Smith J.G. and Duncan A.J.                          | 1944 | Elementary Statistics and Applications, McGraw-Hill Book Co. Inc. 304.    |

- |   |      |  |
|---|------|--|
| Smith E.J., Davis L.<br>Coleman P.J. and Sonnet C.P.                          | 1962 | Science, <u>139</u> , 1099.  |
| Snyder C.W., Neugebauer M.<br>and Rao U.R.                                    | 1963 | J. Geophys. Res., <u>68</u> , 6361.  |
| Stern D.  | 1964 | Planet. Space Sci., <u>12</u> , 973.                                       |
| Stoker P.H. and Carmichael H.   | 1971 | Astrophys. J. <u>169</u> , 357.  |
| Stoker P.H., Raubenheimer B.C.<br>and Van der Walt A.J.                       | 1971 | Proc. 12th Int. Conf. on<br>Cosmic Rays, Denver, <u>3</u> , 870.           |
| Stormer C.  | 1936 | Astrophys. Norway <u>2</u> , No.1.   |
| Stozhkov Y. and<br>Charakhchyan T.N.  | 1968 | Can. J. Phys., <u>46</u> , S927.   |
| Subramanian G. and<br>Sarabhai V.   | 1967 | The Astrophys. J. <u>149</u> , 417.  |
| Subramanian G.  | 1971 | J. Geophys. Res., <u>76</u> , 1093.  |
| Suga K., Sakuyama H.,<br>Kawaguchi S. and Hara T.                             | 1971 | Phys. Rev. Lett. <u>27</u> , 1604.   |
| Svalgaard L.  | 1968 | Danish Meteorological<br>Institute Geophysical<br>papers R.6, August 1968. |
| Svalgaard L.  | 1972 | Preprint   |
| Teegarden R.J., McDonald F.B.<br>Trainor J.H., Roelof E.C. and<br>Webber W.R. | 1973 | Proc. 13th Int. Cosmic<br>Ray Conf., Denver, <u>2</u> ,<br>749.            |
| Thomson D.M.  | 1971 | Planet. Space Sci., <u>19</u> , 1169.                                      |
| Thomson D.M.  | 1972 | Planet. Space Sci., <u>20</u> , 2196.                                      |
| Treiman S.B.  | 1952 | Phys. Rev., <u>86</u> , 917.   |
| Van Allen J.A.  | 1973 | Proc. 13th Int. Cosmic<br>Ray Conf., Denver, <u>2</u> , 750.               |
| Venkatesan D. and<br>Dattner A.   | 1959 | Tellus, <u>11</u> , 116.   |



- Verschell H.J., Mendell R.B. 1971 Proc. 12th Int. Conf.  
Korff S.A. and Roelof E.C. Cosmic Rays, Hobart, 2, 705.
- Waddington C.J. 1962 J. Phys. Soc. Japan,  
17, Suppl. A-III, 63.
- Webber W.R. 1962 Prog. in Elementary  
Particle and Cosmic Ray  
Phys., 6, 75.
- Webber W.R. 1968 Proc. Int. Conf. Cosmic  
Rays (Calgary), A, 148.
- Webber W.R. 1969 Proc. Leningrad Conf.  
page 118.
- Wenk G. 1961 Thesis, Imperial College,  
London.
- Wilcox J.M. and Ness N.F. 1965 J. Geophys. Res. 70, 5793.
- Wilcox J.M. 1972 Private communication  
to Thomson D.M.
- Yoshida S., Akasofu S.I. 1968 J. Geophys. Res., 73, 3377.  
and Kendall P.C.
- 